

**GRAVITY ANOMALIES, GEODYNAMIC MODELLING
AND
THE EASTERN VENEZUELA BASIN EVOLUTION**

BY

INÍRIDA RODRÍGUEZ MILLÁN

A THESIS SUBMITTED FOR THE DEGREE OF

DOCTOR OF PHILOSOPHY

AT THE

UNIVERSITY OF DURHAM

DEPARTMENT OF EARTH SCIENCES

2013

GRAVITY ANOMALIES, GEODYNAMIC MODELLING AND THE EASTERN VENEZUELA BASIN EVOLUTION

BY

INÍRIDA RODRÍGUEZ MILLÁN

Geophysical Engineer, Central University of Venezuela
Magister Scientiarum, University of Leeds, UK.

ABSTRACT

This work examines the tectonic evolution of the Eastern Venezuela foreland basin by analysis of gravity anomalies and geodynamical modelling. Gravity data (8°N-12°N and 60°W-66°W) were processed to produce gravity anomaly maps, the most prominent feature being the minimum of -200 mGal isostatic, Bouguer and free-air anomalies associated with the basin. Positive gravity values characterize the northern terranes. Backstripping analysis of the sedimentary successions of four boreholes penetrating the Eastern Venezuela basin was applied to evaluate the history of subsidence. This demonstrated that an early passive margin phase (Cretaceous to early Oligocene) was followed by Oligocene to Recent tectonic subsidence of the foreland basin linked to the northern coastal compressional tectonic belt. Geohistorical analysis shows a major contribution to subsidence from early Oligocene, renewed during mid-Miocene times, in response to the loading of the South American plate on its northern margin. This tectonic loading pattern is younger from north to south. The observed gravity anomaly paired in eastern Venezuela is adequately reproduced by crustal models along profiles OO' and II' showing the isostatic negative anomaly over the foreland basin, primarily caused by the 10-13 km of sediments, the downwarping of dense lower crust and Moho down to 48 km depth. The positive gravity anomalies to the North are associated with southward thrusting of metamorphic and magmatic terranes, and dense Caribbean lithosphere. Dense subducting mantle may also be contributing to the northern positive anomaly belt as deep seismicity suggests.

Two mechanisms were applied to explain the formation of the Eastern Venezuela foreland basin during a collisional regime. First, the "hidden load" approach explains the deflection but includes an intracrustal load whose magnitude is around a third of the supracrustal loads computed by an iterative process. This gives rise to a major misfit between the gravity anomaly computed for the structural model which takes into account all the geological and geophysical constraints when the contribution of the "hidden load" is included in the calculations. Second, since the hidden load hypothesis fails to explain the gravity profiles, a remaining viable explanation is release of compressional strain energy involving N-S crustal shortening involving faulting. I therefore explored a fault-based hypothesis which does not depend on hidden gravitational loads, but takes into account the clear relationship between the subsidence and the complementary uplift. In conclusion the prime cause of the evolution of the system depends on the forces on fault planes as they move, where the tractions on a thrust fault develop when a frictionless fault occurs in response to horizontal deviatoric compression of an elastic layer. As compression acts at the edges of the plate, the stresses are re-orientated producing the movement of the two plates along dipping fault planes (including the El Pilar fault). This led to the formation of the Eastern Venezuela foreland basin and linked uplift of the Eastern Serranía del Interior by spasmodic release of elastic strain energy.

GRAVITY ANOMALIES, GEODYNAMIC MODELLING AND THE EASTERN VENEZUELA BASIN EVOLUTION

CONTENTS

	PAGE
Abstract	ii
Contents	iii
List of figures	v
List of tables	xiv
Acknowledgments	xvi

CHAPTER 1 INTRODUCTION

1.1. Introduction	2
1.1.1. The objectives of this research	2
1.2. The Caribbean plate.	3
1.2.1. Eastern Caribbean plate boundary zone	14
1.2.2. Evolution of the Eastern Caribbean plate	21
1.2.3. Southern Caribbean plate boundary zone.	24

CHAPTER 2 EASTERN VENEZUELA TECTONIC SETTING

2.1. Introduction	29
2.2. Geology prior to Jurassic tectonism.	30
2.2.1. Guayana Shield.	30
2.2.2. Post-Cambrian and pre-Jurassic	33
2.3. Jurassic rifting: Extensional domain	34
2.4. Passive margin phase: Early Cretaceous to Eocene.	36
2.5. The northern overthrusting domain	39
2.5.1. Araya-Tobago terrane	39
2.5.2. Eastern Venezuela foreland thrust and fold belt.	44
2.6. The Eastern Venezuela foreland basin.	46
2.6.1. Oligocene to Present time.	47
2.6.2. Regional Tertiary to Present structures.	51
2.7. The structure of the Eastern Venezuela basin.	55
2.8. Key elements for the evolution of the Eastern Venezuela basin.	58
2.9. Seismicity in eastern Venezuela.	62

CHAPTER 3 SUBSIDENCE IN THE EASTERN VENEZUELA BASIN

3.1. Sedimentary basins.	67
3.1.1. Sedimentary basins classification.	67
3.2. Passive-Margin basins.	68
3.3. Foreland basins.	69
3.4. Mechanisms of basin formation.	70

3.4.1. An introductory review.	70
3.5. Sedimentation vs. Subsidence in the Eastern Venezuela foreland basin.	74
3.5.1. Tertiary subsidence of the Eastern Venezuela foreland basin.	75
3.5.2. Sediment loading effect.	83

CHAPTER 4 GRAVITY ANOMALIES

4.1. Gravity anomalies in Eastern Venezuela.	91
4.2. Gravity data reduction.	91
4.2.1. Complete Bouguer anomaly.	93
4.3. Gravity anomaly maps of Eastern Venezuela.	94
4.4. Isostatic anomalies.	99
4.4.1. An introductory review.	99
4.4.2. Isostatic anomalies Eastern Venezuela -Airy and Pratt-.	102
4.4.3. Bouguer and free-air anomalies vs. topography.	104
4.4.4. Gravity anomaly-topography admittance and coherence analysis techniques.	110
4.5. Two-dimensional gravity modelling.	111
4.5.1. Constraints from borehole data.	112
4.5.2. Constraints from seismic data.	113
4.5.3. Constraints from density measurements.	115
4.5.4. Spectral analysis from gravity data.	118
4.5.5. Crustal sections in eastern Venezuela.	119
4.5.6. Seismicity and gravity modeling.	127

CHAPTER 5 EASTERN VENEZUELA FORELAND BASIN FORMATION

5.1. Introduction.	132
5.2. Flexure of the continental lithosphere.	133
5.2.1. Some theoretical considerations.	133
5.2.2. A flexural model for the Eastern Venezuela foreland basin.	137
5.3. Flexural modelling in the Eastern Venezuela foreland basin.	146
5.3.1. Effect of topography-thrusts-sediments.	146
5.3.2. Estimation of hidden loads.	151
5.3.3. Hidden load effect.	153
5.4. Results from flexural modelling.	155
5.4.1. Results Profile 00'	157
5.4.2. Results Profile II'	160
5.5. The origin of the "hidden load".	164
5.6. The stress release mechanism.	167
5.7. The nature of the hidden load subsurface load required to explaining the Eastern Venezuela basin subsidence and its relation to subduction.	172
5.8. Mantle dynamic topography and tectonic overview	174

CHAPTER 6	SUMMARY AND CONCLUSIONS	179
	BIBLIOGRAPHY AND REFERENCES	188
APPENDIXES		
APPENDIX A.1	SEDIMENTATION vs. SUBSIDENCE STRATIGRAPHIC ZONAL DISTRIBUTION	216
APPENDIX A.2	SEDIMENT LOADING EFFECT BACKSTRIPPING	229
APPENDIX B	FINITE ELEMENT METHOD FOR FLEXURE	233
APPENDIX C	GRAVITY DATA CATALOGUE EASTERN VENEZUELAN BASIN	241
APPENDIX D	EARTHQUAKE DATA CATALOGUE EASTERN VENEZUELAN BASIN	267

LIST OF FIGURES

FIGURE		PAGE
1.1	Regional tectonic setting of the Caribbean exhibiting the most striking structural features of the Caribbean region.	4
1.2	Diachronous eastward displacement of the Caribbean plate relative to the North and South American plate with numbered, solid black lines representing the inferred locations of the leading edge of the Caribbean plate at these times (modified from Lugo and Mann, 1995; taken from Escalona and Mann, 2011).	6
1.3	Map of seismic activity in the Caribbean region. Approximate epicentre's location from International Seismology Center –ISC.	8
1.4	Satellite Free-Air anomaly map of the Caribbean region. Gravity data from Sandwell and Smith (2009).	10
1.5	Bouguer Anomaly map of the Caribbean region. Gravity data from Sandwell and Smith (2009).	11

1.6	Magnetic anomaly map of the Caribbean region. Magnetic data from EMAG2: Maus et al. (2009)	12
1.7.	Heat flow measurements in the Caribbean region. Values are in heat-flow units (1 h.f.u. = 1 $\mu\text{cal cm}^{-2} \text{s}$). Compiled from Epp et. al. (1970), Erickson et al. (1972), Simmons and Horai (1968) and Lee and Clarck (1968). After Bowin (1976), generated by Arnaiz-Rodríguez (2012, in press).	13
1.8.	Seismic line BOL30 (From Aitken et al., 2011, Fig. 5): A) Uninterpreted seismic reflection data. B) Interpreted seismic reflection data. C) Interpreted seismic refraction data from Christeson et al. (2008).	19
1.9.	Seismicity in the Eastern Caribbean: Lesser Antilles Island Arc. Depth: Yellow=0-35 km; red=36-70 km; green=71-150 km; blue =151-300 km. Data from ISC: 1904-2009. Taken from Ughi (2009).	20
1.10	Cenozoic plate reconstructions and cross-sections of the southeastern Caribbean to propose models for Grenada and Tobago basin evolution. Plate reconstructions from Aitken et al. (2011) modified from Mann and Escalona (2011).	23
2.1.	Geographical and tectonic setting of the Eastern Venezuela basin in the northern South America borderland.	29
2.2A	Auyantepuy seen from the south. Location: 5° 48' 15" N, 62° 28' 03" W. Courtesy: Isabel Hernandez (2010).	31
2.2B	Roraima seen from its top, from the north with north-south direction. Location: 5° 12' 08" N, 60° 44' 07" W. Courtesy: Janckarlos Reyes, 2010.	31
2.3.	Crustal sections from seismic refraction survey along W-E and N-S profiles in the Guayana Shield. Velocities are in km/s. Vertical exaggeration 3:1 (Schmitz et al.,1999; Chalboud,2001).	32
2.4.	Tectonic and geological framework showing the main structural features in Eastern Venezuela, as well as location of profiles OO' and II'. Relevant structures in the area after Bellizzia et al. (1976), Feo Codecido et al. (1984), Di Croce (1995) and Hung (2005).	34

2.5. Seismic Stratigraphy and idealized well log of the Eastern Venezuelan basin. (Modified from Cobos, 2002; Duerto, 2007)	48
2.6. Simplified Cronostratigraphic chart of the Eastern Venezuelan basin. From Di Croce et al. (2000), modified by Duerto (2007).	50
2.7. Schematic regional NW-SE cross-section of the northeastern part of Venezuela. Vertical scale exaggerated 4-times. (After Chevalier, 1994; Duerto, 2007)	52
2.8. Location of seismic sections (blue lines) shown in section 2.7, this chapter. Modified after Duerto (2007)	55
2.9A Seismic section R-6, north section, interpreted by Duerto (2007).	56
2.9B Seismic section R-6, south section, interpreted by Duerto (2007)	57
2.10A Seismic profile R-10 which runs in E-W direction. Interpreted by Duerto (2007).	57
2.10B Seismic profile R-9, east of R-10, shows three main structural features: high angle reverse faults, a listric fault system and a low angle fault system. Interpreted by Duerto (2007).	58
2.11. Geological cross sections depicting the tectonic and structural evolution of the Eastern Venezuela basin. Stratigraphy is highly generalized. Restored fault geometries are based in part on quantitative restorations of seismic-based cross-sections (Taken from Summa et al., 2003).	62
2.12. Distribution of seismicity in Eastern Venezuela. Focal depths 0-20 km depth.	63
2.13. Distribution of seismicity in Eastern Venezuela. Focal depths 20-80 km depth.	64
2.14. Distribution of seismicity in Eastern Venezuela. Focal depths >80 km depth.	65
3.1. Simple stretching model, after McKenzie (1978).	72
3.2. Diagram to illustrate the relation $t=d ((\rho_m - \rho_w) / (\rho_m - \rho_s))$ in gravity loading mechanism assuming Airy isostasy,	

where ρ_m is the mantle density, ρ_w is the water density and ρ_s is the sediments density.	73
3.3. Borehole-well location map and zonal distribution according to sedimentation-rate in the study area. Numbers 1 to 10 in grey circles are identification of subzones 1 to 10 respectively. Dots indicate well location. Blue squares indicate backstripped wells.	75
3.4. Stratigraphic sections characteristic of subzones 1 to 10 in Eastern Venezuela.	77
3.5A-B. Sequence Cretaceous to Present time in Eastern Venezuela illustrating the zonal distribution of sediments according to sedimentation-rate in the study area. 3.5A. Cretaceous. 3.5B. Oligocene.	79
3.5C-D. Sequence Cretaceous to Present time in Eastern Venezuela illustrating the zonal distribution of sediments according to sedimentation-rate in the study area. 3.5C. Lower Miocene. 3.5D. Mid Miocene.	80
3.5E-F. Sequence Cretaceous to Present time in Eastern Venezuela illustrating the zonal distribution of sediments according to sedimentation-rate in the study area. 3.5E. Upper Miocene-Pliocene. 3.5F. Present.	81
3.6. Top Basement Structure - Total Sediment Fill, Eastern Venezuela. Modified after Summa et al. (2003). The thickest sediment fill lies within the gravity low showed in dashed blue lines.	82
3.7A-B. Total (yellow+green) and tectonic (green) subsidence of the Eastern Venezuela basin, from wells PER and ALT. Borehole-well location in Fig. 3.3. Age scale.	86
3.8A-B. Total (yellow+green) and tectonic (green) subsidence of the Eastern Venezuela basin, from wells CA1 and QUI. Borehole-well location in Fig. 3.3. Age scale	87
3.9A-B. Integrated total (yellow) and tectonic (green) subsidence curves of the Eastern Venezuela basin, from wells QUI, ALT,	

CA1 and PER. Dashed orange lines indicate pulses of tectonic subsidence. Borehole-well location in Fig. 3.3.	88
4.1. Shaded relief topographic map of the area of study in Eastern Venezuela. OO' and II' are modelled sections.	92
4.2. Bouguer Anomaly Map of the area of study: Eastern Venezuela. Contour intervals (dashed lines) 50 mGal. OO' and II' are modelled sections.	96
4.3. Free-Air Anomaly Map of the area of study: Eastern Venezuela. Contour interval (dashed lines) 50 mGal. OO' and II' are modelled sections.	98
4.4. Illustrative diagram for Airy and Pratt anomaly computations. (From Bott, 1971a).	101
4.5. Isostatic anomaly map: Airy compensation $T=35\text{km}$, Eastern Venezuela. Contour interval (dashed lines) 50 mGal.	103
4.6. Isostatic anomaly map: Pratt compensation $D=100\text{km}$, Eastern Venezuela. Contour interval (dashed lines) 50 mGal.	104
4.7. Upward continuation of Bouguer anomalies 5000 m. Contour interval (dashed lines) 50 mGal. OO' and II' are modelled sections.	106
4.8. Upward continuation of free-air anomalies 5000 m. Contour interval (dashed lines) 50 mGal. OO' and II' are modelled sections.	107
4.9. Free-air and Bouguer anomalies related to topography along profile OO'.	108
4.10. Free-air and Bouguer anomalies related to topography, along profile II'.	109
4.11. Map of the Caribbean-South America interaction zone showing the location of seismic transects carried out in the framework of BOLIVAR and GEODINOS projects. (Taken from Schmitz et al., 2008).	114
4.12. Moho map from BOLIVAR and GEODINOS data (Schmitz et al., 2008).	115

4.13. Final velocity model for profile 65W shown with (top) a 5x vertical exaggeration and (bottom) no vertical exaggeration. Modified after Bezada et al. (2010)	116
4.14. Depth determination from spectral analysis of gravity data.	118
4.15. Structural models for profiles OO' and II' illustrating the near surface structure and the observed Bouguer anomaly.	120
4.16. Bouguer gravity model along profile OO' in Eastern Venezuela.	122
4.17 Bouguer gravity model along profile II" in Eastern Venezuela.	123
4.18 Bouguer gravity model along profiles OO' and II", showing the contribution of the sedimentary sequence of the Eastern Venezuelan basin.	124
4.19 Bouguer gravity models along profiles OO' and II' to test the structural or seismic models proposed by Clark et al. (2008).	126
4.20 Bouguer gravity model along profile OO' showing hypocentral depth for earthquakes of magnitude > 5	128
4.21 Bouguer gravity model along profile II' showing hypocentral depth for earthquakes of magnitude > 5	130
5.1 The assumed loading scheme describing the emplacement of loads onto the continental lithosphere at mountain ranges and formation of associated foreland basins. (After Karner and Watts, Figure 9, 1983).	138
5.2A. Loading scheme for flexural modelling at the Eastern Venezuela foreland basin. 1= Surface Load. 2 = Subsurface Load. 3 = Sediments.	139
5.2B. Geological crust-section illustrating the loading scheme in the area of study. 1 = Above sea level topography. 2 = Subsurface load including the thrusts of the Eastern Serrania del Interior, Araya-Paria terrane and the magmatic arc-platform Margarita-Los Testigos. 3=Infilling sediments of the Eastern Venezuela foreland basin.	139

- 5.3. Location of profiles OO' and II' illustrating end-positions of the broken South American plate (I-II-III, shown by red lines). I= Grenada Basin (SW end). II= Margarita-Tobago forearc basin. III= El Pilar fault. 141
- 5.4. Diagram to illustrate the flexural modelling. Surface (topography) and subsurface (thrust and terranes) load spectra are applied over the lithosphere (a thin, elastic, broken plate) and the flexural response calculated and compared with the observed data. 143
- 5.5. Combined effect of surface, subsurface loads and sediments in the deflection of an elastic plate with elastic thickness 10, 25, 35 and 50km, for position of the broken-end of the plate at I. 148
- 5.6. Combined effect of surface, subsurface loads and sediments in the deflection of an elastic plate with elastic thickness 10, 25, 35 and 50km, for position of the broken-end of the plate at III. 149
- 5.7. Flexural response of the South American plate to the combined surface and subsurface load, for a choice of elastic thickness of 10, 25, 35 and 50 km and positions of the broken-end of the plate at I, II and III, along: A.- Profile OO' and B.- Profile II'. 150
- 5.8. Free-air anomaly map with corridors 100 km wide, used to evaluate the mean free-air anomaly and estimate the average load per unit area. 152
- 5.9A. Loading scheme for flexural modelling at the Eastern Venezuela foreland basin. 1=Surface Load. 2=Subsurface Load. 3=Sediments. 4=Hidden Load. 154
- 5.9B. Geological crust-section illustrating the loading scheme
In the area of study. 1 = Above sea level topography.
2 = Subsurface load including the thrusts of the Eastern Serrania del Interior, Araya-Paria terrane and the magmatic arc-platform Margarita-Los Testigos. 3 = Infilling sediments of the Eastern Venezuela foreland basin. 4 = Hidden Load. 154
- 5.10. Effect of the modified loading scheme onto the foreland plate, $T_e=25\text{km}$. Bouguer anomaly controlling the basement deflection; hidden load not included into calculations. Continuous line in free-air and Bouguer anomaly profiles

- represent calculated anomalies for the crustal section and dots are observed gravity values. 155
- 5.11. Effect of the modified loading scheme onto the foreland plate, $T_e=25\text{km}$. Flexural model as in Figure 5.11 but hidden load included in gravity calculations. Continuous line in free-air and Bouguer anomaly profiles represent calculated anomalies for the crustal section and dots are observed gravity values. 156
- 5.12. Flexural model along profile OO', with broken-end position I (SW Grenada basin) produced according to the modified loading scheme. Continuous line in free-air and Bouguer anomaly profiles represent calculated anomalies for the crustal section and dots are observed gravity values. 158
- 5.13. Flexural model along profile OO', with end-position II (Margarita-Tobago forearc basin). $T_e=23\text{km}$. Continuous line in free-air and Bouguer anomaly profiles represent calculated anomalies for the crustal section and dots are observed gravity values. 159
- 5.14. Flexural model along profile OO', with end-position III (El Pilar Fault). $T_e=20\text{km}$. Continuous line in free-air and Bouguer anomaly profiles represent calculated anomalies for the crustal section and dots are observed gravity values. 160
- 5.15. Flexural model along profile II', with end-position I. (SW Grenada basin) produced according to the modified loading scheme. Best fit for $T_e=20\text{km}$. Continuous line in free-air and Bouguer anomaly profiles represent calculated values for the modelled crustal section and dots are observed values. 161
- 5.16. Flexural model along profile II', with end-position II. (Margarita-Tobago forearc basin). $T_e=15\text{km}$. Continuous line in free-air and Bouguer anomaly profiles represent calculated values for the modelled crustal section and dots are observed values. 162
- 5.17. Flexural model along profile II', with end-position III (El Pilar Fault). $T_e=15\text{km}$. Continuous line in free-air and Bouguer anomaly profiles represent calculated values for the modelled crustal section and dots are observed values. 163

5.18 Bouguer gravity model along profile OO' illustrating the effect of the "hidden load" when it is included in the calculations.	165
5.19 Bouguer gravity model along profile II' illustrating the effect of the "hidden load" when it is included in the calculations.	166
5.20. Schematical diagram to demonstrate how tractions on a thrust fault develop when a frictionless fault occurs in response to horizontal compression of an elastic layer.	169

FIGURES IN APPENDIXES:

Diagrams illustrating:

(A) Thickness of sediments. (B) Depth to basement.

(C) Rate of sedimentation. Characteristic of the Eastern Venezuela basin.

A.1. Subzone 1. (Wells 35, 36, 76 and 147)	217
A.2. Subzone 2. (A.2a. Wells 1 and 101)	219
Subzone 4. (A-2b. Wells 18 and 25)	219
A.3. Subzone 3. (Wells 48, 101, 102 and 108)	220
A.4. Subzone 5. (Wells 127, 128, 129 and 130)	222
A.5. Subzone 6-8. (A.5a. Wells 9 and 6, 138 and 118).	223
A.6. Subzone 7. (Wells 140, 79, 91 and 90)	225
A.7. Subzone 9. (Wells 154, 153, 91 and 156)	227
B.1. Diagram to illustrate the flexural modelling applying Finite Elements Method –FEMFLEX (From Arnaiz-Rodriguez, 2011).	235
B.1.1 Flexure of the South American plate in response to the surface (topography) plus subsurface (foreland thrust belt) loads.	236
B.1.2 Flexural response of the South American plate to the combined effect of surface and subsurface loads, plus a vertical force F_P acting downwards.	237
B.1.3 Flexural response of the South American plate to the combined effect of surface and subsurface loads, plus a horizontal force F_H acting at the top of the plate.	237

B.1.4 Flexural response of the South American plate to the combined effect of surface and subsurface loads, a small vertical force F_V plus two horizontal forces F_H acting as a couple at the top and bottom of the plate.	238
B.1.5 Flexural response of the South American plate to the combined effect of surface and subsurface loads, a vertical force F_V plus a couple of horizontal forces F_H acting at the top and bottom of the plate.	238
B.1.6 Flexural response of the South American plate to the combined effect of surface and subsurface loads, plus a couple of horizontal forces F_H acting at the top and bottom of the plate, a small vertical force F_V acting at the top and a vertical force $F_P = 0.5L$ acting downwards.	239

LIST OF TABLES

TABLE	PAGE
1.1. Summary of Crustal Properties in the SE Caribbean Region (Modified after Case et al., 1990; and Pindell et al., 2005)	27
4.1. Densities used for Bouguer Anomaly Computation.	117
5.1. Summary of parameters assumed in flexural modelling.	145
5.2. Loading masses for flexural modelling.	157

TABLES IN APPENDIXES

A.1. Input and Output Data for Backstripping Wells QUI, ALT, PER and CA1.	231
D.1. Seismologic database: Earthquakes with magnitude > 5	268

“The copyright of this thesis rests with the author. No quotation from it should be published without the prior written consent and information derived from it should be acknowledged.”

ACKNOWLEDGMENTS

I would like to thank the Consejo de Desarrollo Científico y Humanístico and the Faculty of Engineering of the Universidad Central de Venezuela for giving me time and financial support throughout my research for my Ph.D. thesis at Durham University, which I also acknowledge with thanks for being my second *alma mater* in England.

I wish to express my very special thanks to Professor Graham K. Westbrook for his supervision during the first stage of my research; his guidance and comments are very much appreciated. My profound acknowledgment to Professor Martin H. P. Bott for sound advice and for his invaluable support and encouragement in giving me the opportunity to revive and conclude this research, because it would not have been possible to accomplish it at all without his unceasing inspiration, suggestions and constant presence. My gratitude goes also to Dr. Jhonny Imber for allowing me the opportunity to conclude this research.

I am most indebted to Dr. Garry Karner for specific advice relating to flexural modelling and for allowing me access to his computer subroutines. It is a pleasure to record these names, as well as those of Professor John F. Dewey, James Pindell, Naomi Ussami and Webster Monjak, for many stimulating and fruitful discussions concerning the tectonic of the Caribbean and South America regions. I would also thank former Petróleos de Venezuela and FUNVISIS SA, Caracas, for supplying technical information about the Eastern Venezuela basin; and to the GEODINOS-BOLIVAR project, which provided substantial recent information to support my research.

This study could not have been possible without the cooperation of a large number of people; foremost amongst my colleagues at the Universidad Central de Venezuela Mónica Martiz and Nuris Orihuela, both dear friends whose confidence and support I deeply appreciate; my students and

research assistants of Gravity and Magnetic Methods throughout the years, Antonio, Adriana, Ignacio, very very specially Josmat for well data processing and modelling, and Mariano for the new maps and FEM models, all of whom I will forever consider my academic children; the expertise of draftsmen Samuel and Raul; the support and patience of José Luís Bifano in helping with the graphs; Alexka and Richard with the data; Anays for keeping me company on campus at night; Morella Mikati in the Library; Paola with her indispensable touch of artistry; my very dear friends Moni and Mary for welcoming me in their homes and caring for me during long hours of work; and my lifelong friend Lucy for her revisions and many helpful suggestions.

I am deeply grateful to my friends Lourdes and Michael Watts for many hours devoted to helping me improve the clarity of the manuscript, and to my goddaughters Gaby and Andrea who helped very much with the references. My appreciation and a special vote of heartfelt thanks go to Mirtha Sara Morales, for her invaluable and cheerful assistance in what I thought were the final stages of this work. For their friendship, my warmest thanks to Gill Lyons, Margaret McCollum and most specially to Marie Shearer for every kind of help and for always making me feel at home in Durham.

My best thanks are due to Dr. Nicolás Bianco C., present Academic Vicerrector of the Universidad Central de Venezuela, for allowing me to share his significant work as part of the authorities of our University. Working with him and following his leadership inspired me to take the first steps in reviving this research.

Finally I owe a very special thanks to my parents for inspiration and continuous loving support, to my brother Jesús for encouragement throughout my academic career and last, but far from least, to my son Oscar for his love and patient tolerance of my periods of absence while I was working on the thesis.

IN THE LOVING MEMORY OF MY FATHER

TO MY MOTHER

FOR MY SON, OSCAR

CHAPTER 1

INTRODUCTION

1.1. INTRODUCTION

Although geological and geophysical investigations have added greatly to the knowledge of the structure and tectonics of the Caribbean area in recent years, the tectonics of the Caribbean plate and particularly those of its southern margin is still the subject of controversy.

This work examines the tectonic evolution of the southern Caribbean margin, especially the Eastern Venezuela foreland basin, through an analysis of gravity anomalies. Chapter 1 of this thesis provides a brief literature review of the geology and geophysics of the Caribbean region. Chapter 2 focuses on the Eastern Venezuela tectonic setting, summarizing the general aspects related to the evolution of the Eastern Venezuela basin. Chapter 3 describes and analyzes the sedimentation vs. subsidence in the Eastern Venezuela foreland basin, based on borehole data. Chapter 4 is devoted to processing and interpretation of gravity anomalies. The flexural modelling and the strain release mechanism applied in the Eastern Venezuela foreland basin are described and compared in Chapter 5. The final summary and conclusions are presented in Chapter 6.

1.1.1 THE OBJECTIVES OF THIS RESEARCH

The main objective of this research is to determine a crustal model of the eastern part of Venezuela through an analysis of gravity anomaly data, borehole and geological data, together with flexural and strain release mechanisms applied to basin modelling to help understanding the tectonic subsidence and evolution of the Eastern Venezuelan basin.

Among the specific objectives to fulfill the purposes of this study we consider: (1) To evaluate the response of the South American plate to loads corresponding to the weight of the topography and thrust sheets associated with plate convergence, as well as the possibility of combining it with the effects of forces acting upon or beneath the lithospheric plate. (2) To constrain the effective elastic thickness of the lithosphere in the eastern part of Venezuela

and possible locations of the South American plate breaks northwards. (3) To study the earthquakes distribution below the region and its association with possible discontinuities between zones of contrasting density structure. (4) To study subsidence patterns from borehole data of the Eastern Venezuela basin.

1-2. THE CARIBBEAN PLATE

In the context of Plate Tectonics, the Caribbean region has been interpreted as a zone of interaction between the Caribbean plate and the North and South American plates. A general view of the Caribbean plate shows that it covers approximately the extension of the Caribbean Sea and is surrounded by four plates, namely: North America, South America, Cocos and Nazca. A simplified map showing the most striking structural features of the Caribbean region and the location of the study area onland Venezuela is shown in Figure 1.1.

Active subduction margins delineate the western and eastern boundaries of the Caribbean plate at the Middle America trench and the Lesser Antilles island arc respectively; while sea-floor spreading, strike slip and thrust areas characterize its northern and southern multibranch boundary zones (Burke et al., 1980; Sykes et al., 1982; Mann and Burke, 1984; Burke, 1988; James, 2003; Pindell et al., 2005).

The literature of the Caribbean region, both on land and offshore, is voluminous and particularly over the last 30 years has been characterized by the publication of mostly specialized studies that have improved and refined our knowledge of the Caribbean area. More recently, a great deal of geological and geophysical information has been added to it, throughout the BOLIVAR (**B**roadband **O**cean-**L**and **I**nvestigations of **V**enezuela and the **A**ntilles arc **R**egion) and GEODINOS (**G**eodinámica Reciente del Límite **N**orte de la Placa **S**udamericana - Recent Geodynamics of the Northern Limit of the South American Plate) projects in the Caribbean and South American plates interaction zone.

Following definitions of geological provinces in the Caribbean region by Speed et al. (1984), Case et al. (1990) and Pindell et al. (2005), a summary of the main characteristics of the most relevant features of the Caribbean plate and

boundary zones is presented in Table 1.1, and should be examined in conjunction with the location map on Figure 1.1.

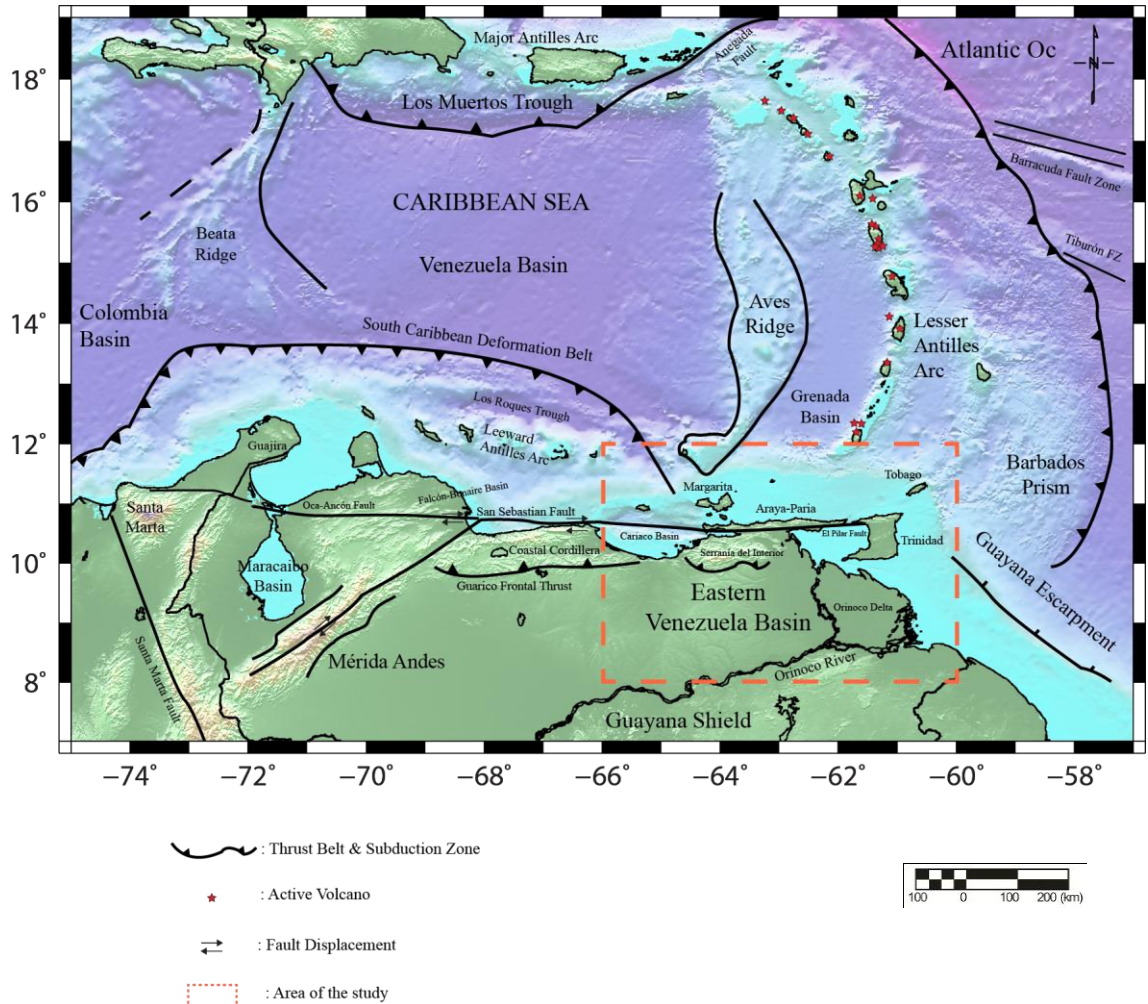


Figure 1.1. Regional tectonic setting of the Caribbean exhibiting the most striking structural features of the Caribbean region. Red rectangle shows the area of study: The Eastern Venezuela foreland basin, onland Venezuela.

The following general remarks may, however, be of interest:

- The region occupied by the Caribbean basin, on the whole, can be considered as a product of Jurassic spreading of the North and South American plates, and concomitant generation of oceanic lithosphere (Ladd, 1976; Pindell and Dewey, 1982; Pindell et al., 2005).

- It is also well accepted that the modern Caribbean plate has always migrated eastward relative to North and South American plates, and its displacement has influenced the tectonics of the area since the Jurassic (Jordan, 1975; Mann et al., 1990). Pindell and Barrett (1990) have proposed that the direction of Caribbean plate motion has not remained steady but has changed several times throughout the Cenozoic. In this context it is interesting the recognition of a late middle Miocene change in the Caribbean-North American azimuth from E to ENE, and the Caribbean-South American azimuth from ESE to E, which resulted in wholesale changes in tectonic development in both the northeastern and southeastern Caribbean plate boundary zones (Pindell and Kennan, 2001a; 2007a-b).
- Crustal properties of the Caribbean lithosphere are not typical of other major ocean basins. As Fox and Heezen (1975) have established, over much of the Caribbean basin, seismic refraction measurements reveal anomalous oceanic crust 10 to 25 km thick, and a substantial part of the Caribbean is underlain by two crustal layers with average velocities of 6.2 and 7.2 km/sec, values that do not correspond to the typical velocities of 5.0 and 6.8 km/sec for oceanic layers 2 and 3. In close coincidence with this, Escalona and Mann (2011) state that the Caribbean plate possesses an oceanic crustal thickness ranging from 8 to 20 km.
- Two main alternatives have been proposed to explain the origin of the Caribbean: the plate is either a fragment of Proto-Caribbean lithosphere, originally generated by seafloor spreading between North and South American plates, which means that its easterly translation has been small (Sykes et al., 1982; James, 2009; Meschede and Frisch, 1998) or it is a fragment of Pacific lithosphere that has moved a large distance to the east relative to the Americas during Cenozoic time (Hess, 1953; Malfait and Dinkleman, 1972; Burke *et al.*, 1984; Pindell *et al.*, 1988; Pindell and Kennan, 2001a). Nowadays, most authors agree that the Caribbean plate was formed as an oceanic plateau during Late

Cretaceous in the near eastern Pacific region and migrated eastwards relative to the North and South American plates, behind an east-facing Great Arc of the Caribbean to its present position (Burke et al., 1984; Burke, 1988; Pindell and Barrett, 1990; Mann, 1999; Pindell et al., 2005; Escalona and Mann, 2011). The difference between the two hypotheses is based mainly in different interpretations of the paleomagnetic and geochemical evidence (Schmitz et al., 2008).

The displacement of the Caribbean plate relative to North and South American plates, showing the inferred locations of the leading edge of the Caribbean plate through time is shown in Figure 1.2. (Lugo and Mann, 1995; Escalona and Mann, 2011).

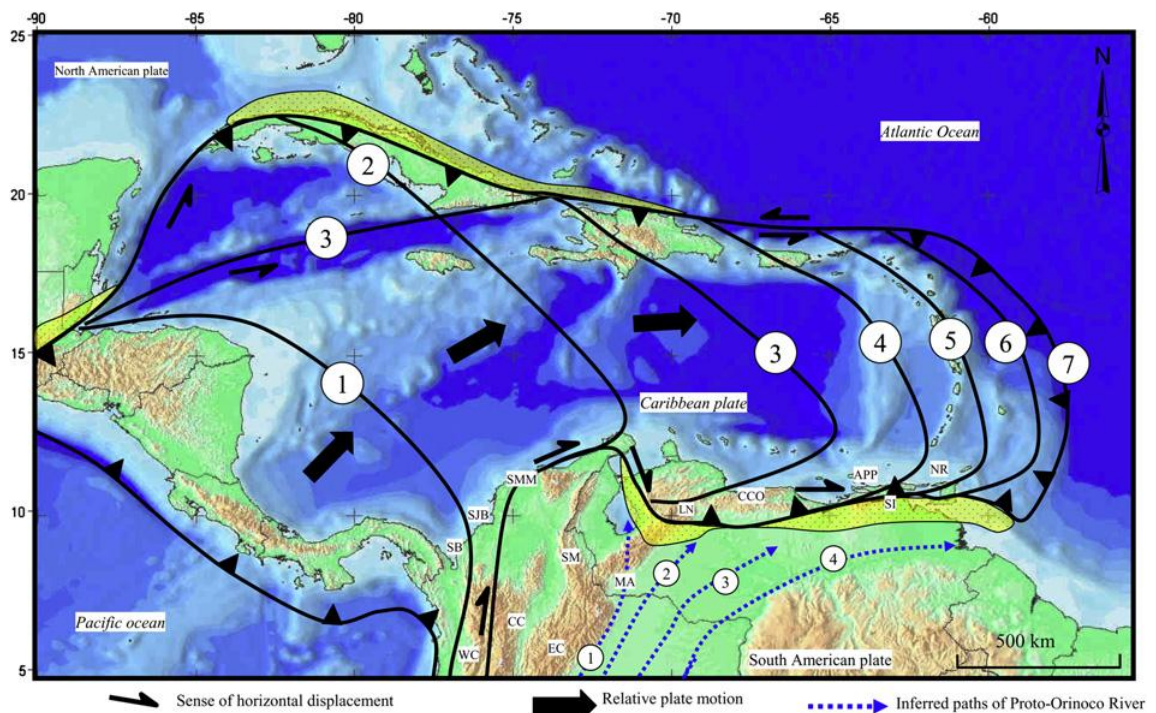


Figure 1.2. Diachronous eastward displacement of the Caribbean plate relative to the North and South American plates with numbered, solid black lines representing the inferred locations of the leading edge of the Caribbean plate at these times: 1 = Late Cretaceous (~80 Ma); 2 = middle Paleocene (~60 Ma); 3 = middle Eocene (~44 Ma); 4 = middle Oligocene (~30 Ma); 5 = middle Miocene (~14 Ma); 6 = Pliocene (~5 Ma); and 7 = Recent (modified from Lugo and Mann, 1995). Yellow, stippled areas represent foreland basins produced by diachronous oblique convergence between the Caribbean, North American and South American plates. Abbreviations: SB = Sinu belt, WC = Western Cordillera, SJB = San Jacinto belt, SMM = Santa Marta massif, CC = Central Cordillera, EC = Eastern Cordillera, SM = Santander massif, MA = Mérida Andes, LN = Lara nappes, CCO = Cordillera de la Costa, APP = Araya-Paria peninsula, SI = Serranía del Interior, and NR = Northern Range of Trinidad. Blue, dashed lines represent inferred paths of the proto-Orinoco River at the following times: 1 = Paleocene (~60 Ma); 2 = middle Eocene (~44 Ma); 3 = middle Miocene (~14 Ma); and 4 = Recent. (Taken from Escalona and Mann, 2011).

- Rifting between South and North American plates started in Late Jurassic-Early Cretaceous, and was followed by prolonged Cretaceous subsidence in a passive margin setting (Pindell and Kennan, 2001b; Mann et al., 2006). The passive margin phase was interrupted by progressive west-to-east collision of the Caribbean arc with the passive margin in the Late Paleocene-Early Eocene western Venezuela at the Maracaibo basin region (Pindell and Barrett, 1990; Lugo and Mann, 1995; Escalona and Mann, 2006); and during the Neogene in the area of eastern Venezuela and Trinidad (Erlich and Barrett, 1992; Di Croce et al., 1999; Pindell and Kennan, 2001b, 2007a).
- Apparently, no major plate boundary has extended through the Caribbean interior, except through the Cayman Trough, since the reorganization of relative plate motions in the Eocene, Miocene to Recent time was marked by lithospheric flexure adjacent to active compressional margins, diffuse rifting beneath the western Caribbean and a great influx of terrigenous sediments, especially from South America (Holcombe, 1977; Holcombe et al., 1990; Pindell et al., 2005).
- The seismicity of the Caribbean area ranks it among the most active areas in the world (Sykes and Ewing, 1965). However, the paucity of seismic activity in the interior region of the plate contrasts with the ring of seismicity around the Caribbean plate, as to confirm that earthquake epicenters appear to be largely limited to locations of crust-crust contact (Figure 1.3).

Among the studies that have contribute to improve the configuration of downgoing seismic zones, seismic troughs and strike-slip faults (Sykes et al., 1982; Speed et al., 1984, 1993; Pérez and Aggarwal, 1981; McCann and Pennington, 1990) and to provide more accurate estimates of the rate of relative motion of the Caribbean and surrounding lithospheric plates, it is worth mentioning those of Jarrard (1986) and Speed et al. (1993) reporting that the rate of convergence today is faster in the north (37 mm/year relative to North America plate) than in the south (13 mm/year relative to South America plate);

and also those of Mann et al. (1990), based on their review of Caribbean neotectonics, concluding that the most reliable rates of North America-Caribbean interplate displacement on major strike-slip faults in Late Neogene times reach an amount of 20 mm/year. Compared to other arc systems, the Caribbean arc system has a slow convergence rate and low magma production rates (Wadge, 1984).

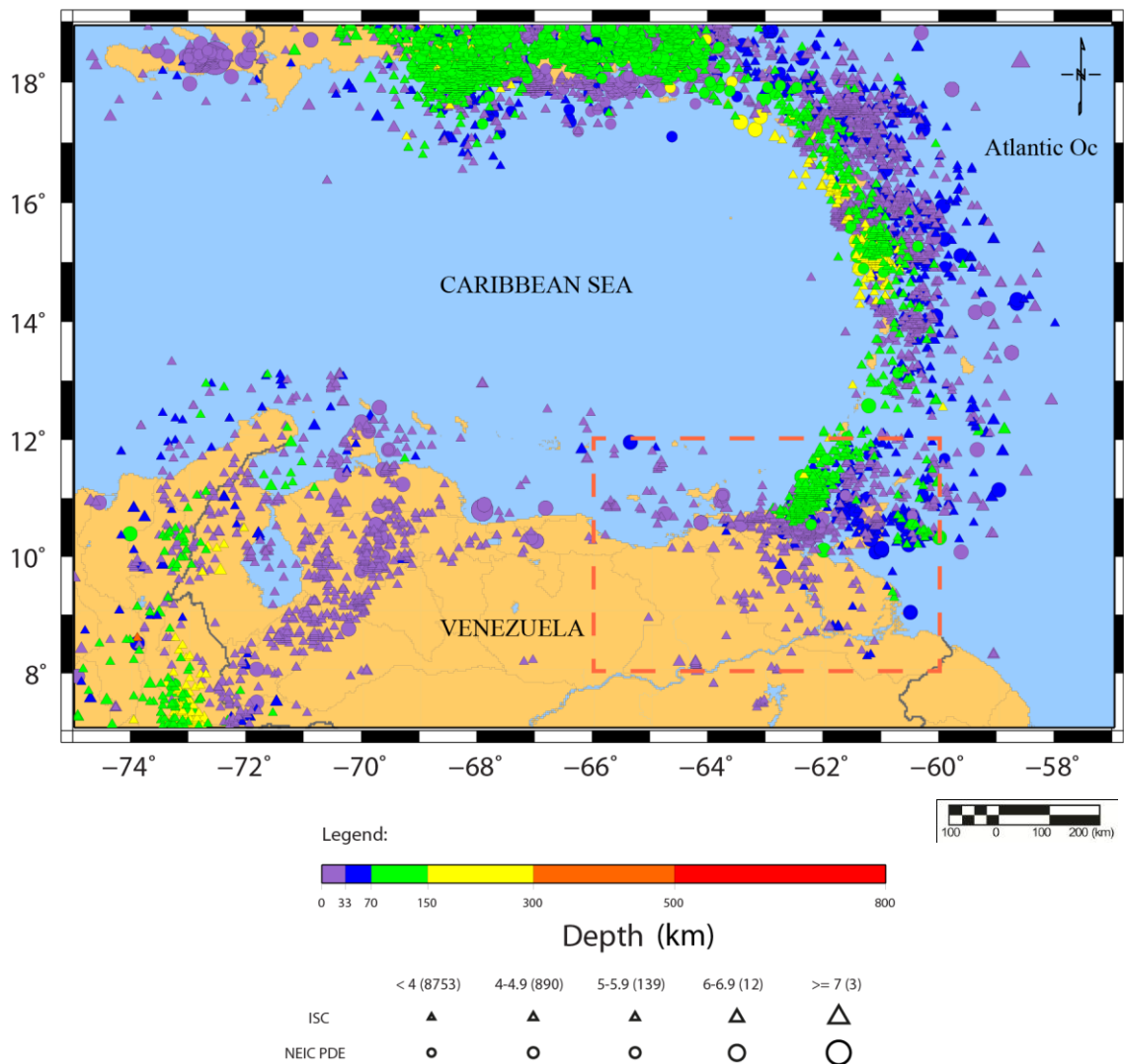


Figure 1.3. Map of seismic activity in the Caribbean region. Approximate epicentres location from International Seismology Center (ISC).

More recently, GPS-based geodetic data show that the present-day Caribbean plate moves ~20 mm/year eastwards relative to the South America plate along east-west-striking, right-lateral strike-slip faults in Venezuela and Trinidad

(Pérez et al., 2001; Weber et al., 2001, 2010; Trenkamp et al., 2002). In addition to large strike-slip faults, two subduction zones are shown in the Caribbean area on Figures 1.1 and 1.2: (1) On the west, underthrusting of the Caribbean plate at low angles ($\sim 18^\circ$) to the east and southeast, beneath western and central South America, forming the accretionary prism along the South Caribbean deformed belt (van der Hilst and Mann, 1994; Taboada et al., 2000); and (2) Subduction of the Atlantic Ocean plate ($\sim 38^\circ$) beneath the Caribbean plate, in the eastern Caribbean, forming the Barbados accretionary prism (Westbrook, 1975). The Atlantic lithosphere is presently subducting to the west to a depth of 150 km beneath the Lesser Antilles arc and the dip of the subducting slab varies from $\sim 50^\circ$ in the north to near vertical in the south near Grenada (Stein et al., 1988; Ladd et al., 1990; Russo and Speed, 1992; Speed et al., 1993; Wadge and Shepherd, 1984; Wadge, 1994).

As summarized by Escalona and Mann (2011) and Aitken et al. (2011), during Cenozoic time, the Caribbean plate has converged with the North and South American plates in an oblique and diachronous manner (Clark et al., 2008; Erlich and Barrett, 1990; Pindell and Barrett, 1990). The point of collision between the leading edge of the Caribbean plate and the South American continent moved from western and central Venezuela in the Paleogene to eastern Venezuela in the Neogene. The location of present-day convergence is somewhere between the Paria peninsula of Venezuela and the Northern Trinidad range.

The gravity and magnetic anomalies, and heat flow are as follows:

- Gravity anomalies, both free-air and Bouguer, in the Caribbean region are among the largest in the world (Bowin, 1976). Values of free-air anomalies (FAA) range from highs greater than +200 mGal over the Greater Antilles, down to lows of about -300 mGal over the Los Muertos trough. Bouguer anomalies (BA) for a density of 2.67 gm/cm^3 range from highs in excess of +350 mGal in the Atlantic Ocean, down to lows more negative than -150 mGal along the Venezuelan Andes and -200 mGal over the Eastern Venezuela foreland basin, as shown in Fig 1.4 and 1.5

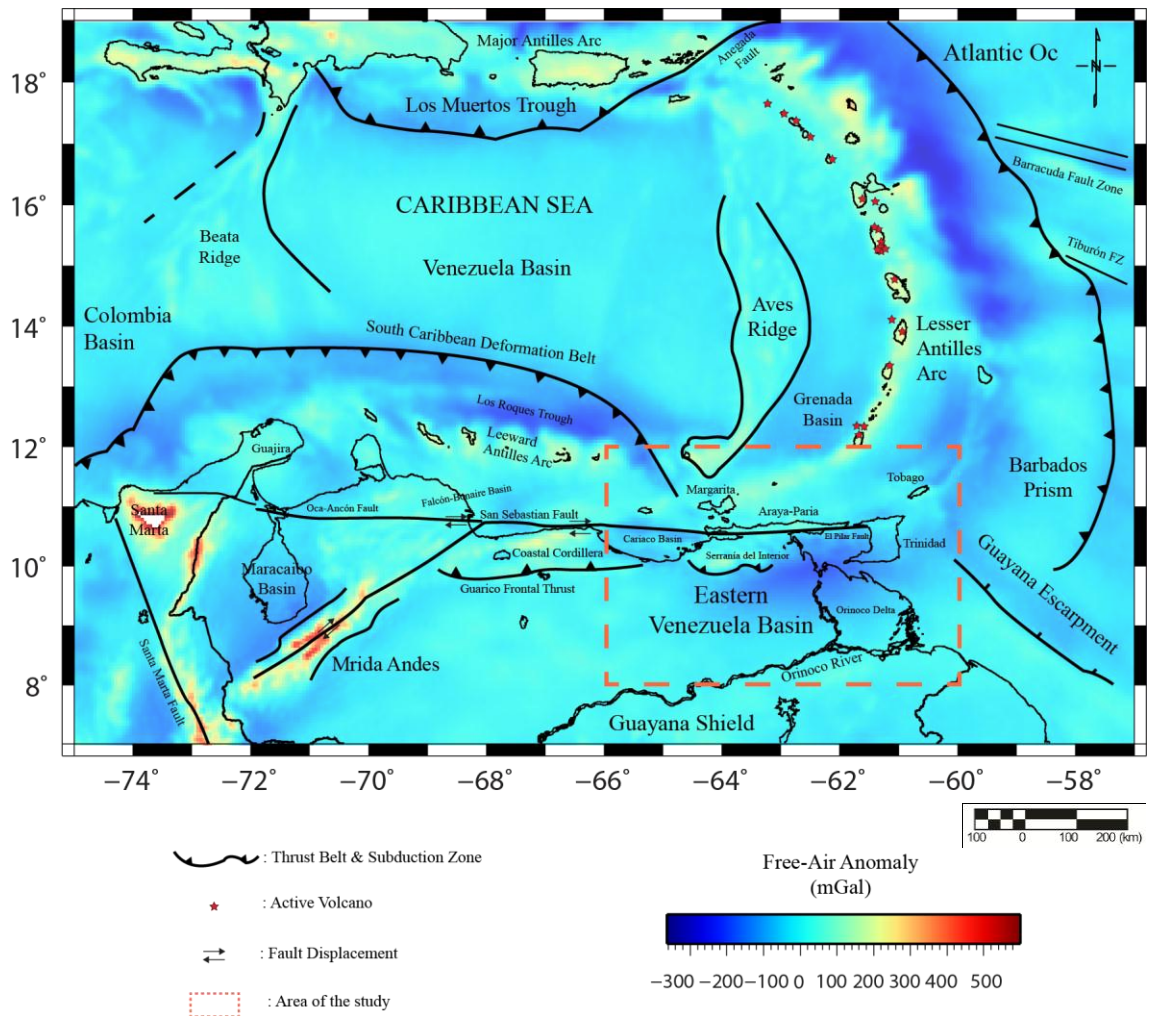


Figure 1.4. Satellite Free-Air anomaly map of the Caribbean region. Gravity data from Sandwell and Smith (2009), Scripps Institution of Oceanography, Universidad de California, San Diego.

- The magnetic anomalies exhibit a very variable non-symmetrical pattern throughout the Caribbean region. As depicted in Figure 1.6 north-northeasterly trending magnetic anomalies related to an Atlantic spreading center have been identified in the northeastern extreme of the area (Burke et al., 1984). Crustal magnetic anomalies with similar trends have been identified in the Venezuela basin (Pindell, 1985; Ghost et al., 1984; Diebold and Driscoll, 1995) while the Colombia basin exhibits E-W trends, as shown by Christofferson (1973). The magnetic response of the triangular section southeast of the Venezuela basin, although exhibiting

a significant attenuation in the banded component of magnetic anomaly, this does not disappear entirely allowing affirm that the entire subsurface of the Eastern Caribbean has oceanic crustal material formed by spreading of an oceanic ridge (Orihuela and García, 2011). The magnetic anomalies over the Lesser Antilles magmatic arc have a distribution apparently related to igneous centers, as indicated by Westbrook in Speed et al. (1984).

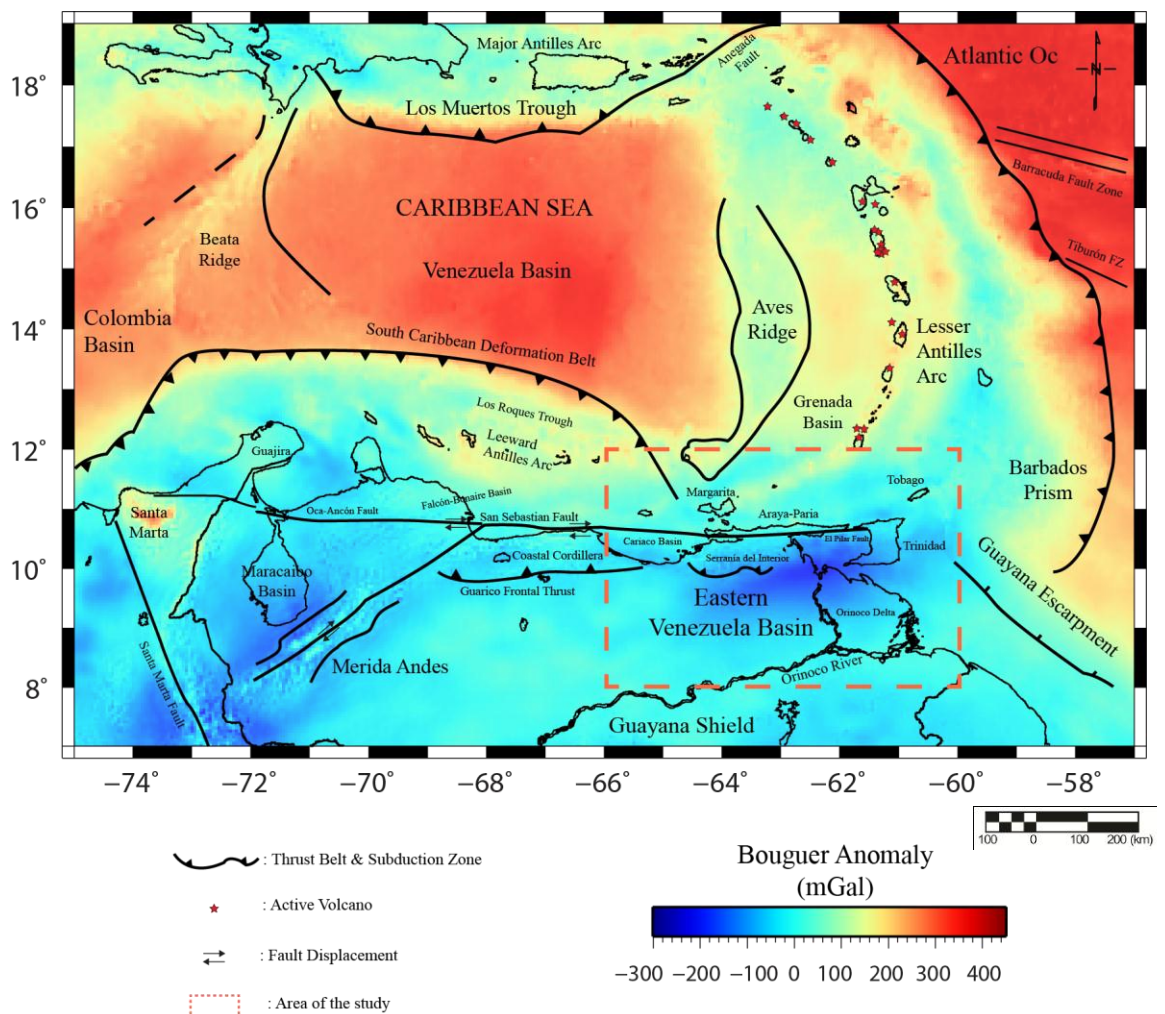


Figure 1.5. Bouguer Anomaly map of the Caribbean region. Gravity data from Sandwell and Smith (2009), Scripps Institution of Oceanography, Universidad de California, San Diego.

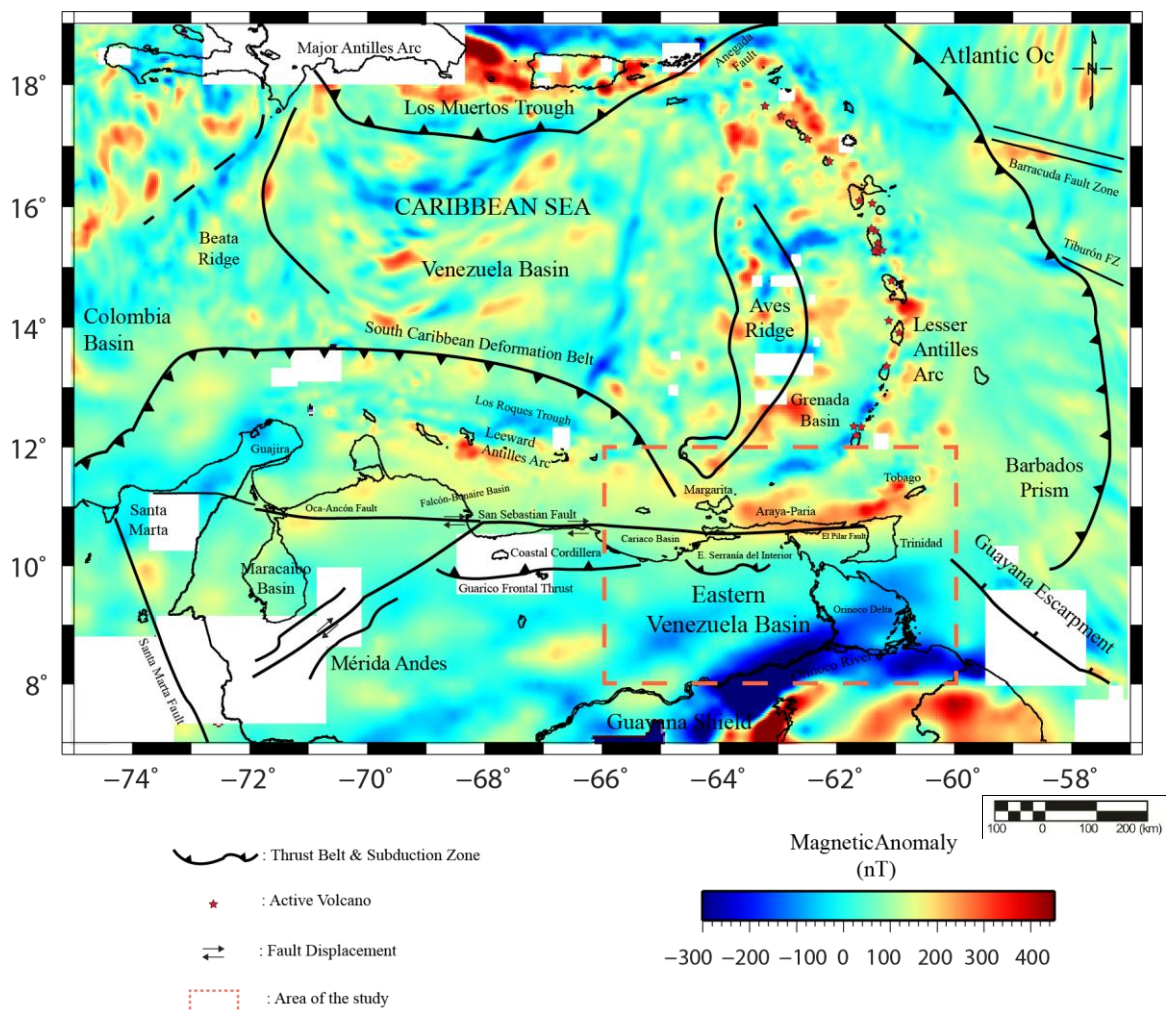


Figure 1.6. Magnetic anomaly map of the Caribbean region. Magnetic data from EMAG2: Maus et al. (2009)

- Heat-flow measurements are sparse or even absent over some places in the Caribbean area. A map of heat-flow distribution in this region (Figure 1.7), with data compiled from Bowin (1976, Figure 15; from Epp et al., 1970; Erickson et al., 1972; Simmons and Horai, 1968; Lee and Clark, 1966) generated by Arnaiz-Rodríguez (2012, in press) shows that heat-flow values in the Caribbean are generally uniform, lying within the range of 1 to 2 heat-flow units. Slightly above-average heat-flow values occur in the area of Los Muertos trough, and over the southern Venezuela basin. Slightly below-average heat-flow values occur in northern and southern parts of the Colombia basin, and eastwards of the Lesser Antilles island arc, where Schoonmaker and Ladd (1984) have indicated

that the general trend on the whole correlates well with the regional geology of the area. Heat-flow values greater than 1 heat-flow unit (between 3 and 4 heat-flow units) occur above the Aves ridge and the Lesser Antilles Arc, and also in Guárico basin, central Venezuela, and in the western part of Venezuela. These values of heat-flow are anomalous respect to other foreland basins in the world and also different to those predicted by theory for this kind of tectonic setting.

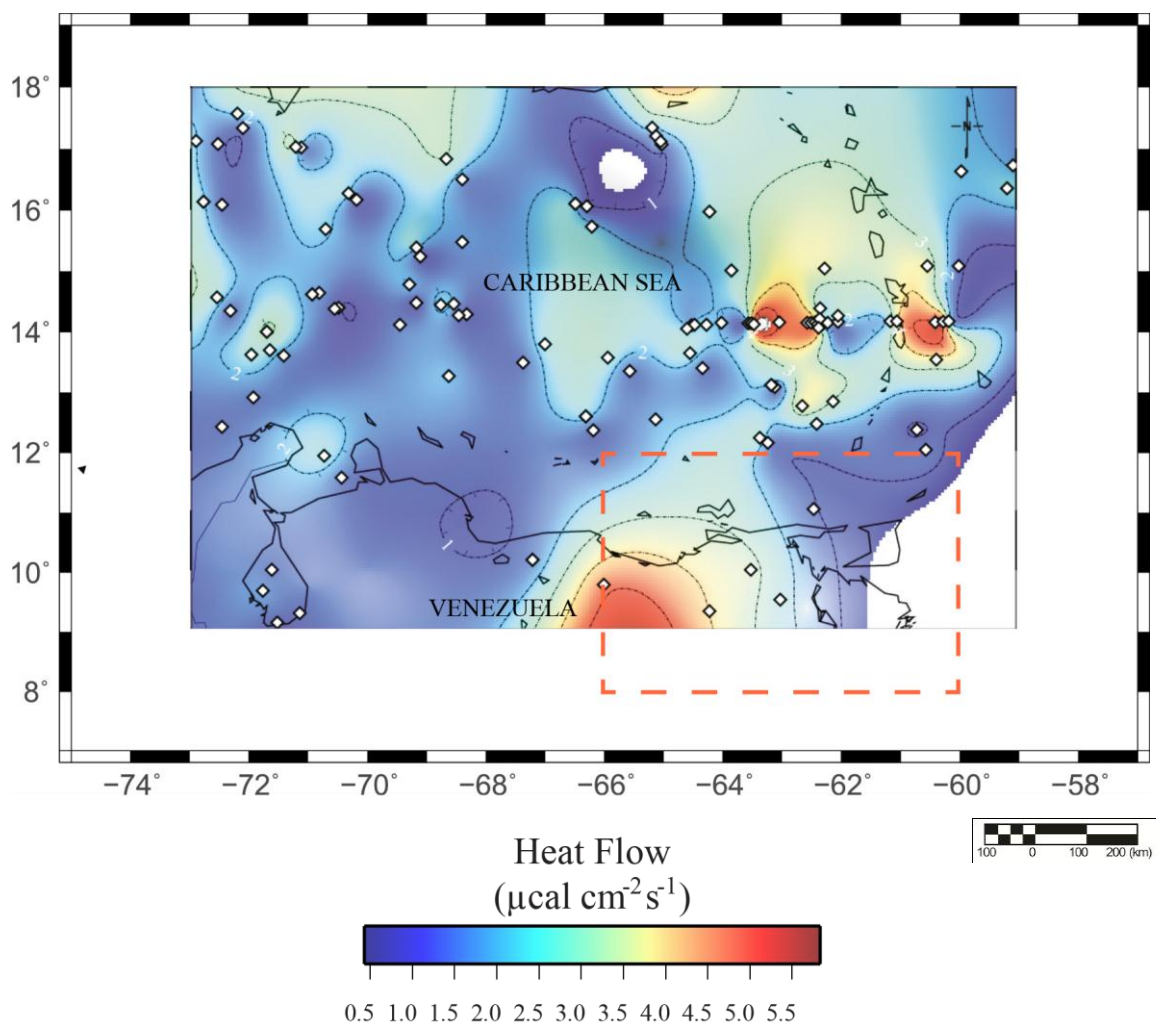


Figure 1.7. Heat flow measurements in the Caribbean region. Values are in heat-flow units (1 h.f.u. = $1 \mu\text{cal cm}^{-2} \text{s}^{-1}$). Compiled from Epp et al. (1970), Erickson et al. (1972), Simmons and Horai (1968) and Lee and Clark (1966). After Bowin (1976), generated by Arnaiz-Rodríguez (2012, in press).

The work herein contains a synthesis of the existing knowledge of the Geology and Geophysics of the Caribbean region and it will be endeavoured to account for these observations when discussing the gravity results in the northeastern Venezuelan borderland. Most pertinent papers to this synthesis are referred in Sykes et al. (1982), Case et al. (1984), Mann et al. (1990), Pindell et al. (2005), Escalona and Mann (2011).

Geologic and tectonic maps that have proved most useful to the author in interpreting the area, have been compiled or edited by Bellizzia et al. (1976), Martín (1978), Case and Holcombe (1980), Case et al. (1984) and MacDonald (1990), as well as Garrity et al. (2005) and Hackley et al. (2006) for the Venezuelan area. Geophysical maps of Bowin (1976), Bonini et al.(1978), and those compiled by Arnaiz-Rodríguez and Garzón (2012) provide a general overview of the Caribbean plate and close surrounding areas; those of Kearey et al. (1975), Westbrook and Jackson, in Speed et al. (1984), and Ughi (2009) provide a detailed coverage of the eastern Caribbean area.

1.2.1. EASTERN CARIBBEAN PLATE BOUNDARY ZONE

The most prominent structural features outlined along the eastern Caribbean plate boundary zone are, from west to east, the Venezuelan basin, the Aves ridge, the Grenada basin, the Lesser Antilles magmatic arc, the Tobago-Margarita trough (forearc basin) and the Barbados accretionary prism (Figure 1.1).

The eastern boundary of the Caribbean plate is delineated by the Lesser Antilles deformed belt, where the Caribbean plate is shallowly underthrust by the Atlantic lithosphere at a slow convergence rate (~20 mm/year, Mann et al., 1990). Some 100 to 300 km west of the oceanward deformation front is the lithospheric subduction trace where crystalline rocks of both, the Caribbean and Atlantic plates, are supposed to have made the initial contact (Speed et al., 1984). This zone of crust-crust contact appears to follow directly the axis of minimum Bouguer anomaly; whose values are increasingly more negative southwards (Figure 1.5), suggesting that the deformed sediments of the accretionary prism thicken towards the south.

The crust-crust contact trace of the Caribbean-Atlantic plates is also approximately coincident with the westernmost extent of magnetic anomalies from the Atlantic igneous crust, as stated by Speed et al. (1984) (Figure 1.6).

On the basis of rock type and age, a double chain of islands has been recognized northwards of the volcanic island of Dominica at the Lesser Antilles island arc (see Fig. 1.1, around 15°N of latitude): the Volcanic Caribbees and the Limestone Caribbees (Martin-Kaye, 1969). The first, i.e.: the northwestern andesitic volcanism; the second, i.e.: the northeastern branch (Dominique to Sombrero) consists of shallow-water limestones of Miocene to Recent age, lying over a pre-Miocene volcanic platform. Southwards (Dominica to Grenada), a single chain of islands with Miocene to Recent volcanism (Bouysse et al., 1990; Macdonald et al., 2000), stands on the narrower magmatic platform of the Lesser Antilles.

Along the Lesser Antilles arc, the depth of the slab of subduction is also variable, reaching 140-160 km in the northern region (Saba to Guadeloupe), 180 km (Dominica to Martinique) and 100-140 km (St. Vincent to Grenada) (Wadge y Shepherd, 1984). It is unlikely that the downgoing Atlantic plate extends much further west than the active arc, particularly in the southeastern Caribbean (Macdonald et al., 2000). This condition is likely due to the complex interactions between the Caribbean plate, the downgoing Atlantic plate, and the South American continent in the southeastern Lesser Antilles arc (Aitken et al., 2011).

The volcanic activity in the area suggests that subduction developed from the Late Cretaceous to Recent (Case et al., 1984; Ysaccis, 1997). In this area the Barracuda fault zone, the boundary between the North and South American plates, subducts under the Caribbean plate and it's probably related to the ancient subduction of the proto-Caribbean plate (Pindell & Kennan 2007b).

These differences north to south of the Greater Caribbean arc and associated terranes are likely explained by: (1) separately subducting North American (North Atlantic) and South American (South Atlantic) plates (Wadge and

Shepherd, 1984), (2) subducting oceanic ridges (e.g. Barracuda) beneath the Caribbean plate (Bouysse, 1988), and/or (3) the oblique interaction of the South American continent with the southern Caribbean plate margin (Russo and Speed, 1992).

A continuous belt of positive gravity anomalies, both free-air and Bouguer anomalies (Figures 1.4 and 1.5), follows the Lesser Antilles magmatic arc; FAA gradients being sharper in the southern chain of islands (Bowin, 1976; Speed et al., 1984). Large positive Isostatic anomalies, of the order of +50 mGal, are also found along the Lesser Antilles (Kearey, 1974,1976) and along the northeastern front of the arc platform, where bathymetric shoaling, diminishing depth to crystalline basement and mainly thickening of the upper-arc crust have been interpreted. A series of gravity lows, over the accretionary prism, follows closely the trend of the Lesser Antilles forearc basin; southwards, two free-air anomaly trends can be identified, one along the Tobago trough forearc basin and other following the Barbados basin.

Flanking the western boundary of the magmatic arc platform it is the backarc Grenada basin (maximum water depths ~ 3.0 km), with typical Caribbean basin velocity structure of thickened oceanic type: subsediment basement of about 1.5 km in thickness and 5.3 km/sec seismic velocity, overlying a 6.2 km/sec, 6.0 km thick layer, and a 7.4 km/sec, 6.5 km thick layer (Boynton et al., 1979; Holcombe et al., 1990; Christeson et al., 2008). On the northern portion, tectonically influenced by the bathymetry, the basin exhibits an irregular pattern of gravity anomalies, with negative values increasing toward the south end of the basin, where the bathymetry is smooth and the depth of the basement is greater (Speed et al., 1984; Aitken, 2005).

The southern Grenada basin, with sediments as thick as 13 km, is floored by crystalline basement and bounded by normal faults along the adjacent Aves ridge and Lesser Antilles arc. The heat-flow through the Grenada basin ($1.42\text{--}2.45 \mu\text{cal cm}^{-2} \text{sec}^{-1}$; Clark et al., 1978) seems to be significantly lower than in other backarc basins undergoing active spreading. Any spreading is certainly no younger than mid-Miocene and probably older (Speed et al.,1984).

Among other provinces of the eastern Caribbean, there is the Tobago basin, an arcuate-shaped forearc basin with as much as 14 km of sedimentary fill. It is bounded by the Lesser Antilles arc to the west and the Barbados accretionary prism to the east. To the southwest, the Tobago basin extends up to the Margarita trough, offshore area of easternmost Venezuela (Ysaccis, 1997). From refraction data, Christeson et al. (2008) measured thicknesses (6–8 km) and velocities (5.5–7.3 km/s) for the crust underlying the Tobago basin to be consistent with normal oceanic crust. Most previous models for the Tobago basin attribute its tectonic origin, shape in map view, and tectonic control on its fill to a thrust system at the eastern edge of the growing Barbados accretionary prism (Speed et al., 1984; Westbrook et al., 1988; and Ladd et al., 1990). The approximate depths to Moho discontinuity beneath Grenada and Tobago troughs, either side of the magmatic arc platform, are about 21 and 25 km respectively (Biju-Duval et al., 1978; Boynton et al., 1979).

The Barbados accretionary prism is the product of sediments offscraped and underplated as the Atlantic oceanic lithosphere subducts westward beneath the eastwardly advancing Caribbean plate (Westbrook et al., 1988). Because the prism has undergone continuous or episodic growth since at least the Eocene (Speed et al., 1989), the prism is presently between 100 and 300 km wide and up to 20 km thick. Prism rocks consist of accreted, clastic and pelagic rocks (Ladd et al., 1984). The 400 km long deformed zone at the western limit of the Barbados accretionary prism is called the Inner Forearc deformed belt (IFDB) and is attributed to backthrusting of the prism over the Tobago basin (Westbrook et al., 1988; Torrini and Speed, 1989).

Farther west, some 240 km west of the Lesser Antilles island arc, there is the Aves ridge, a submerged northerly trending uplift of volcanic composition (Biju-Duval et al., 1978), regarded by Case et al. (1984) as a late-Cretaceous Paleogene magmatic arc. It was probably east-facing (Speed et al., 1989) forming an arcuate continuation of the Greater Antilles, along which subduction of Atlantic lithosphere beneath the eastern Caribbean occurred during late Cretaceous to Eocene times (Malfait and Dinkelman, 1972; Pindell, 1985). Its

crustal character, which is similar to that of the Lesser Antilles, and the types of igneous rocks found in the area, strongly support the hypothesis that the Aves ridge is primarily an extinct island arc (Holcombe et al., 1990).

Depths to the Aves ridge's crestal region are about 1 km, but in the north (at about 15° N) the ridge crops out in the Venezuelan Aves Island; there, the swell is mostly covered by calcareous and arenaceous sediments. The thick cover of deposits over most of the ridge and the absence of young volcanic rocks suggest that the Aves ridge has been comparatively an inactive feature during most of the Tertiary (Holcombe et al., 1990). Seismic and gravity investigations in the area suggest that Moho beneath the horst-graben like structure of the Aves ridge is relatively deep, of the order of 40 km (Kearey, 1976; Westbrook in Speed et al., 1984; Ughi, 2009). There is clear evidence, coming from the presence of a deep and strong erosional surface, diachronous low-to-mid Miocene, on the Aves ridge, to indicate that the swell must have undergone tectonic subsidence during Miocene times (Speed et al., 1984).

To illustrate the crustal structure of the Caribbean, Figure 1.8 shows the seismic line BOL30 acquired in the BOLIVAR project in 2004, where structures as Venezuela basin, Aves ridge, Grenada basin, Lesser Antilles arc, Tobago and Trinidad islands have been interpreted (Aitken, 2005).

Later, Christeson et al. (2008) analyzed the same seismic line and described similarities between the velocity structure and crustal thicknesses of the Aves ridge and the Lesser Antilles arc (~ 24–26 km), implying that magmatic processes have remained moderately steady over time. In both cases, it is noticeable the abrupt change in the velocity of the sediments (2.0 km/s) against the basement (6-6.3 km/s) at 6-7 km depth.

Seismic activity along the Eastern Caribbean-Atlantic boundary zone has so far been examined by many authors; early earthquake first motion studies (Molnar and Sykes, 1969; Chase and Bunce, 1969) revealed that the oceanic lithosphere is plunging beneath the Caribbean in a westerly direction, along the Lesser Antilles. McCann et al. (1982) showed that the downgoing seismic zone

follows the bend of the arc, and that the earthquake zone is continuous from near the surface to depths of about 140 km. Wadge and Shepherd (1984), on the basis of precise hypocentral location of earthquakes (1978-84), coincide with this interpretation and established two distinct segments along the arc: north of 14.5° N, trends NNW, dips 60°-50°, and south of 14.5°N, trends NNE, dips variable from 50°- 45° in the north, to vertical in the south.

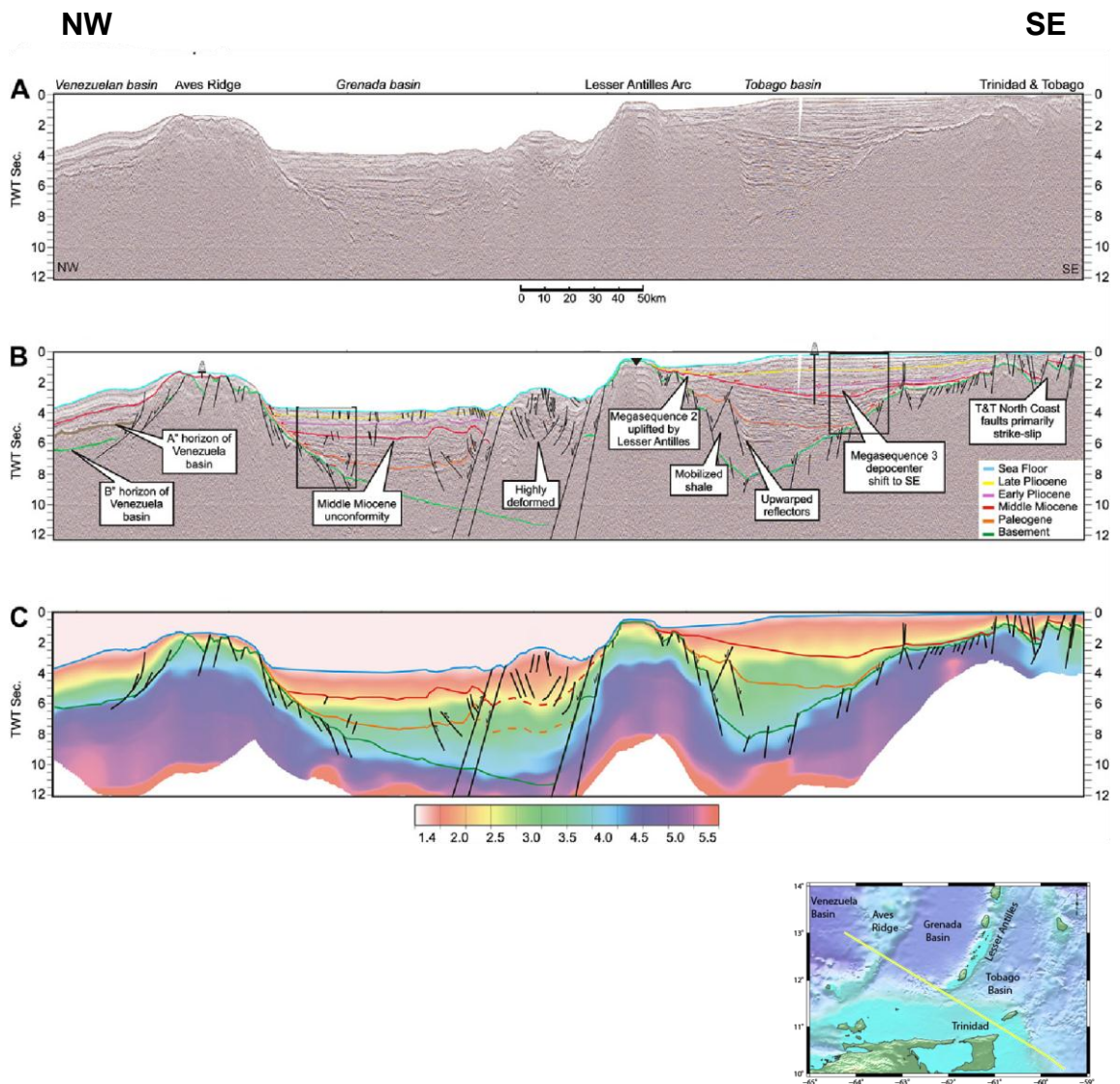
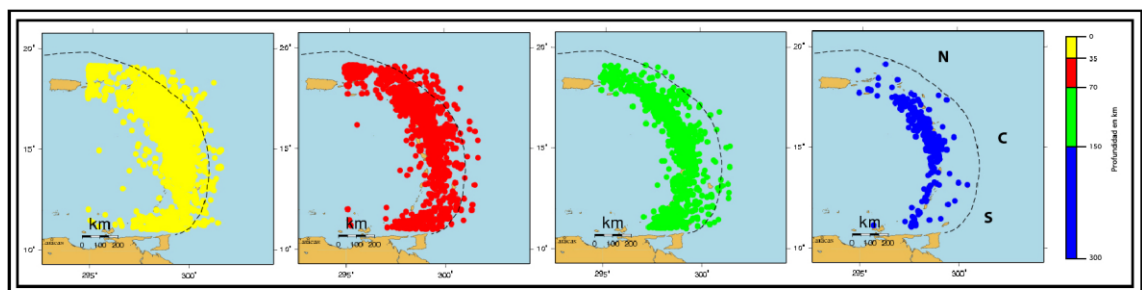


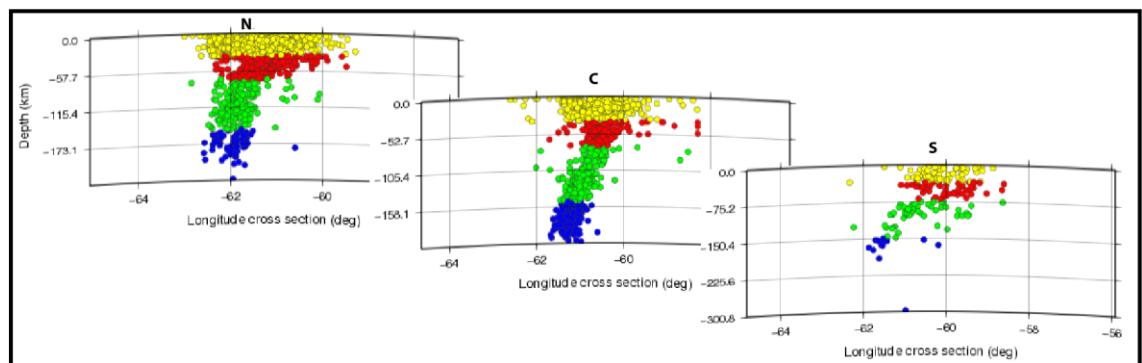
Figure 1.8. Seismic line BOL30 (From Aitken et al., 2011, Figure 5): A) Uninterpreted seismic reflection data. B) Interpreted seismic reflection data. C) Interpreted seismic refraction data from Christeson et al. (2008). As shown in the inset location map, from west to east the following structures have been identified: a) Venezuelan basin, b) Aves ridge, c) Grenada basin, d) Lesser Antilles arc, e) Tobago basin, and f) Trinidad and Tobago islands.

As shown in Figure 1.3, most hypocenters are confined to a seismic zone about 50 km wide that dips some 60° westward beneath the arc. Focal mechanism determinations have revealed that recent activity along the arc exhibits the combined effect of intraplate normal and deep strike-slip faulting, with few small to moderate size interplate thrust events, suggesting that subduction in this region is largely aseismic (Speed et al., 1984). It is unlikely that the downgoing Atlantic plate extends much further west than the active arc, particularly in the southeastern Caribbean (Macdonald et al., 2000).

In a very elegant account, Ughi (2009) presented three W-E sections across the Lesser Antilles island arc (North, center and South), showing the focal distribution of earthquakes (International Seismological Centre –ISC, data for 1904-2009). Hypocentral seismic depths for ranges of 0-35 km, 36-70 km, 71-150 km and 151-300 km, were plotted to show their distribution in depth, evidencing the geometry of the slab of subduction of the Atlantic beneath the Caribbean plate, as well as the increment in the dip from south to north, and that deep seismicity is lower in the south (Figure 1.9).



A) Epicentral location of earthquakes



B) Hypocentral location of earthquakes in vertical sections across North (N), Center (C) and South (S).

Figure 1.9. Seismicity in the Eastern Caribbean: Lesser Antilles island arc. Depth: Yellow = 0-35 km; red = 36-70 km; green = 71-150 km; blue = 151-300 km. Data from ISC: 1904-2009. Taken from Ughi (2009).

At this stage it is interesting to point out that, although geologic data for the opening of the Atlantic suggest that the Caribbean region was one of extension -and hence of seafloor spreading for approximately 135 my (from 200 to 65 my B.P., Burke et al., 1984)- the early spreading history between the North American and South American plates at the site of the present Caribbean plate has remained obscure, mainly because much of the oceanic crust created as the North American and South American plates drifted apart, has most probably been subducted beneath the Caribbean arc systems from the Mesozoic to the Present (Burke et al., 1984; Ghosh et al., 1984; Pindell et al., 1988, 2005).

The dominant features within the Venezuela basin, a Cretaceous oceanic plateau that constitutes the core of the Caribbean plate, are the NE-SW linear magnetic anomalies with maximum values around 200-300 nT and minimum of the order of 150 nT. Along the southern periphery of the basin, there is a series of E-W trending anomalies over the Leeward Antilles basin (Silver et al., 1975; Ghosh et al., 1984); and over the extreme eastern edge of the basin and the Aves ridge, there is a series of poorly defined N-S linear magnetic anomalies.

The Venezuelan basin comprises an anomalously thick (17–20 km) two-layer oceanic plateau (Boynton et al., 1979; Driscoll and Diebold, 1999; Fox and Heezen, 1975). The bathymetric interior of the Venezuelan basin is flat, with only mild deformation of a uniform 3.0 km thick layer of pelagic sediments and clastic sediments shed off the Aves ridge from the east and from the South American continent to the south (Draper et al., 1994).

1.2.2. EVOLUTION OF THE EASTERN CARIBBEAN PLATE

After discussing previous tectonic models proposed by authors like Tomblin (1975), Bouysse (1988), Pindell and Barret (1990), to explain the origin of the Grenada basin, Aitken et al. (2011) integrated stratigraphic and tectonic evolution of Late Cretaceous to Recent volcanic arcs and associated basins in the southeastern Caribbean Sea using seismic reflection data, wide-angle seismic refraction data, well data and onland geologic data; and propose a new

tectonic model for the opening of the Grenada and Tobago basins and the 50–250-km eastward jump of arc volcanism from the Late Cretaceous Aves ridge to the Miocene to Recent Lesser Antilles arc in the southeast Caribbean. The striking similarity of the half-graben structure of the Grenada and Tobago basins that flank the Lesser Antilles arc, their similar smooth basement character, their similar deep-marine seismic facies, and their similar Paleogene sediment thickness mapped on a regional grid of seismic data suggest that the two basins formed as a single, saucer-shaped, oceanic crust Paleogene forearc basin adjacent to the now dormant Aves ridge.

Following Aitken et al. (2011, Figure 15), the succession of tectonic events that they proposed to explain the evolution of the Grenada and Tobago basins, in the southeastern Caribbean plate, Figure 1.10, include:

(1) Paleogene extension of the preexisting forearc of the Great Arc of the Caribbean (Aves ridge) by the mechanisms of slab rollback and flexural subsidence.

Figure 1.10A: Paleocene (~60 Ma): Aves ridge with single forearc basin began to converge with the South American plate.

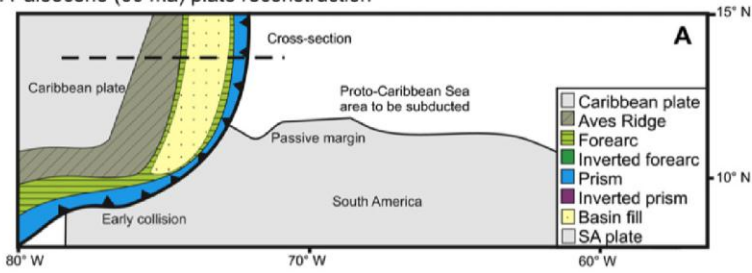
(2) Flexural and thermal subsidence that ceased in the Middle Eocene, and produced a wide, deep-marine forearc basin with some 8 km of sediments originated primarily from the South American passive margin.

Figure 1.10B: Middle Eocene (~40 Ma): slow rollback of the slab increased, creating flexural subsidence. Forearc basin widened from approximately 190 km wide to 260 km wide. The downgoing slab shifted seaward, and volcanism ceased in the now dormant Aves ridge.

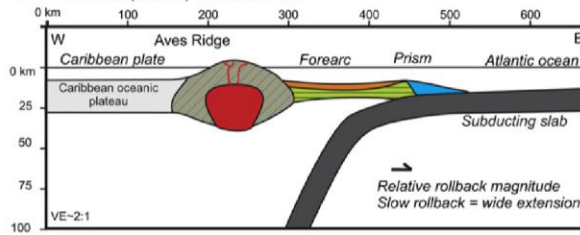
(3) Oblique plate convergence of the Caribbean with the South American plate during the Late Oligocene to Middle Eocene, causing a backthrust response in the thinned crust of the Grenada/Tobago forearc basin.

Figure 1.10C: Oligocene (~30 Ma): relative slab rollback decreased, and partial inversion of the thinned and weakened forearc crust occurred. This could be a mechanism of convergence in the top of the forearc crust according to the flexural subsidence model, aided by a rising plutonic melt that ultimately produced the volcanism in the Neogene Lesser Antilles arc.

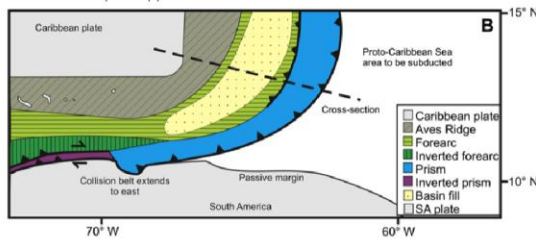
A. Paleocene (60 ma) plate reconstruction



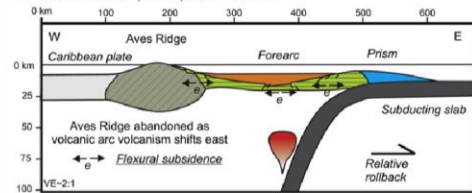
B. Paleocene (60 ma) cross-section



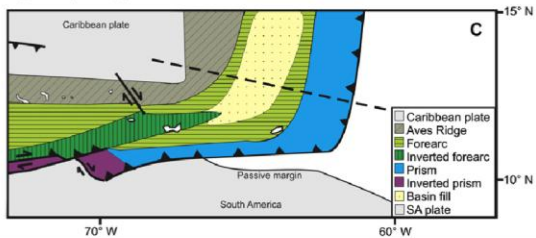
A. Middle Eocene (40 ma) plate reconstruction



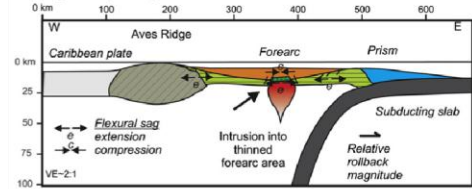
B. Middle Eocene (40 ma) cross-section



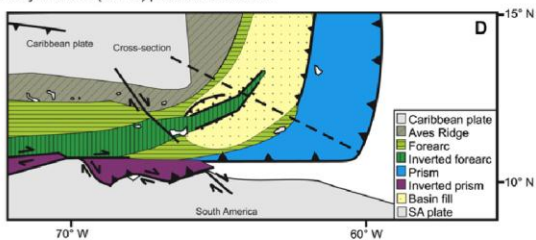
A. Oligocene (30 ma) plate reconstruction



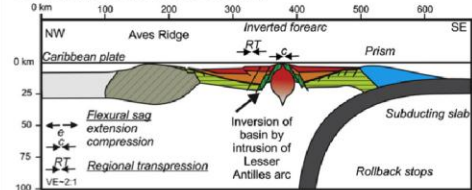
B. Oligocene (30 ma) cross-section



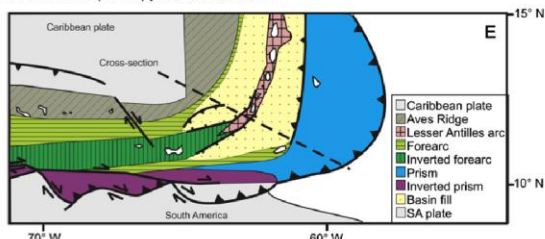
A. Early Miocene (20 ma) plate reconstruction



B. Early Miocene (20 ma) cross-section



A. Late Miocene (10 ma) plate reconstruction



B. Late Miocene (10 ma) cross-section

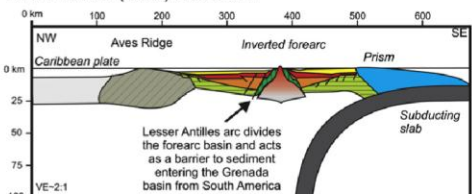


Figure 1.10. Cenozoic plate reconstructions and cross-sections of the southeastern Caribbean to propose models for Grenada and Tobago basin evolution. Plate reconstructions from Aitken et al. (2011) modified from Mann and Escalona (2011).

(4).Transpressional deformation uplifted the thinned crust of the forearc in a west-to-east direction from Margarita Island to the southern Lesser Antilles (Grenada to St. Vincent islands). This uplift divided the westward Grenada basin and the eastward Tobago basin by Early to Middle Miocene time.

Figure 1.10D: Early Miocene (~20 Ma): Continued inversion of the forearc occurred, increased by the regional transpression derived from the oblique convergence between the Caribbean plate and the passive margin of Eastern Venezuela. Slab rollback stopped.

(5) Transpression gave way to transtension in the region during post-Middle Miocene. Then oblique convergence between the Caribbean and South American plates changed from convergent to strike-slip along their boundary.

Figure 1.10E: Late Miocene (~10 Ma): Lesser Antilles volcanism was active above the inverted crust of the forearc. The Lesser Antilles arc divided the Grenada and Tobago basins into two basins.

The late Miocene to Recent depositional histories of the Grenada and Tobago basins are distinct because of the isolation of the Grenada basin by growth and uplift of the Neogene Lesser Antilles volcanic ridge. This model has the advantage of explaining in a simple manner, not only the origin of the Grenada basin, but the formation of the Tobago basin and the associated end of the magmatism at the Aves ridge, all through the same process.

1.2.3. SOUTHERN CARIBBEAN PLATE BOUNDARY ZONE

The most outstanding feature along the southern boundary of the Caribbean plate is, at the southwestern corner, the Maracaibo basin (Fig. 1.1, 2.1) with its prolific hydrocarbon production. Negative free-air and Bouguer anomalies occur all over this area possibly associated with deep basins of thick sedimentation; while positive pronounced highs of Bouguer anomaly occur over the Santa Marta massif (about 180 mGal, Fig. 1.5) and the Guajira uplift (about 100 mGal, Fig. 1.5), and some steep gradients are present across the Oca and Santa Marta fault systems (Kellogg and Bonini, 1982).

Separating the inner Caribbean basins from the continental South America plate, from north to south, there is the Southern Caribbean deformed belt, a complex Neogene band with folds and thrusts of E-NE trend related to oblique

convergence of the Central Caribbean with northern South America. Jurassic-Lower Cretaceous, "Pacific-derived", Caribbean ophiolite bodies were probably dragged and stretched (arc-parallel) southeastward during the Late-Jurassic to Early Cretaceous (Pindell and Kennan, 2001b).

Recent interpretations based on tomographic and seismic studies along the Caribbean's southern boundary suggest active subduction of the Caribbean plate beneath the continental South American plate in Colombia and western Venezuela (van der Hilst, 1990), particularly under the Falcón basin (Fig. 1.1, 2.1; Rodríguez and Sousa, 2003; Sousa et al., 2005).

Towards the east of Venezuela (i.e. under the Eastern Serranía del Interior thrust belt; Fig. 1.1, 2.1) a change in subduction polarity is observed; in this area the continental South American lithospheric mantle is subducting under the oceanic Caribbean plate (Russo and Speed, 1994; Jácome et al., 2003). In this model, strike-slip movement constitutes a minor component of oblique convergence. In support of this interpretation minor strike-slip movement (less than 150 km) has been reported by Audemard and Giraldo (1997), in a regime of strain partitioning with oblique convergence between the Caribbean and South American plates

On the whole, this plate boundary is associated with transform and thrust faulting (Fig.1.1) and forms a complex subduction system that extends along the Colombia, Venezuela and Trinidad coastal margins (Stephan et al., 1985, 1990; Biju-Duval et al., 1982; Schubert, 1984; Mann and Burke, 1984; Mann et al., 1990; Pindell et al., 2005). Transpressive orogenic belts and foredeep basins have formed in response to the Caribbean collision with the South American plate which developed diachronously from west to east since the Cretaceous (Ave Lallemand, 1997; Giunta et al., 2002), being the southern continental margin area characterized by flexure of the South American continental crust (Escalona and Mann, 2011).

Although there is considerable seismicity in northern South America and the adjacent Caribbean Sea floor (Fig. 1.3), there is not widespread agreement on

the location of the plate boundary defined by the seismicity. This now appears to be due to the complex nature of the boundary (partly transform, along multiple branches, and partly convergent, although at a slow rate, McCann and Pennington, 1990). The major Caribbean-South American plate boundary in northeastern Venezuela is a series of strike-slip faults, all exhibiting some seismicity (Molnar and Sykes, 1969). The earthquake focal mechanisms provide strong support for the right oblique collision model of Caribbean South American plate (Russo et al., 1993; Sisson et al., 2005).

Southwards, the easterly trending Leeward Antilles terrane, a chain of uplifted block-islands with positive gravity expression, stands off the northern coast of Venezuela. This platform, that was probably a primitive magmatic arc, is bounded by the Los Roques trough on its northern margin and on its southern flank by a series of basins along the Venezuelan borderland including the easterly trending Falcón-Bonaire and the deep Cariaco basins. A belt of very negative free-air anomaly (-200 mGal) occurs all over the trace of the Southern Caribbean deformation belt, reaching minimum values along the Los Roques basin (for location of geological features and associated gravity anomalies the reader is referred to Figs 1.1, 1.4 and 1.5).

In short, it can be said that the crust is very heterogeneous along the widely distributed southern margin of the Caribbean, where a complex history of extension, thrusting and strike-slip faulting started at least since the Cretaceous and developed all throughout the Cenozoic.

In the mainland of Venezuela it is worth mentioning striking elements such as the Mérida Andes Cordillera, the Coastal Cordillera with ultrabasic complexes and nappes up to the Guárico Frontal thrust. Eastwards, the Araya-Paria and Tobago terrane, the Eastern Venezuela deformed belt -Eastern Serranía del Interior- and the Eastern Venezuela foreland basin above the cratonic area of the Guayana Shield, forming the stable craton upon which the basin developed (Figs 1.1, 2.1). The southern margin of the Caribbean plate and its interaction with South America is discussed fully in Chapter 2.

TABLE 1.1. SUMMARY OF CRUSTAL PROPERTIES IN THE SE CARIBBEAN REGION (Modified after Case et al., 1990; and Pindell et al., 2005)

Area or Province	Principle Data Source S= Seismic G= Gravity	Thickness (exclusive of water) km	Inferred Crustal Type	Gravity Anomalies	Age	Remarks
VENEZUELA BASIN	SG	17-20	Oceanic	FAA≈0	Pre-Coniacian	3000-5000m in depth.
AVES RIDGE	SG	25-35	Extinct island arc	N-S trending highs and lows.	Late Cretaceous Paleogene	This uplift is regarded as a Late Cretaceous – Paleogene magmatic arc
GRENADA BASIN	SG	18-25	Oceanic? in South	Negative anomalies	Possibly Paleogene	1000-2000 m thick in the North and as much as 4000 m in the South
LESSER ANTILLES Magmatic Arc Platform	G	30-35	Island arc volcanic units	Positive gravity anomaly belt occurs parallel the island arc	Early Tertiary time.	Active seismicity
LESSER ANTILLES Trough-forearc basin	SG	14-25	Accretionary	Arcuate pair of positive (over the arc-masif) and negative (over the edge of the Caribbean plate) anomalies. FAA≈100-200 mGal	The oldest igneous rocks exposed in the islands are Late Cretaceous	Boundary zone. Active seismicity predominantly convergent with well developed seismic Wadati-Benioff zone and volcanic arc.
BARBADOS RIDGE COMPLEX	G	25-30	Oceanic, continental	BA minimum	Early Eocene	
SOUTH CARIBBEAN DEFORMED BELT	SG	15-25	Accretionary. Mainly Oceanic	Low	Neogene	Difuse E-W band of earthquakes. Broad zone of convergence, strike-slip faulting. Also extensional normal faulting between offset strike-slip faults between Caribbean and SA
LEEWARD ANTILLES TERRANE	SG	20-25	Accretionary, Oceanic	Positive FAA and BA of more than 100 mGal	Middle Cretaceous?	Paleomagnetic data suggest large clockwise rotations since Cretaceous time
SOUTH CARIBBEAN ISLAND CHAIN			Oceanic (North) or Undefined	BA local highs ≈150 mGal	Early Cretaceous to early Tertiary	
CARIBBEAN MOUNTAIN SYSTEM	G	25-35	Continental, (or undefined in the South)	BA≈-50, +50 mGal	Palaeozoic	Metamorphic grades range from greenschist to amphibolite or higher facies
ANDEAN CORDILLERA	G	35-40	Continental	BA≈-150 mGal	Precambrian	The range is bisected by the active Bocono fault. Moderate seismicity
SUB ANDEAN BASINS	G	25-40	Continental	BA lows	Precambrian basement	Local Paleozoic, thick Cretaceous and Cenozoic sequences fill these basins.
GUAYANA SHIELD	GS	30-43/45-48	Continental	Positive BA and FAA	Precambrian	Practically stable since late Precambrian times

CHAPTER 2

EASTERN VENEZUELA TECTONIC SETTING

2.1. INTRODUCTION

Several tectonic units can be distinguished in eastern Venezuela along the northern South America borderland (Figures 2.1, 1.2). The most relevant of those elements took their present configuration from Tertiary times when major orogenic events developed in the area.

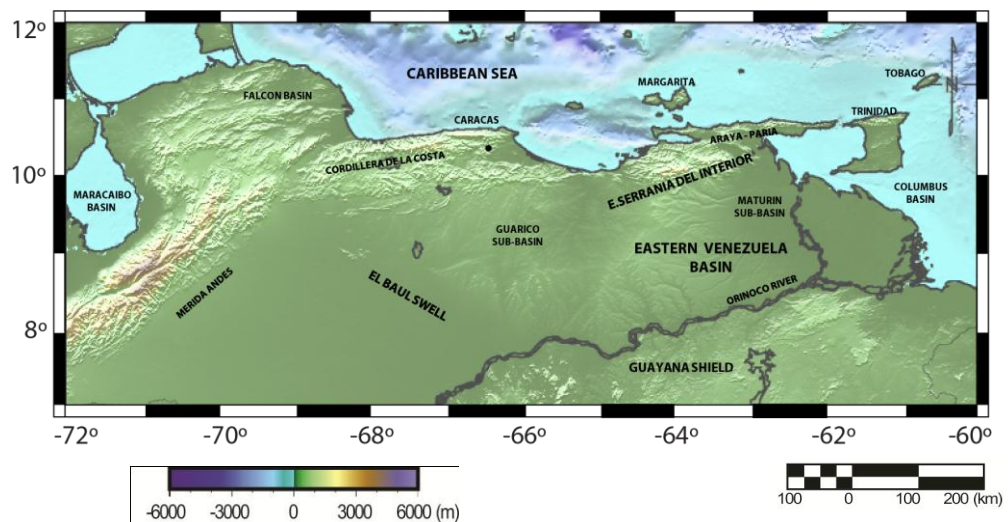


Figure 2.1. Geographical and tectonic setting of the Eastern Venezuela basin in the northern South America borderland.

Generally, the main features in eastern Venezuela are found within the following tectonic settings: the Guayana Shield, the Eastern Venezuela foreland thrust and fold belt (Eastern Serranía del Interior), the Araya-Tobago terrane and the Eastern Venezuela foreland basin. Two sub-basins can be distinguished in the continental area: the Guárico sub-basin, farther west up to the El Baúl Swell; the Maturín sub-basin, main depocenter of the Eastern Venezuela basin, and farther east the offshore Columbus basin. Most of the following geologic statements are based to a large extent on descriptions given by González de Juana et al. (1980), Bellizzia et al. (1981), Arstein et al. (1982), DiCroce et al. (1999) and Ostos et al. (2005), supported by mapping developed during the petroleum exploration in Venezuela, as well as from synthesis of Caribbean geology and tectonic, such as those of Menevén (1982), Case et al. (1984), Speed (1985), James (2003) and Pindell et al. (2005).

2.2. GEOLOGY PRIOR TO JURASSIC TECTONISM

2.2.1. THE GUAYANA SHIELD

The crystalline basement of the Precambrian Guayana Shield crops out southward of the Orinoco River. This cratonic area is made up mostly of metasedimentary and igneous rocks, with granite batholiths of homogeneous composition as well as greenschists widely distributed (Case et al., 1984). From near sea-level, the rolling surface of the Guayana Shield rises slowly southward to vast mesas rising about 1200-1800 m above the surrounding savannas, such as the Auyantepui and Roraima (Figure 2.2A-B). On top of much of these higher regions a sequence of little deformed, unmetamorphosed rocks -Roraima series- overlies most of the earlier Pre-Cambrian basement (Donovan, 1994).

Five tecto-thermal and tectonic events have been recognized over the shield; the most recent of all, the Orinoquean, developed about 1300-850 my. B.P. (Martín, 1974a; González de Juana et al., 1980). However, the Guayana Shield, whose rocks may be as old as 3.7 by, has been rather stable in terms of compressional tectonic during most of the Phanerozoic time. The craton, as part of the South America plate, has moved relatively westward from Africa since the Mesozoic opening of the Atlantic Ocean and has undergone substantial vertical uplifting during the Cretaceous and Cenozoic.

Four erosional levels have also been reported at the Guayana Craton, namely: Kamarata, the oldest one of unknown age (1000 m); Imataca, Cretaceous (600-700m); Caroní-Aro, Tertiary (200-300 m and 400-500 m) and Llanos-Orinoco, Pliocene to Recent times (80-150 m) (González de Juana et al., 1980; Mendoza, 2005).

Results of seismic refraction data from the Guayana Shield (Fig. 2.3) suggest a mean crustal velocity of 6.6 km/s and a depth of 49-48 km for the Moho discontinuity in this area (Schmitz et al., 1999; Chalboud, 2001).



Figure 2.2-A. Auyantepui seen from the south.
Location: $5^{\circ} 48' 15''$ N, $62^{\circ} 28' 03''$ W.
Courtesy: Isabel Hernández (2010).

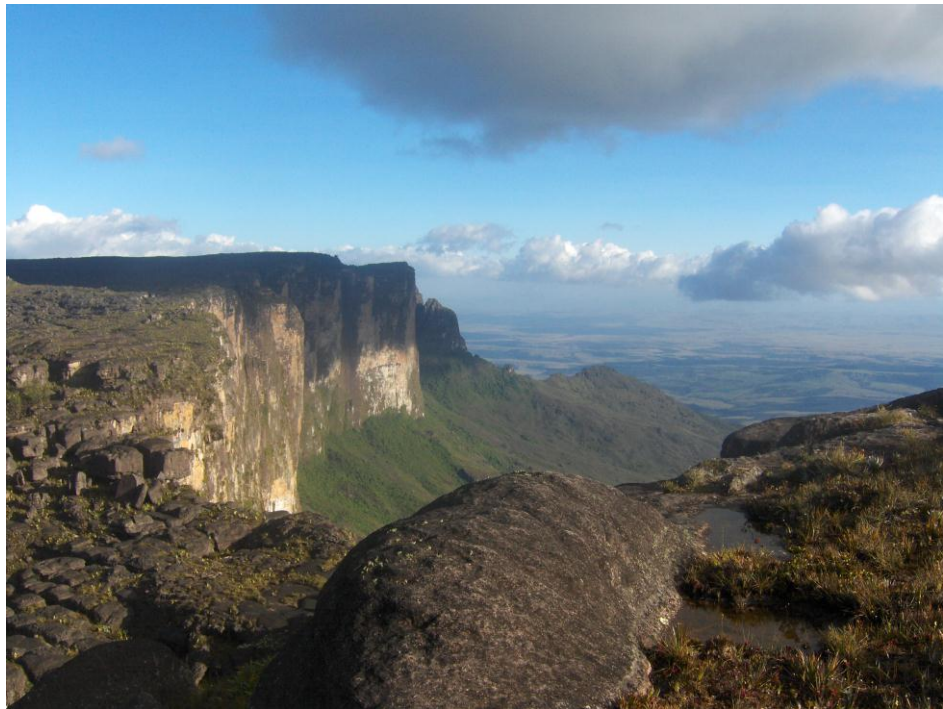


Figure 2.2-B. Roraima seen from its top, from the north with north-south direction.
Location: $5^{\circ} 12' 08''$ N, $60^{\circ} 44' 07''$ W.
Courtesy: Janckarlos Reyes (2010).

From refraction data along profiles W-E and N-S on the Guayana Shield, Chalboud (2001) interpreted a two layers upper crust, a shallow one, 8-10 km thick, with velocities from 6.1 km/s (west) to 6.0 km/s (east), and a deeper one with variable velocities from 6.3 km/s (west) to 6.2 km/s (east) reaching depths of 20-21 km. For the lower crust, two layers have been interpreted, the first one at 30-32 km depth with variable velocities from 6.6 km/s (west) to 6.7 km/s (east) reaching depths of 20-21 km. For the lower crust, two layers have been interpreted, the first one at 30-32 km depth with variable velocities from 6.6 km/s (west) to 6.7 km/s (east), and the deepest one, down to the Moho discontinuity (45 km), with velocities of 6.95 km/s (west) and 6.9 km/s (east). Upper mantle velocity is 8.2 km/s.

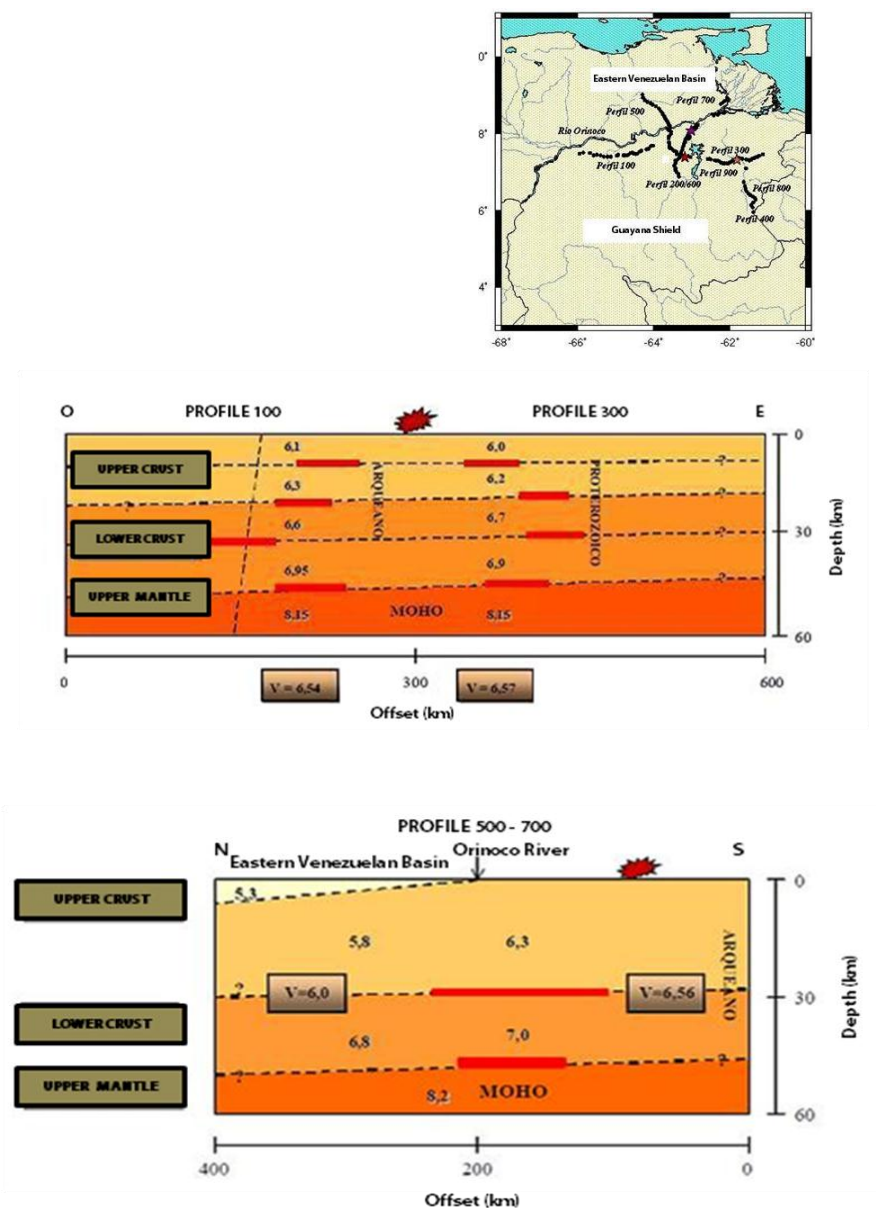


Figure 2.3. Crustal sections from seismic refraction surveys along W-E and N-S profiles in the Guayana Shield. Velocities are in km/s. Vertical exaggeration 3:1. (Schmitz et al.,1999; Chalboud, 2001).

2.2.2 POST-CAMBRIAN AND PRE-JURASSIC

The effects of two main Paleozoic orogenies have been reported in Venezuela (Caledonian: 300-450 my. B.P. and Hercynian: 200-300 my. B.P.; González de Juana et al., 1980); however, as far as this work is concerned, the most relevant is the uplift of El Baúl Swell, which is formed by an alkaline granite (287 ± 10 my. (Rb/Sr) - 270 ± 10 my. (K/Ar), Santamaría and Shubert, 1974) that projects northwestwards from the Guayana highlands and marks the westernmost limit of the Eastern Venezuela basin (see Figure 2.1 for location and González de Juana et al. (1980), Feo Codecido et al. (1984), Menéndez (1994), Viscarret and Urbani (2005), Arraiz and Dinis (2008) and Arraiz et al. (2008) for details). It is most probable that El Baúl, as other dated plutons of Permian age referred by Burke et al. (1984), might be interpreted as related to convergence and final collision between the North and South American plates at that time, and probably, as Arraiz et al. (op.cit) state from their gravity modelling, the rocks of El Baúl Swell extend down to 8.5 km in depth, overlaying a deeper arcuate structure related to the Guayana Shield.

This period records the deposition over an irregular basement with deep depressions of the Hato Viejo and Carrizal formations, where a great thickness (some 1200 m) of unmetamorphosed sediments of these two formations has been preserved. The Hato Viejo Formation, the older one, is non-fossiliferous and consists mainly of arkosic and quartzitic sandstones of probable nearshore marine environment (Hedberg, 1950; Bartok et al., 1985; LEV, 2008), which grades upward into the Carrizal Formation (early Cambrian (?) in age), a homogeneous siltstone and claystone sequence with minor interbedded fine grained sandstones. The sedimentary record suggests that the rifting along eastern Venezuela was at least Pre-Barremian (Erlich and Barrett, 1992; Ríos, 2002) whereas radiometric dates on igneous rocks indicate a Late Triassic-Early Jurassic age (Feo Codecido et al., 1984)

During Triassic-Jurassic times, the Hato Viejo and Carrizal formations were exposed to erosion, which is why they probably only remain in deep basement depressions. Intense volcanic activity has also been reported

during the Guacamayas Volcanic Group event (192 ± 3.8 my. K/Ar) in the El Baúl area.

2.3. JURASSIC RIFTING: EXTENSIONAL DOMAIN

The earliest apparent traces of the presence of extensional regimes in eastern Venezuela is probably the uplift of the cratonic area of Guayana, reported by González de Juana et al. (1980) as a Triassic-Jurassic event, and the existence of a graben-type structure in the Espino area (Figure 2.4), where a complete record through the pre-rifting into the rifting stages seems to be present (Ríos, 2002).

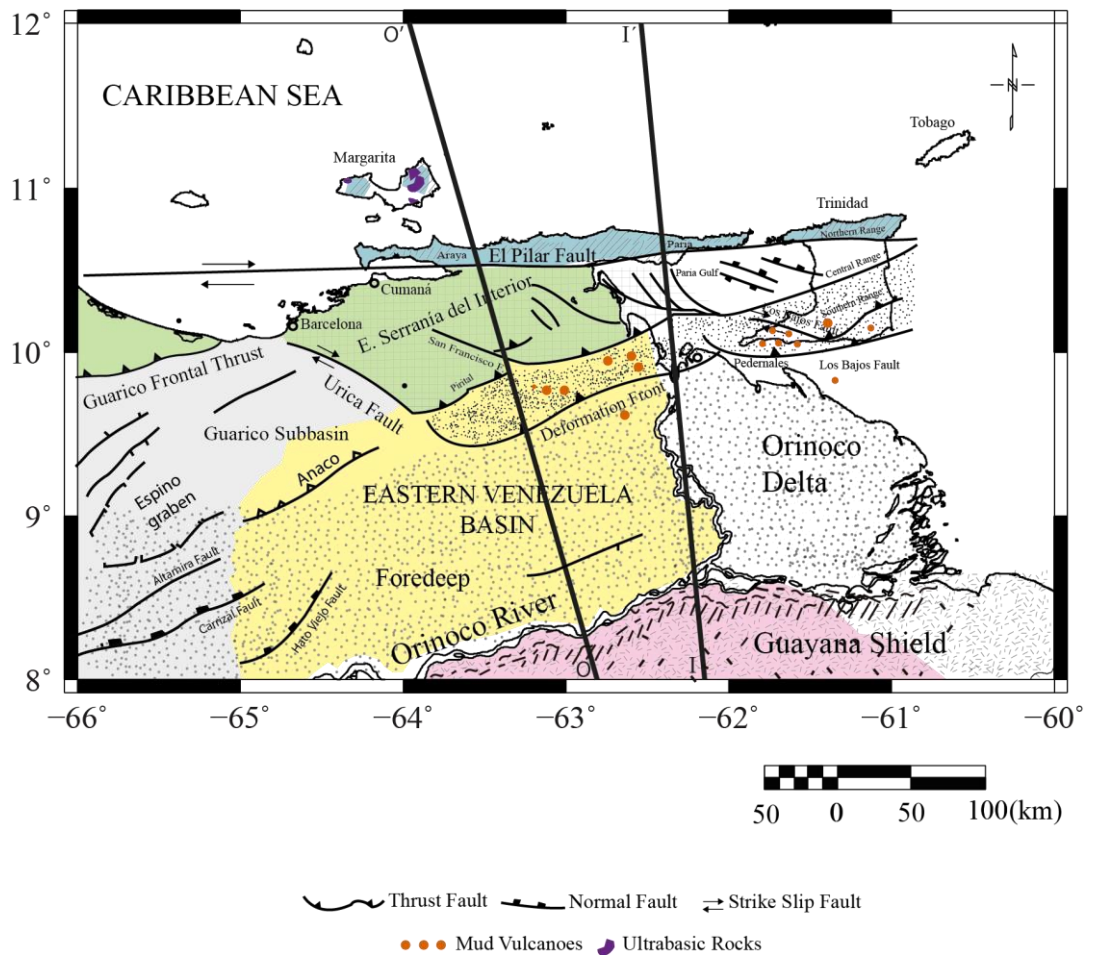


Figure 2.4. Tectonic and geological framework showing the main structural features in Eastern Venezuela, as well as location of profiles OO' and II'. Relevant structures in the area after Bellizzia et al. (1976), Feo Codecido et al. (1984), Di Croce (1995) and Hung (2005).

At this stage the evolution of the Eastern Venezuela basin has to be dealt with in the context of the North and South American plate's separation. Evidence of rifting between these two plates in Eastern Venezuela is difficult to find, mainly because the rocks that might uncover the Jurassic to Early Cretaceous rifting phase are buried beneath a very thick sedimentary sequence.

However, the presence of evaporites (Late Jurassic-Early Cretaceous (135 my. B.P.) in at least three wells drilled in the Gulf of Paria (lying in the eastern part of the basin) is very strong evidence of the production of rift basins in the area (Burke et al., 1984; Burke, 1988) and hence in the Eastern Venezuela basin. Furthermore, the 1.6 km thick sequence of red-beds and interbedded basaltic flow (113 m thick and 162 my. age) reported by Feo Codecido et al. (1984) at the northeasterly trending Espino graben (Fig. 2.4), seems to indicate that a rifting event might have been felt in that area as early as in Mid to Late Jurassic time; according to syntheses of Caribbean tectonics suggesting that the separation of the North and South American plates might have occurred during the Mid Jurassic (Pindell et al., 1988; Ross and Scotese, 1988; Pindell and Kennan, 2009). The African and South American plates drifted apart most probably during the Mid Cretaceous (some 110 my. ago, Burke et al., 1984; Pindell et al., op. cit.) after the relative tectonic quiescence of the Early Cretaceous.

In Eastern Venezuela, the sedimentation that took place from the initial rifting phase occurs over the continental northeastern edge of the South American plate, thought to have been an Atlantic-type ocean margin developed along the southern border of the Proto-Caribbean sea during Jurassic to Cretaceous times (Maresch, 1974; Speed, 1985; Pindell et al., 1988, 2005). There, the Precambrian sialic crust of the South American plate extends well east of the longitude of Trinidad (Case and Holcombe, 1980) probably to the base of the eastern continental slope.

Since at least the Barremian-Aptian (120-110 my. B.P.), the shelf and coastal region of northeastern Venezuela started to subside and the incipient ocean margin kept accumulating sediments with the typical pattern of shallow marine deposits near the craton, to deep sea-water facies northward to the open ocean; there, the stratigraphic evidence shows that the sedimentary facies distribution was controlled by the basement topography.

However, it is difficult to ascertain the full extent to which the South American continental crust was stretched before splitting in Late Jurassic to Early Cretaceous times and the magnitude of the initial subsidence. This latter factor is strongly dependent on the thickness and density of the continental crust (McKenzie, 1978), but knowing the amount of extension, both the initial and thermal subsidence can be computed. Among the numerous uncertainties involved, a rough estimate of the initial subsidence gives values of 1.3 to 4.3 km; minimum thicknesses of shelf deposits (Barranquín Formation), with seabed depth probably of the order of 1.3 to 2.5 km.

2.4. PASSIVE MARGIN PHASE: EARLY CRETACEOUS TO EOCENE.

This phase spans the end of rifting in Late Jurassic or earliest Cretaceous to the onset of active tectonism in the Eocene.

The beginning of the transgressive cycle of Cretaceous age in eastern Venezuela is a matter of uncertainty because the base of the Barremian-Aptian Sucre Group, the oldest autochthonous rocks deposited in the area, is unknown. However, it is generally accepted that the Cretaceous transgression, as a whole, began during the Barremian-Aptian (with the deposition of the Barranquín Formation consisting of quartzitic sandstones interbedded with arenaceous shale and lesser amounts of limestone (Hedberg, 1950; Guillaume et al., 1972; Erikson, 1994). It extended southwards over the flattened cratonic area, whose slow and progressive subsidence continued up to the Santonian. Subsequently, red beds

associated with graben fill have been identified at the base of the Barranquín Formation (around 2800 m depth) in the Macal wells, and have been assigned the informal name of the Macal Formation of Late Jurassic age (Aquino and Arreaza, 2005; Aquino, 2006).

Continental shelf to shallow water marine sediments of the Temblador Group were deposited over the comparatively stable platform north of the Guayana Shield and east of the El Baúl Swell; farther north -bordering the open ocean- the Sucre, Guayuta and Santa Anita groups formations were laid down (González de Juana et al., 1980; Muñoz, 1985).

In the south, the Temblador Group lies unconformable over the northern flank of the Guayana Craton and represents all the Cretaceous sedimentation in the southern rim of the basin. To the north, the Lower Cretaceous Sucre Group consists of a neritic-coastal seaward limestone sequence, typified by interfingering and lateral equivalence of facies (Rosales, 1972; González de Juana et al., op.cit.). During Mid Cretaceous, the maximum southwards extension of the transgressive cycle took place, all in a period characterized by a general deepening of the sea. Then, the deposition of the Guayuta Group occurred under euxinic conditions with thick limestones and dark shales of the Querecual Formation to the north and neritic-coastal sandstones, shales and limolites to the south.

The Upper Cretaceous sedimentation, a characteristic deep basin filling sequence, began gradually with the fossiliferous deep-sea shales and fine-grained calcareous sandstones of the San Antonio Formation, and followed during the Maestrichtian, at a faster rate, with the deposition of the sandstones of the San Juan Formation which reflects the onset of a regressive cycle (Renz et al., 1958; González de Juana et al., 1980).

Towards the end of the Cretaceous and into the Paleocene, some events possibly correlated with the North American Laramidean orogeny occurred in this zone as follows:

(1) In inland Venezuela, the Guayana and El Baúl cratonic areas, with their Cretaceous sedimentary covers, were uplifted, exposing to erosion the southern and western parts of the Cretaceous Eastern Venezuela basin; this period of erosion might account for the lack of Paleocene-Eocene sedimentation in a great portion of the Eastern Venezuela basin. While erosion was going on in the south, sedimentation was continuous in the north throughout the Late Cretaceous and early Tertiary with the deposition of dark shales of the Santa Anita Group, consisting of the Vidoño and Caratas Formations (Renz et al., 1958; González de Juana et al., 1980). The thinning or lack of deposition of the Caratas Formation in the south, suggests that flexural upwarping of area immediately north of the Guayana Shield may have been coincident with this first phase of compression-transpression and foreland basin development in the Guárico sub-basin (Erich and Barrett, 1992). Mid to late Eocene uplift age is also supported by radiometric and stratigraphic data from Margarita Island (Chevalier et al., 1995).

(2) Farther north, somewhere to the north of its present position (Speed, 1985) or farther west (Pindell, 1985; Burke et al., 1984) intense tectonism including regional metamorphism, igneous activity and uplifting, was taking place (Martín, 1974b; González de Juana et al., 1980) to give shape to the metamorphic terrane now exposed along the Araya-Paria peninsula.

From the structural point of view, two main fault systems have been recognized at this stage in the Eastern Venezuela basin; these are: normal faults, with strike parallel to the regional trend of the basin, and dip either north -towards the trough- or south -towards the craton-, and a set of transverse faults across the basin. As reported in the literature, there is a remarkable lack of folding in the Cretaceous formations on the meridional flank of the basin; there is apparently no deformation of the Upper Cretaceous in the Eastern Venezuela basin.

2.5. THE NORTHERN OVERTHRUSTING DOMAIN

2.5.1. ARAYA-TOBAGO TERRANE

The Araya-Tobago terrane, as depicted in Figure 2.4, comprises the metamorphic rocks of the Eastern Cordillera de la Costa (Coastal Range) at the Araya-Paria peninsula in Venezuela, those of the Northern Range of Trinidad and Tobago Island. This terrane is limited on its northern boundary by the southwestern edge of the Lesser Antilles-Tobago trough (forearc basin, Margarita-Tobago in Fig. 1.1) and on its southern border, along the Araya-Paria isthmus, by the foreland thrust and fold belt on continental South America (Case et al., 1984; Speed, 1985).

The Araya-Paria peninsula and Northern Trinidad range (Fig. 2.4) consist of metamorphic rocks exhumed during mid to late Miocene collision of the arc terranes of the Caribbean plate and the continental South America plate (Speed, 1985; Cruz et al., 2004). Notably the Dragón - Mango gneiss occurs in the Paria peninsula (Carboniferous age, Urbani, LEV, 2008).

The continuity of the metamorphic belt eastwards towards Trinidad has been confirmed through seismic experiments carried out by Bassinger et al. (1971). They observed that an undeformed sedimentary cover above the Araya-Tobago terrane is of variable thickness and much of it lays over a regional unconformity of late Miocene or subsequent age (Speed et al., 1991).

From field observations on the Araya-Paria peninsula, three generations of metamorphic rocks of the Eastern Cordillera de la Costa have been identified (Vignali, 1977; Vierbuchen, 1979). The nearly isoclinal folding gives the region an apparent homoclinal structure of ENE-WSW strike with regional dip towards the NNW and evident drag folding and fold-type lineations throughout the sequence. Shortening occurs in NNW-SSE direction. Investigations of Ave Lallemand (1997) and Alvarado (2005) recognized that all rocks of the Araya-Paria peninsula were deformed during two orogenic

events (D1&D2). D1 structures are syn-metamorphic and related to subduction/collision processes. D2 structures are postmetamorphic and related to south-southeastward thrusting of the Cordillera de la Costa belt and the formation of the Serranía del Interior fold and thrust belt.

Three phases of faulting, with different characteristics and ages have also been described by Vignali (1977) throughout the metamorphic range. First, there is a zone characterized by ophiolitic melanges, ENE trending, in contact with metamorphic rocks of amphibolite-almandine facies with siliceous facies. At the isthmus, the abrupt contact between the metamorphic rocks of the Eastern Cordillera de la Costa and the sedimentary rocks of the Eastern Serranía del Interior occurs over a structurally chaotic zone, marked by the presence of ultramafics, serpentinites and lavas; here, metamorphic rocks of Cretaceous to Eocene (?) age are thrust over strata of the foreland deformed belt (Vierbuchen, 1979; Vignali, 1979) in a region where an important amount of N-S shortening might have occurred.

Second, there is a series of long postmetamorphic fractures trending $N60^{\circ}$ - $30^{\circ}E$ and dipping northwards, where strong strike-slip activity appears to have ended in late Eocene, not having affected the recent sediments. And, third, there are numerous transverse faults (NNW and NNE strike) with right or left strike-slip motion, which seem to be the result of stresses with maximum tension acting in a NE-SW direction (Vignali, 1979).

Furthermore, according to recorded and present evidence of motion along the ENE faults in eastern Venezuela, three chronological stages can be recognized: Cretaceous-Eocene (normal faults), Eocene (thrust faults) and Recent (normal and strike-slip). The thrust-type faults are probably related to the uplift of the mountain range and the normal faults series delineate horst-graben like structures along it. It is also likely that normal faults were turned into reverse high angle faults and finally true thrusts, as a consequence of the tectonic processes later affecting the area (González de Juana et al., 1980). Thus, contemporaneous stresses are probably reactivating ancient structures as well as forming new ones.

Apparently, the major geologic elements of the metamorphic range were generated during the Mesozoic although important questions about their origin, development, and present tectonic role are still unanswered. The following facts need to be taken into account when interpreting the tectonics of the region:

(1) The metamorphic rocks of the Cordillera de la Costa in the north and the sedimentary rocks of the Serranía del Interior in the south are in close contact along either a thrust or strike slip fault or a combination of both, and also along a narrow elongated belt partially covered by sea-water or alluvial deposits.

(2) Limited igneous activity of continental nature is represented by granitic intrusive bodies, mostly sills concordant with the surrounding rocks and in many cases exhibiting the same pattern of deformation. For details see Santamaría and Schubert (1974).

(3) The presence of rocks of ultramafic complexes (serpentinite, peridotite, dunite) is very often associated with metamorphosed basic rocks (gabbro, amphibolite, volcanic), where the volcanic rocks occur as interleaved lenses subparallel to the ENE trending foliation or to strike-slip faults, all integrated into the metamorphic mountain range.

(4) The metamorphic rocks grade from greenschist to prehnite-pumpellyite and zeolite facies. The regional trend of increasing metamorphism within the rocks of the Eastern Cordillera de la Costa (Araya-Paria peninsula) is from south to north, and also from SE to NW (Schubert, 1972; Maresch, 1974; González de Juana et al., 1980; Ave Lallemand, 1997). At the latitude of the Araya peninsula, the Cordillera de la Costa belt split into a northern high grade and southeastern low grade metamorphic belt. The northern belt is characterized by the occurrence of eclogite on Margarita Island, blue schists in the Carúpano basin and staurolite and kyanite schists on the Araya peninsula. The age of metamorphism is Mid Cretaceous to Late Cretaceous. The southern low-grade belt consists of chlorite-grade

metasedimentary rocks; the age of the low-grade metamorphism appears to be middle Tertiary. On Tobago Island the metamorphic terrane consists mainly of amphibolite and pelitic schists, faulted against arc-volcanic rocks of probable Mid Cretaceous age. Metamorphic rocks also crop out offshore on Margarita and other smaller islands to the east and west (Navarro, 1977).

(5) The time span between Late Cretaceous and late Miocene records the entire process from the protolith formation of the rocks of the Araya-Tobago terrane through to the metamorphism and deformation of the complex. Upper Jurassic to Upper Cretaceous scarce fossils have been found in Trinidad and Cretaceous fossils in Venezuela. Furthermore, determinations of age of the metamorphism in the Araya-Paria peninsula are based mostly on correlations with metamorphic rocks dated in Margarita; however, it is probable that neither the protoliths nor the metamorphic rocks of the Araya-Paria peninsula and of Margarita Island are related (Speed, 1985).

Within this fundamental framework there are a few aspects where agreement seems to exist; these are:

(1) The entire metamorphic unit has been strongly folded and thrust toward the south, together with the Mesozoic and Paleogene sediments of the Eastern Venezuela foreland deformed belt (Vignali, 1979; González de Juana et al., 1980; Chevalier, 1993; Ysaccis, 1997; Ostos et al., 2005).

(2) Major shortening in a NNW-SSE direction has occurred throughout the area, across the Araya-Tobago terrane and the Eastern Venezuela foreland deformed belt.

(3) Although it is difficult to precisely identify a time for each stage of evolution of the whole complex, the complete process of rock generation, metamorphism and deformation took place between Cretaceous and Miocene. Fission track analyses indicate that the Serranía del Interior and the

Cordillera de la Costa belt were both exhumed during the Eocene and Oligocene (42 – 28 Ma; Sisson et al., 2005).

(4) A first phase of compressional deformation probably occurred in mid-to-late Eocene and a second one, with reactivation of faults, in the Miocene.

There are also some aspects still subject to much debate, mostly because of gaps existing in the tectonic knowledge of the area; among these it is interesting to mention:

(1) The metamorphic terrane substrate and related deep structure, as well as the kinematic of the El Pilar fault zone, about which there are two schools of thought:

- The terrane is allochthonous with a north dipping basement underlain by South America continental crust; in this case the current El Pilar fault is a post-emplacment structure and the terrane is a product of thin skinned tectonic (Speed, 1985).
- The terrane lies above a discrete lithosphere joined to the South American plate by a steeply dipping suture; therefore, the El Pilar fault marks this collision zone characterized by either continuous or reactivated motion through time (Silver et al., 1975; Sykes et al., 1982; Pindell, 1985).

(2) The origin of the metamorphic rocks of the Araya-Tobago terrane and its tectonic emplacement. Nowadays, most researchers are focusing their attention on the idea of a terrane that formed at a subduction island arc complex during mid-Mesozoic (Bell, 1971; Bellizzia, 1972; Maresch, 1974; Speed, 1985; Pindell, 1985; Erlich and Barrett, 1990; Ave Lallemand, 1997 among many others). Margarita and Tobago Islands comprise forearc elements of the Great Arc whose metamorphism indicates burial to varying depths (Maresh et al., 2000a-b; Rekowski and Rivas, 2005). The remaining

controversy, closely related to aspect (1), lies in the time and mechanism of collision; thus, the arc terrane was either thrust as a series of nappes (Speed et al., 1984) or carried along a large strike-slip fault zone (Pindell et al., 2005) during Mesozoic (?), early Tertiary (?) or late Tertiary (?).

These controversial aspects will be examined together with the gravity modelling and the evolution of the Eastern Venezuela foreland basin in Chapters 4 and 5. However, my inclination is for a model of eastern Venezuela where the continental South American plate is overridden by a complex of metamorphic nappes whose emplacement gave rise to the uplift of the Serranía del Interior and contemporaneous formation of the Eastern Venezuela foreland basin.

2.5.2. EASTERN VENEZUELA FORELAND THRUST AND FOLD BELT

The foreland thrust and fold belt province in Eastern Venezuela is mainly made up of the intracontinental strata of the Eastern Serranía del Interior, a series of unmetamorphosed Cretaceous to middle Eocene rocks with local Oligocene to Miocene synorogenic sediments that extends, trending about N70°E, for some 200 km from Barcelona and continues eastward off the western coast of the Paria gulf, as far as Trinidad, where the belt comprises deformed strata as young as Oligocene. The northern limit of this tectonic unit follows the Venezuelan coastline and islands between Barcelona and Cumana, along the southern coast of the Cariaco gulf and the isthmus between the Araya-Paria peninsula and Venezuela; the southern boundary is the southernmost frontal thrust (Fig. 2.4 for location).

Autochthonous sediments of the belt include Lower Cretaceous shelf deposits of the Barranquín Formation which are considered to mark the beginning of the passive margin phase (Higgs, 2007). This represents the lowermost sequence exposed in the belt developed over the subsident flank of the Guayana Craton, being progressively more marine towards the north

as a result of southward transgressive seas. An identical relationship is observed in sedimentary rocks of Late Cretaceous and Paleocene age.

Along the foreland deformed belt (Fig. 2.4), the main structural elements include: (a) thrust and reverse faulting parallel or subparallel to the trend of the folds, predominantly along the strike of the range, (b) WNW to NW oblique faults mostly with right strike-slip sense of motion, and (c) minor scale NE faulting. Coeval southeast vergent thrusting in the Eastern Serranía del Interior and right lateral strike-slip along the faults suggest strain partitioning (Ave Lallemand, 1997). East-west strike slip faults are coeval with thrust faults and they share the same decollement surface (Hung, 2005).

Southward overriding and thrusting of ENE strike bounds in the Eastern Serranía del Interior, suggesting a major SSE trend of shortening across the belt (González de Juana et al., 1980; Speed et al., 1982), apparently the result of decollement tectonics (Chevalier, 1993). Daal et al. (1989) identify three levels of decollement in eastern Venezuela: The basal pre-Cretaceous level, whose depth range is 7 to 12 km (Lilliu, 1990), forms the main decoupling of the allocthonous strata; a middle Aptian level, which generates the structures of the Serranía del Interior, and a late Oligocene level responsible of the Miocene folding in the Eastern Venezuela basin.

The deformed fold and thrust belt generally follows a N15E trend. The most significant structure is related to the Pirital thrust, which follows a N30E trend, with decreasing fault displacement eastwards (Fig. 2.4). Detachment levels are located in the Paleozoic rocks for westward verging structures and in the syn-rift sequence for eastward verging structures (Duerto, 2007).

The tectonic evolution of the whole belt is associated with the uplift of the Eastern Serranía del Interior in eastern Venezuela as a late orogenic phenomenon, evident only after the middle-upper Eocene hiatus. Thus, the deposition of early Oligocene formations marks the beginning of a new sedimentary cycle (González de Juana et al., 1980; Arstein et al., 1982; Ostos et al., 2005) where the eastern sedimentary range as a positive

element came to form the northern flank of the Tertiary Eastern Venezuela foreland basin formed thereby.

2.6. THE EASTERN VENEZUELA FORELAND BASIN

The Eastern Venezuela foreland basin is an ENE trending and east plunging structural and sedimentary trough, some 400 km long and 200 km wide, situated in the northeastern part of Venezuela (see Figures 2.1 and 2.4 for location). The physiographic basin is bounded on the north by the Eastern Venezuela foreland thrust and fold belt, on the east by the Atlantic Ocean, on the south by the Guayana Shield and on the west by the Espino graben. The basin, as a whole, has accumulated thicknesses of Cretaceous to Recent sediments up to twelve or even more kilometers.

Pioneering regional interpretations of the area were given in the fifties by Hedberg (1950), Young et al. (1956) and Renz et al. (1958). More recent studies, besides the obligatory reference text of González de Juana et al. (1980), include those of Arstein et al. (1982), Sánchez & Russomanno (1982), Muñoz (1985), Yoris and Ostos (1997) and Ostos et al. (2005) where an up-to-date compiled version of the geology, geophysics and geochemistry of the basin, mostly related to the petroleum industry, has been presented; and those of Daal et al. (1989), Aymard et al. (1990) and Erlich and Barrett (1992) where detailed stratigraphic data has helped to constraint and refine models of the geohistory of Northeastern Venezuela. The details will not be repeated here. However, the most important conclusions, mainly based on facts rather than ideas or models from those authors, will be summarized in order to lay the foundations for the interpretation to be carried out in this work.

- The ancestral Eastern Venezuela basin came into existence in Early Cretaceous or possibly Late Jurassic times over a region that had been subjected to invasions of the sea over the Precambrian Guayana basement during Paleozoic and early Mesozoic. The Cretaceous Eastern Venezuela basin remained as a main deposition belt, lacking active vulcanism, throughout the transgressive Cretaceous period into

early Tertiary. Erosion was widespread during Paleocene to Eocene, after which a new sedimentary cycle started in the recently formed Tertiary Eastern Venezuela basin, limited on its northern flank by the uplifting of the Eastern Serranía del Interior. Sedimentation was continuous through the mid-to-late Tertiary and into the Pleistocene, during a period of intense tectonic activity throughout the area. The summarized stratigraphy of Eastern Venezuela basin is shown in the Figure 2.5.

- As can be seen from this brief outline of the Eastern Venezuela basin history, the basin developed in a complex tectonic setting and it experienced substantially different processes through time. At least three main stages in time-evolution have characterized the basin: the pre-Early Cretaceous, the Early Cretaceous to Eocene and the Eocene to Present.
- The first period comprises the development of the pre Mesozoic basins over the cratonic area of Guayana before the North and South American plates drifted apart. The second period corresponds to the establishment of the original structural Cretaceous Eastern Venezuela basin over the passive continental margin of the South American plate, above which the Tertiary foreland basin was to be generated. The third stage corresponds to the period of evolution of the Eastern Venezuela foreland basin, focal point of this work, to its current configuration.

2.6.1. OLIGOCENE TO PRESENT

During this phase of foreland basin development the Eastern Venezuela basin was superimposed on the older passive margin sequences.

Following Stainforth (1965) and based on surface and subsurface data and seismic sections, Arstein et al. (1982) and Duerto (2007) recognized four regional sedimentary cycles in Eastern Venezuela during the Cenozoic. The

onset of each sedimentary cycle is marked by a transgressive phase, whose major subsidence is represented by a regional shale interval named after the biozone that typifies it. The cycle closes with a regressive phase. The following review of the basin Tertiary sedimentation is organized chronologically, from earlier to most recent (Fig. 2.5):

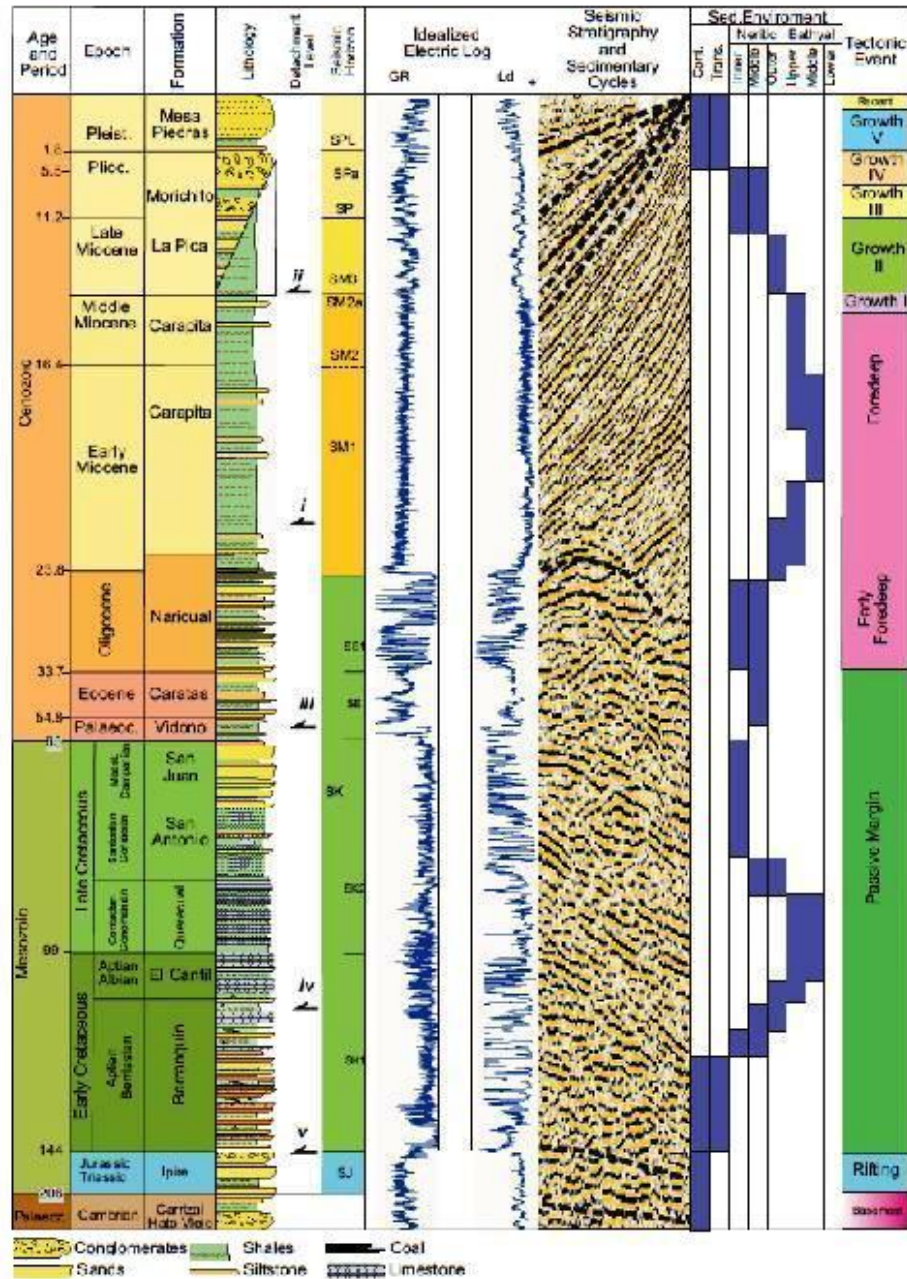


Figure 2.5. Seismic Stratigraphy and idealized well log of the Eastern Venezuelan basin. (Modified from Cobos, 2002; Duerto, 2007).

(1) The Oligocene cycle rests unconformable over eroded basement rocks after the Eocene hiatus. This cycle is represented by the predominantly marine Roblecito and La Pascua formations on the west, and by the more continental Naricual, Areo and Los Jabillos formations on the east. The Oligocene marks the onset of the subsidence of the Eastern Venezuela foreland basin, whose depocenter was located northwest, with 2700 m thickness of sediments (Muñoz, 1985; Erlich and Barrett, 1992). First stratigraphic signs of uplifting of the Eastern Serranía del Interior are the paralic episode of Naricual and the conglomeratic sedimentation of Los Jabillos Formation (González de Juana et al., 1980).

(2) The lower Miocene cycle is preserved in the northern parts of the basin and in the Eastern Serranía del Interior. The sedimentation, transitional to marine facies, comprises Oficina-Anaco and Capiricual formations in the west, and Capaya, Carapita and Uchirito in the east. After shifting eastwards, during early Miocene, the axis of the foredeep became close to the current position of the mountain range. The zone of frontal sheets developed during the sedimentation of the shales of the Carapita Formation. The order of appearance of each sheet is with the youngest to the south, due to tectonic transport from the northwest toward the southeast (Chevalier, 1993).

(3) The middle Miocene cycle was deposited in a southern continental environment close to Guayana (sandstones of Merecure Formation) and in open sea to the north (dark shales and turbidites, Carapita Formation). Maximum thicknesses of sediments are now found at the thrust areas, affected by compressive tectonic (Subieta, 1988).

(4) The upper Miocene-Pliocene cycle is represented by the Freites and La Pica formations in the south-southeast, being present mostly in the subsurface of the easternmost part of the basin. By this time the basin was gradually filling, especially its southern and western rims; the end of this cycle is an evident eastward regressive phase.

Sedimentation in the basin subsequently continued through the Pleistocene and still does in the Orinoco River deltaic zone and the Columbus basin further east (Garciacaro et al., 2011). The youngest stratigraphic unit in the Eastern Venezuela foreland basin is the Pleistocene Mesa Formation which rests unconformably over older rocks; this sequence thickens northwards.

The Pleistocene was, in general, a period of intense tectonic activity, evident by continuous folding and overthrusting affecting marine and continental deposits throughout the area, also by normal and transcurrent faulting. Uplift of the fold belt intensified into the Pleistocene as the Maturin subbasin filled to the south (Ostos et al., 2005). The sedimentary fill became increasingly continental and diapirism reached the surface. This tectonic activity was probably a reflection of the Antillean orogeny reported to have occurred in the Caribbean during this period (González de Juana, 1977). It became less intense during the Upper Pleistocene when only gravitational effects are observed, mostly at reactivated faults. During the Holocene, the vertical activity has continued and currently the entire region is exposed to erosion.

A simplified chronostratigraphic chart of the Eastern Venezuelan basin, illustrating both the timing and stratigraphic record and tectonic events is shown in Figure 2.6 (Di Croce et al., 2000, modified by Duerto, 2007).

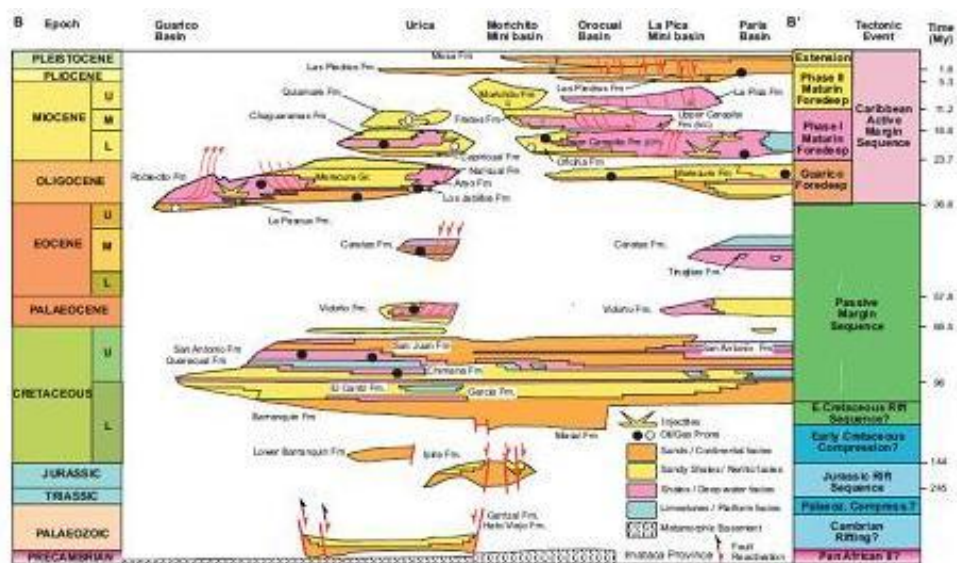


Figure 2.6. Simplified Chronostratigraphic chart of the Eastern Venezuelan basin. From Di Croce et al. (2000), modified by Duerto (2007).

2.6.2. REGIONAL TERTIARY TO PRESENT STRUCTURES

A review of the main structural characteristics of the Tertiary Eastern Venezuela foreland basin, mostly based on González de Juana et al. (1980), Arstein et al. (1982), Muñoz (1985), Daal et al. (1989), Yoris and Ostos (1997) and Ostos et al. (2005), follows herein:

- The lower Miocene regional structure in Eastern Venezuela was a monocline dipping north where faulting, mostly normal along EW and NE-SW trending faults, sometimes affected basement blocks. The upper Miocene was a period controlled by widespread compressional structures in the north; thrusts were developed even along pre-Cretaceous normal faults, and these locally emplaced Cretaceous rocks over Miocene deposits. The compressional provinces comprise the foreland thrust and fold belt extends southwards, beyond the Pirital thrust, as seismic data from Munro and Smith (1984) and Duerto (2007) suggest. In the south, on the contrary, a mostly tensional regime was present with normal faulting accentuated along a hinge line (Renz et al., 1958).
- Over the whole area and clearly associated with the Tertiary sedimentation, there is a NE-SW trending fault system of possible growing type with dips north or south. The youngest faults developed in the Eastern Venezuela foreland basin are Upper Miocene (?) to Pliocene, long transcurrent faults of NW-SE to WNW-ESE trend, such as Urica, San Francisco and Los Bajos faults, which appear to change strike and terminate on northeasterly striking thrust faults (Fig. 2.4). The WNW strike of these faults is thought to mark the direction of plate convergence which began in late Eocene or Oligocene time in western Venezuela and progressed eastward to a point today on the Araya-Paria peninsula (Mann et al., 1990; Pindell et al., 2005).

- Urica, with its 10 km wide fault-zone, appears to be the southernmost limit of the Eastern Venezuela foreland deformed belt (Fig. 2.4) and it is considered as a possible paleofracture of Precambrian age, reactivated during the collision process as a dextral strike slip fault (Daal et al.,1989). An elegant account of this fault has been given by Munro and Smith (1984) and later by Erikson (1994) who point out the importance of this fault as seismic has revealed that despite Neogene thrusting, reflectors of the basement are deeper on the coast side of the Urica fault than on the west side. It's also noticeable that for approximately 100km west of the Urica fault, no formations older than Eocene are exposed.

As can be seen, the late Tertiary was a period of intense tectonism in the northern boundary of the Eastern Venezuela foreland basin, which is evident not only because of the extensive faulting and folding, but because there is stratigraphic evidence suggesting that the basin was affected by a major northward basement tilting during the late Miocene and by two successive eastward tilting phases, the first in the late Miocene and the second in the Pliocene.

A regional picture of the structure of the eastern part of Venezuela, as proposed by Chevalier (1994), is shown in Figure 2.7 to illustrate the Eastern Venezuela basin and the main structural elements present in the area.

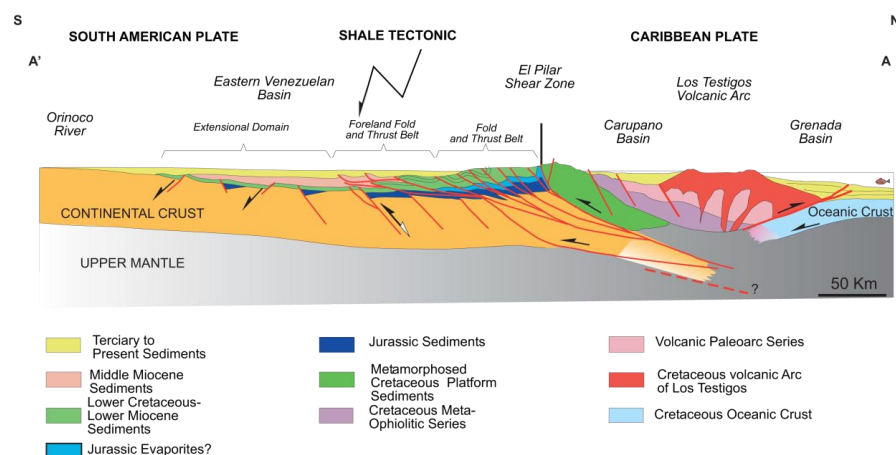


Figure 2.7 Schematic regional NW-SE cross-section of the northeastern part of Venezuela. Vertical scale exaggerated 4-times. (After Chevalier, 1994; Duerto, 2007)

To fully understanding the overall tectonic setting of the Eastern Venezuela foreland basin, here are some other noteworthy features closely connected to its evolution:

(1) An excellent review of the El Pilar fault, summarizing the great variety of ages, sense and magnitude of displacement along this fault has been presented by Schubert (1979) and new contributions or ideas about it can be found in Vierbuchen (1984), Speed (1985); Robertson and Burke (1989), Ysaccis (1997) and Ostos et al. (2005). However, there seems to be an agreement in describing the present El Pilar fault as a right lateral strike-slip fault zone that marks the boundary between the Araya-Tobago terrane and the continental South American plate, at least in Venezuela (Vignali, 1979; Speed, 1985; Speed et al., 1991). Major discrepancies still exist regarding the nature of the fault during the process of collision between the Caribbean and South American plates, and the amount of offset (tens to hundreds of kilometers). Special attention should be paid to this point because the markers for the estimates are allochthonous. A great deal of uncertainty remains.

There seems to be no-stratigraphic evidence of Holocene-to-present motion along El Pilar fault zone; however, seismicity and active hot-springs suggest that the tectonic activity still persists (Pérez and Aggarwal, 1981; Urbani, 1989; respectively). Some evidence of seismicity areas come from the destructive earthquake of magnitude $M_n = 6.4$ and focal depth of 9.4 km, occurred along the El Pilar fault on July 9th, 1997. Pure dextral strike-slip movement generated a surface rupture with a mean coseismic right-lateral displacement of about 0.25m, without visible vertical component (Romero et al., 1998). The main shock was located at 10.54°N and 63.5°W , with a focal depth of 9.4 km. The aftershock activity was concentrated on east-west trending fault plane dipping about 60° - 70° north, down to 15 km in depth (Romero et al., 1998; Schmitz et al., 1998; Choy et al., 1998). In dealing with the modelling and evolution of the Eastern Venezuela foreland basin, it will be necessary to refer to the critical role of the El Pilar fault in the Caribbean-NE Venezuela collision.

(2) The easternmost extreme of the Eastern Venezuela foreland basin, Paria gulf, Columbia basin and Trinidad Island: Throughout its evolution, the Eastern Venezuela basin remained always open to the east, where great thicknesses of sediments were accumulated; there, four Tertiary sedimentary cycles, correlatable with those occurring in Venezuela, have been reported (Stainforth, 1965; Garciacaro et al., 2011; and Escalona & Mann, 2011; for details). The physiographic provinces in Trinidad Island have their exact counterpart in Venezuela; thus, the Northern Range forms the eastward continuation of the Venezuelan Cordillera de la Costa, and consists of low-to-medium grade metamorphic rocks of Late Jurassic to Early Cretaceous age (Bassinger et al., 1971; González de Juana et al., 1980; Robertson and Burke, 1989; Donovan, 1994).

(3) The Central and Southern mountain ranges of Trinidad, a complex of Tertiary sedimentary rocks highly folded and thrust southwards along WSW-ENE trending faults, are considered to be the extension of the Eastern Venezuela foreland thrust and fold belt towards the east. The Eastern Venezuela and Trinidad deformed belts exhibit analogous characteristics in terms of stratigraphy and regional structure symptomatic of a compressional regime; although it appears that the orogenic pulses have been diachronous, becoming progressively younger from west to east, the effect of compressive stresses in Trinidad persisted after they had died away in the west (Salvador and Stainforth, 1968). There is also an interesting account (Ritter, 2007) about the influence of vertical tectonic in the region, in response to the formation of the Gulf of Paria, a pull-apart basin resulting from dextral wrenching along the El Pilar fault in Venezuela.

(4) The clear continuity of the main structural features of the Eastern Venezuela foreland basin, from Venezuela up to Trinidad, is also evident along the WSW-ENE trending belt exhibiting sedimentary vulcanism (see Figure 2.4), much of which is related to shale diapirism as confirmed by seismic studies from Giraldo et al. (2000) and Duerto and McClay (2002). Active mud volcanoes associated to subduction complexes have been reported by Hamilton (in Miall, 1990); in the study area this activity appears to

have occurred at least since the late Miocene and extends farther northeastwards up to the Barbados accretionary complex (Westbrook and Smith, 1983; Urbani, 1991). Mud diapirism is also abundant in the southern part of the complex, mostly south of the Tiburón Rise (at about 15°N of latitude) and increases southwards, with the thickness of the Orinoco submarine fan (Brown and Westbrook, 1987, 1988).

Duerto (2007) in his analysis of mud volcanism in eastern Venezuela concluded that it simultaneously evolved with the foreland fold belt in two main periods from W to E. The first episode began during the late Miocene and the second one during the Pliocene. The last episode of volcanic activity in the eastern part has continued from the Pleistocene to Recent.

2.7. THE STRUCTURE OF THE EASTERN VENEZUELA BASIN.

A set of seismic profiles in eastern Venezuela has been interpreted by Duerto (2007) to show the geometry of the structure of the Eastern Venezuela basin. His study along these representative lines, clearly shows the west to east variation in structural style along the strike of the foreland fold and thrust belt evolution. As a sample to illustrate the main structures across the Eastern Venezuela Basin, I have chosen seismic profile R-6 which runs NW-SE and has been divided into two sections (For location see Figure 2.8).

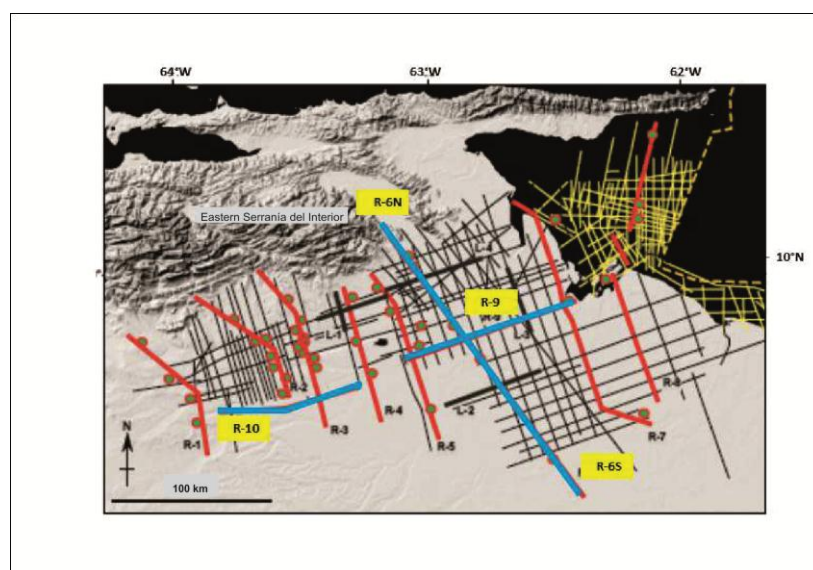


Figure 2.8. Location of seismic sections (blue lines) shown in section 2.7, this chapter. Modified after Duerto (2007)

Figures 2.9-A and 2.9-B illustrate profile R-6 (Duerto, 2007; Fig. 4.16a and 4.16b) where it is possible to see deep seated thrust sheets displacing Pre-Cretaceous to Oligocene units towards the south, listric faults with a southward sense of motion in both parts of the line and shallow structures which deform Plio-Pleistocene strata.

There are also seismic profiles R-10 and R-9 running E-W, and shown in Figures 2.10-A and 2.10-B, from W to E. Seismic interpretation of R-10 suggests the presence of two main groups of structures, deep-seated reverse faults involving Cretaceous and Pre-Cretaceous units, and listric faults dipping eastwards involving lower to middle Miocene units. The interpretation of profile R-9, located east of R-10, shows three main structural features: high angle reverse faults whose sense of motion is southwards and involves Pre-Cretaceous to Oligocene units, a listric fault system developed above the previously described, that usually dips eastwards and only involves the lower to middle unit (the foredeep sequence), and some low angle fault system.

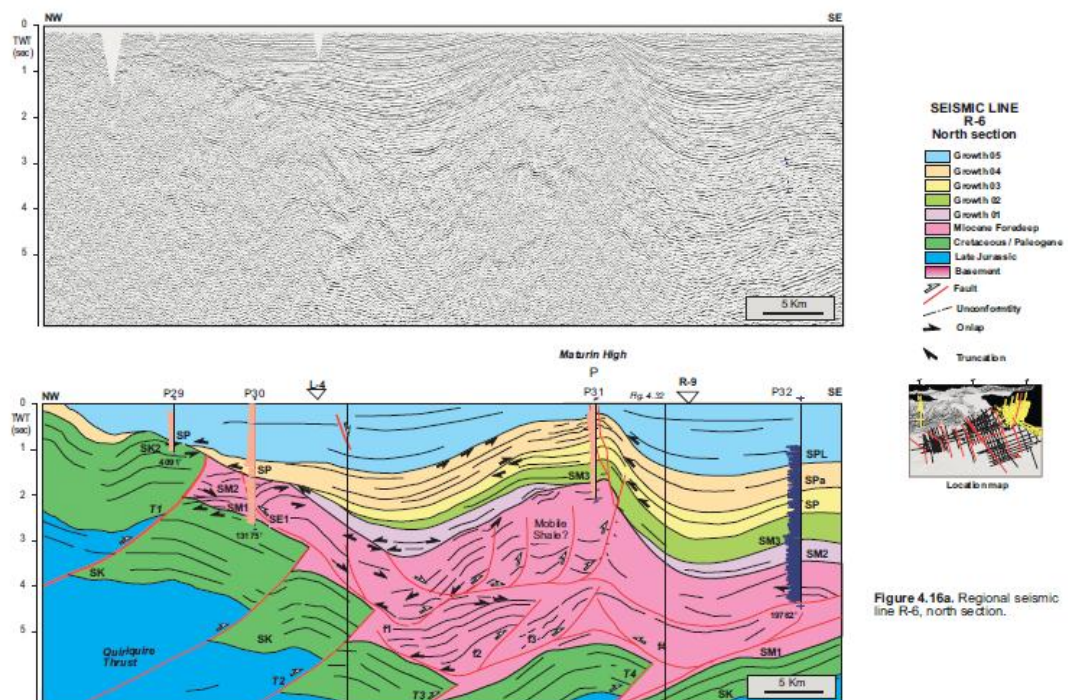


Figure 2.9-A. Seismic section R-6, north section, interpreted by Duerto (2007).

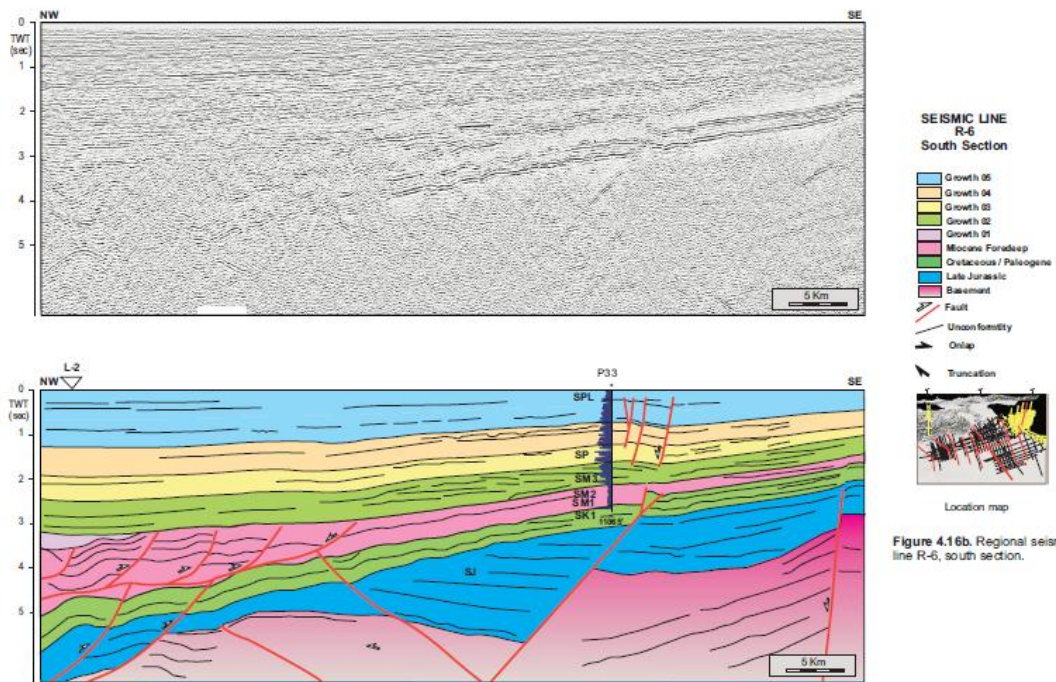


Figure 4.16b. Regional seismic line R-6, south section.

Figure 2.9-B. Seismic section R-6, south section, interpreted by Duerto (2007).

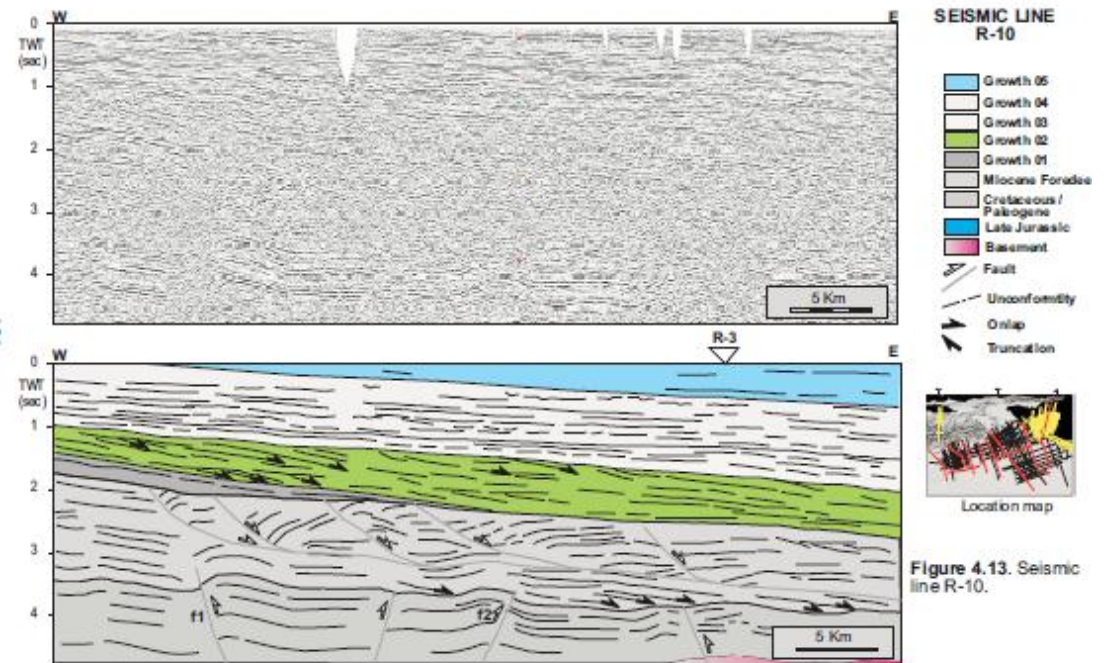


Figure 4.13. Seismic line R-10.

Figure 2.10-A. Seismic profile R-10 which runs in E-W direction. Interpreted by Duerto (2007)

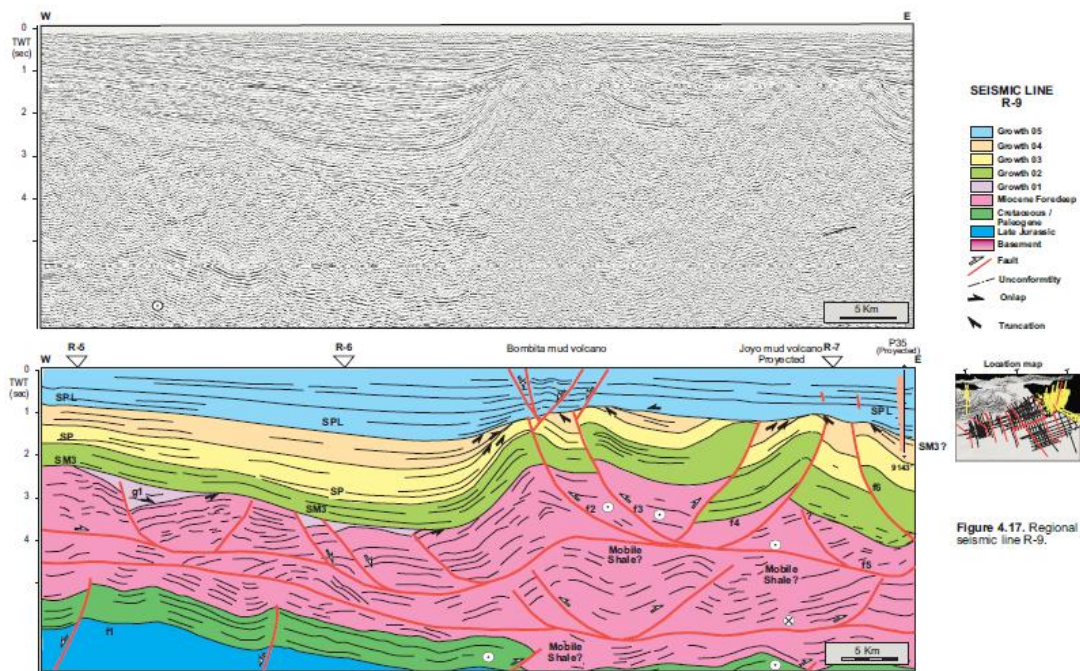


Figure 4.17. Regional seismic line R-9.

Figure 2.10-B. Seismic profile R-9, east of R-10, shows three main structural features: high angle reverse faults, a listric fault system and a low angle fault system. Interpreted by Duerto (2007).

2.8. KEY ELEMENTS FOR THE EVOLUTION OF THE EASTERN VENEZUELA FORELAND BASIN.

The end of the Eocene marks an important period in terms of plate tectonics in the Caribbean; 38 my. B.P. marks the onset of eastward movement of the Caribbean (Bell, 1972; Ladd, 1976; Speed, 1985; Pindell, 1994) relative to the North and South American plates, as well as the beginning of the Lesser Antilles Arc volcanism (Pindell and Dewey, 1982). This is reflected in the Eastern Venezuela foreland basin genesis and its early evolution: Margarita Island had emerged by the end of the Eocene (González de Juana, et al., 1980) and according to Speed (1985) overriding started near the Cariaco gulf in late Eocene or early Oligocene.

The collision-suturing stage in eastern Venezuela records all the history of the Tertiary Eastern Venezuela foreland basin, which after the Late Cretaceous-early Eocene orogeny was limited on the north by the Eastern

Venezuela foreland thrust and fold belt, and superimposed on the Cretaceous one. The Eastern Venezuela foreland basin was then asymmetrical from north to south, opened eastwards, bordered by coastal plains on its western and southern flanks, and with its deeper zones at the north and east.

The meta-igneous terrane, developed during the Cretaceous north or northwest of the basin, was pushed southwards, possibly even during the Paleocene (González de Juana, 1977) compressing the trough and sedimentary cratonic cover of the Cretaceous basin; the uplift of the Guayana Shield was perhaps the first sign of collision (Speed, 1985). After the orogenic pulse of the late Eocene, the Eastern Serranía del Interior was uplifted within the foreland thrust and fold belt province, and this tectonic loading of the shelf caused a major subsidence of the Eastern Venezuela foreland basin on the continent side of the deformed belt. Then, by the end of Tertiary times, the collision of the Araya-Tobago terrane caused extensive overthrusting on the northern flank of the Eastern Venezuela foreland basin, while southward, near the craton, no major deformation had occurred (González de Juana et al., 1980).

A key element of the foreland basin fill, related to its evolution, is its syntectonic character (Miall, 1990). For instance, the presence of conglomeratic alluvial sequences, such as those of Los Jabillos Formation in the Eastern Venezuela foreland basin, may represent major phases of basin alluvial sedimentation that could be related to uplift pulses. The Los Jabillos Formation (early Oligocene) provides the first recorded stratigraphic evidence of uplift in the Eastern Venezuela foreland basin, but later conglomeratic intervals have also been registered at the base of each sedimentary cycle during the Tertiary evolution of the basin, suggesting that the deposition and associated subsidence of the foreland basin was effectively continuous through renewed pulses probably reflecting the advance of the nappes over the continent.

The bulk of sediments in the Cretaceous Eastern Venezuela basin were derived from the southern cratonic area of Guayana and its western extension, whereas in Tertiary times the adjacent growing thrust and fold belt became a new source of sediments; although not easy, dating this time-span is very important to understand the evolution of the foreland basin. The Miocene formations evidently show the presence of sediments of a northern proximal provenance, which means that by the Miocene the Eastern Serranía del Interior was already a positive feature in northern Venezuela, but the collision process might have started at least in early Oligocene. The maximum subsidence of the basin occurred during the mid Miocene; to further explore this matter, the relationship between sedimentation and subsidence in the Eastern Venezuela foreland basin is studied in Chapter 3.

A recent model of Eastern Venezuela basin evolution from Summa et al. (2003, Fig. 5) nicely illustrates the tectonic and structural evolution of eastern Venezuela along a line of generalized section that runs across the Eastern Venezuela basin, from the edge of the Guayana Shield outcrop up to El Pilar fault zone. A very brief summary of the main features and stages of this process, from Late Cretaceous to Present (see Fig. 2.9), follows herein:

- 92 Ma: Cretaceous sedimentation occurred in a passive margin setting above Jurassic and Early Cretaceous rift fill. Between 92 and 20 Ma several important disruptions to this “passive” margin occurred (Speed, 1985) as our subsidence data also support, mainly seen in the subsidence curve of well QUI (Fig. 3.8B and 3.9B) where I have identified at least 2 episodes of tectonic subsidence (early Oligocene and early Miocene) that could be interpreted in terms of lithospheric loading of the continental South American plate on its northern margin.
- 20 Ma: Allochthonous nappes, approached from the northwest as the Caribbean plate was moving eastwards. These were emplaced onto the South American plate, and the Tertiary Eastern Venezuela basin represented by a deep foreland flysch trough was formed.

- 15.5 Ma: Oblique convergence between the Caribbean and South American plates continued to drive shortening, as reflected by the obduction of Caribbean nappes (present-day Araya-Paria metamorphic rocks exposed at the Coastal Cordillera) in mid Miocene. In this model, tectonic uplift occurred during times of significant convergence between the Caribbean and South American plates. During times of relatively low convergence along the transform boundary, the relaxation of transpressive stresses allowed for regional isostatic rebound. Major regional unconformities during 15.5 and 10 Ma may be attributed to these isostatic uplift events. Interpretation of seismic reflection data indicates that thrust faults in this area ceased to be active shortly after 15.5 Ma.
- 10 Ma: Fault-related and isostatic processes continued to drive regional uplift and erosion, with the development of the regional unconformity at around 10 Ma. The inferred hinge-line separating regions of significant uplift and erosion from those that primarily subsided shifted southward from the leading edge of the Caribbean allochthonous toward the region near the southern limits of the modern Serranía del Interior.
- Present time: The Serranía del Interior remains a significant topographic feature, with the El Pilar fault as the tectonic boundary that separates, at the surface, parautochthonous rocks of the Serranía del Interior from allochthonous metamorphic rocks of the Araya-Paria peninsula. The axis of the Maturín basin has shifted slightly southward, with a thick Pliocene section deposited there by the eastward-migrating proto-Orinoco river system south of the deformation front.

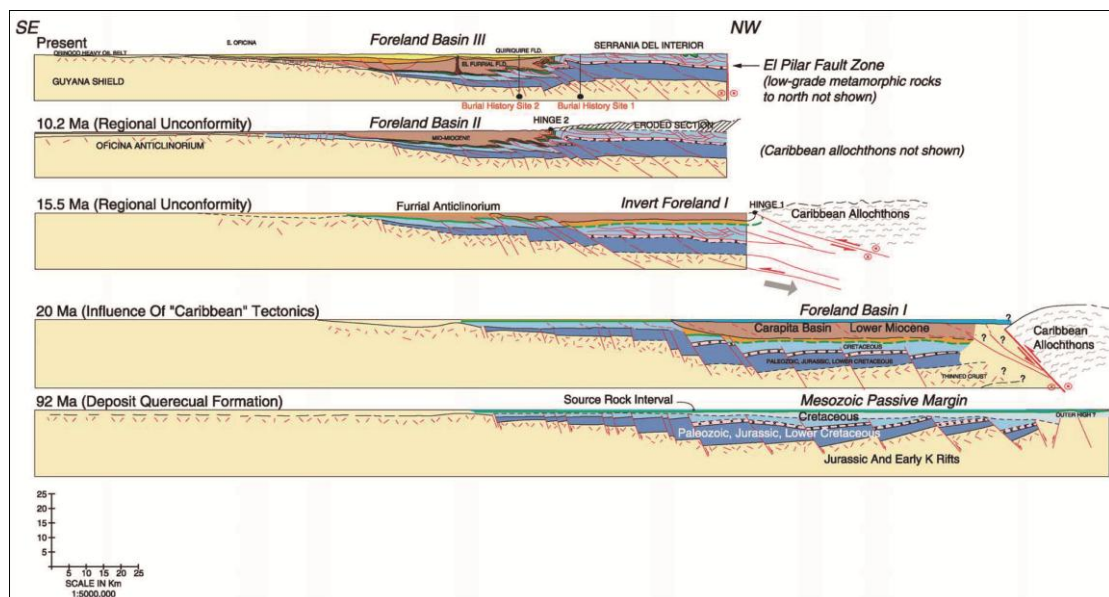


Figure 2.11. Geological cross sections depicting the tectonic and structural evolution of the Eastern Venezuela basin. Stratigraphy is highly generalized. Restored fault geometries are based in part on quantitative restorations of seismic-based cross-sections. (Taken from Summa et al., 2003)

2.9. SEISMICITY IN EASTERN VENEZUELA

This section is devoted to investigate the distribution of the seismic activity below eastern Venezuela for focal depths of 0-20 km, 20-80 km and greater than 80 km, as shown in Figures 2.12, 2.13 and 2.14. Relating the seismicity shown on these maps to the main structural features in eastern Venezuela (Figure 2.4) it can be observed that near shallower seismicity (Fig. 2.12) is mostly concentrated along the eastern segment of the El Pilar fault (from 63° W eastwards) and NW-SE strike-slip faults as Los Bajos in the Paria Gulf. Deep seismicity (Fig. 2.14) is mostly concentrated around 11°N – 62.25°W, north of the Paria peninsula, just at the southernmost extreme of the Lesser Antilles Arc (Fig. 2.13 and 2.14).

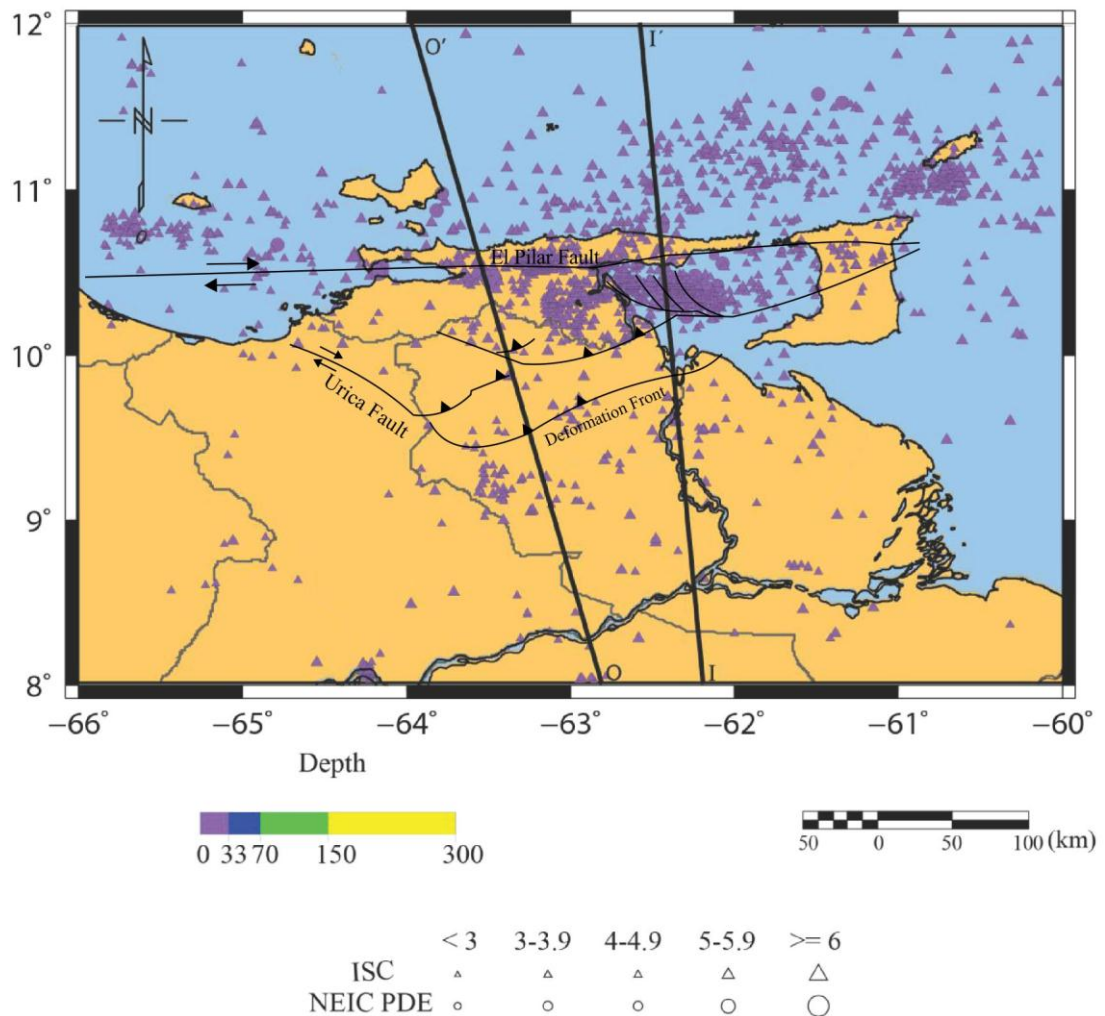


Figure 2.12 Distribution of seismicity in Eastern Venezuela. Focal depths 0-20 km

Deep focal mechanisms related to the Lesser Antilles Arc extend northwestward off the Trinidad Island and the eastern Venezuela coast (Wadge and Shepherd, 1984; Speed, 1985; Westbrook and McCann, 1986). Dextral strike-slip is active only as far east as the Gulf of Paria, and not within or east of Trinidad Island (Russo et al., 1993). On land and south of the El Pilar fault, mainly from 10°N southwards the seismicity is diffuse. It is also noticeable that high magnitude seismicity (> 5) is scarce and diffuse.

Seismicity data obtained from the Cariaco earthquake of June 1997 improved greatly the knowledge about the structure of El Pilar fault zone, which appears to be a high angle fault, extending northwards at depths of the order of 10-12 km (Romero et al., 1998).

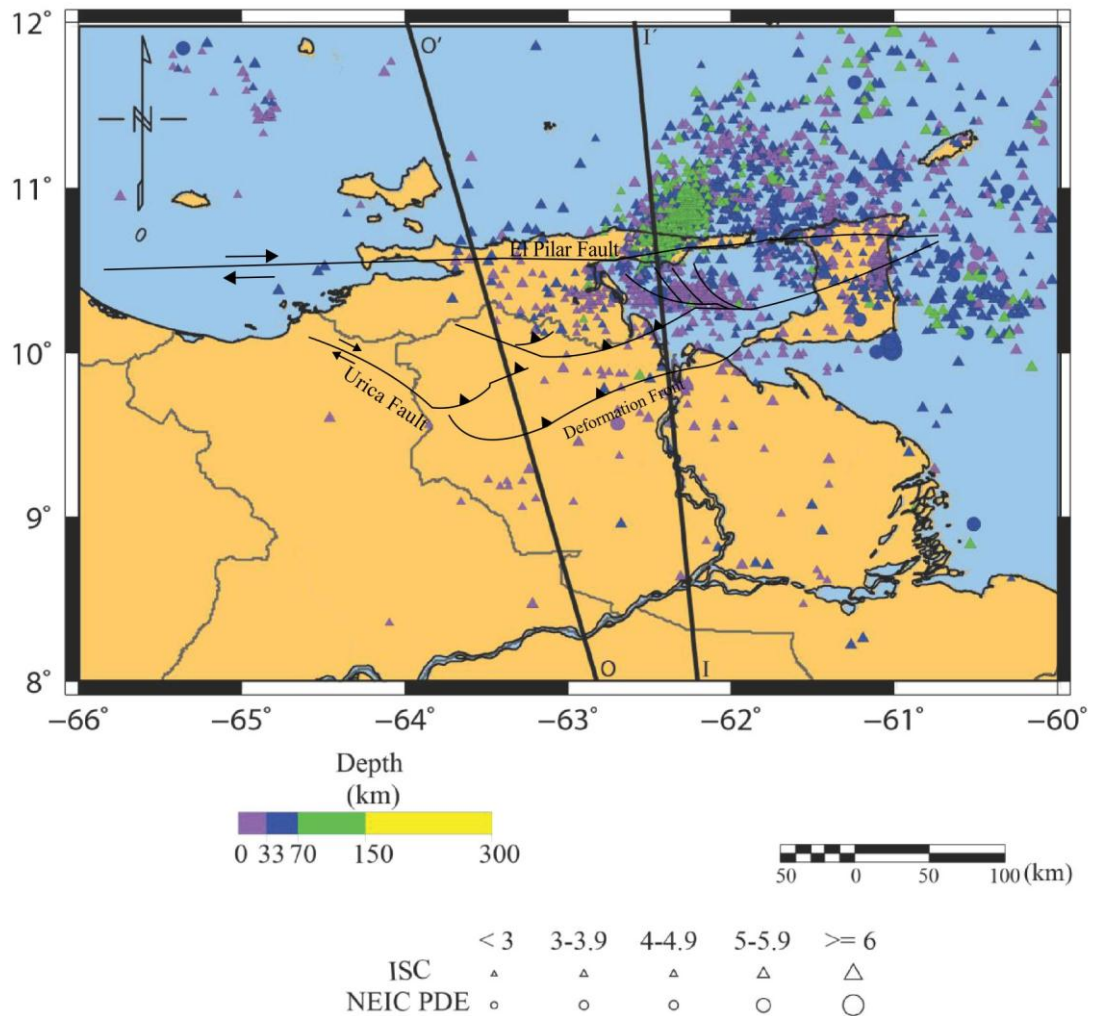


Figure 2.13 Distribution of seismicity in Eastern Venezuela. Focal depths 20-80 km depth.

Earthquake focal mechanisms obtained for events along El Pilar fault show that they are effectively restricted to the upper crust and indicate right-lateral strike-slip on nearly vertical planes (Audemard, 2006; Russo et al., 1993; Speed et al., 1991). According to Audemard (2009) the geometry of the El Pilar fault is an inheritance of an old high-angle thrust fault related to the collision stage of the margin. It must be also underlined that there are no records of very large earthquakes in eastern Venezuela during the last 5 centuries, which suggests that the segmentation of the fault by transpressional or transtensional relays reduces the size of the rupture area (Audemard, 2007).

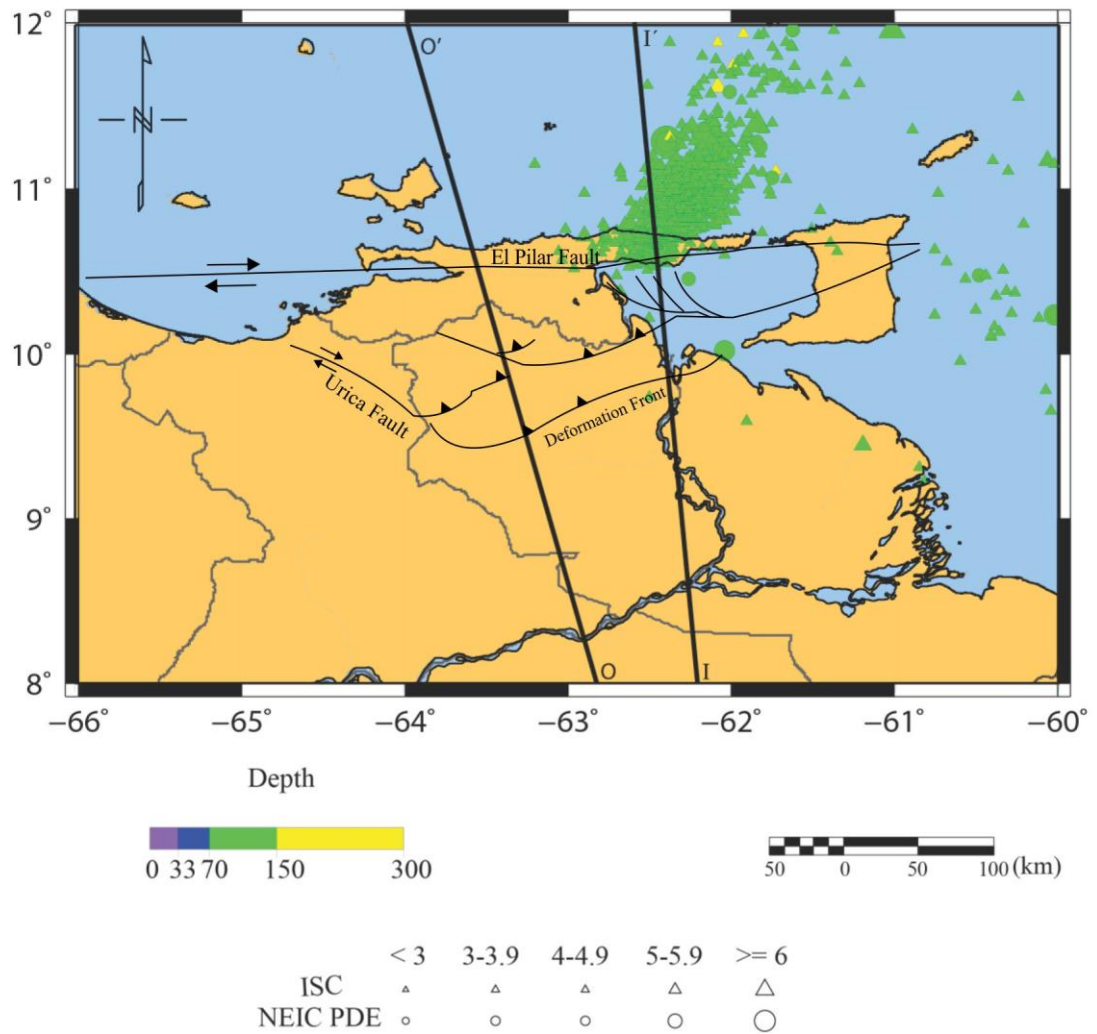


Figure 2.14. Distribution of seismicity in Eastern Venezuela. Focal depths >80 km depth.

Jouanne et al. (2011) suggest a shallow locking depth or an aseismic component along the upper part of the El Pilar fault and based on the asymmetry of displacement gradients on both sides of the El Pilar fault suggest that the fault is not vertical at the lithospheric scale. In their opinion, aseismic displacement could affect the ductile part of the El Pilar fault dipping northwards below the Araya-Paria peninsula and Margarita Island.

CHAPTER 3

SUBSIDENCE IN THE EASTERN VENEZUELA BASIN

3.1. SEDIMENTARY BASINS.

3.1.1. SEDIMENTARY BASINS CLASSIFICATION.

Nowadays, within the plate tectonics frame of reference, three main criteria are used to classify most sedimentary basins, namely: the type of crust on which the basin rests, the position of the basin relative to the plate margins and the type of plate interaction occurring during the process of sedimentation if the basin lies close to a plate margin (Dickinson, 1974; Sleep, 1974; Bally and Snelson, 1980; Miall, 1990; Allen and Allen, 2000). The first of these parameters concerns the type of substratum below the sedimentary basin; in this context the normal continental crust and the standard oceanic crust are two end members, with a range of transitional-type crust in between (Menard, 1967; MacDonald, 1972). In general, basins floored by continental crust develop typically shallow marine to non-marine sedimentation, while those basins overlying oceanic crust are all of deep marine facies.

The second factor deals with the location of the basin over a rigid lithosphere or a mobile belt and the third one emphasizes the plate boundary behaviour and the processes occurring at its margins. The fact that these three factors can change through time implies that different stages in a basin evolution might be simply superimposed in the same orogenic belt. The Eastern Venezuela basin is a good example of this. Following Miall (1990) classification, the current Eastern Venezuela basin, as being developed during collision and suturing, can be defined as a “foreland basin”, resting on the continental South American crust. However, the Tertiary Eastern Venezuela foreland basin has been superimposed on the precursor Cretaceous basin developed over the continental margin of northern South America, after the North and South American plates separation; so, this ancestral Eastern Venezuela basin was a passive continental margin (Atlantic ocean-type margin basin).

The whole development of the Eastern Venezuela basin can, then, be explained through two stages in evolution: the first, when the basin

developed as a "passive-margin basin" covering a span of time since pre-Cretaceous times to the early Eocene, and a second period, from early Eocene to Present time, when it evolved as a "foreland basin".

For each stage in the basin evolution the following three aspects should be considered:

- (1) The stratigraphy and structure of the basin.
- (2) The plate tectonic setting and the processes involved in the genesis of the basin.
- (3) The mechanisms of crustal subsidence.

The prime and basic concepts concerning the stratigraphy and structural characteristics of the Eastern Venezuela basin, through time, were outlined in Chapter 2; whereas, the following sections will be devoted to the principles of the other two aspects, which will be considered and integrated to the first one in this Chapter 3.

3.2. PASSIVE-MARGIN BASINS

Passive continental margins (Atlantic-type margins) are characterized by seaward thickening prisms of marine sediments overlying a faulted basement with syn-rift sedimentary sequences, often of continental origin. They overlie earlier rift systems which are generally sub-parallel to the ocean margins (Allen & Allen, 2000). The series of plate tectonic settings characterizing the successive stages of the process of continental splitting include graben and half-graben development and deposition of continental red-beds intercalated with volcanic flows. Once the zone of rupture has been established, rapid subsidence accompanied by deposition of evaporites occurs. A slow subsidence follows and may persist for perhaps 50-80 my. There is also a rapid accumulation of thick clastics as a basal phase (Dickinson, 1974; Schneider, 1972; Veevers, 1981).

Through time the margin continues evolving with its characteristic sedimentary facies over the continental shelf (paralic sediments, thickening of strata, carbonate platforms), slope (thin strata) and rise (dark shales, turbidites). When the strictly thermal subsidence is complete, absent other external forces, the margin remains in an intraplate realm facing an open ocean. The duration of the entire process seems to vary considerably depending on the regional spreading patterns.

Thus, the process of continental separation has led to the formation of a topographic depression, which if filled with sediments will become a sedimentary basin. Passive margins are formed in the context of continental break-up with formation of new oceanic crust between an extreme stretching of the continental crust at the time of break-up (thinning may be of the order of a factor of 5 adjacent to the oceanic crust, decreasing landwards) and subsequent thermal subsidence (also decreasing landwards) as the underlying upper mantle hot spot cools (time constant about 60 my). Through this process a zone of transitional crust and lithosphere has been developed between the continent and the adjacent oceanic basin. Sediments deposited over this type of transitional crust will then overlay basement rocks of continental blocks of uncommon crustal thickness.

3.3. FORELAND BASINS

These basins are commonly related to continental collision in the plate tectonic framework. In compressional regimes where either continent-continent or continent-arc/terrane collisions are developed, the edge of the continental plate is deformed into a fold-thrust belt (Dewey, in Miall, 1990). The crust may, then, be thickened by a factor of two, giving rise to a mountain belt where metamorphic and plutonic rocks of the arc, as well as upthrust masses of different rock nature, may be exposed. Due to the loading of the superimposed thrust sheets, the craton responds by flexure of the lithosphere (Beaumont, 1981). The trough formed through this process is filled with sediments derived from the adjacent positive areas

and the sediment load itself contributes to the crustal depression; as the process continues, undeformed continental basement and cover rocks may also be affected by folding and thrusting, becoming then a contributory source of sediments to the basin. The basins resulting from these collision processes are floored by continental crust. Foreland basins are then easily defined as the sedimentary basins lying between the front of a mountain chain and the adjacent craton (Allen et al., 1986).

The depositional style and lithological composition of the sediments in a subsiding foreland basin are strongly influenced by tectonism and climatic variance (Miall, 1990). Tectonism and basin subsidence control the regional architecture of the trough, as well as climate influences weathering, eustatic sea-level and variability of sediment discharge within the basin (Schwans, 1988; Galloway, 1989). The greatest thickness of foreland basin fill occurs adjacent to the thrust front as a consequence of greatest subsidence nearest the load (Miall, op. cit.).

When the upper crust is thrust-faulted, the subsidence and complementary uplift may also be caused by the vertical component of the net equal but opposite force distributions acting on the reverse fault plane each time the fault moves in response to compressive shortening of the elastic layer, rather than gravity loading. As Bott (1990) has shown, surface downflexure produced by slab downpull may give rise to wide borderland sedimentary basins such as the Po basin.

3.4. MECHANISMS OF BASINS FORMATION.

3.4.1. AN INTRODUCTORY REVIEW.

Various mechanisms have been proposed to account for the formation of sedimentary basins, the subsidence of the basin being a common factor, and hence an essential parameter to evaluate. In general, three main causative factors appear to be involved in the subsidence of basins; these are:

(1) Thermal events: provide a mechanism to explain the apparent exponential decay of the rate of subsidence with time, after the primary thermal event, which may be due either to the uplift of the lithosphere by thermal expansion or else due to crustal thinning, being followed by erosion and subsequent cooling of the lithosphere which, then, subsides isostatically (Sleep and Sneel, 1976; McKenzie, 1978; Turcotte, 1980).

Additional effects contributing to thermal subsidence might include the injection of dense basic or ultrabasic intrusives (Sheridan, 1969; Bally, 1980) and the metamorphism of lower crustal rocks to eclogite or granulite facies (Falvey, 1974; Haxby et al., 1976). However, processes other than erosion, intrusions or metamorphism should be invoked if thicknesses of sediments exceeding 4 km are to be taken into account (Bott, 1980).

McKenzie (1978) has suggested that the subsidence associated with the development of a basin is initiated by stretching of the continental lithosphere, which causes thinning of the crust and passive upwelling of hot asthenosphere. Then, the rapid initial tectonic subsidence is followed by a slower "thermal" subsidence, at a rate proportional to the square root of time, as conduction re-establishes the normal geothermal gradient (McKenzie, op. cit.; Sclater et al., 1971). This model contains one adjustable parameter β which is the amount of extension, as illustrated in Figure 3.1, and exhibits a close resemblance to the thermal models used to explain the subsidence in oceanic regions (Parsons and Sclater, 1977). Following McKenzie (1978) the uniform extension model has been applied to investigate the subsidence history in a variety of basin settings and conditions (Jarvis and McKenzie, 1980; McKenzie et al., 1980; Keen and Barret, 1981; Royden and Keen, 1981).

(2) Gravity loading: attributes the subsidence of the lithosphere in response to a load (Walcott, 1972; Steckler & Watts, 1978; Turcotte, 1980; Watts, 2001). In its simplest form, this hypothesis assumes local Airy isostasy. The main role of the load is amplifying the subsidence caused by

other primary mechanism (Watts and Ryan, 1976) by a factor between two and three, depending on the mean density of the sediments filling the basin (Bott, 1980). In this situation the total thickness of marine deposits that may accumulate in the trough is given by:

$$t = d ((\rho_m - \rho_w) / (\rho_m - \rho_s)) \quad (3.1)$$

where d is the initial water depth, and ρ_m , ρ_w and ρ_s are the upper mantle, water and sediment densities respectively, as illustrated in Figure 3.2.

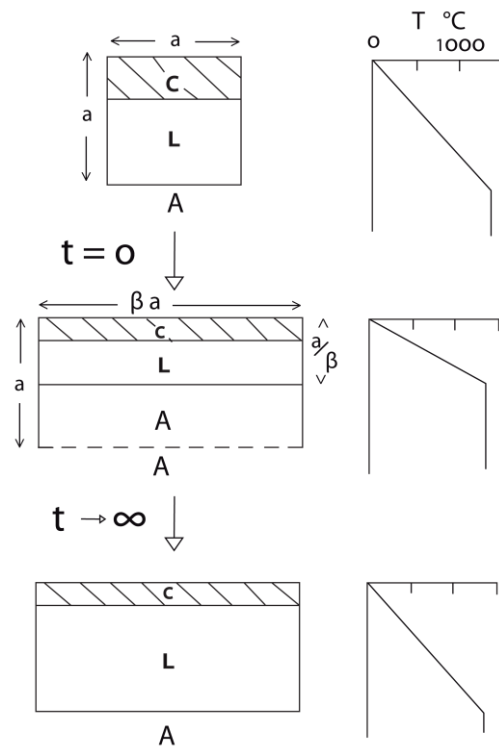


Figure 3.1. Simple stretching model, after McKenzie (1978).

Sketch to show the principal features of the subsidence model. At time $t=0$ a piece of thermally equilibrated continental lithosphere is extended by β . Since the temperature of the material remains unchanged during extension, isostatic compensation causes upwelling of hot asthenosphere. Cooling of this hot material produces subsidence as the temperature perturbation decays. Continental crust is assumed to be conserved during extension and its radioactivity neglected. The discontinuity in the temperature gradient between the lithosphere and the asthenosphere is an artefact of the model which could be removed by considering the details of the convective heat transport in this region. However, the heat flux and subsidence would be little affected.

A more adequate approach is perhaps to consider the lithosphere as a thin elastic plate and investigate its flexure in response to sediment loading by elastic beam theory. The flexural rigidity D is the parameter that describes the mechanical behaviour and strength of the lithosphere and is defined as:

$$D = E \cdot T_e^3 / (12(1 - \nu^2)) \quad (3.2)$$

where E is Young's modulus, T_e is the plate thickness and ν is the Poisson's ratio.

Flexural models have been addressed by many authors (Walcott, 1970a; Watts and Ryan, 1976; Turcotte and Ahern, 1977; Turcotte, 1980; Beaumont, 1981; Karner and Watts, 1983; Watts, 2001) and I will revert to them in detail when discussing the flexural models at the Eastern Venezuela foreland basin.

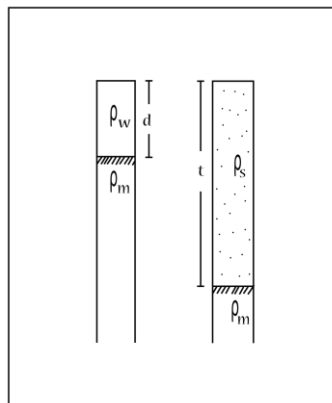


Figure 3.2. Diagram to illustrate the relation $t=d((\rho_m - \rho_w) / (\rho_m - \rho_s))$ in gravity loading mechanism assuming Airy isostasy, where ρ_m is the mantle density, ρ_w is the water density and ρ_s is the sediments density.

(3) Response of the crust to stresses: Applied forces of whatever origin cause stresses which result in deformation or strain. The simplest view of applied forces is of those due simply to the weight of an overlying

rock column, known as *lithostatic stress*. The difference between the actual stress and the lithostatic stress is a tectonic contribution known as *deviatoric stress*, which can be either tensile or compressive. (Allen and Allen, 2000). The release of these lithospheric deviatoric stresses is the prime cause of origin of most continental basins (Bott, 1976). Tensional stress release is associated with continental break-up and plateau uplifts within continental interiors as in the present East African rifting zone, and probably during the Early Cretaceous in northern Venezuela. Compressional stress release applies particularly to continental regions adjacent to converging plate boundaries, including transpressional ones as in eastern Venezuela since the Early Tertiary.

The shelf subsidence near the continental margins by thinning of the crust either by stretching during the continental splitting or by the oceanward creep of continental crustal material is a response of the crust to stresses acting upon it (Bott, 1971a-b, 1980; Bally, 1980). The resulting isostatic subsidence of the continental side of the continental margin may lead to the formation of a sedimentary basin. It is always possible that more than one mechanism operates in passive margin evolution. However, a basic model of lithospheric extension followed by cooling is the starting point for analysis of passive margin subsidence.

3.5. SEDIMENTATION vs. SUBSIDENCE IN THE EASTERN VENEZUELA FORELAND BASIN

A quantitative analysis of Cenozoic sedimentation and subsidence has been carried out in the Eastern Venezuela foreland basin; it is based on the geological evaluation of: 160 boreholes, structural maps of different horizons at depth, facies distribution maps of Oligocene, lower, middle and upper Miocene to Pliocene sedimentary cycles and seismic sections.

Most of this material was made available to me from unpublished information gathered during the petroleum exploration of the area by Petroleum Companies or reported by Arstein et al. (1982) and Muñoz

(1985). Data from offshore Venezuela boreholes was taken from Talukdar (1983) and Goddard (1988)

3.5.1. TERTIARY SUBSIDENCE OF EASTERN VENEZUELA FORELAND BASIN

In an attempt to estimate the time and magnitude of the subsidence of the Eastern Venezuela foreland basin, diagrams of thickness, depth to basement and rate of sedimentation, all versus time, were constructed for the 160 wells analyzed in this work; a location map of these boreholes is shown in Figure 3.3. All available details of the boreholes I have used in the compilation, synthesis and analysis of the passive margin and foreland basin sediments are fully listed in Appendix A.1.

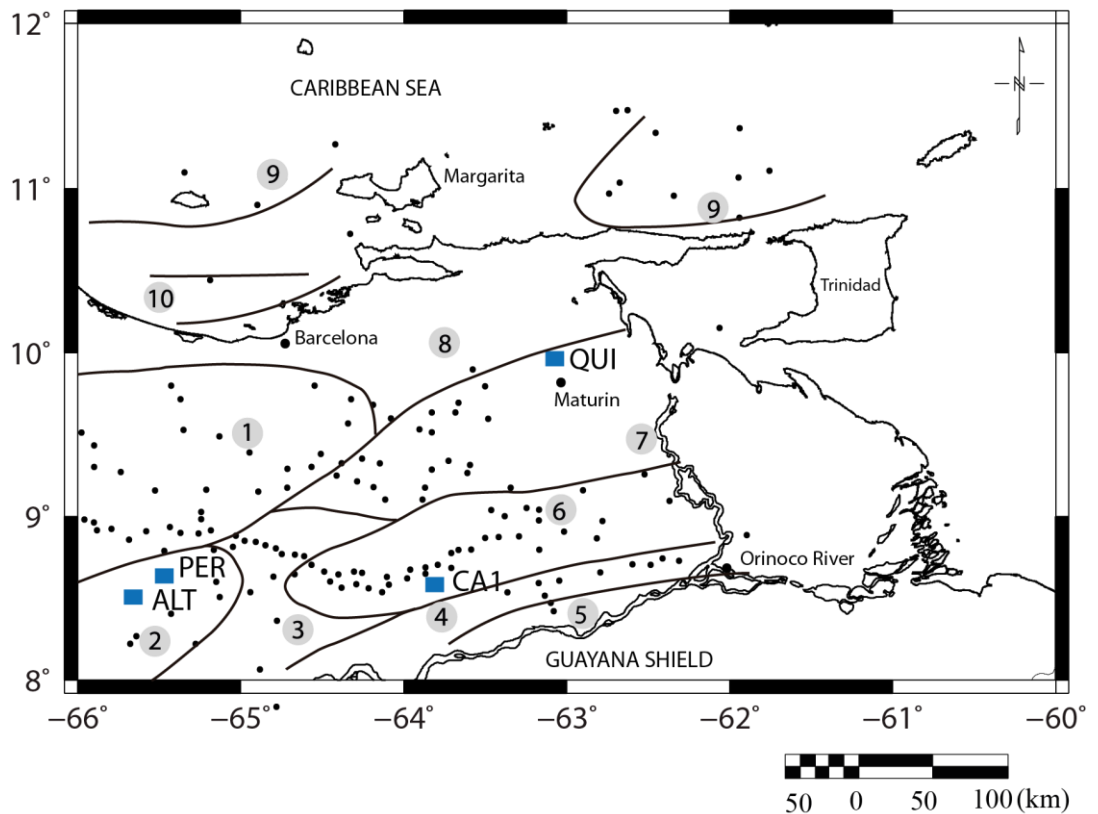


Figure 3.3. Borehole-well location map and zonal distribution according to sedimentation-rate in the study area. Numbers 1 to 10 in grey circles are identification of subzones 1 to 10 respectively. Dots indicate well location. Blue squares indicate backstripped wells.

Once the complete set of sedimentation-subsidence diagrams was analyzed and correlating among themselves, it was possible to delimit 8 subzones with distinct characteristics in terms of stratigraphy, subsidence pattern and basement of the Eastern Venezuela foreland basin, plus 2 subzones offshore north of Venezuela. Figure 3.4 shows this zonal distribution based on generic sedimentation-rate vs. time histograms (Appendix A.1); in addition, a generalized stratigraphic column of each subzone is depicted.

A detailed description of subzones 1 to 10 is given in Appendix A.1. Summarizing, the evidence obtained from the sedimentation-subsidence rates zonal distribution in Eastern Venezuela, lead to the following conclusions:

(1) Two distinct basement units underlie the Eastern Venezuela basin, namely: the Paleozoic-Precambrian section or directly the Precambrian craton. The first is preserved in the area west of 64.5° W (subzones 1-2-3), while towards the east (subzones 4-5-6) the basement drilled is the Precambrian Guayana Shield. To the north, beneath the foreland deformed belt, although not yet drilled because of the thick Cretaceous-Cenozoic sedimentary section deposited there, the Paleozoic-Precambrian basement might be present. Farther north, offshore Venezuela and Trinidad, pre-Cretaceous igneous-metamorphic rocks resembling those exposed in the Araya-Paria peninsula have been drilled; this fact suggests the northwards extension of the igneous-metamorphic terrane.

(2) Cretaceous sedimentary rocks are widespread all over the basin, except in subzones 4 and 5, bordering the craton, south of the hinge line. There, middle Miocene and upper Miocene-Pliocene strata overlie directly the Precambrian basement. This might be interpreted not only as a result of erosion and deposition in transgressive marine facies over the shield (González de Juana et al., 1980; Arstein et al., 1982), but as a probable consequence of wedges of younger sediments being pushed from the north

in the foreland deformed belt. The Cretaceous sedimentary sections thicken towards the north, where they are definitely affected by the compressive regime prevailing in the area.

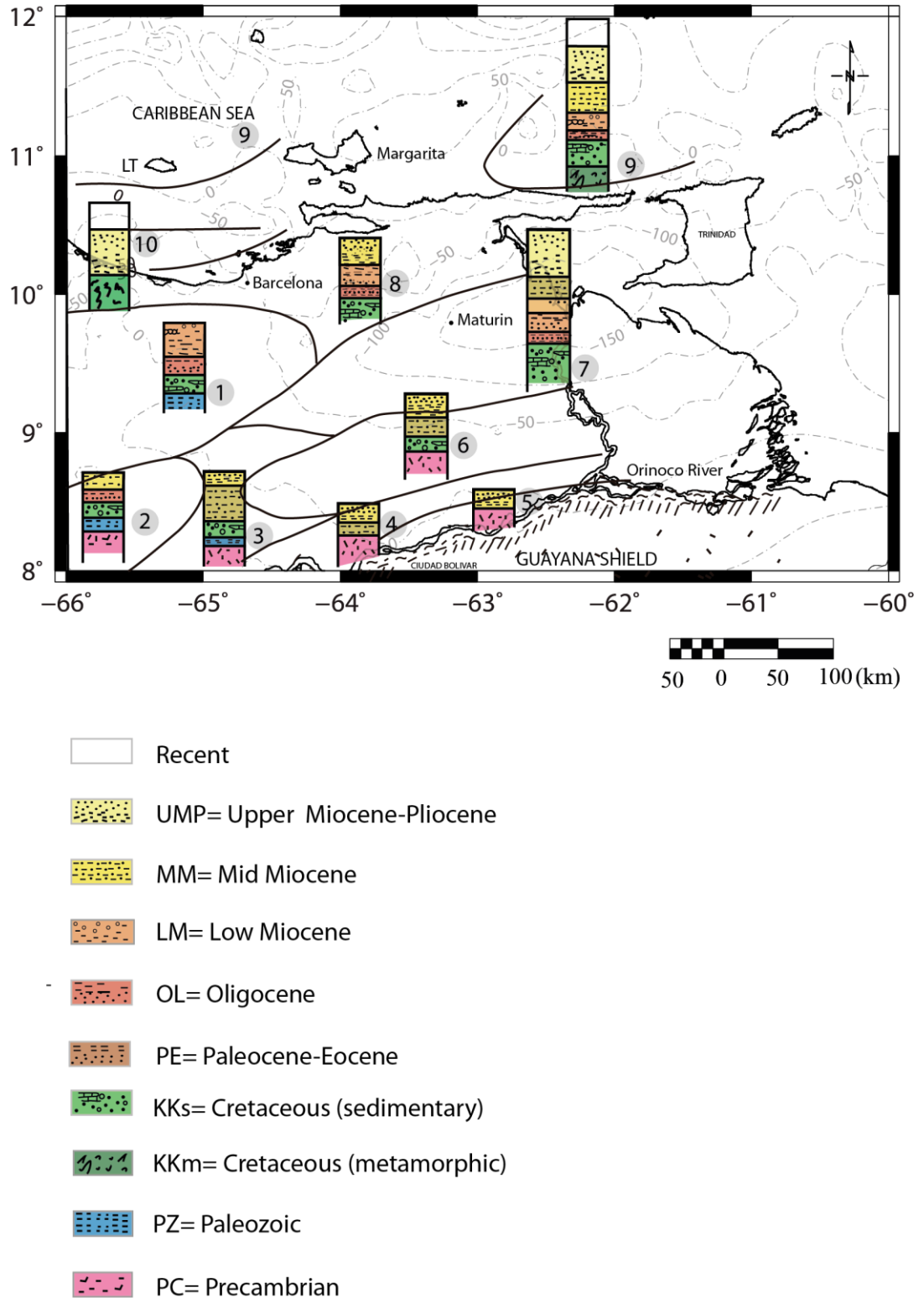


Figure 3.4. Stratigraphic sections characteristic of subzones 1 to 10 in eastern Venezuela. Dashed contours are free-air anomalies in mGal.

(3) The Paleocene-Eocene sequence has been preserved only locally (subsurface, subzone 6) and in the Serranía del Interior, confirming the hitherto held view that a period of erosion affected the whole area during these times.

(4) The Oligocene to lower Miocene sequence was deposited over most of the basin area, north of the present latitude 9°N. The maximum thicknesses of Oligocene -lower Miocene deposits are found in the western parts of the basin (subzone 1) where a well-developed trough, probably related to the Guárico Frontal thrust, was in the process of being filled.

(5) The middle Miocene sedimentation is preserved all over the basin except in its northwestern rim, and the maximum thicknesses of sediments appear to be located along a north-easterly trend, running through Maturín. This period records the maximum sedimentary rates and associated subsidence of the foreland basin. From the upper Miocene to the Pliocene the sedimentation was continuous throughout the foreland basin, whose depocenter was located along an ENE belt at the present latitude of 9.5° N.

Figure 3.5A illustrates the passive margin phase of the Eastern Venezuela basin. In the distribution of sediments during the Oligocene (Fig. 3.5B) it is shown that maximum deposition occurred around 10°N. Evidence of no-deposition in zones 3-4-5-6 (Oligocene) and also zone 2 (lower Miocene, Fig. 3.5C) is probably consequence of uplift in response to the loads applied further north. Middle Miocene axis of sedimentation has migrated southward since the Eastern Venezuela basin was closed because of the Eastern Serranía del Interior uplift (Fig. 3.5D).

Sedimentation continued through the Present time, and the depocenter of the basin lies nowadays over a wide area, offshore eastern Venezuela, in the Gulf of Paria and the Orinoco delta front, clearly coincident with the minimum free-air anomaly overprinted on maps of the area of study (Figures 3.5 A-F, where dashed contours are free-air anomalies in mGal).

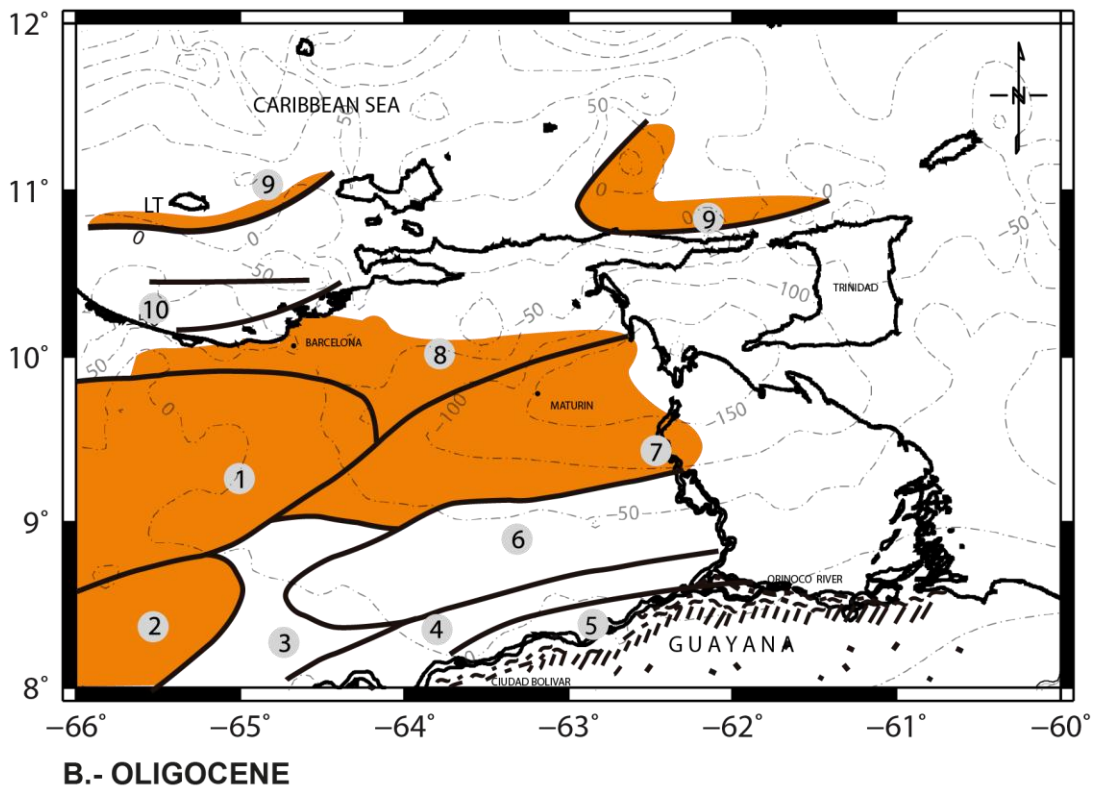
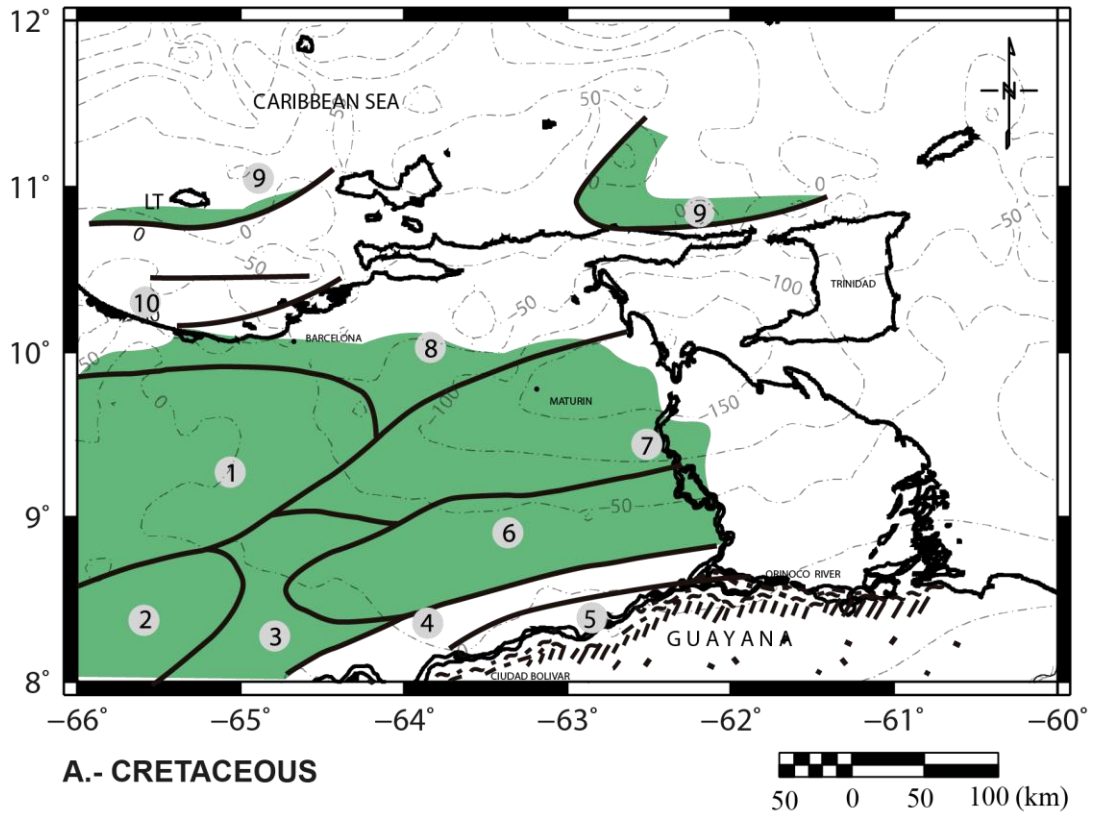


Figure 3.5A-B. Sequence Cretaceous to Present time in Eastern Venezuela illustrating the zonal distribution of sediments according to sedimentation-rate in the study area. 3.5A. Cretaceous. 3.5B. Oligocene. Dashed contours are free-air anomalies in mGal.

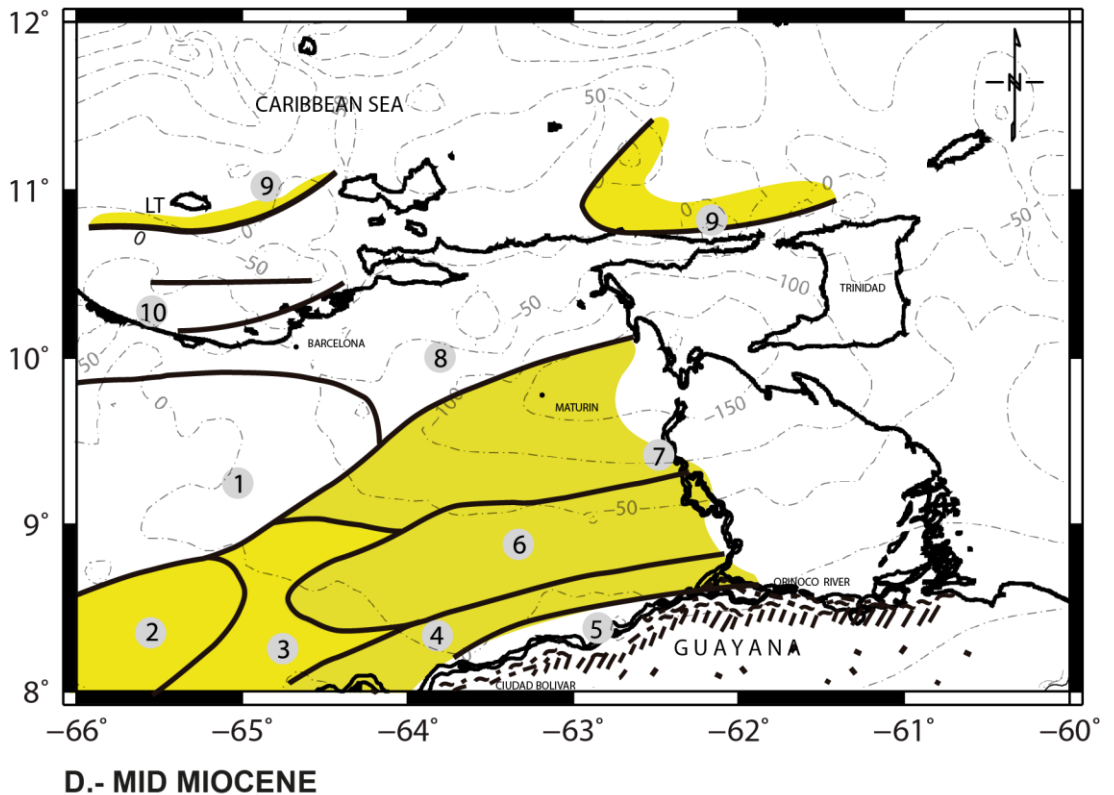
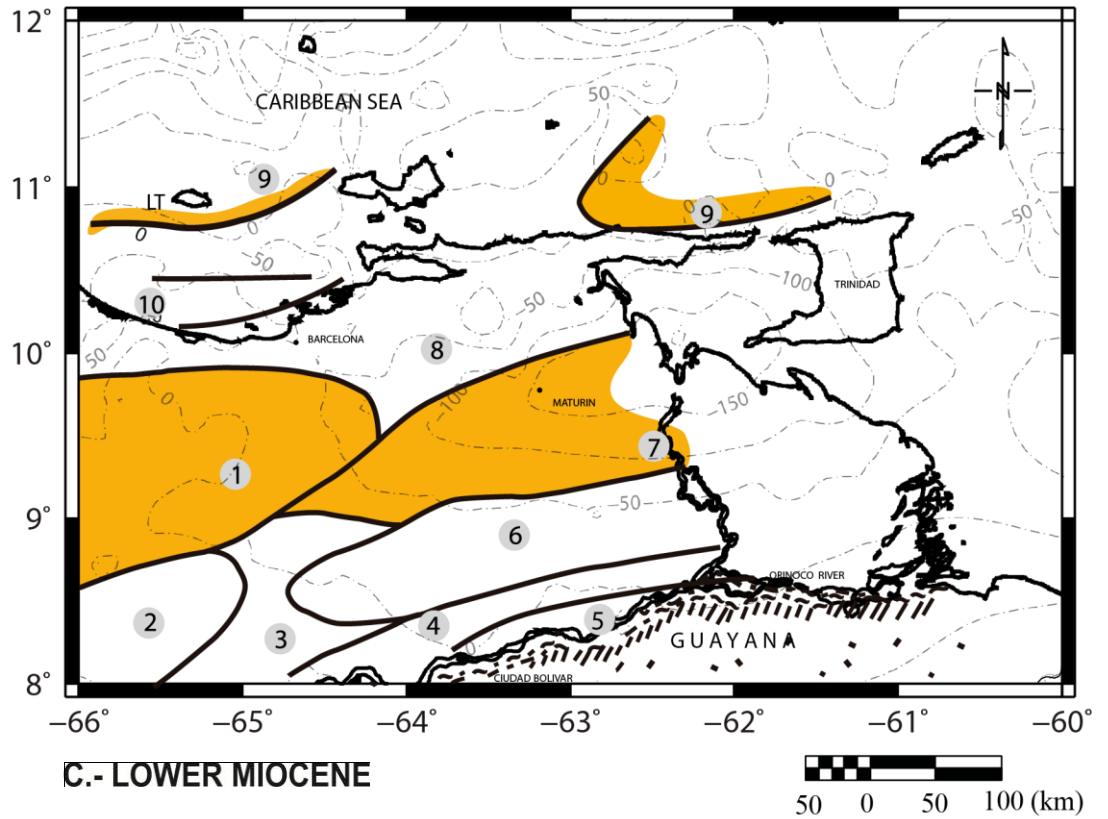


Figure 3.5C-D. Sequence Cretaceous to Present time in Eastern Venezuela illustrating the zonal distribution of sediments according to sedimentation-rate in the study area. 3.5C. Lower Miocene. 3.5D. Mid Miocene. Dashed contours are free-air anomalies in mGal.

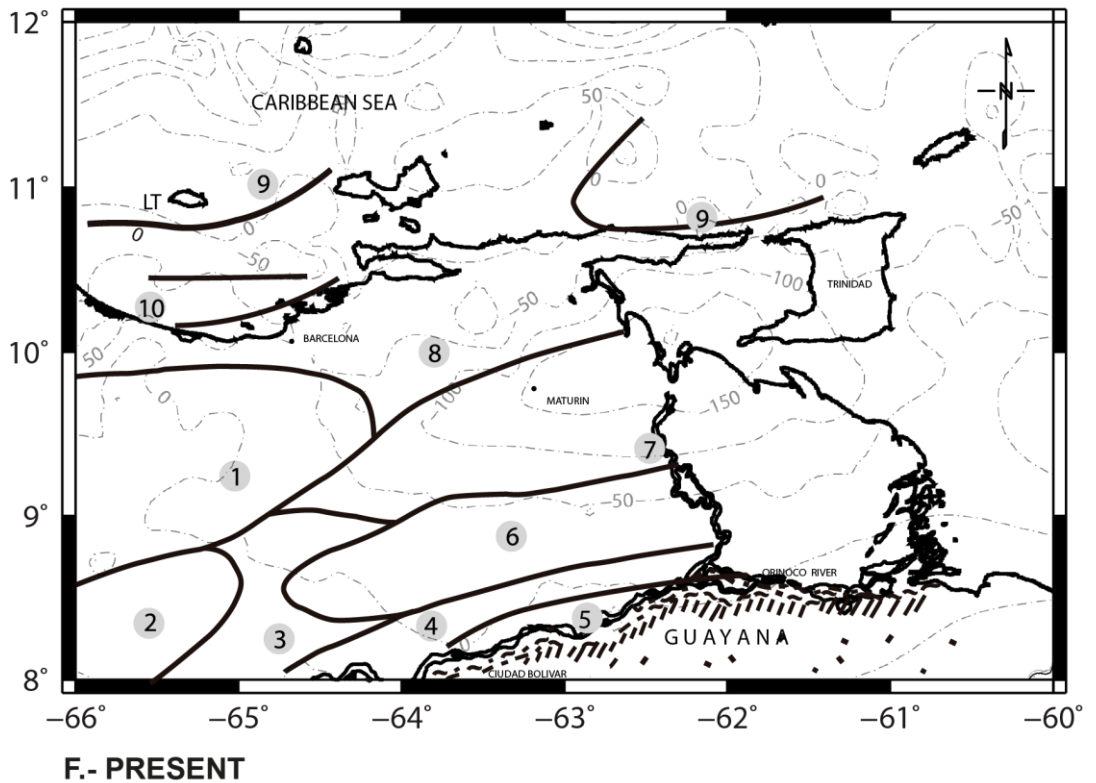
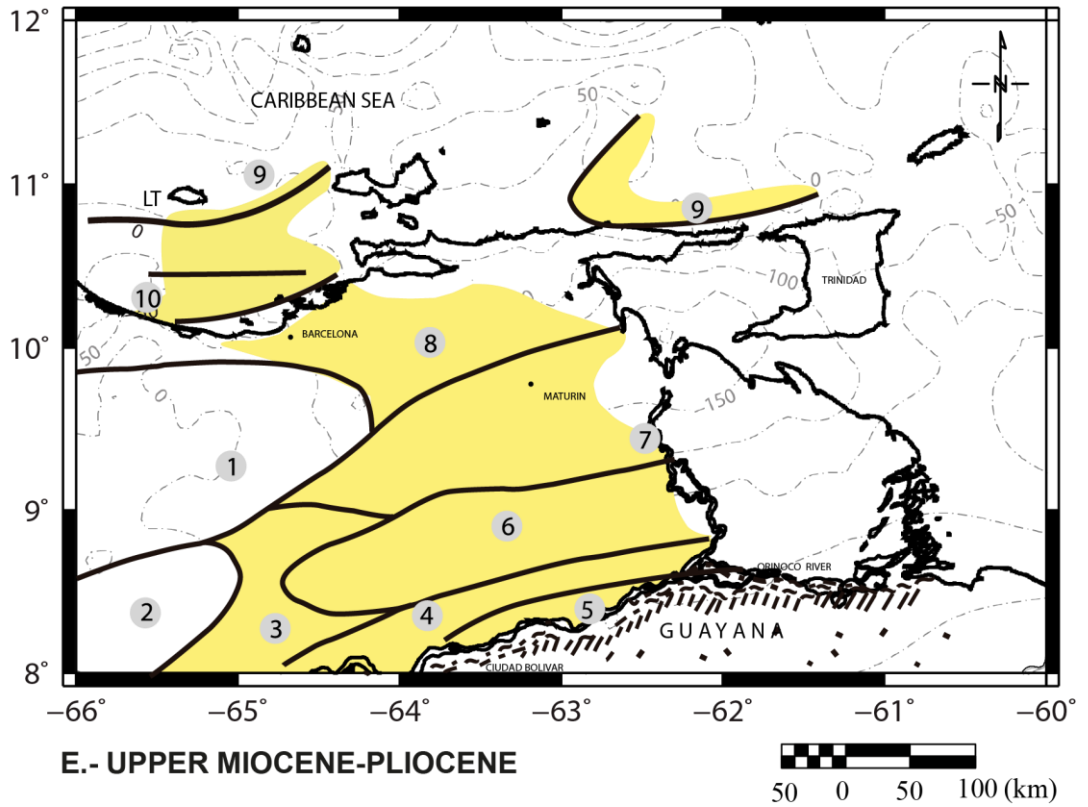


Figure 3.5E-F. Sequence Cretaceous to Present time in Eastern Venezuela illustrating the zonal distribution of sediments according to sedimentation-rate in the study area. 3.5E.Upper Miocene-Pliocene. 3.5F.Present. Dashed contours are free-air anomalies in mGal.

An interpretative map showing the distribution of sedimentary thickness across the Eastern Venezuela basin, modified after Summa et al. (2003) is depicted in Figure 3.6. This map is based on a compilation of constraints from petroleum drilling, seismic sections and published maps, with interpretations of Paleozoic and basement penetrations from the literature, and estimates of top crystalline basement from magnetic data. Basement is variable, but usually consists of Precambrian or Paleozoic crystalline rocks. The main depocenters shown in this top of basement map are located at the Espino graben (up to 10 km depth), the Maturín foredeep (more than 10 km depth) and offshore Trinidad, Columbus basin (some 12 km depth). Contours of free-air anomaly have been overprinted on this map to illustrate the relation between the depocenters and the minimum values of gravity.

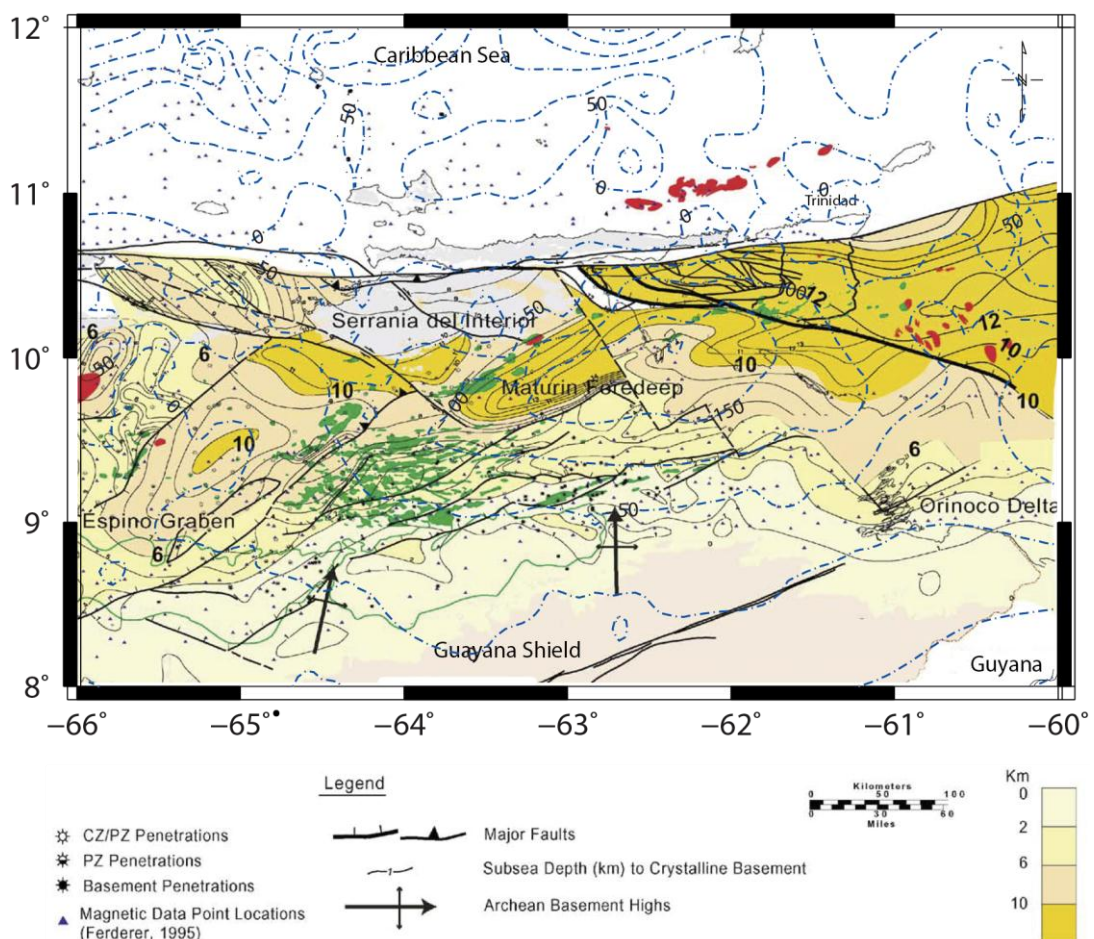


Figure 3.6. Top Basement Structure - Total Sediment Fill, Eastern Venezuela. Modified after Summa et al. (2003). The thickest sediment fill lies within the free-air anomaly low showed in dashed blue lines.

3.5.2. SEDIMENT LOADING EFFECT.

The geohistory analysis, as Allen and Allen (2000) summarized, aims at producing a curve for the subsidence and sediment accumulation rates through time. In order to do this, three corrections to the present stratigraphic thicknesses need to be carried out:

(1) Decompaction: present-day compacted thicknesses must be corrected to account for the progressive loss of porosity with depth of burial. The decompaction technique seeks to remove the progressive effects of rock volume changes with time and depth. As any compaction history, being affected by lithology, overpressuring, diagenesis, and other factors is likely to be complex, some general relationships to hold good over large depth ranges are needed.

(2) Palaeobathymetry: the water depth at the time of deposition determines its position relative to a datum (such as present-day sea level).

(3) Absolute sea level fluctuations: changes in the paleosea level, relative to today, also need to be considered.

In addition, the subsidence curves give an immediate visual impression of the nature of the driving force responsible for basin formation and development. Applying the technique of geohistory analysis or “*backstripping*” (defined by Allen & Allen (2000) as “*the exercise of partitioning the subsidence due to tectonics and that due to sediment loading*”) the effect of the sediment load on driving subsidence is removed, and the tectonic subsidence can be isolated.

The different types of sedimentary basins have varying tectonic subsidence and uplift curves. Rift-type basins tend to have concave-up curve with the subsidence fast early on after rifting and then slow later on. Foreland basins, in contrast, have concave-down curve with the subsidence slowest early on and then fastest later on. Strike-slip basins generally subside

rapidly and their backstripped curves show features of both rift-type and foreland-type basins.

Porosity variations with depth are defined by a function that decreases exponentially with depth (Sclater and Christie, 1980). The porosity ϕ at depth z is given by:

$$\phi = \phi_0 e^{-cz} \quad (3.3)$$

where ϕ_0 is the surface porosity and c (the reciprocal of the distance over which ϕ decreases by e) is a coefficient that is dependent on lithology and describes the rate at which the exponential decrease in porosity takes place with depth (Allen and Allen, 1990).

In reviewing the stratigraphy and mechanisms of evolution of the Eastern Venezuela basin, two main stages have been differentiated. The first, accounts for the development of the Cretaceous Eastern Venezuela basin as an Atlantic-type margin, and the second for the evolution of the Tertiary Eastern Venezuela foreland basin. To understand the complete process, it is necessary to distinguish the different factors contributing to the subsidence of the basin. In this context, it is important to evaluate the sedimentary loading effect, so that the subsidence due to other causes can be isolated.

An attempt was made to determine the history of subsidence in the Eastern Venezuela basin, following Steckler and Watts (1978), and Watts (2001). A model assuming local Airy isostatic response to the sediment load and accounting for the effects of sediment compaction was used, and the computations were made with the computer program developed by Waltham (2001). The subsidence curves representing the basement burial history are the total subsidence (cumulative depth to basement, shown in green plus yellow) and the tectonic subsidence after backstripping (without sea level and palaeobathymetric corrections, shown in green).

Data concerning the age of sediments, depth to different horizons, environment of deposition, and porosity-depth relation curve were obtained for the analysis of four wells in eastern Venezuela, PER, ALT, CA1 and QUI wells. These data were backstripped and also corrected using Vail et al. (1977) values for eustatic sea level, and palaeobathymetric data of the wells being studied (see Figure 3.3 for location, and Appendix A.2 for details about the computations with the computer program developed by Waltham (2001)). The subsidence curves of the four backstripped wells are shown in Figures 3.7A-B and 3.8A-B.

In spite of some uncertainties involved in the data, mostly regarding the initiation of rifting and the age of the sediments, these curves provide very useful qualitative information on basin evolution. In this particular case, the subsidence curves for the sequence underlying the foreland basin deposits (i.e. Late Cretaceous to early Oligocene) exhibit an initial high subsidence rate (except at well CA1) which decreases roughly exponentially with time and thus represents the passive margin stage of the Eastern Venezuela basin; within the limitations of sampling they are consistent with thermal subsidence, but more detailed well data would be necessary for proper assessment. No indication of a rift phase in well CA1 (Fig. 3.8A) is due to absence of information about older sequences in the well.

The resulting total and tectonic subsidence curves illustrate clearly that the subsidence in the Eastern Venezuela basin was concomitant with deposition during all the passive margin phase, and that a major contribution of tectonic loading was present from early Oligocene and renewed during the Mid Miocene. Wells in the south exhibit less pronounced subsidence and rebound trends in comparison to the well QUI in the north, which reflects the highest sedimentation rates (of the order of 20m/my in the Oligocene and >100m/my in the Miocene).

The onset of the foreland basin sedimentation is marked by the Oligocene subsidence which is presumably a response to the lithospheric loading of

the continental South American plate on its northern margin (Figures 3.7 to 3.8). There we can see how the magnitude of both, total and tectonic subsidence, vary across the basin increasing from south to north.

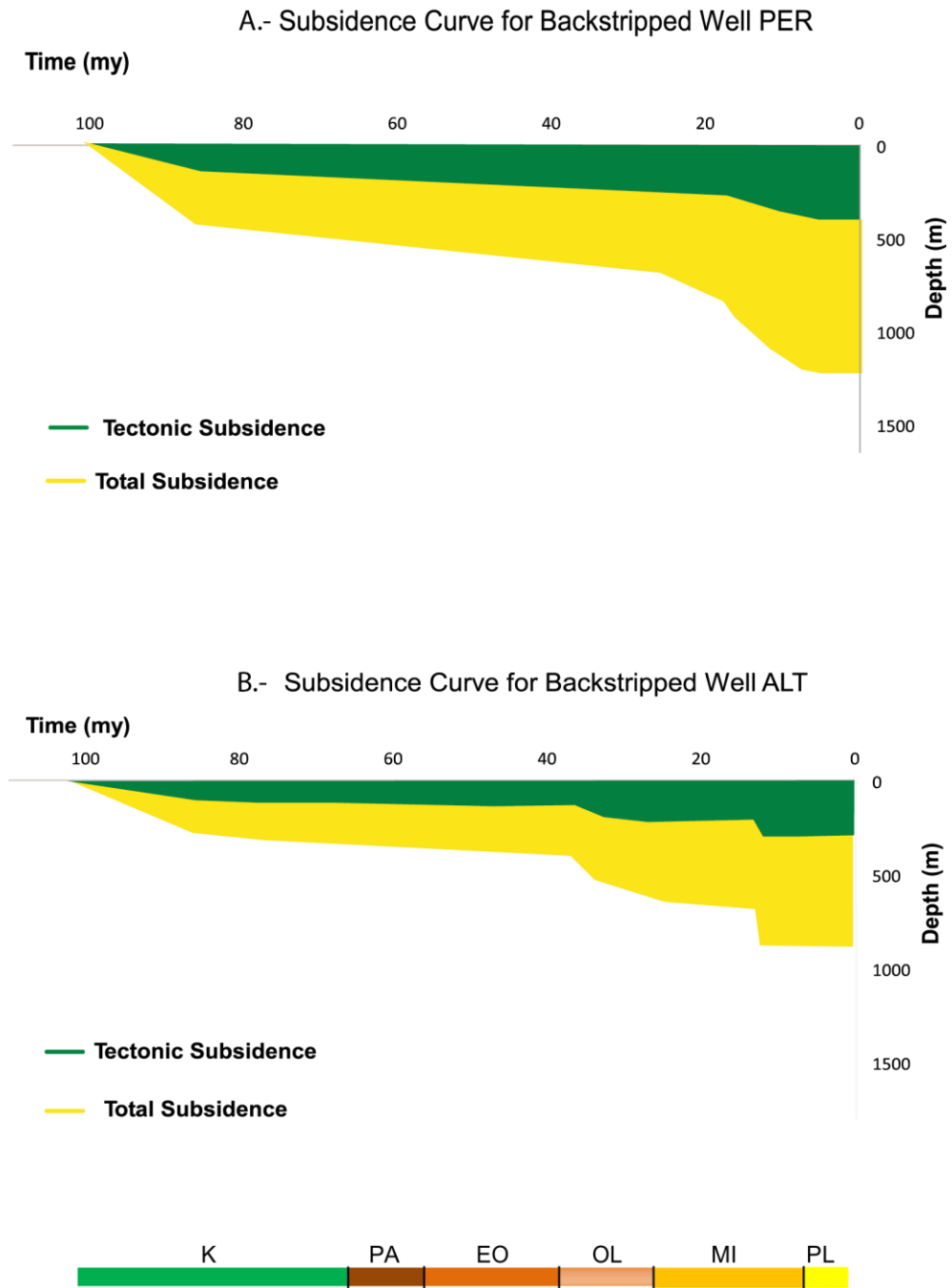


Figure 3.7A-B. Total (yellow+green) and tectonic (green) subsidence of the Eastern Venezuela basin, from wells PER and ALT. Borehole-well location in Fig. 3.3. Age scale: Cretaceous (K), Paleocene (PA), Eocene (EO), Oligocene (OL), Miocene (MI) and Pliocene (PL).

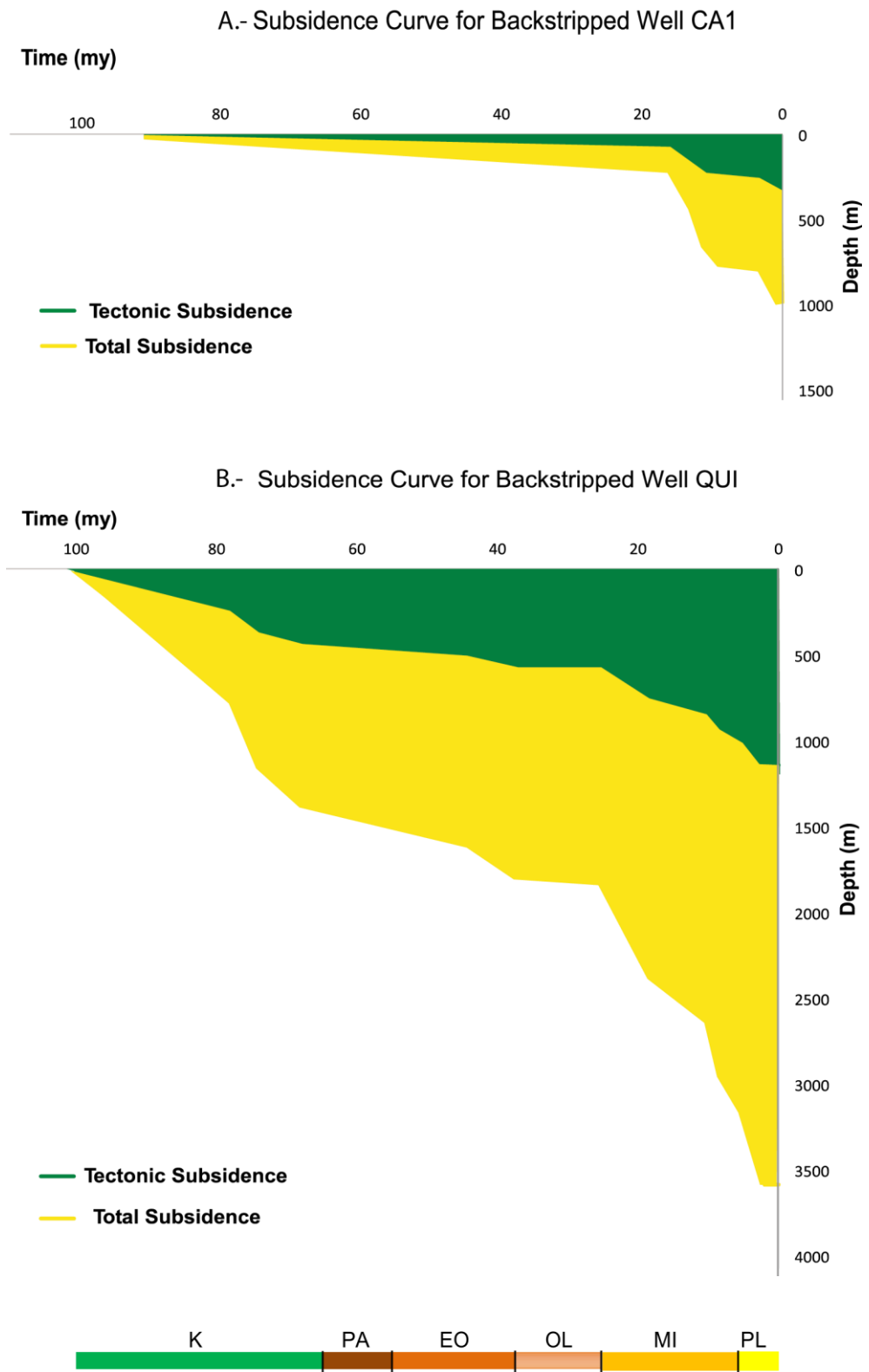


Figure 3.8A-B. Total (yellow+green) and tectonic (green) subsidence of the Eastern Venezuela basin, from wells CA1 and QUI. Borehole-well location in Fig. 3.3. Age scale: Cretaceous (K), Paleocene (PA), Eocene (EO), Oligocene (OL), Miocene (MI) and Pliocene (PL).

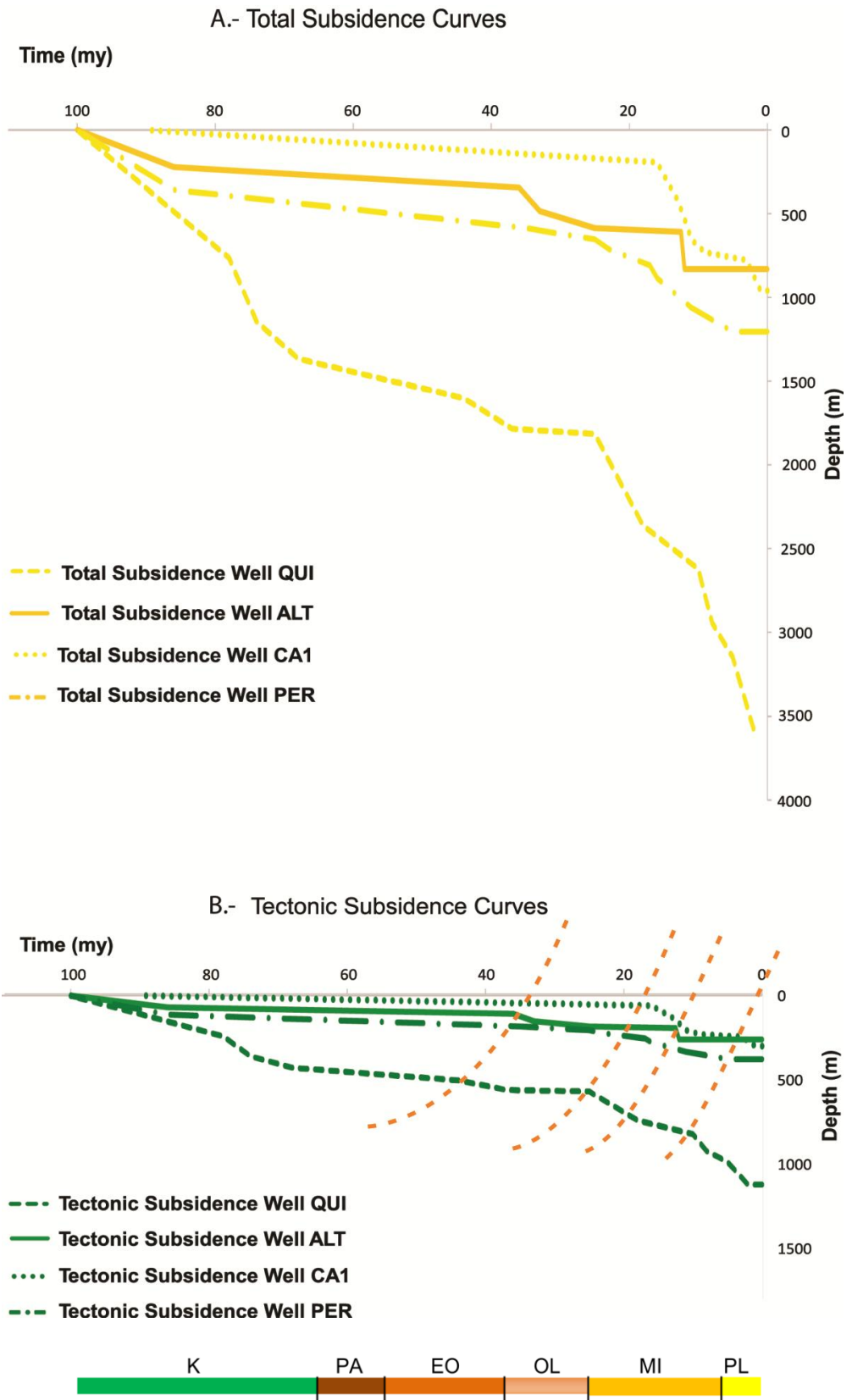


Figure 3.9A-B. Integrated total (yellow) and tectonic (green) subsidence curves of the Eastern Venezuela basin, from wells QUI, ALT, CA1 and PER. Dashed orange lines indicate pulses of tectonic subsidence. Borehole-well location in Fig. 3.3.

In their study about basin subsidence mechanism of the Caribbean-South American plate boundary, Escalona and Mann (2011) interpreted a progressive younger pattern of tectonic loading along the margin from west to east. From our total and tectonic subsidence integrated curves for wells QUI, ALT, CA1 and PER (Fig. 3.9) I could say that this tectonic loading pattern is also younger from north to south; the effect of tectonic loading is notorious in well QUI (Fig. 3.8B) during early Miocene, whereas in the wells closer to the Guayana craton major impact is observed during mid Miocene. It is also interesting pointing out that an incipient uplift is inferred to occur during early Miocene in wells ALT, CA1 and PER which may represent the isostatic rebound response to the loads applied in the north, i.e.: Caribbean obduction, emplacement of nappes and thrusts.

Observing the tectonic subsidence curves, from Oligocene to Present time, it can be noticed that pulses of tectonic subsidence are first registered in the north (well QUI) and later on in wells located further south (CA1, PER, ALT) as shown by orange dashed lines in Fig. 3.9B representing advanced fronts of tectonic subsidence. Some kind of periodicity in episodic pulses of major subsidence between quiescence times (13, 10, 9 my) could also be inferred and probably related to the stress release mechanism described by Bott (1990) which will be discussed in Chapter 5.

CHAPTER 4

GRAVITY ANOMALIES

4.1. GRAVITY ANOMALIES IN EASTERN VENEZUELA

The existence of a prominent negative gravity anomaly in Eastern Venezuela has long been recognized (Bowin, 1976; Bonini, 1978) as it may represent the largest negative free-air anomaly on Earth, where the topography is above sea level. A few models have been proposed to account for this gravity minimum; however, the subject is still a matter of interesting debate and hence the motivation for this research. A full evaluation of gravity anomalies in eastern Venezuela will be accomplished, and the conditions of isostatic equilibrium and crustal structure of the area will be examined.

Data consisting of: (a) observed or measured gravity (g in mGal), (b) elevation (meters), (c) latitude and longitude (degrees, minutes and seconds) for each gravity station were available to process and calculate the gravity anomalies within the work area (Figure 4.1) extending between latitudes 8° and 12° N and longitudes 60° and 66° W. Most of these data were collected during gravity surveys (1980-90) in eastern Venezuela.

The data were compiled from a Caribbean Gravity Data Catalogue at Durham University. The source of land gravity data is: Cartografía Nacional, Ministerio de Energía y Minas, Petroleum Companies in Venezuela and Princeton University. Sea gravity data are from: U.S. Geological Survey, Woods Hole Oceanographic Institution, Lamont-Doherty Geological Observatory and National Oceanographic and Atmospheric Administration.

4.2. GRAVITY DATA REDUCTION

Gravity data were reduced to sea level to calculate free-air and complete Bouguer anomalies. In doing so, the observed gravity values were referred to the theoretical gravity values through the Geodetic Reference System 1967 (GRS67) at sea level, using the Mittermeyer (1969) formula, ϕ being the latitude of the station:

$$g_{\phi} = 978031.85 (1 + 0.005278895\sin^2 \phi + 0.000023462\sin^4 \phi) \text{ mGal} \quad (4.1)$$

To reduce the gravity measurements to sea level, the normal gravity gradient or free-air correction: $0.3086h$ (mGal) was used. The *free-air anomaly* was computed from:

$$\text{FAA (mGal)} = g + 0.3086h - g_{\phi} \quad (4.2)$$

where the elevation h is in meters and positive above sea level.

After applying the Bouguer correction: $0.04191\rho_b h$ representing the attraction of an infinite flat slab of thickness h (m) and density ρ_b (g/cm^3), the simple Bouguer anomaly was computed from the expression:

$$\text{BA (mGal)} = g + 0.3086h - 0.04191 \rho_b h - g_{\phi} \quad (4.3)$$

and h , the height of the station in meters, is positive above sea level.

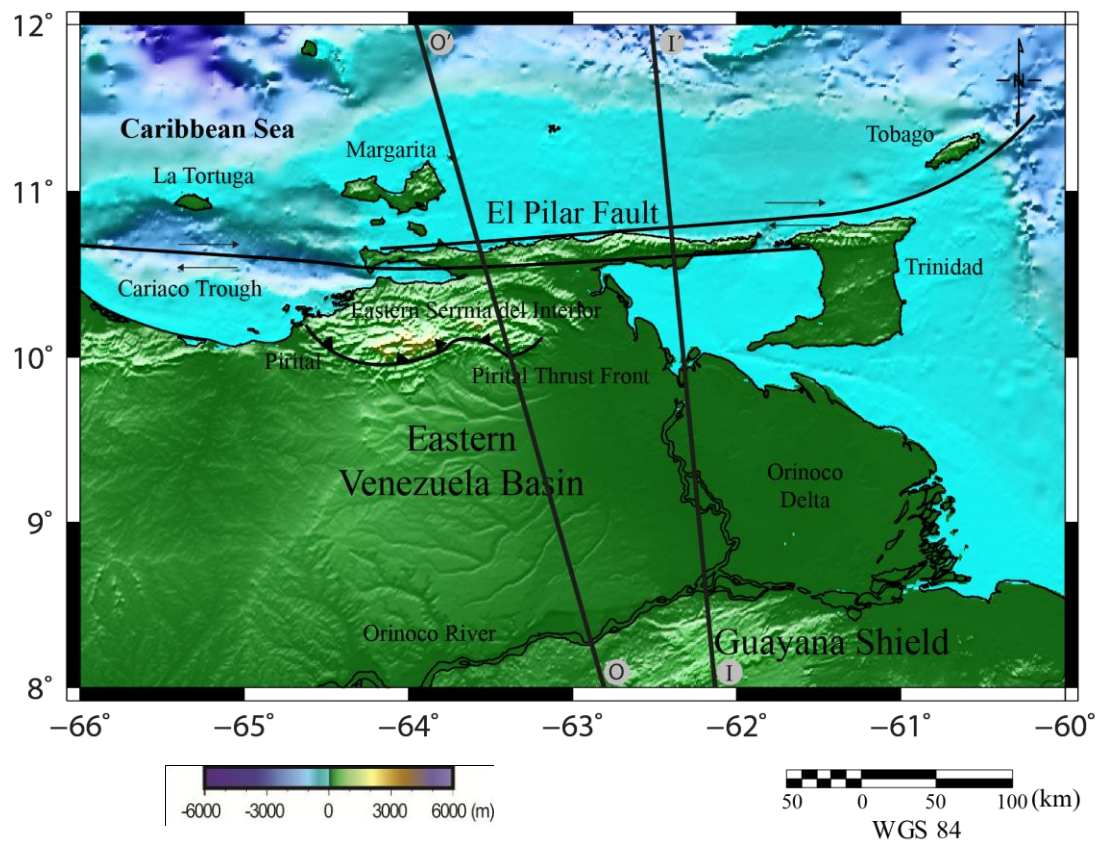


Figure 4.1. Shaded relief topographic map of the area of study in eastern Venezuela. OO' and II' are modelled sections.

Although no work has been published about the quality of the gravity data in the area, a rough estimate of error in accuracy of gravity measurements (~0.03 mGal), location (~10-20 m) and elevation of stations (~5 m) will lead to random errors which are probably negligible due to the regional character of this investigation. The most serious systematic error in the Bouguer anomaly values arises from errors in the density values above datum. If this error were $\pm 0.3 \text{ g/cm}^3$, probably an upper limit, then the error in the Bouguer anomaly would be of the order of 1.25 mGal for each 100 m of elevation above datum; stations with heights in excess of 200m, on the other hand, represent less than 20% of the total number of stations in the area (see Figure 4.1).

It has been recognized that if important density changes occurs in an area, errors of several tenths of a mGal may result using the average density instead of the density values, to calculate Bouguer anomalies, even in an area of moderate topography (Vajk, 1956). Due to the contrasting differences in the lithological character of the rocks constituting the distinct tectonic provinces in the work area, different values of density were used for the calculations. Data for surface densities were available from sample measurements and density logs of some boreholes drilled in the area, and are listed in Table 4.1. Where no direct data were at hand, assumptions were made with sound geological deduction.

4.2.1. COMPLETE BOUGUER ANOMALY

In gravity maps of eastern Venezuela previously published (Folinsbee, 1972; Bonini et al., 1978) terrain corrections were not applied, probably on account of the gentle topography of the area. Although it must be valid for most of the southern part of the work area, the foreland deformed belt and the Araya-Paria Peninsula on land and the islands and small basins offshore Venezuela, exhibit steep topographic (Fig. 4.1) and bathymetric contours respectively. Hence it was considered necessary to include terrain

corrections and produce complete Bouguer anomalies for the purposes of this study.

In order to compute the topographic corrections it was necessary to convert the terrain data, as provided by topographic and bathymetric maps (Source: Topographic maps of Venezuela, Cartografía Nacional scale 1:100,000 and 1:500,000; Bathymetric charts from Perry (1984) and Bartholomew (1975, sheets 117 and 119, scale 1:5,000,000)) into digital form to be used with the computer package SPIDGRA (Becerra and Rodríguez, 1985) at the Lab of Geophysical Interpretation, Universidad Central de Venezuela. The elevation data, in and outside the study area, were digitized in order to cover the effects of terrain from a gravity station up to the M-zone in the Hammer (1939) scheme.

As expected, calculated terrain correction values grade from 0 to 1 mGal in flat areas (8° - 10° N), are of the order of 5 mGal at the mountains and Margarita Island, and reach values up to 10 mGal at sea stations. Once all the corrections were applied, a Gravity Data Catalogue was produced where the following information is given in Appendix C for each of the 1397 gravity stations processed: Identification-number, latitude and longitude (degrees), height (m), and gravity anomalies (mGal).

4.3. GRAVITY ANOMALY MAPS OF EASTERN VENEZUELA

Once the gravity data had been reduced, the resulting Bouguer and free-air gravity anomalies were contoured to produce the Bouguer and free-air anomaly maps of the study area, using General Mapping Tool –GMT (Wessel and Smith, 1995); these maps are presented in Figures 4.2 and 4.3. For references to geographical and geological features the reader is referred to Figures 1.1, 2.1 and 2.4)

The main and most striking feature of the *Bouguer anomaly map* is the gravity minimum of about -200 mGal centered around Pedernales (10°N, 62.2°W) at the Orinoco River mouth (Fig. 4.2; see Fig. 2.4 for location). To elaborate on it, the anomaly belt with a fairly constant N70°E trend widens eastward and, from a qualitative point of view, there seems to be a clear correlation between the Bouguer anomalies and the major geological structures in the area. The gravity contours follow almost exactly the margins of the Eastern Venezuela foreland basin; so, perpendicular to contours roughly parallel to each other, over an area some 70 km north of the Orinoco River, the gravity gradients are of the order of 0.7 mGal/km and from this zone, that might represent the hinge line of the crystalline basement, the gravity values decrease northwards at a rate of about 1.5 – 1.75 mGal/km, down to the minimum anomaly, suggesting the uniform south-to-north dip of the basement. The minimum itself coincides with the southernmost front of the nappes of the foreland deformed belt province.

Towards the east, the main anomaly goes through the Gulf of Paria and Trinidad Island, and continues in NE direction to meet the negative belt of gravity anomalies of the Lesser Antilles.

The northern flank of the anomaly exhibits, on the contrary, a steeper gravity gradient of the order of 2.2 – 2.5 mGal/km, with the zero anomaly contour being at the Araya-Paria Peninsula. This area with steep gravity gradients and more irregular contours reflects the complex structure of the foreland thrust and fold belt, and the metamorphic Araya-Tobago terrane.

A gravity gradient of the order of 2.0 mGal/km follows closely the contact between these two complexes and also the trend of El Pilar fault zone, up to the eastern end of the Araya-Paria isthmus. There, at the Paria peninsula, the Bouguer anomaly gradient reaches values around 4.2 mGal/km, suggesting a steeper contact zone or change in density contrast at least near the surface, between the previously mentioned tectonic units.

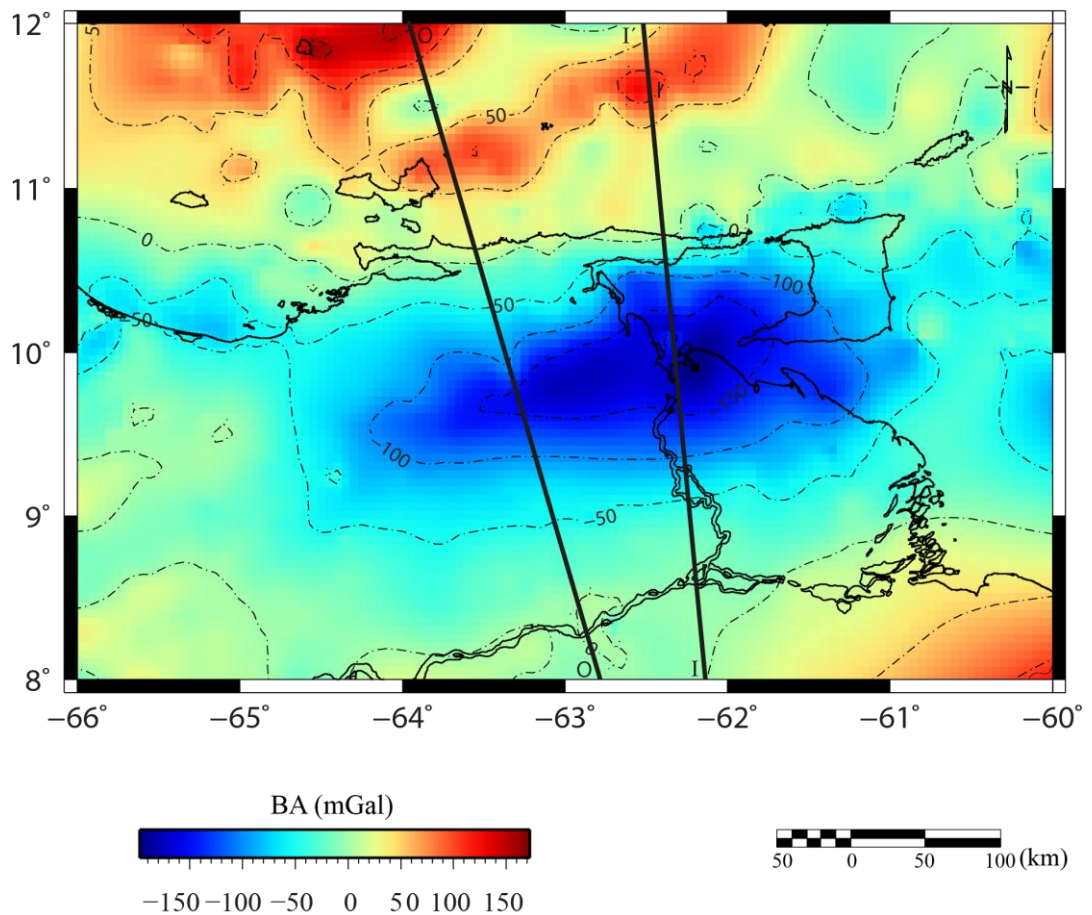


Figure 4.2. Bouguer Anomaly Map of the area of study: Eastern Venezuela. Contour intervals (dashed lines) 50 mGal. OO' and II' are modelled sections

On the western side of the area, at about 65° W of longitude, the main anomaly abruptly changes its NE trend and develops a flank with positive Bouguer anomaly values (+10 to +20 mGal) which marks the western margin of the basin. Within this area, a relatively negative anomaly trend (western-end at about 8.75° N, 66° W) is certainly the gravity expression of the Espino Graben, flanked by positive anomalies possibly related to highs of the basement such as the Altamira high. To the north, along the meridian 66° W, at about 10° N, there is a minimum, some -20 mGal, associated with the Guárico Frontal thrust and just a little bit further north, a WNW trend of negative gravity anomalies follows the offshore Urica fault, with a minimum of

-70 mGal occurring over the thick sedimentary sequence at the Barcelona embayment shelf.

Positive Bouguer anomalies exist over most of the northern part of the study region, offshore Venezuela, all in a very irregular pattern with many local maximum and minimum closures reflecting the intricate structure of the area. There are some remarkable small circular and elongated local but high amplitude Bouguer anomalies on the northern overthrust plate; the circular ones are probably associated to basic/ultrabasic intrusions and must provide a significant contribution to the load on the northern plate.

However, there are two clearly distinguishable ENE trend anomalies, more or less parallel to each other; the southern one follows the strike of the Margarita-Tobago forearc basin, and exhibits a local minimum lower than -10 mGal. The northern one, with a local maximum in excess of +150 mGal, delineates the Margarita-Los Testigos platform which is the southwesternmost extreme of the Lesser Antilles magmatic platform. Both anomaly belts tend to support the continuity of the structures associated with them, as well as the irregular topography of the underlying basement. Positive Bouguer anomalies occur also at the northwestern border of the work area, over the La Blanquilla platform and the easternmost extension of the Bonaire basin (see Fig. 1.1, 2.4 for location).

Most gravity studies aiming to investigate the crustal structure are based on Bouguer anomaly data and those oriented to geoid investigations on free-air anomalies. Free-air anomalies provide a first fair indicator of the isostatic equilibrium conditions in the Earth and they exhibit a strong correlation with local topographic variations, hence, their importance in supporting studies related to crustal structure.

Free-air anomalies in Eastern Venezuela (Figure 4.3) exhibit a pattern quite similar to that of the Bouguer anomalies described in the foregoing section, with negative values in inland Venezuela, reaching near-to-zero values

around the coastline, and increasing progressively towards positive anomalies. At about 63.5° W – 10.25° N, a local free-air anomaly maximum in excess of +50 mGal coincides with a local high topography of the Eastern Serranía del Interior.

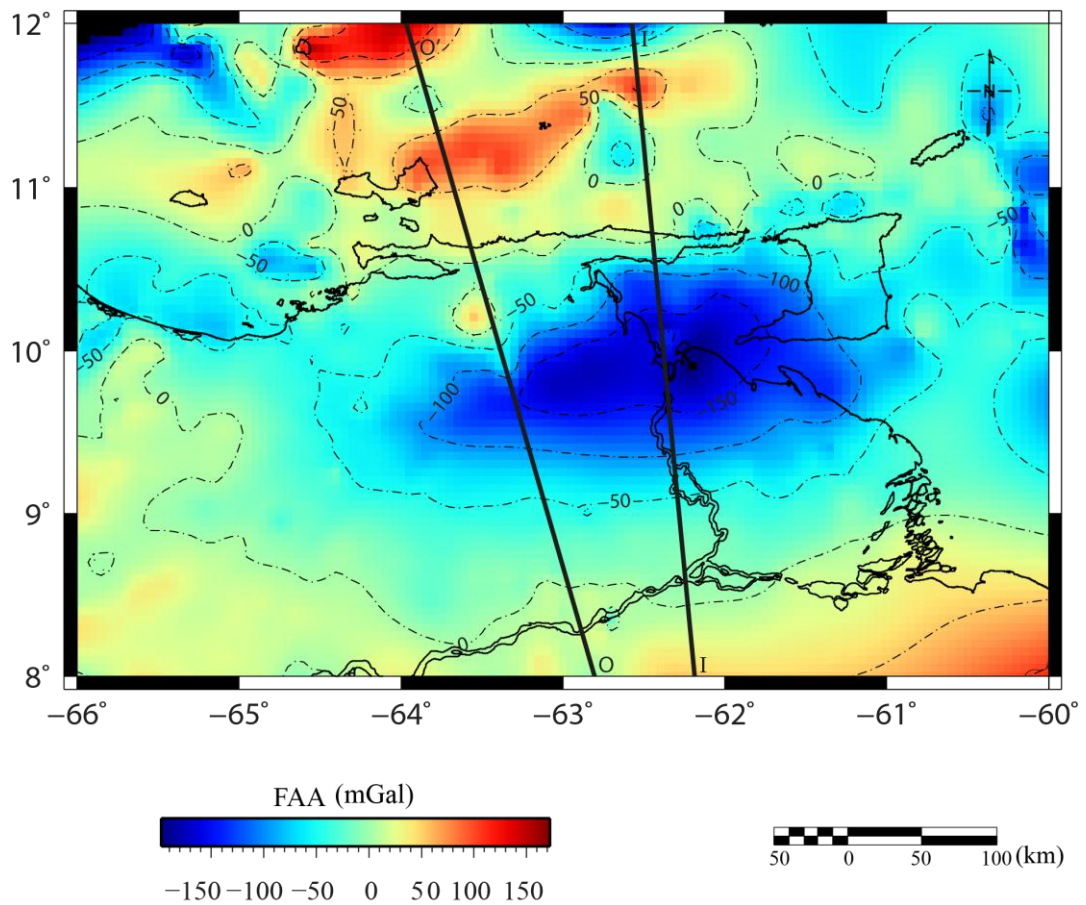


Figure 4.3. Free-Air Anomaly Map of the area of study: Eastern Venezuela. Contour interval (dashed lines) 50 mGal. OO' and II' are modelled sections

The three main northeasterly trending alignments, i.e. the positive belt of the Margarita-Los Testigos magmatic arc platform, the minimum along the Margarita-Tobago forearc basin and the negative anomaly belt of the Eastern Venezuela foreland basin are continuous features, parallel to each other, suggesting that a genetic relationship might exist (see Fig. 4.3 and 2.4 for location).

4.4.- ISOSTATIC ANOMALIES

The concept of Isostasy implies that at a certain depth D (compensation depth), hydrostatic equilibrium prevails, no matter whether the surface topography of the region under consideration is a mountain, low-land or ocean. The purpose of isostatic studies through gravity anomalies is to investigate in which way and to what extent different topographic features around the world are compensated at depth, and if they are not, to find an explanation for deviations from isostatic equilibrium.

4.4.1. AN INTRODUCTORY REVIEW

The earliest and still commonly used isostatic models are those of Pratt (1854) and Airy (1855) who, working independently, proposed an explanation for the isostatic behaviour of the Earth. Although differing in the mechanisms to account for isostatic equilibrium, both hypotheses share the common conviction that the mountain masses must be compensated at depth directly beneath the topography. Thus, Pratt's (op. cit.) original assumption was that "*the higher the mountain, the smaller the density of the Earth's crust*"... and vice-versa for the oceans. Later, Hayford and Bowie (1912) derived the required formulae and computed a set of tables to calculate the corrections.

The Pratt-Hayford isostatic system, as known in current times, presupposes that isostatic compensation is accomplished by lateral variations in the density of the outer layers of the Earth (equivalent to lithosphere perhaps) to support the variations in load created by the variations in the elevation of the Earth's surface, through:

$$\rho_p = \rho_o (D / (D + h)) \quad \text{for land stations} \quad (4.4)$$

and

$$\rho_p = (\rho_o D + \rho_w h) / (D+h) \quad \text{for marine stations} \quad (4.5)$$

where: D is the depth of compensation, ρ_p is related to the elevation above sea level where ρ_o is the reference density corresponding to zero elevation, and ρ_w is the water density, as shown in Figure 4.4

Airy (1855) according to his “*mountain-root*” theory postulated the existence of light “*roots*” beneath the continents and heavy “*antiroots*” beneath the oceans to compensate the topographic masses.

Heiskanen (1953) developed tables for isostatic reductions; the Airy theory assumes local and complete isostatic compensation through the relations:

$$t = h \cdot \rho_c / (\rho_m - \rho_c) \quad \text{for land stations} \quad (4.6)$$

and
$$t = h ((\rho_c - \rho_w) / (\rho_m - \rho_c)) \quad \text{for ocean stations} \quad (4.7)$$

where t is the depth of root, h is the height of the topography, ρ_c is the crustal density, ρ_m is the substratum density and ρ_w is the water density (Figure 4.4); all assumed densities are constant. The thickness of the crust with zero elevation regarding sea level is T .

A third mechanism is due originally to Vening Meinesz (1931) who modified the Airy model and proposed a regional isostatic compensation system. According to this mechanism the topography can be considered as a load over the crust, which behaves like an elastic plate and bends in response to such a load. The amount of downbending of the crust is then used to determine the effect of the isostatic compensation.

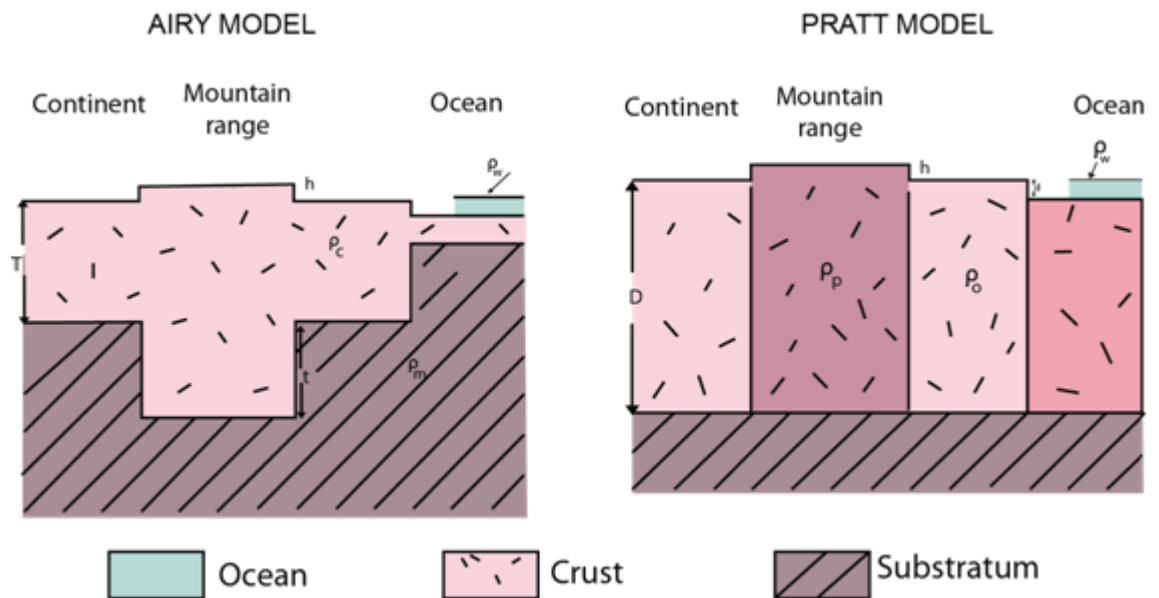


Figure 4.4. Illustrative diagram for Airy and Pratt anomaly computations (From Bott, 1971a).

Airy model: t =depth of root; h =height of the topography; ρ_c = crustal density; ρ_m = substratum density; ρ_w = water density; T =thickness of the crust with zero elevation regarding sea level.

Pratt model: D =depth of compensation; h =height of the topography; ρ_p = density related to the elevation above sea level where ρ_o = reference density corresponding to zero elevation; ρ_w = water density.

In summary, the Airy hypothesis gives the best simple model for isostasy of major folded mountain ranges such as the Alps and the Andes, and also of isostasy at passive continental margins. On the other hand, the Pratt hypothesis gives the best simple model for ocean ridges and continental plateau uplifts (eg. Colorado Plateau and Basin-and-Range in western U.S.A., East African uplift) which were not known about in early days. The compensation in both these is caused by the underlying region of hot, and hence low density, upper mantle. Also low density granitic bodies extending to depths of ~ 10 km in the continental crust are often associated with local uplifts which are locally compensated by the granite (depth of compensation 10 km). Many examples occur in England and Scotland, including uplift of the Lake District and northern Pennines. So the two early hypotheses share the honours about equally (Bott, 1971a).

4.4.2. ISOSTATIC ANOMALIES EASTERN VENEZUELA -AIRY AND PRATT.

Initially the isostatic anomalies in Eastern Venezuela have been examined in the light of the two traditional hypotheses (Pratt, 1854; Airy, 1855). In doing so, isostatic anomalies for both models were calculated using a computer program developed for such a purpose. The calculations are based on a digitized elevation data -topography and bathymetry- extending from 5° N to 14° N of latitude, and 57° W to 69° W of longitude. Data source consisted of: Topographic maps of Venezuela, Cartografía Nacional, scale 1:100,000; 1:500,000; Bathymetric charts, Perry (1984) and Bartholomew (1975), sheets 117 and 119, scale 1:5,000,000.

Maximum isostatic corrections are of the order of 15 mGal. Isostatic anomalies for different compensation depths were derived, and the resulting anomalies do not show significant differences among themselves. Figure 4.5 illustrates the Isostatic Anomaly Map, Airy-model, for compensation depth of 35 km, and Figure 4.6 the resulting Isostatic Anomaly Map for compensation depth of 100 km in the Pratt-model. No matter the depth of compensation assumed for the computations, the principal features of the gravity anomaly over the Eastern Venezuela basin are little changed; which is, of course, a consequence of the low topography of this area. The isostatic anomaly maps do not exhibit remarkable differences from the free-air anomaly map in Figure 4.3. The main differences lie in the region of the Coast Ranges.

For an area of low topography, free-air, Bouguer and isostatic gravity anomalies of small values should be expected. That is not the case in eastern Venezuela, where the main anomaly reaches values more negative than -190 mGal. In Heiskanen and Vening Meinesz (1958) terminology, the characteristic pattern of minimum anomaly over the low topography of the Eastern Venezuela basin corresponds to an area of overcompensated surface topography. But, it should be understood in the sense that no local, Airy or Pratt, compensation mechanisms can account for the isostatic

equilibrium in the work area, a conclusion we have anticipated, and so other mechanisms will be explored.

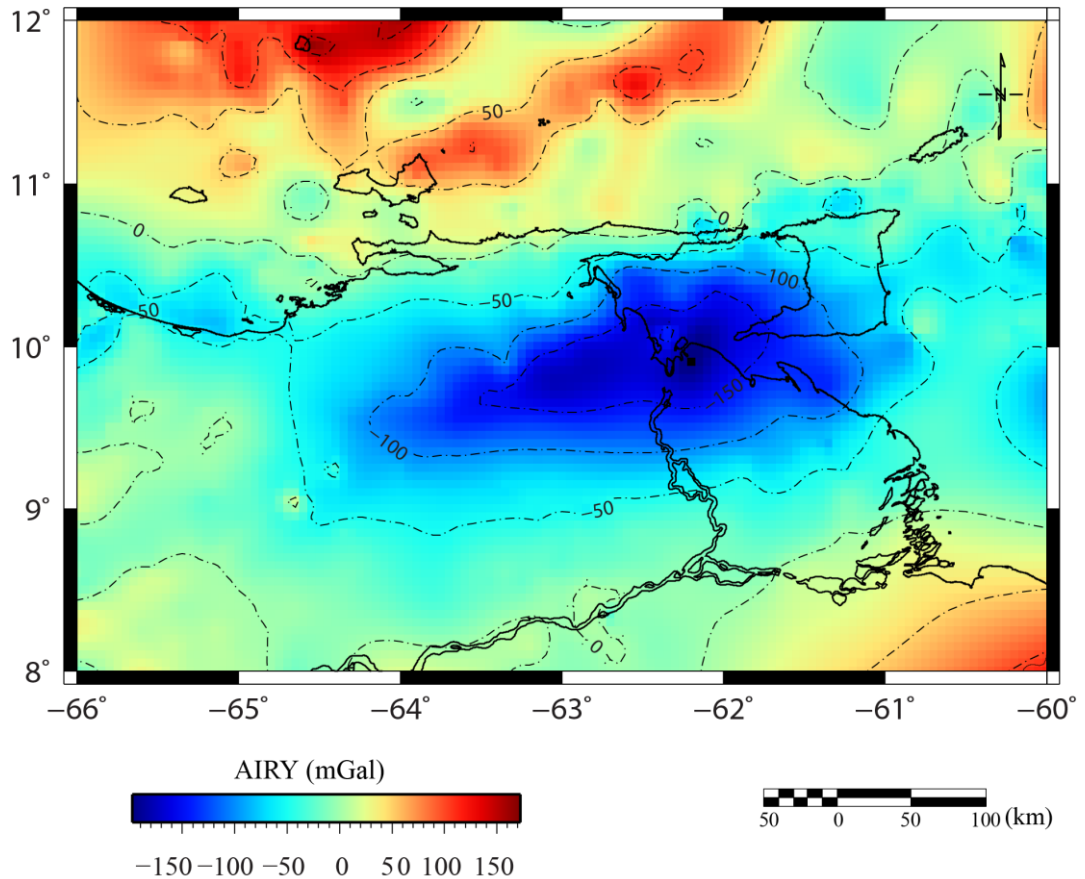


Figure 4.5. Isostatic anomaly map: Airy compensation $T=35\text{km}$, Eastern Venezuela. Contour interval (dashed lines) 50 mGal.

It may be worthwhile to mention that when local compensation is assumed to compute isostatic anomalies in an area, when the compensation is actually regional, the resulting isostatic reductions will be too large for stations at high elevation; therefore, isostatic gravity anomalies at high topographic elevations will be more positive than they should be. The opposite is true for marine stations (Heiskanen and Vening Meinesz, 1958).

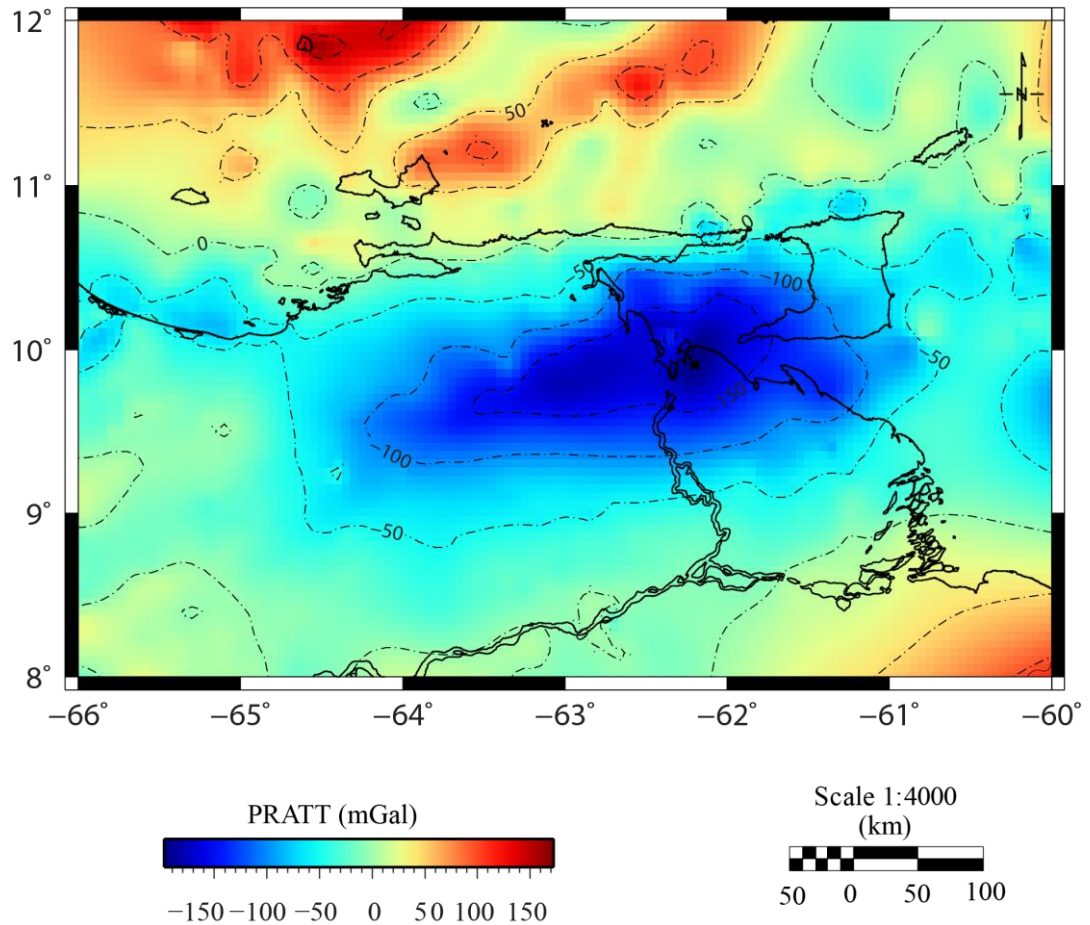


Figure 4.6. Isostatic anomaly map: Pratt compensation $D=100\text{km}$, Eastern Venezuela. Contour interval (dashed lines) 50 mGal.

4.4.3. BOUGUER AND FREE-AIR ANOMALIES vs. TOPOGRAPHY

By comparing Bouguer, free-air anomalies and topography one can get an idea about the isostatic conditions over an area. At long wavelengths, a high correlation between Bouguer anomalies and the topography has been observed, whereas free-air anomalies are small, suggesting the counter-balance between the attraction of the topography and that of the compensation (Lewis and Dorman, 1970; Dorman and Lewis, 1970). At shorter wavelengths, free-air anomalies are highly coherent with topography while the correlation between Bouguer anomalies and topography decreases. These correlations can be used to study the flexure of the elastic lithosphere

under loading (Turcotte and Schubert, 1982, 2002) because the load due to a mountain range with large horizontal scale (hundreds of kilometers) deflects the lithosphere downward and the excess mass of the mountain topography is compensated at depth by lighter crustal rocks depressing the Moho.

As the Bouguer gravity anomaly corrected for topography does not take into account the effect of the compensating density distribution, Bouguer anomalies over mountain ranges are strongly negative as gravity measurements have largely confirmed (Banks et al., 1977; Turcotte and Schubert, 2002) and free-air anomalies are near zero as a consequence of no net mass difference required by isostasy.

As a first approach to investigate a regional mechanism for isostatic compensation in Eastern Venezuela, the relationship between Bouguer, free-air anomalies and topography is analyzed and discussed along profiles 00' and II' whose location is shown in Figures 4.1, 4.2, 4.3 and 2.4. Both profiles were constructed including information projected onto the transect lines, from 50 km wide corridors, over the regional Bouguer and free-air anomaly maps produced by upward continuation 5000 m height (Figures 4.7 and 4.8 respectively) using the package Oasis montaj (Geosoft, 2010).

Data were extended southward to include the topographic elevation of the Guayana highlands, which as shown in the next chapter, is probably produced by flexural uplift. The source of gravity data between 8° to 12° N is the free-air and Bouguer anomaly maps of this study with data for 6° to 8° N taken from Graterol (1978).

Upward continuation is considered a clean filter because it produces almost no side effects that may require the application of other filters or processes to correct (MAGMAP, from Geosoft, 2010). Because of this, it was used to remove or minimize the effect of shallow sources and noise in grids.

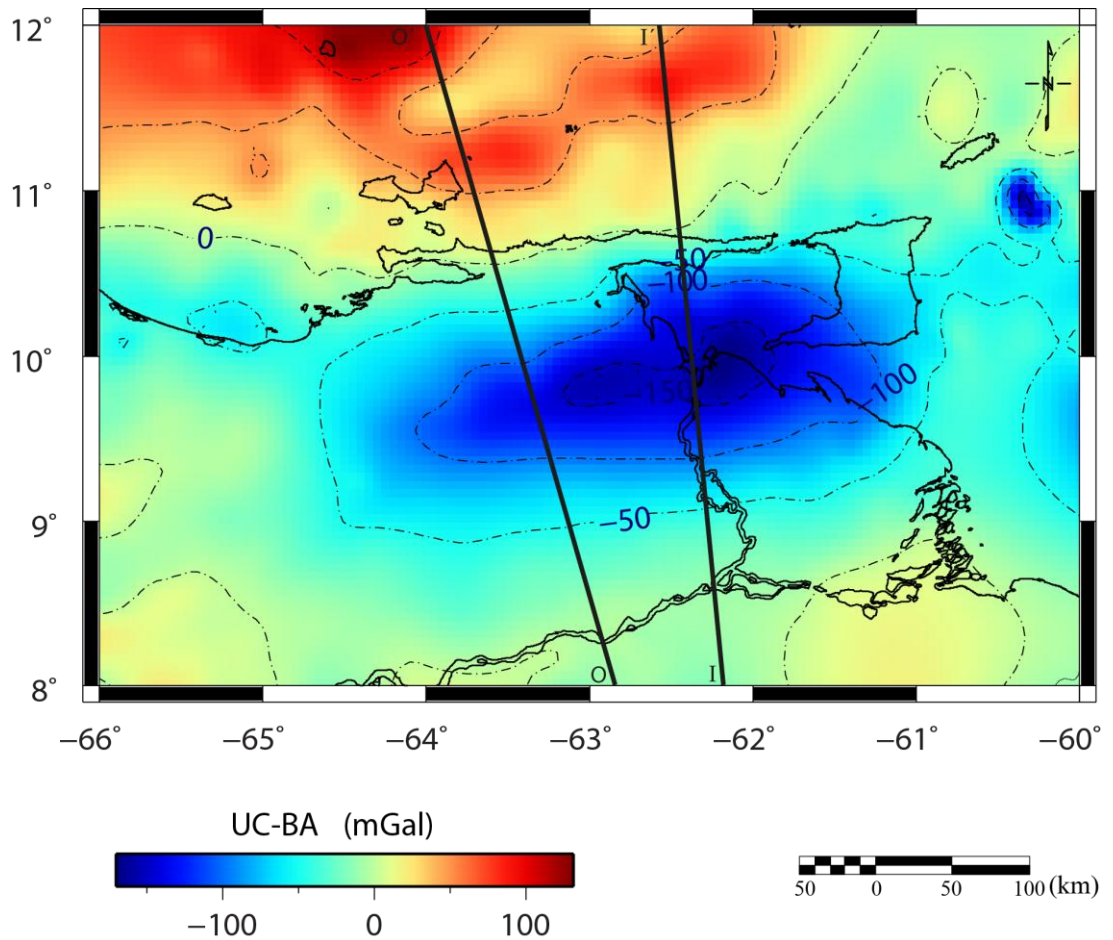


Figure 4.7. Upward continuation of Bouguer anomalies 5000 m. Contour interval (dashed lines) 50 mGal. OO' and II' are modelled sections

Profile OO' (Figure 4.9) extends from the Guayana highlands in the south, with N15°W strike, to the Grenada basin, passing across the Eastern Serranía del Interior, where maximum heights are about 1300 m. Close correlation with free-air anomaly is shown over this short-wavelength topographic feature, as well as with Margarita Island, the Guayana highlands and the Grenada depression. However, at longer wavelength the correlation is poor, with the minimum anomaly occurring over a region of low topography (elevations around 100 m). No mirror effects are present between the Bouguer anomalies and the topography; the long wavelength of the Bouguer anomaly being controlled by the Bouguer anomaly minimum.

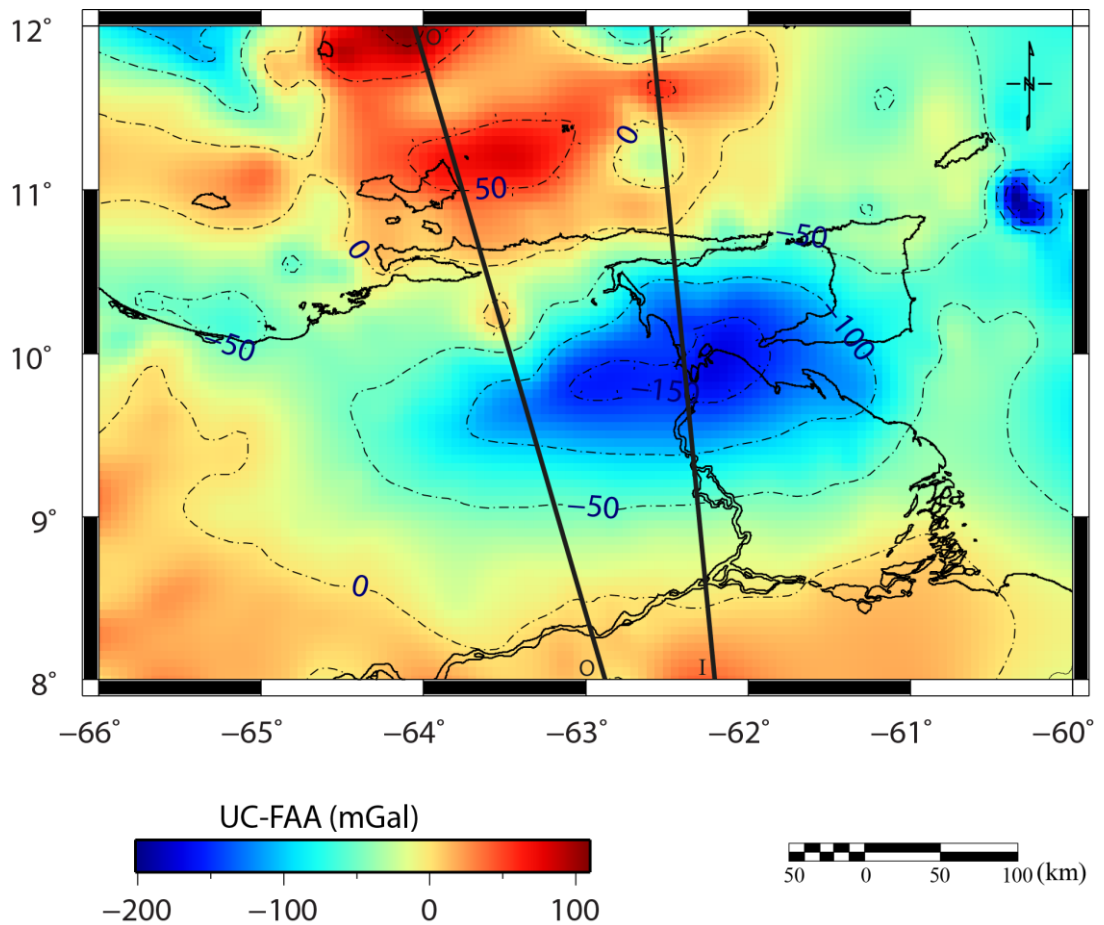


Figure 4.8. Upward continuation of free-air anomalies 5000 m. Contour interval (dashed lines) 50 mGal. OO' and II' are modelled sections.

Profile II' (Figure 4.10) extends also from the Guayana Craton, with N5°W strike, up to the Grenada depression. Most of the topography along this profile is near sea level; hence no major correlation exists between both free-air or Bouguer anomalies, and the topography at the minimum anomaly zone. Free-air anomalies and topography are clearly coherent at short wavelengths over the Guayana highlands and at the northern end of the section, over the Grenada basin.

An interesting point is that both of these profiles exhibit the characteristic positive-negative gravity anomaly couple identified in areas such as the Alps and the Appalachians and their associated foreland basins, and have been

interpreted in terms of convergence, suturing and collision during mountain building processes (Karner and Watts, 1983; Thomas, 1983).

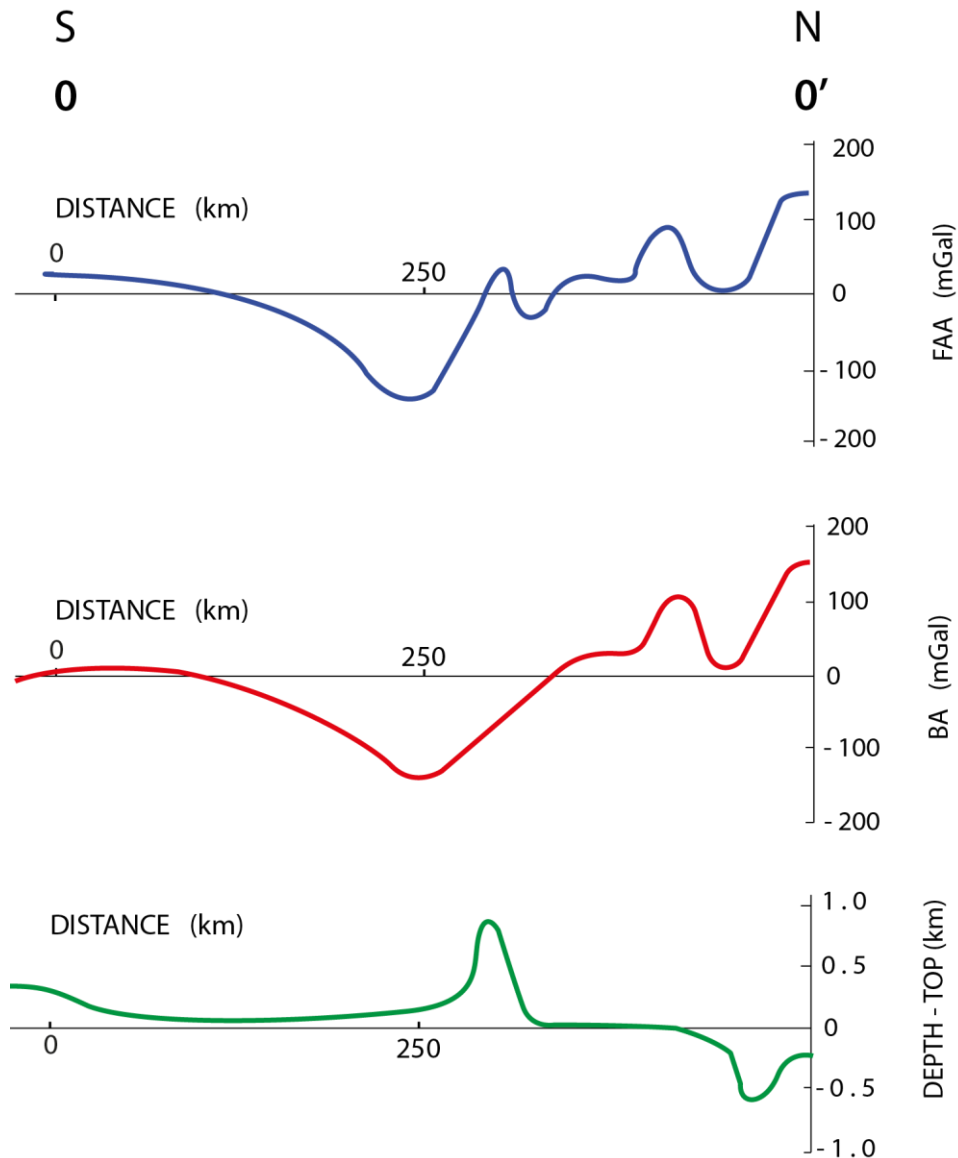


Figure 4.9. Free-air and Bouguer anomalies related to topography along profile OO'.
(For location see Figures 4.8, 4.7 and 4.1 respectively)

Following these authors' terminology the outer gravity high (OGH) along profiles OO' and II' coincides with the Guayana highlands in the south, the outer gravity low (OGL) is associated with the Eastern Venezuela foreland basin and the inner gravity high (IGH) on the north with Araya-Paria terrane and the Margarita-Los Testigos magmatic arc platform (see Figure 2.4 for

location). The gravity anomalies in eastern Venezuela cannot be explained by local isostatic models, because these classical mechanisms account only for vertical compensation of surface topography. The horizontal displacement of masses associated with plate convergence and the finite flexural rigidity of plates offer a possible explanation of these anomalies.

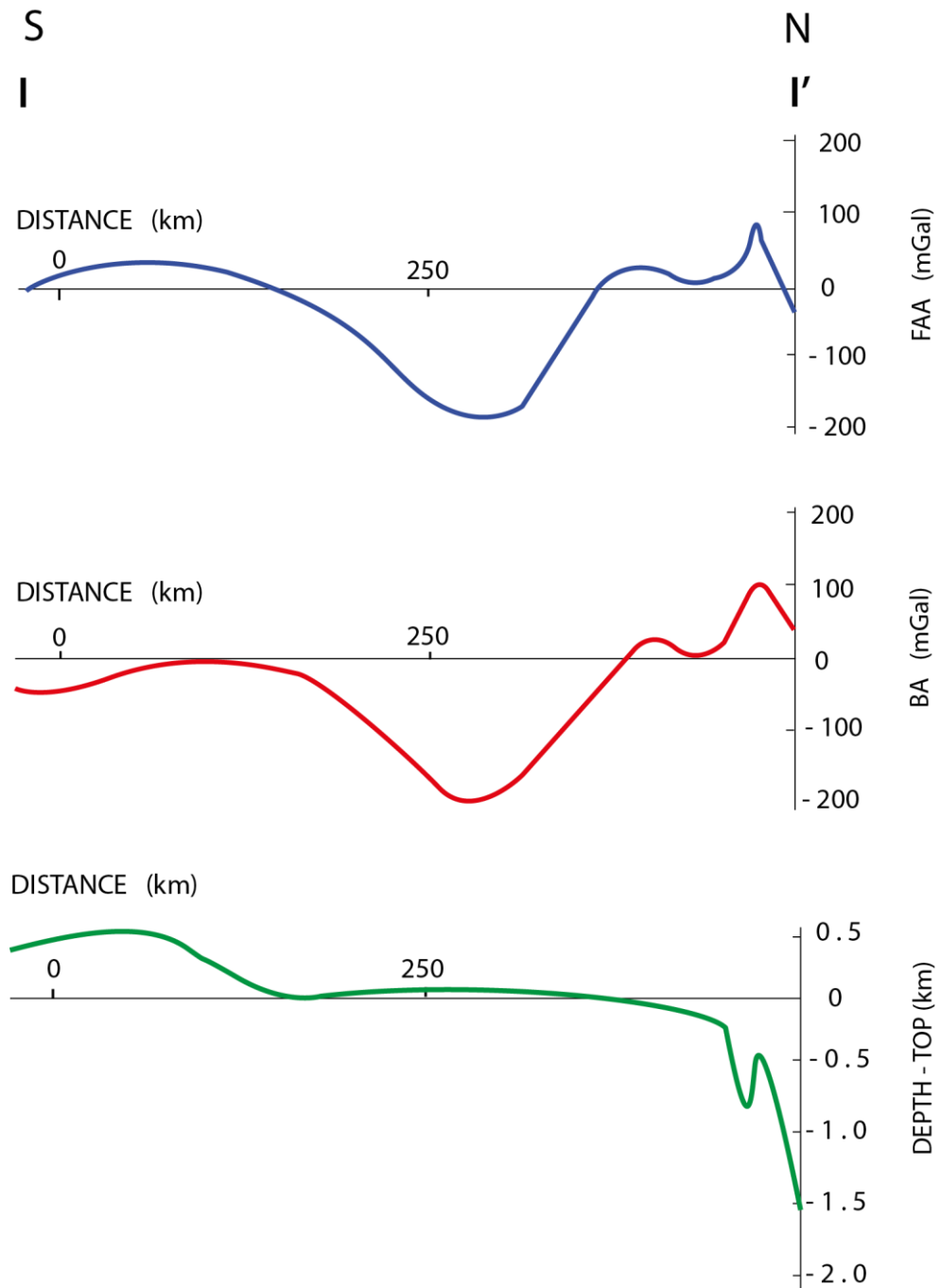


Figure 4.10. Free-air and Bouguer anomalies related to topography along profile II'. (For location see Figures 4.8, 4.7 and 4.1 respectively)

4.4.4. GRAVITY ANOMALY-TOPOGRAPHY ADMITTANCE AND COHERENCE ANALYSIS TECHNIQUES

The admittance or linear transfer function is the Fourier transform of the linear filter operating on the topography that best predicts the gravity field in the least-squares sense. This is a convenient way to describe the relationship between the topography and the gravity anomalies that are associated with the isostatic compensation of the topography (Bechtel et al., 1987). The Bouguer anomaly coherence and the free-air admittance are statistical methods that determine the relationship between the Bouguer and free-air gravity anomalies and the topography as a function of wavelength. Both methods have been used to find a “best fit” of the elastic thickness T_e by minimizing the root-mean square difference between observed and predicted coherence and admittance functions (Pérez-Gussinye and Watts, 2005). The estimation of the coherence between Bouguer gravity anomalies and topography in the frequency domain has been used by authors such as Bechtel et al. (1990). They show that the relationship between these parameters is very different for surface and subsurface loads that are applied to an elastic plate but Forsyth (1985) demonstrated that the interpretation of the admittance function may yield a biased model of the compensation mechanism if there is both surface and subsurface loading of the lithosphere.

Examples of coherence studies are as follows: Ebinger et al. (1989) provided a consistent basis for comparison between the effective elastic thickness (T_e) beneath subregions of East Africa and the Afar plateau. Hartley et al. (1996) estimated the effective T_e of the African lithosphere, with the purpose of isolating that part of the gravity field which cannot be accounted for by flexure and must be caused by other processes such as mantle convection acting below the lithosphere. Audet and Mareschal (2007) tested and used a wavelet-based method to obtain estimates of the effective elastic thickness of the lithosphere and its anisotropy in the Canadian Shield. This method has not been used in the present work because of the dominance of continuing thrust faulting in the tectonic mechanism which complicates the relationship between the gravity anomalies and topography.

4.5. TWO-DIMENSIONAL GRAVITY MODELLING

Two-dimensional gravity modelling was carried out at the Lab of Geophysical Interpretation, Central University of Venezuela, using the capabilities of Oasis montaj (Geosoft, 2010). GM-SYS, the basic program from which the gravity anomalies are calculated, computes the gravitational attraction of the proposed model composed by a series of semi-infinite horizontal slabs with a sloping end-face. The gravity effect of the slab is given by:

$$g(\text{mGal}) = 13,34 \Delta\rho \left[\theta_2 (Z_2 - Z_f) - \{ (X_1 - X_f) \sin\theta + (Z_1 - Z_f) \cos\theta \} \right. \\ \left. \{ \ln(r_2 / r_1) \sin\theta + (\theta_2 - \theta_1) \cos\theta \} \right] \\ \text{(From Talwani et al., 1959) (4.8)}$$

where $\Delta\rho$ is the density contrast (g/cm^3) across the slab. The total gravity effect at each observational point is obtained by adding the effects of the n-slabs that represent the model.

GM-SYS (Oasis montaj, Geosoft, 2010) requires the observed gravity data at station points located along a profile and an input model (coordinates of the vertices of the bodies, densities) to be provided by the user. The program computes the gravitational attraction of the proposed model and interactively allows the model to be altered (changes in density and body points can be made following the program menu) until a reasonable fit between the observed and computed anomalies is achieved. Correlation coefficient and standard errors are calculated at this stage. The output of the program consists of the resulting model plotted in cross-section together with the observed and calculated anomalies.

In this study two-dimensional gravity models along profiles OO' and II' were produced to investigate the crustal structure of the Eastern Venezuela foreland basin area. The basic assumption of the structural feature being two-dimensional for gravity modelling purposes is fully satisfied in eastern

Venezuela, where the regional structure is dominated by the east-west to east-northeasterly trend of the Eastern Venezuela foreland basin, its associated foreland deformed belt and adjacent terranes, and clearly related to the gravity anomaly trend with the same orientation.

4.5.1. CONSTRAINTS FROM BOREHOLE DATA

Data from 160 borehole wells in the work area (Figure 3.3) have been analyzed in section 3.5.1 related to the stratigraphic evolution of the Eastern Venezuela basin. This information has also been used to constrain the depth to basement and to the top of other major discontinuities in the geological sections. There, well data located within a 50 km wide corridor were projected onto the transect lines OO' and II' to delineate the topography of the crystalline basement as well as the top of Cretaceous sedimentary rocks and the Oligo-Miocene sequence. So, three main sedimentary units with distinctive lithologic characteristics have been defined along the profiles:

UNIT	SEQUENCE
1 -----	Upper-Miocene - Pliocene -----
2 -----	Oligocene - Mid-Miocene -----
3 =====	Cretaceous =====
	Crystalline Basement

Twelve wells provided information of the crystalline basement depth along OO' profile, and eight along II' profile, constraining the top of the basement from the Orinoco River up to latitude 9.1° N and 9.2° N respectively, where a sedimentary sequence about 2.4 km thick overlies the craton. The top of the Cretaceous unit is constrained at about latitude 10.2°N – 10.5°N of underlying 4.0 km of Tertiary sediments. Offshore Venezuela two wells allow controlling the top of the metamorphic terranes, at a depth of 4.5-5.0 km.

4.5.2. CONSTRAINTS FROM SEISMIC DATA

Interpreted seismic reflection sections resulting from a compilation of onland seismic surveys in eastern Venezuela (Muñoz, 1985, section Orinoco - Tortuga Island, and Yopales – Pato; and Duerto, 2007) were used to constrain the depth to the sedimentary units and basement along profiles OO' and II'. For offshore Venezuela, the depth to the acoustic basement was controlled using refraction surveys conducted by Ewing et al. (1957), Edgar et al. (1971) and more extensively using the maps of thickness of sediments above acoustic basement and depth to acoustic basement, both of which were compiled by Westbrook et al. in Speed, Westbrook et al. (1984).

As indicated by Edgar (1958), beneath the continental shelf of northeastern Venezuela, a depth to Moho of about 25-30 km was assumed, also used for gravity modelling by Bradley (1979) and Ainscough (1983). Additional seismic data concerning the depth to the Moho discontinuity in the area nearby include the Venezuelan Basin, 13 km (Diebold et al., 1981), the Aves Swell, 40 km, south Grenada Basin, 20 km (Boynton et al., 1979; Ughi, 2009) and Guayana Shield, 35-45 km (Schmitz et al., 1999; Chalboud, 2001).

A very important effort has been made since 2004, throughout an interdisciplinary geophysical and geological research carried out within the framework of the BOLIVAR (**B**roadband **O**cean-**L**and Investigations of **V**enezuela and the **A**ntilles arc **R**egion) and GEODINOS (**G**eodinámica Reciente del Límite **N**orte de la Placa **S**udamericana – Recent Geodynamics of the Northern Limit of the South American Plate) projects conducted by Rice and Houston Universities from USA, and several institutions in Venezuela as FUNVISIS, the Central University of Venezuela and the Simón Bolívar University, with the purpose of investigating the geodynamics of the Caribbean-South America plate boundary zone.

In this context, active seismic measurements were taken in 2004 in northern Venezuela and in the southeast Caribbean as reported by Levander et al.

(2006). See Figure 4.11 for location of seismic transects carried out in the framework of BOLIVAR and GEODINOS projects, and Figure 4.12 where a preliminary Moho map of northern Venezuela, product of the contributions of these projects, is exhibited (Schmitz et al., 2008).

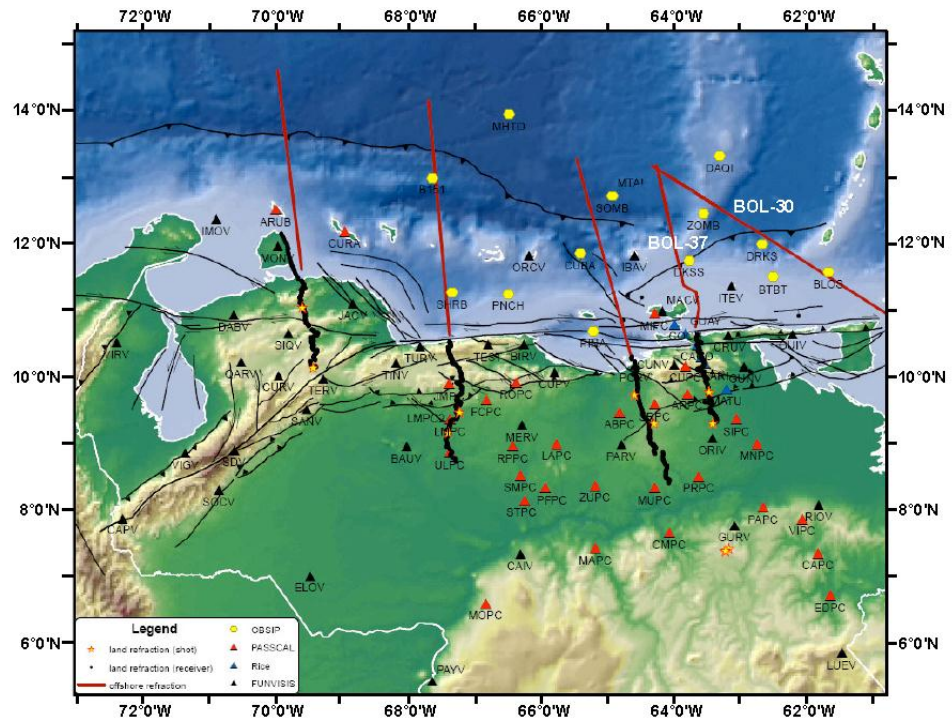


Figure 4.11. Map of the Caribbean-South America interaction zone showing the location of seismic transects carried out in the framework of BOLIVAR and GEODINOS projects. Red lines are reflection profiles on the sea, black lines are refraction profiles inland Venezuela, yellow points are OBS; red, blue and black triangles are seismological stations. (Taken from Schmitz et al., 2008)

Among these contributions it is also interesting mentioning the velocity model proposed by Bezada et al. (2010) along profile 65W (Figure 4.13) where they do not observe a sharp contrast in Moho depth and crustal velocities across the El Pilar fault zone as was expected from BOLIVAR work in other areas of the South America-Caribbean.

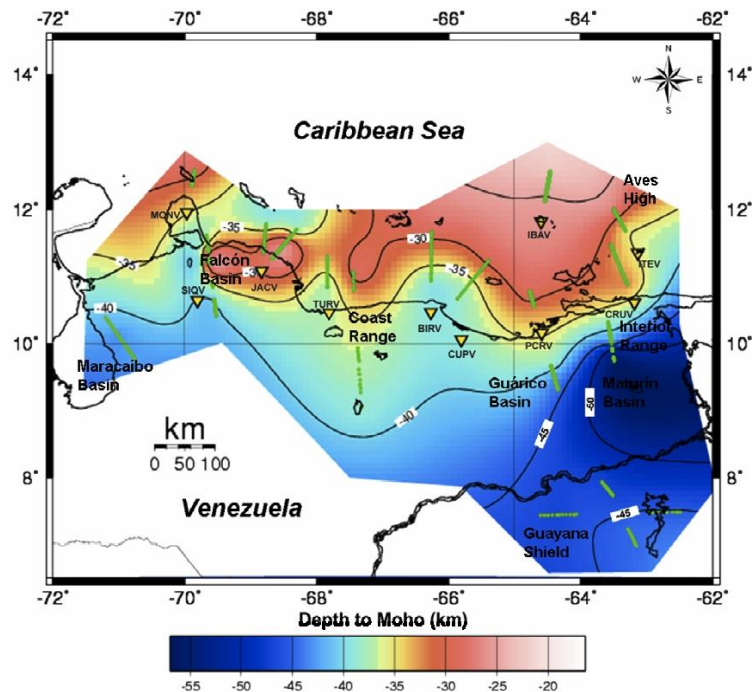


Figure 4.12. Moho map from BOLIVAR and GEODINOS data (Schmitz et al., 2008).

4.5.3. CONSTRAINTS FROM DENSITY MEASUREMENTS.

The density of rocks exposed at the surface provided some control for shallow depth. The result of density measurements from samples of rocks of the study area (collected by members of the staff and students of the Geology Department of the Central University of Venezuela during geological surveys and field work) are summarized in Table 4.1. Additional constraints on density values come from published measurements (Hedberg, 1936; Renz et al., 1958; Vierbuchen, 1979; Rodríguez et al., 2009) and from core samples and density logs run in some wells in the basin area.

Where no data from wells were available to constrain the density at depth, density values were assigned on the basis of depth of burial of sediments or relating compressional velocities from seismic refraction profiles to rock densities through the empirical velocity-density curves of Ludwig et al. (1970) which are indicative of the general trend for commonly occurring rocks.

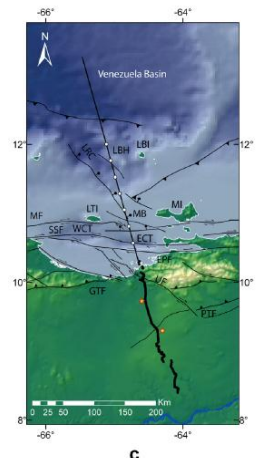
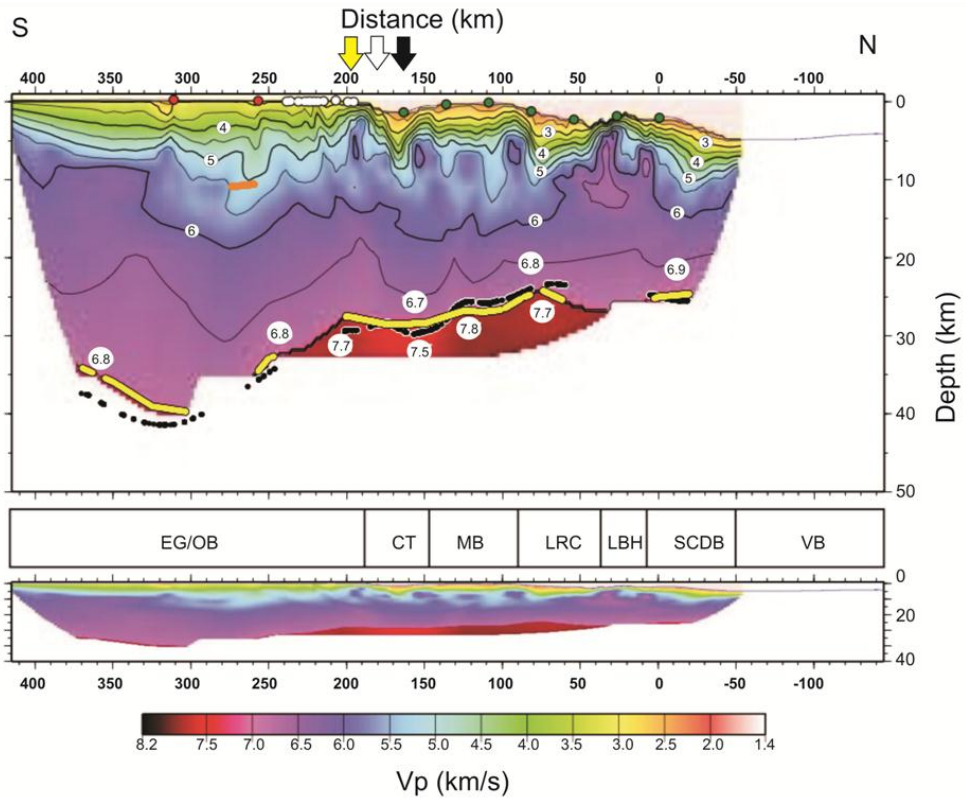


Figure 4.13. Final velocity model for profile 65W shown with (top) a 5x vertical exaggeration and (bottom) no vertical exaggeration. Velocities in the lower crust and upper mantle labeled in km/s. Isovelocity contour interval is 0.5 km/s, with thicker contours labeled. Green dots indicate the location of OBSs, white dots indicate the location of Texan stations with picked records, red dots indicate the location of land shots. Yellow dots in the bottom of the model correspond to bounce points of modelled PmP reflections referred to in the text as rat trace Moho; the tomographic Moho is indicated in black. Orange dots at a depth of ~ 10 km between model distances 260 and 280 km represent bounce points of the intracrustal phase interpreted as a reflection from the base of the Espino graben. VB, Venezuela basin; SCDB, Southern Caribbean Deformed Belt; LBH, La Blanquilla high; LRC, Los Roques canyon; MB, Margarita basin; CT, Cariaco trough; EG/OV, Espino graben/Oriental basin (Eastern Venezuela basin). Black arrow shows the location of the San Sebastian fault, white arrow shows the location of the El Pilar fault, and yellow arrow shows the location of coastline. Modified after Bezada et al. (2010)

TABLE 4.1. DENSITIES USED FOR BOUGUER ANOMALY COMPUTATION

		DENSITY g/cm ³
ρ_w :	Sea water	1.027
ρ_{qs} :	Quaternary sediments	2.1
ρ_{ts} :	Tertiary sedimentary rocks	2.3
ρ_{ks} :	Cretaceous sedimentary rocks	2.4
ρ_{km} :	Cretaceous metamorphic rocks	2.67
ρ_i :	Igneous rocks	2.7

REFERENCE DENSITIES FROM SAMPLE'S MEASUREMENTS

GEOLOGIC UNIT	AGE	LITHOLOGY	DENSITY g/cm ³
Querecual	Late Cretaceous	Limestone	2.53-2.55
Caratas	Eocene	Limestone	2.69-2.61
		Sandstone	2.51
San Juan	Late Cretaceous	Sandstone	2.51-2.43-2.32
El Cantil	Early Cretaceous	Limestone	2.50
Barranquín	Early Cretaceous	Sandstone	2.38
		Limestone	2.52

REFERENCE DENSITIES FROM DENSITY LOGS OF WELLS TE AND BO
EASTERN VENEZUELA BASIN

GEOLOGIC UNIT	AGE	DENSITY g/cm ³	SOURCE *
Las Piedras	Pleistocene	2.05-2.25	TE
La Pica	Late Miocene	2.10	BO
		2.13-2.25	TE
Carapita (surface)	Mid Miocene	2.15	BO
Naricual (surface)	Oligocene	2.45	TE-BO
Naricual (depth)	Oligocene	2.57-2.64	TE
San Antonio	Late Cretaceous	2.27-2.34	BO
San Juan	Late Cretaceous	2.22-2.30	BO
Vidoño	Paleocene	2.40-2.65	BO
Caratas	Eocene	2.42	BO

* NOTE: TE and BO are the names of the wells.

4.5.4. SPECTRAL ANALYSIS FROM GRAVITY DATA

Using the capabilities of MAGMAP (Geosoft, 2010) the technique of spectral analysis was applied to Bouguer gravity anomalies to determine the depth to the source of the anomalies (Figure 4.14). In doing that, a grid (in the space domain) is transferred to and from the wavenumber domain by using a Fast Fourier Transform (FFT). A given potential field function in the space domain has a single and unique wavenumber domain function, and vice-versa. The energy spectrum is a 2D function of the energy relative to wavenumber and direction, and the radially averaged energy spectrum is a function of wavenumber alone and is calculated by averaging the energy at all directions for the same wavenumber.

When considering a grid that is large enough to include many sources, the log spectrum of this data can be interpreted to determine the statistical depth to the tops of the sources (z) using the relationship:

$$\text{Log } E(r) = 4\pi z r$$

The depth of the *ensemble* of sources is easily determined by measuring the slope of the energy (power) spectrum and dividing by 4π .

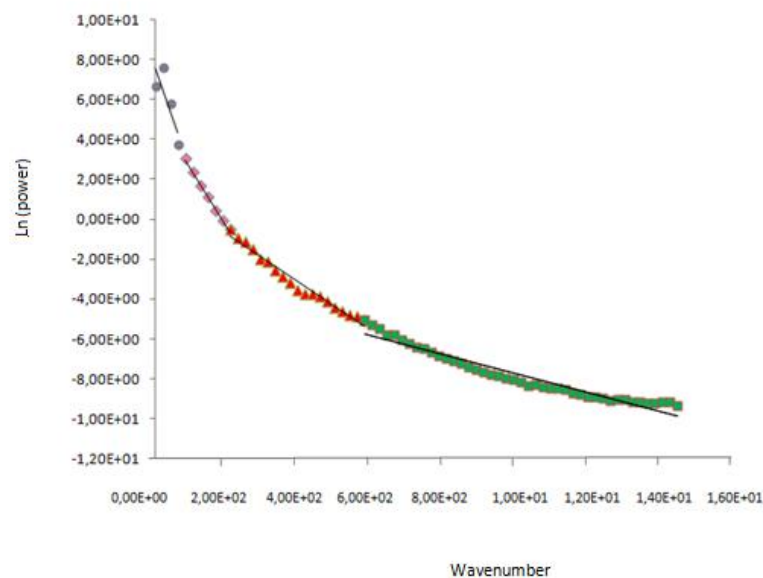






Figure 4.14. Depth determination from spectral analysis of gravity data.

The depths determined from the spectral analysis (Figure 4.14) are as follows:

SYMBOL	S	Z (km)	DESCRIPTION
	-5.40E+02	42.9718346	Moho
	-3.02E+02	24.0323964	Upper-Lower Crust Boundary
	-1.27E+02	10.1063389	Basement
	-4.90E+01	3.8992961	Sediments

More recent interpretation of aeromagnetic data from the Guayana Shield summarized by Rodríguez et al. (2009) has also been used to control depth to the basement determined by spectral analysis.

4.5.5 CRUSTAL SECTIONS IN EASTERN VENEZUELA.

In order to constraint the models, generalized geological cross-sections were constructed along profiles OO' and II' (Figure 4.15). In so doing, all the surface and subsurface data available were used. The geological models were converted into a series of polygons with its corresponding densities to provide the initial input model for the gravity modelling with GM-SYS (Geosoft, 2010). Main geological and geophysical constraints imposed on the model came from: borehole, seismic and spectral analysis of gravity and aeromagnetic data.

Density data from the sources above mentioned and depth information using refraction and reflection lines in the vicinity of the profiles (Ewing et al., 1957; Edgar et al., 1971; Muñoz, 1985; Speed and Westbrook et al., 1984; Schmitz et al., 1999; 2005, 2008) as well as the bathymetry, and depth to basement estimates from spectral analysis of gravity data (Figure 4.14) and from aeromagnetic maps (Rodríguez et al., 2009) provided valuable modelling constraints to make good quantitative estimates of the shallow structure in the investigation area.

On that basis, we consider that the near surface section is accurate and allows modelling the deep crustal structure, investigating subsurface relationships that, being tectonically feasible, would provide a good fit to the observed gravity anomaly.

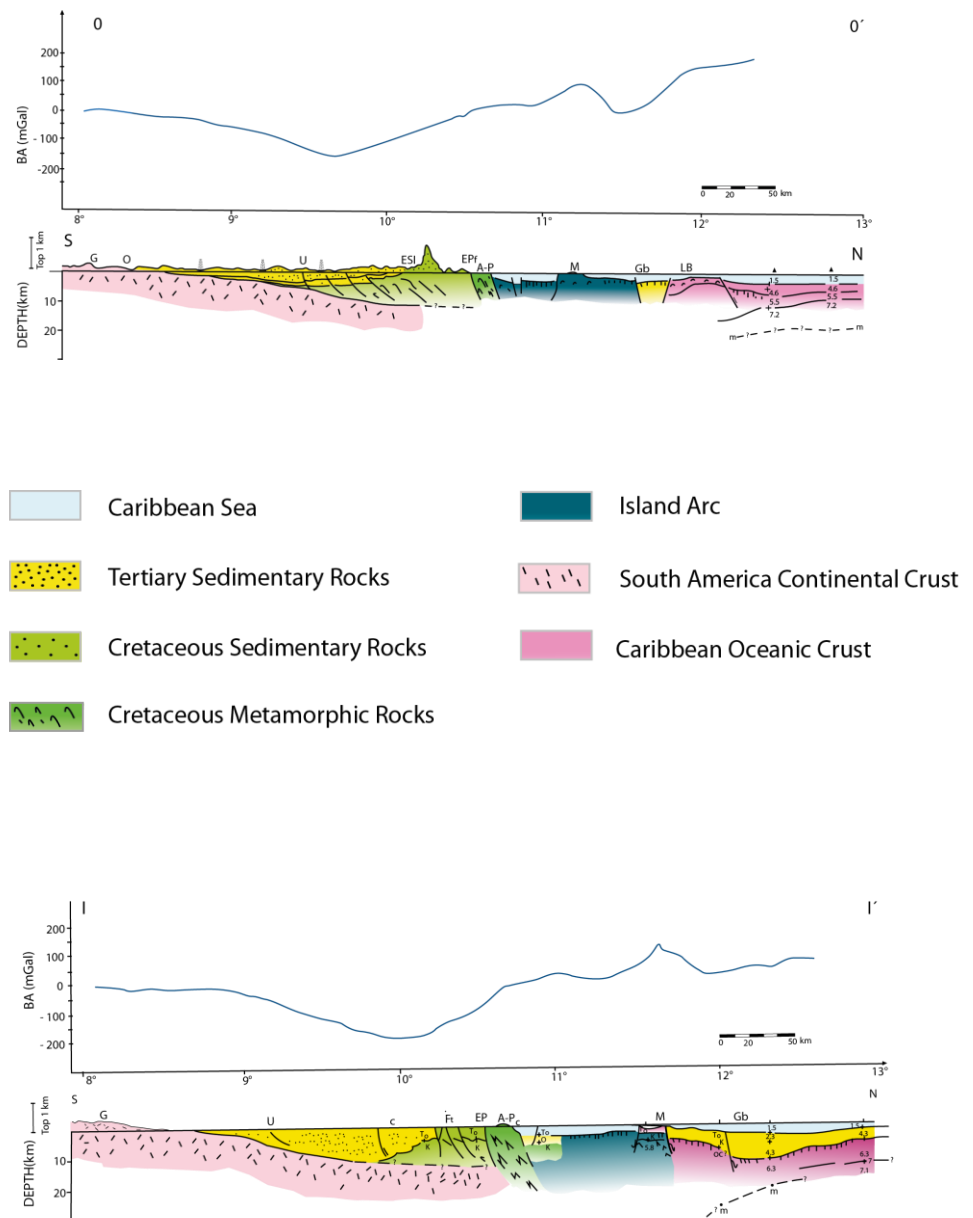


Figure 4.15. Structural models for profiles OO' and II' illustrating the near surface structure and the observed Bouguer anomaly.

The gravity models derived from the structural sections were created using the capabilities of GM-SYS profile 2D-Modelling software (Oasis montaj, Geosoft, 2010) which uses a friendly and interactive interface. Once the geologic model represented by a set of polygonal shape bodies of specific densities is created, GM.SYS calculates and compares the gravity response to the observed measurements, and produces graphic outputs of the models.

The gravity models along profiles OO' and II' are represented in Figures 4.16 and 4.17 to show the fit between observed and calculated Bouguer anomalies, as well as the major features of the structural models whose description follows hereinafter:

- Sedimentary units (1, 2, 3, and 4) represent the upper Tertiary, lower Tertiary and Cretaceous of the Eastern Venezuela basin respectively. It is geologically reasonable to assume that the Cretaceous section might thicken northwards because of thrust repetition, as can be observed in some area wells. The modelling also indicates that the whole sedimentary sequence in the Eastern Venezuela basin might reach thicknesses of around 10-13 km in agreement with seismic and aeromagnetic information (Fig. 3.6).

- The metamorphic Araya – Paria terrane, a body of metasedimentary rocks, has been modeled as a narrow block dipping northward at a high angle. The Margarita – Los Testigos platform, an igneous body resting on high density rocks of accreted terranes. The southern extension of the Aves ridge (paleo island arc) is present at the northern extreme of the profile. Grenada basin is a deep trough filled with sediments of the Tertiary.

- The continental crust of South American plate has been modelled as a two layer crust; the densities constrained from seismic data (Schmitz et al., 1999, 2008; Chalboud, 2001) were assumed as 2.7 g/cm^3 for the upper crust and 2.9 g/cm^3 for the lower crust. The depth to the upper-lower crust boundary (24 km) and Moho (44 km) were also constrained from the spectral analysis in section 4.5.4. The Caribbean oceanic crust was modelled

assuming density values of 2.8-2.85 g/cm³ whereas a value of 3.3 g/cm³ was assumed for the upper mantle, on the basis of seismic data from Schmitz et al. (1999) and Chalboud (2001). The maximum depth of Moho beneath the basin required to fit the observed Bouguer anomaly is ~ 48 km

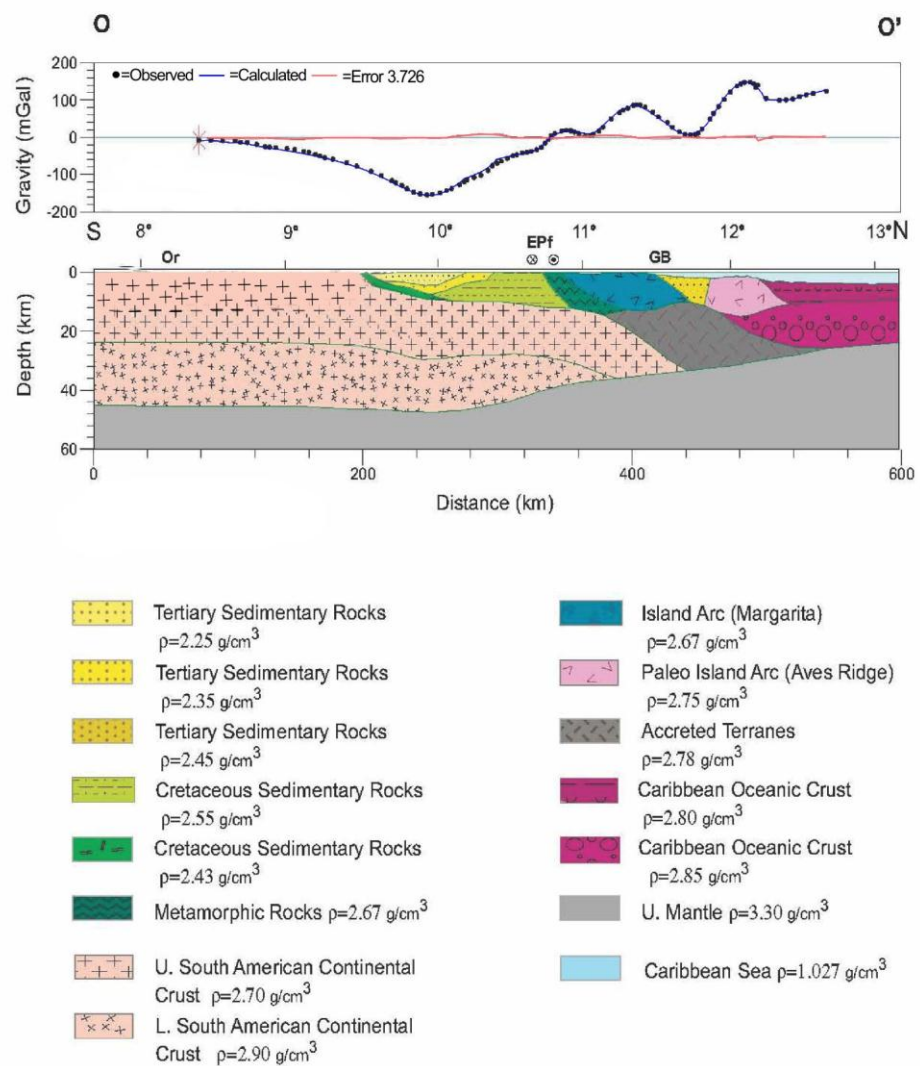


Figure 4.16. Bouguer gravity model along profile OO' in Eastern Venezuela (For location see Fig. 4.2)

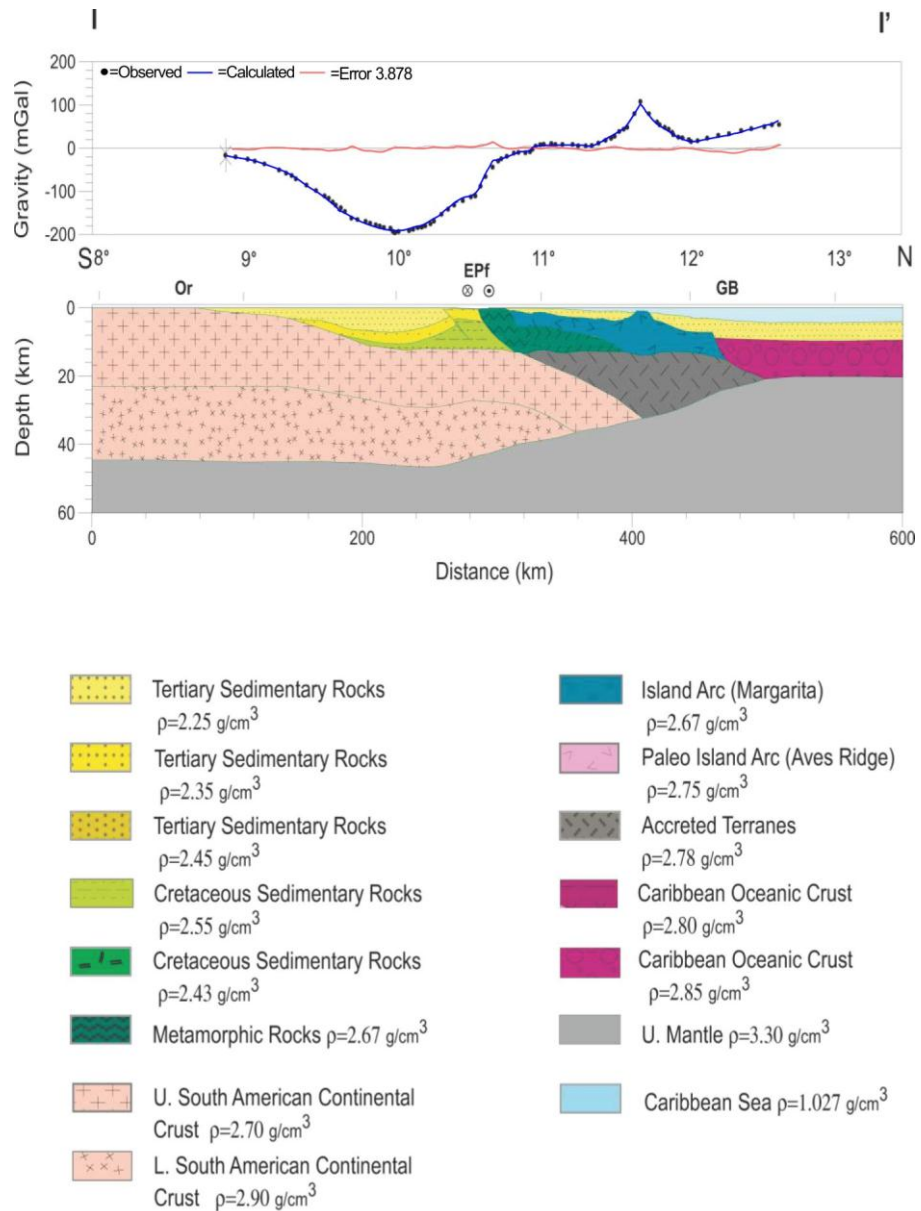


Figure 4.17. Bouguer gravity model along profile II' in Eastern Venezuela (For location see Fig. 4.2).

An estimate of the gravity contribution of the sedimentary rocks infilling the Eastern Venezuela basin is shown in Figures 4.18. There we can observe that the effect of the sediments represents ~ 65-75% of the total Bouguer Anomaly over the Eastern Venezuela basin, along profiles OO' and II' respectively.

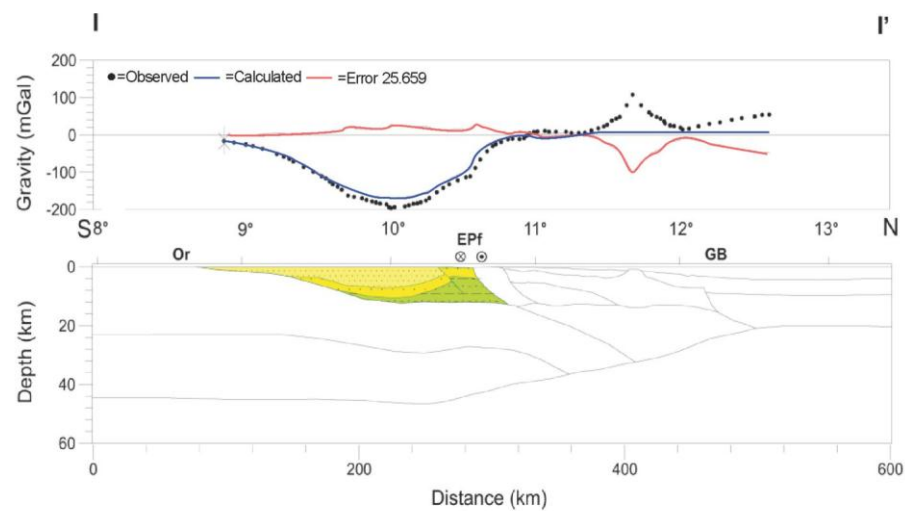
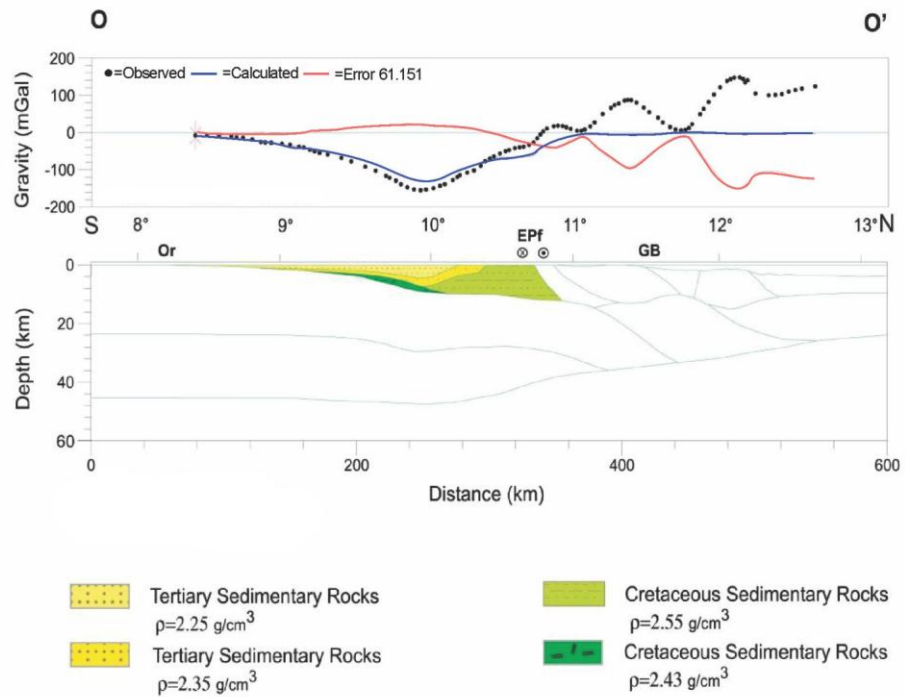


Figure 4.18. Bouguer gravity models along profiles OO" and II', showing the contribution of the sedimentary sequence of the Eastern Venezuelan basin (For location see Fig. 4.2).

Although a reasonable good fit has been obtained for the proposed models, it is important to be aware that gravity solutions are not unique; however, these models represent a very well constrained satisfactory solution to the problem of gravity in Venezuela. The flexural analysis developed in Chapter 5 will provide additional constraints to the model in depth.

An alternative model inspired by the nearly vertical fault hypothesis used in previous studies (Perez et al., 2001; Clark et al., 2008) was also tested. Clark et al. (2008) proposed that the strike-slip plate boundary produced a clean tear through the entire lithosphere, a process that would be currently concentrated at the Paria cluster of seismicity. This tear would separate subducting Atlantic lithosphere from the buoyant South America lithosphere and mark the southern end of the subduction. The body wave tomography data showing the slab south of the strike-slip fault in the tear region suggests a more complicated mechanism for detaching the Atlantic lithosphere from the South American lithosphere than a clean tear.

A rough gravity anomaly was calculated to test that hypothesis, keeping the shallow constraints used for flexural models along profiles OO' and II'. Figure 4.19 illustrates the gravity response of the Clark et al. (2008) model which exhibits an error ~ 200 mGal in excess of the observed anomaly, mostly in the northern area. Apart from the considerations related to the ambiguity of the gravity interpretation, to fit this model it would be necessary to account for a significant density deficit in the northern area, which looks improbable due to the geological characteristics of the region.

Jouanne et al. (2011) suggest a shallow locking depth or an aseismic component along the upper part of El Pilar fault. This suggests that the fault is not vertical at the lithospheric scale. Aseismic displacement could affect the ductile part of the El Pilar fault dipping northwards below the Araya-Paria peninsula and the Margarita Island as suggested by their structural model (Jouanne et al., op. cit., Fig. 2).

El Pilar fault thus has minimal possibilities of being the northern limit of the South American lithosphere, because the loads that could be applied onto the plate, although they would produce the deflection of the Guayana Craton under the basin, fail to produce the fit of calculated to observed gravity anomaly giving higher values than should be expected in the area beneath the foreland belt.

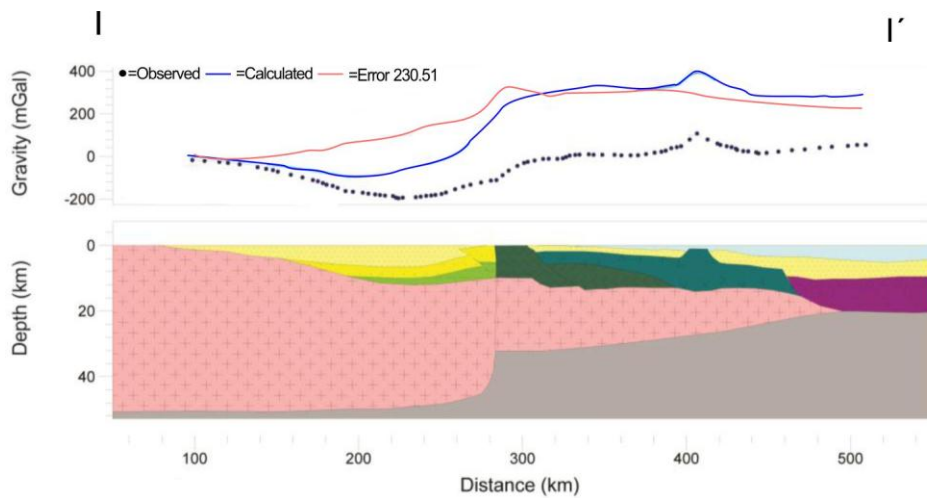
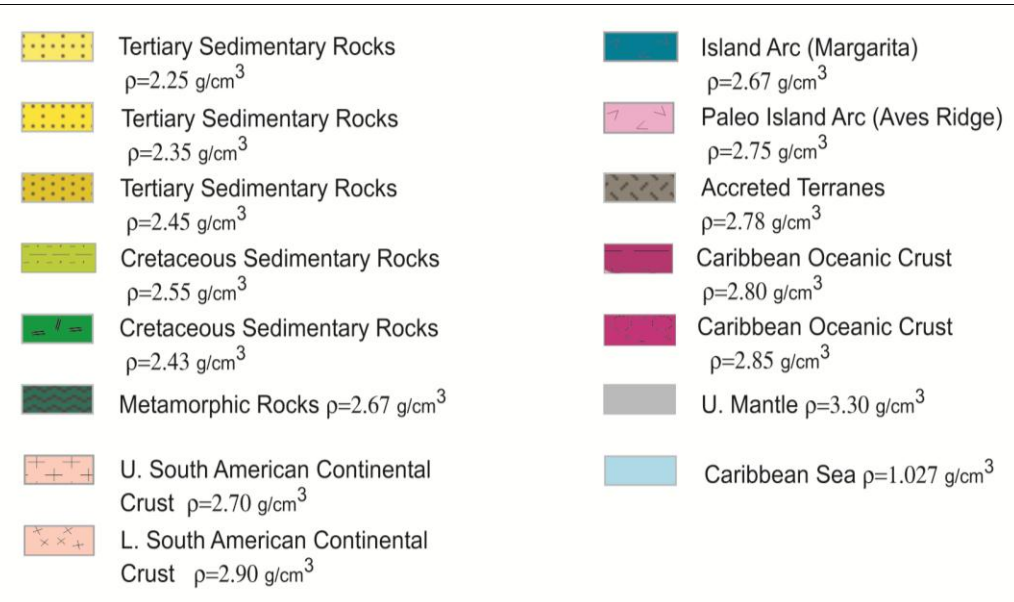
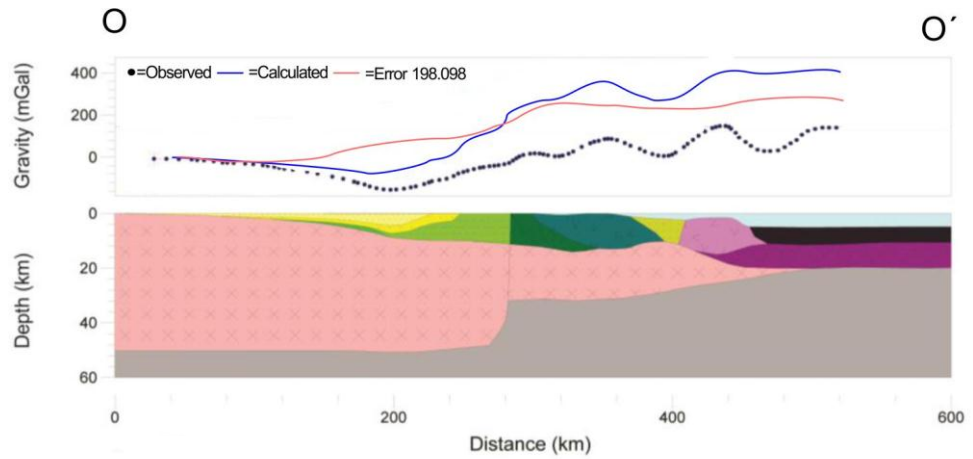


Figure 4.19. Bouguer gravity models along profiles OO' and II' to test the structural or seismic models proposed by Clark et al. (2008).

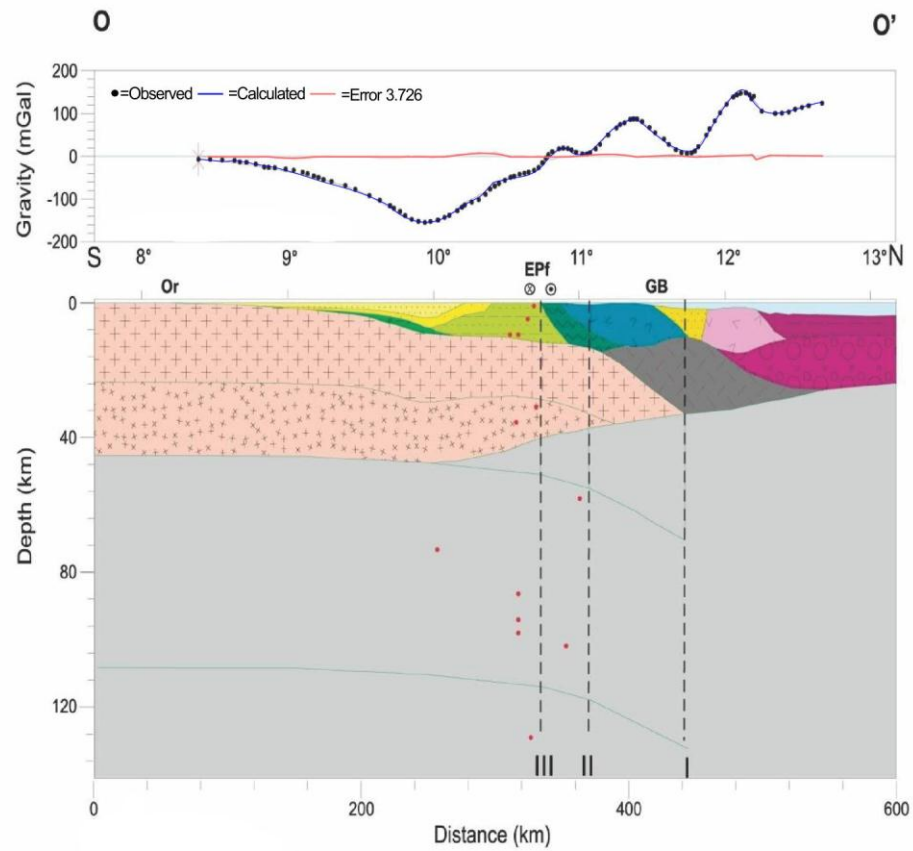
Gravity models along profiles OO' and II' (Fig. 4.16 and 4.17) have been interpreted taking into consideration the geological and geophysical constraints reported in sections 4.5.1 to 4.5.4, which provide strong support to our interpretation, then I can conclude that they represent the best available crustal sections of the area of study in eastern Venezuela.

4.5.6. SEISMICITY AND GRAVITY MODELLING

Hypocentral locations for earthquakes of magnitude >5 (Data in Appendix D, and location in Figures 2.12 to 2.14) were projected onto profiles OO' and II' (Figures 4.20 and 4.21 respectively) where the theoretical lithospheric extension in depth (paralleling the flexural trend) and the possible northern edges of the South American plate are also shown.

Shallow seismicity shown on profiles OO' and II' (0-13 km depth, within the area of the Eastern Serranía del Interior thrust belt) is probably associated with north dipping thrust faults which represent the southern limit of the thrusting structural domain in eastern Venezuela, although Jouanne et al. (2011) suggest lack of significant shortening across the thrusts of the Eastern Serranía del Interior at present. These shallow thrust events indicate that thrusting is active in the area and probably related to transpression between Caribbean and South America plates as proposed by Russo et al. (1993).

It is interesting to observe on profile II' (Figure 4.21) the location of some hypocenters coincident with the interpreted crust-mantle boundary we proposed. Apart from the uncertainties affecting earthquakes locations and the ambiguity in gravity modelling, this might reflect a weakening zone product of the detachment of the northern part of the continental South American crust, i.e. the oceanic or transitional crust product of the South-North American plate break-up. In our model this boundary represents a contrasting crust-mantle density zone ($\Delta\rho \sim 0.4-0.5 \text{ g/cm}^3$) as the one interpreted by Bezada et al. (2010, Fig.6) in their velocity model for profile 65W shown in Figure 4.13.


















- | | | | |
|-------------------------------------------------------------------------------------|-------------------------------------------------------------------|---------------------------------------------------------------------------------------|-------------------------------------------------------------|
|  | Tertiary Sedimentary Rocks
$\rho=2.25 \text{ g/cm}^3$ |  | Island Arc (Margarita)
$\rho=2.67 \text{ g/cm}^3$ |
|  | Tertiary Sedimentary Rocks
$\rho=2.35 \text{ g/cm}^3$ |  | Paleo Island Arc (Aves Ridge)
$\rho=2.75 \text{ g/cm}^3$ |
|  | Tertiary Sedimentary Rocks
$\rho=2.45 \text{ g/cm}^3$ |  | Accreted Terranes
$\rho=2.78 \text{ g/cm}^3$ |
|  | Cretaceous Sedimentary Rocks
$\rho=2.55 \text{ g/cm}^3$ |  | Caribbean Oceanic Crust
$\rho=2.80 \text{ g/cm}^3$ |
|  | Cretaceous Sedimentary Rocks
$\rho=2.43 \text{ g/cm}^3$ |  | Caribbean Oceanic Crust
$\rho=2.85 \text{ g/cm}^3$ |
|  | Metamorphic Rocks
$\rho=2.67 \text{ g/cm}^3$ |  | U. Mantle
$\rho=3.30 \text{ g/cm}^3$ |
|  | U. South American Continental Crust
$\rho=2.70 \text{ g/cm}^3$ |  | Caribbean Sea
$\rho=1.027 \text{ g/cm}^3$ |
|  | L. South American Continental Crust
$\rho=2.90 \text{ g/cm}^3$ | | |

Figure 4.20. Bouguer gravity model along Profile OO' showing hypocentral depth (red dots) for earthquakes of magnitude > 5.

It could equally be explained in terms of a density contrast between the continental crust and part of the detached oceanic or transitional crust because, as Holt et al. (2010) have stated, the lithosphere beneath accretionary crust is not depleted by the melting events which produce the crust, but is compositionally no different from the upper mantle.

As in the Alps where a dense region of cool subducted upper mantle underlies the mountain belt which opposed the isostatic influence of the thickened crustal root (Bott, 2009), a region of high density (detached oceanic or transitional crust, or upper mantle) may underlie the Eastern Venezuelan belt (probably related to transpression rather than simple compression as in the Alps) and may explain the gravity anomaly.

In this scenario, the formation of the Tertiary Eastern Venezuela foreland basin occurred over a plate boundary already formed during an earlier extensional phase (Jurassic-Cretaceous times) and areas of weakness have been subsequently undergoing reactivation.

Deep seismicity shown on profiles OO' and II' (>80 km depth) is mostly concentrated around 11°N, an area where the present-day convergence between the Caribbean and the South American plates is active. Seismicity increases in depth slightly to the north and is also more active eastwards as seen on profile II'. These deep earthquakes seem to be fully consistent with near-vertical cool sinking of the mantle to the north.

The northeastern region of the South American plate, being part of the zone of interaction with the eastern Caribbean plate and the Atlantic slab subducting westward, is an area of intense seismic activity. Seismicity below this region probably occurs in association with mechanical discontinuities connecting zones of contrasting density structure, within the crust or deeper in the mantle, as Tassara et al. (2007) have described in the northeastern margin of the Guayana Shield.

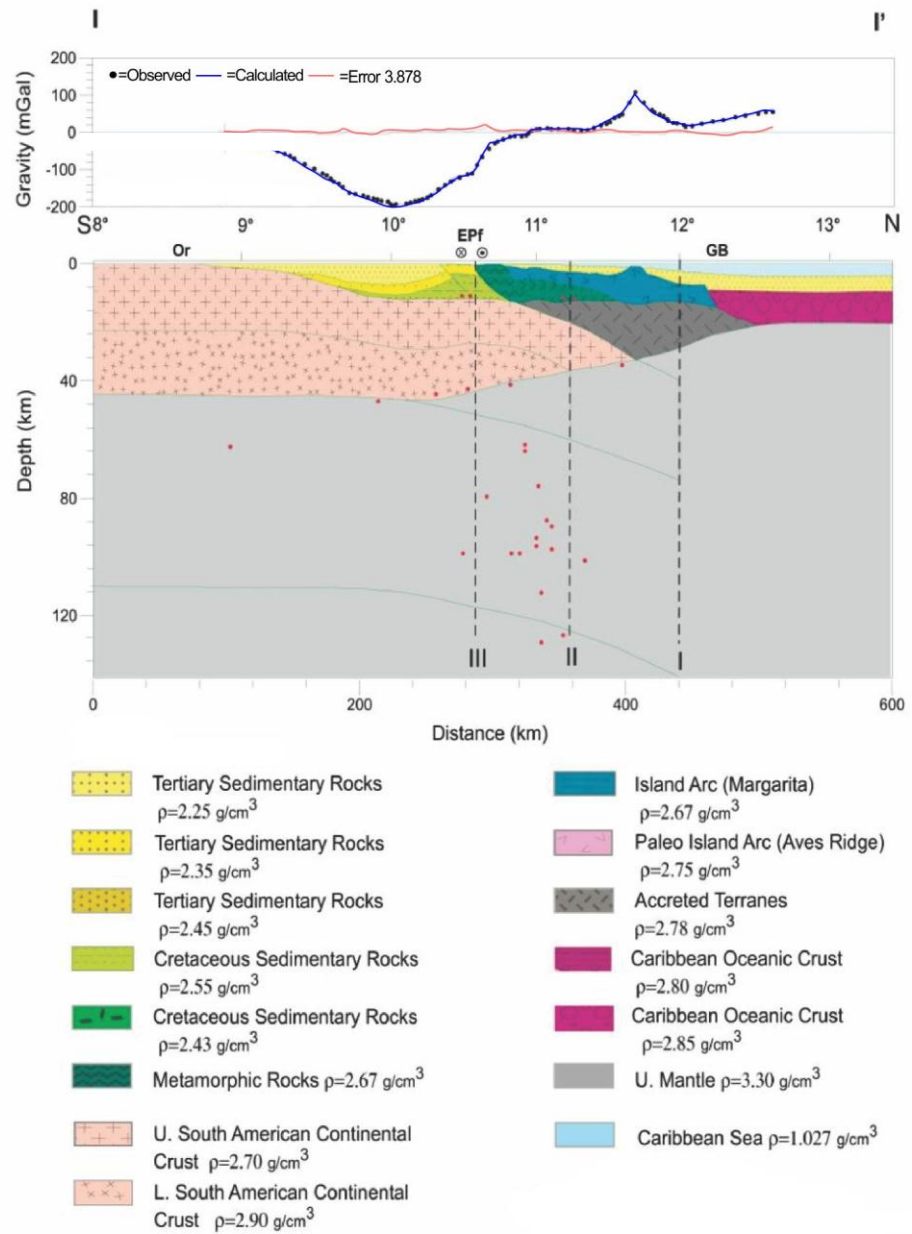


Figure 4.21. Bouguer gravity model along Profile II' showing hypocentral depth (red dots) for earthquakes of magnitude > 5.

CHAPTER 5

EASTERN VENEZUELA FORELAND BASIN FORMATION

5.1. INTRODUCTION.

Chapter 5 deals with the mechanism of formation of the Eastern Venezuela foreland basin and linked Serranía del Interior and Coastal Cordillera uplifts to the north. The primary cause (since the Oligocene) has been N-S transpressive compression at the E-W dextral transform plate boundary separating the Caribbean and the South American plates. This arises during the eastern movement of the Caribbean plate relative to north Venezuela on the South American plate since the Oligocene, when the convergence between the North American and South American plates may have been triggered by an eastward jump of the subduction/island-arc system to the north (?). In mid Miocene times a change in the Caribbean-South American direction of convergence occurred from ENE to E (Pindell and Kennan, 2001a). The mechanism may be related to processes at the northern and eastern Caribbean plate edges which are being forced together. N-S horizontal compressive stress is progressively released as the crust immediately south of the boundary is shortened by reverse faulting and deep plastic crustal thickening with uplift. Additionally, dense Caribbean crust may be obducted into or over the southern crust and Caribbean mantle may be subducted beneath, modifying the loads. To the south of the northern ranges, the spectacular foreland basin develops over the same time interval.

Two approaches have been used in understanding the mechanism of formation of the Eastern Venezuela foreland basin and linked northern compressional ranges. These are: (1) linked to simple flexural analysis involving the concept of "hidden gravitational loads" and (2) explained directly by the mechanism of reverse/thrust faulting in response to N-S ongoing compressive stress. Both of the mechanisms involved flexural analysis which is described in section 5.2. The following sections will be devoted to describe, apply and compare the results from these methods.

5.2. FLEXURE OF THE CONTINENTAL LITHOSPHERE

Pioneering studies of the flexure of the continental lithosphere have followed the explanation proposed for the oceanic lithosphere (Walcott, 1970a-b, 1972; Watts and Talwani, 1974; Bodine and Watts, 1979; Watts, 2001) that the long-term behaviour of the lithosphere in response to the loads placed upon it, may be characterized by the flexure of a thin elastic plate overlying the asthenosphere, the weak layer in which the flow of the mantle takes place. There has also been a number of works dealing with the bending of an elastic lithosphere (Haxby et al., 1976; Watts, 1978; Karner and Watts, 1983) and refinements of the theory using viscoelastic models (Sleep and Snell, 1976; Beaumont, 1978, 1979, 1981; Turcotte, 1979) and elastic-perfectly plastic rheologies (Turcotte et al., 1978; McAdoo et al., 1978).

However it has been shown that, even though it may represent a gross oversimplification to the real Earth behavior, the model of an elastic plate overlying an inviscid fluid is adequate to predict the lithospheric deformation (Karner et al., 1983; Burov and Diament, 1995), particularly for flexural processes occurring in times longer than the relaxation time of the asthenosphere and shorter than that of the elastic lithosphere (Walcott, 1970a-b). It is therefore reasonable to assume, as a first approximation, that the asthenosphere is a dense inviscid fluid when modelling the formation of sedimentary basins over time-scales of 10^7 to 10^8 years (Beaumont, 1978).

5.2.1. SOME THEORETICAL CONSIDERATIONS

The approach to be used here is to assume a simple elastic model, where a "thin plate" represents the continental lithosphere (meaning that its thickness is small in relation to its lateral extent) and then using the basic theory of deformation of an elastic beam developed by Hetenyi (1979).

In its most general form, the vertical deflection or displacement w of an elastic plate in response to a load $h(x)$ is given by:

$$\frac{\partial^2}{\partial x^2} \left[D(x) \frac{\partial^2 w}{\partial x^2} \right] - P(x) \frac{\partial^2 w}{\partial x^2} + \Delta \rho_2 g w = \Delta \rho_1 g h(x) \quad (5.1)$$

where $D(x)$, the flexural rigidity of the plate, is a measure of its resistance to bending, principally determined by the plate thickness (Walcott, 1970a, 1976) and defined as:

$$D(x) = \frac{E T_e(x)^3}{12 (1 - \nu^2)} \quad (5.2)$$

As can be noticed, the flexural rigidity depends on $T_e(x)$ which is the elastic thickness of the plate (i.e. the fraction of the lithosphere that behaves elastically on a geologic time-scale) and also on the intrinsic elastic properties of the plate: E is Young's modulus and ν is Poisson's ratio. Other parameters in (5.1) are: $\Delta \rho_2 = \rho_m - \rho_s$, the density contrast between the material underlying the plate (ρ_m) and the material infilling the deflection (ρ_s); $\Delta \rho_1 = \rho_l$, the density contrast across the surface topography, that is the density of the load; g is the gravitational acceleration, and $P(x)$ is the pre-stress condition or residual stress within the plate before loading.

Residual stresses are defined in the sense of the theory of elasticity as "locked-in" stresses associated with the previous history of the rock. They form a set of stresses in equilibrium on which external stresses may be superimposed (Jaeger and Cook, 1976).

The load $h(x)$ is to be understood in the sense pointed out by Karner and Watts (1983) that any horizontal transfer of mass (for instance, the lateral migration of nappes and thrust sheets and the obduction of ophiolites in compressional regimes, the erosion-deposition cycle of sediments, the stretching of the lithosphere) constitutes a load for the lithosphere. The load may occur either on top of, within or beneath the elastic plate.

It follows from Karner (1985) that, in the absence of knowledge on the thermal history of the plate, the assumptions of constant plate rigidity and hydrostatic pre-stress conditions are adequate. Then, the deformation of the elastic plate in response to a point-load H may be expressed by:

$$D \frac{\partial^4 w}{\partial x^4} + \Delta \rho_2 g w = \Delta \rho_1 g H(x) \quad (5.3)$$

The first term in equation (5.3) represents the flexure due to the stressed elastic plate. Dimensionally $\rho.g.h$ represents a stress, and in particular $\Delta \rho_2 g.w$ represents the resultant stress associated with infilling the deformation with sediments or water, and the buoyancy stress associated with displacing mantle from beneath the plate. The right hand term is the applied load.

In the space domain, the general solution of (5.3) according to Hetenyi (1979) is:

$$w(x) = e^{-\lambda x} (C_1 \cos \lambda x + C_2 \sin \lambda x) + e^{\lambda x} (C_3 \cos \lambda x + C_4 \sin \lambda x) \quad (5.4)$$

where: $\lambda^4 = \Delta \rho_2 g / 4D$ (5.5)

λ is the characteristic of the system, an important factor controlling the elastic deformation, since it includes the flexural rigidity D of the plate as well as the elasticity of the supporting medium (Hetenyi, 1979). The parameter λ has the dimension of $(\text{length})^{-1}$ then $1/\lambda$ is frequently referred as the characteristic length of the system. From equation (5.4) solutions can be derived for thin plates of any length, with any assumed loading and end conditions.

The thin elastic plate has been considered either as a continuous plate (Walcott, 1970a-b; Beaumont, 1978) or as a broken plate (Turcotte et al., 1977, 1978; McAdoo et al., 1978; Karner and Watts, 1983; Beaumont, 1981;

Turcotte, 1979). The deflection solutions for these two cases are, respectively:

$$w_c(x) = \frac{\Delta\rho_1\lambda H}{\Delta\rho_2 2} e^{-\lambda x} (\cos \lambda x + \sin \lambda x) \quad (5.6)$$

$$w_b(x) = \frac{\Delta\rho_1}{\Delta\rho_2} 2 \lambda H e^{-\lambda x} \cos \lambda x \quad (5.7)$$

The difference between these two cases is determined by the boundary conditions imposed at the edge, to counterbalance the bending moment and shearing force created by the distributed load throughout the continuous plate. Details of the derivation of the equations are available in Hetenyi (1979) and Karner (1985) and will be omitted here; only those aspects directly relevant to this study need to be reiterated.

The advantages of working in the frequency domain in order to optimize the calculations of deflection and associated gravity anomalies has long been recognized (Parker, 1973; Banks et al., 1977; Karner and Watts, 1983) as it is a particularly useful and less time consuming technique in which only the spectrum of the applied distributed loads needs be provided to obtain the deflection of even complicated rheologies. In the frequency domain, the deflection of a continuous plate can be expressed, according to Banks et al. (1977), as:

$$W_c(k) = \frac{\Delta\rho_1}{\Delta\rho_2} \left[1 + \frac{D k^4}{\Delta\rho_2 g} \right]^{-1} H(k) \quad (5.8)$$

where $W_c(k)$ is the plate response to the applied load spectrum $H(k)$; k is the wavenumber related to the load wavelength L by $k=2\pi/L$, and $\Delta\rho_1$, $\Delta\rho_2$, g and D as previously defined. Computer subroutines Thrust, Bplate and Cplate from Karner (1985), modified to include specific conditions to be considered for the flexural modeling of the Eastern Venezuelan basin, were used to compute the deflection of the basement, and integrated with Parker (1973)'s subroutine to compute the Bouguer and free-air anomalies in the frequency domain.

5.2.2. A FLEXURAL MODEL FOR THE EASTERN VENEZUELA FORELAND BASIN

When reviewing the mechanisms of basin formation in Chapter 3, I have described the present Eastern Venezuelan basin as a foreland basin related to the Eastern Venezuela foreland deformed belt on the basis of its stratigraphy and structural evolution. Foreland basins and associated mountain building processes (Dewey and Bird, 1970) have been explained in terms of the flexure of the lithosphere after loading.

After the initial proposal of Price (1973), several investigators (Jordan, 1981; Beaumont, 1981; Turcotte and Schubert, 1982, 2002; Karner and Watts, 1983; Watts, 2001) have studied the response of the lithosphere to topographic loading as a mechanism capable of producing foreland basins. However, the gravity anomalies associated with foreland basins and mountain belts were not used as a constraint until Karner and Watts (1983), who evaluated the relationship between gravity anomalies and topography at mountain ranges such as the Alps, the Appalachians and the Himalayas.

In the Eastern Venezuela basin, thus far, we have a foreland basin in an area of low topography, with the signature of an impressive negative free-air and Bouguer anomaly, whose isostatic equilibrium obviously cannot be explained in terms of local compensation. Closely related to the basin, there is a deformed thrust and fold belt, plus a metamorphic terrane and magmatic arc (a complex probably emplaced onto the continental South American plate since the Oligocene) exhibiting positive free-air and Bouguer anomalies; all this in a picture that suggests a regional-type of compensation according to flexural mechanisms.

At this point, the proposition that the Eastern Venezuela foreland basin formed in a foredeep as a result of the downward flexure of the lithosphere under the loading of the terranes and deformed belt occurring north of the 9°N of latitude seems the most probable. I have investigated quantitatively the response of the South American lithosphere to loads associated with the

compressional regime of continent/terrane-arc collision that led to the Eastern Venezuela foreland basin formation, using gravity anomalies as a constraint.

Accordingly, the loading scheme used to compute the deflection of a thin elastic broken plate is depicted in Figure 5.1 (Karner and Watts, 1983). The process is initiated by the obduction of a crustal block and, as the lithosphere flexes in response to the applied load, the block accommodates itself into the flexural depression leaving a significant amount of topography exposed; the trough is then infilled with sediments.

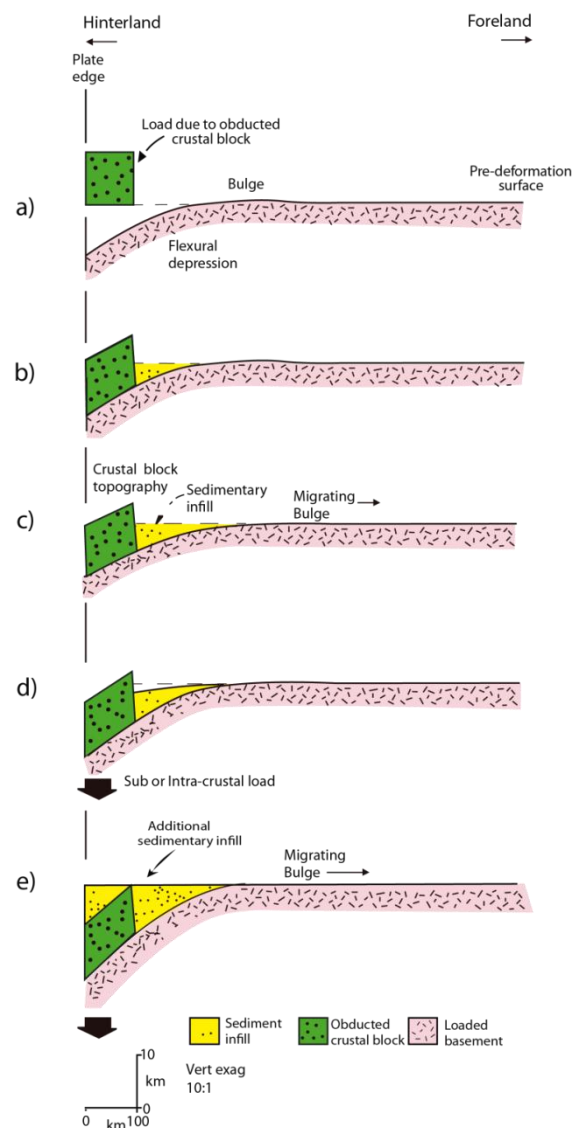


Figure 5.1. The assumed loading scheme describing the emplacement of loads onto the continental lithosphere at mountain ranges and formation of associated foreland basins. (After Karner and Watts, 1983, Figure 9).

Karner and Watts (1983) have shown that even after the sediments completely infill the trough, some topography of the obducted block still remains, and that if this is eroded, given sufficient time, the basement would be expected to rebound, leading to the total destruction of the basin and the obducted block. The fact that many foreland basins still remain, in spite of the peneplanation of their associated mountain belts (for instance: the Appalachians in the Tertiary and the Alps in the Pliocene) led these authors and also Royden and Karner (1984) to suggest that a further load, in addition to the surface topography and obducted block, is acting on or within the lithosphere.

A model to test the formation of the Eastern Venezuela foreland basin as a product of the loading of the South American lithosphere, by the combined effect of topography, thrust slices and nappes emplaced onto the continent plus sediments infilling the trough formed thereby, was developed according to the schematic geologic section shown in Figure 5.2A-B, illustrating the features associated with the loading in the study area.

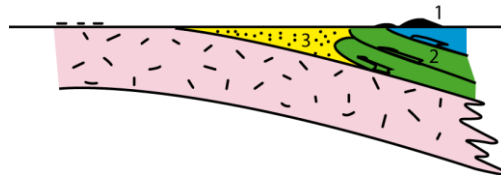


Figure 5.2A. Loading scheme for flexural modelling at the Eastern Venezuela foreland basin. 1 = Surface Load. 2 = Subsurface Load. 3 = Sediments.

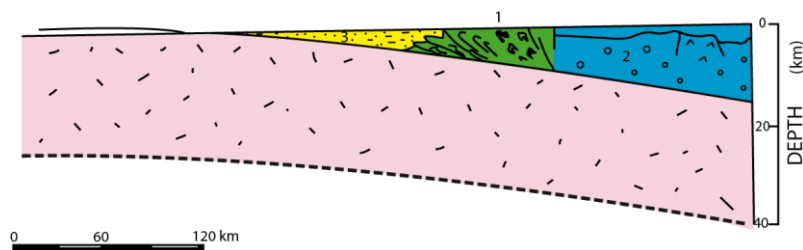


Figure 5.2B. Geological crust-section illustrating the loading scheme in the area of study. 1 = Above sea level topography. 2 = Subsurface load including the thrusts of the Eastern Serranía del Interior, Araya-Paria terrane and the magmatic arc-platform Margarita-Los Testigos. 3 = Infilling sediments of the Eastern Venezuela foreland basin.

In the case under consideration it seems appropriate to model the South American plate as an elastic plate. A stratigraphic argument supports this assumption with other previous considerations. As described in section 3.5 and Appendix A-1, the Eastern Venezuela foreland basin exhibits progressive overstepping of younger strata onto the basement, a pattern that according to Watts et al. (1982, see Figures 4 and 5) and Watts (1992) typifies the sedimentary basins developed in elastic models, in contrast with those developed in viscoelastic models where younger strata are mostly confined to the basin centre (Watts et al., 1982, op. cit.).

I will also consider the South American plate as a broken plate, in cantilever at the Guayana Craton and with the broken end to the north; it does not necessarily mean that the foreland plate is physically broken, although continental splitting occurred at the northern margin of South American in Middle Jurassic (Pindell et al., 1988; Ross and Scotese, 1988). As Royden and Karner (1984) pointed out, the broken slab end might possibly represent a zone beyond which the subducted plate is very weak and hence its ability to transmit bending stresses to the elastic plate would be insignificant.

On the basis of tectonic considerations three end-positions for the broken edge of the foreland plate were chosen (Figure 5.3). These are:

EDGE	LOCATION
I	Grenada Basin (SW end)
II	Margarita - Tobago forearc basin
III	El Pilar fault

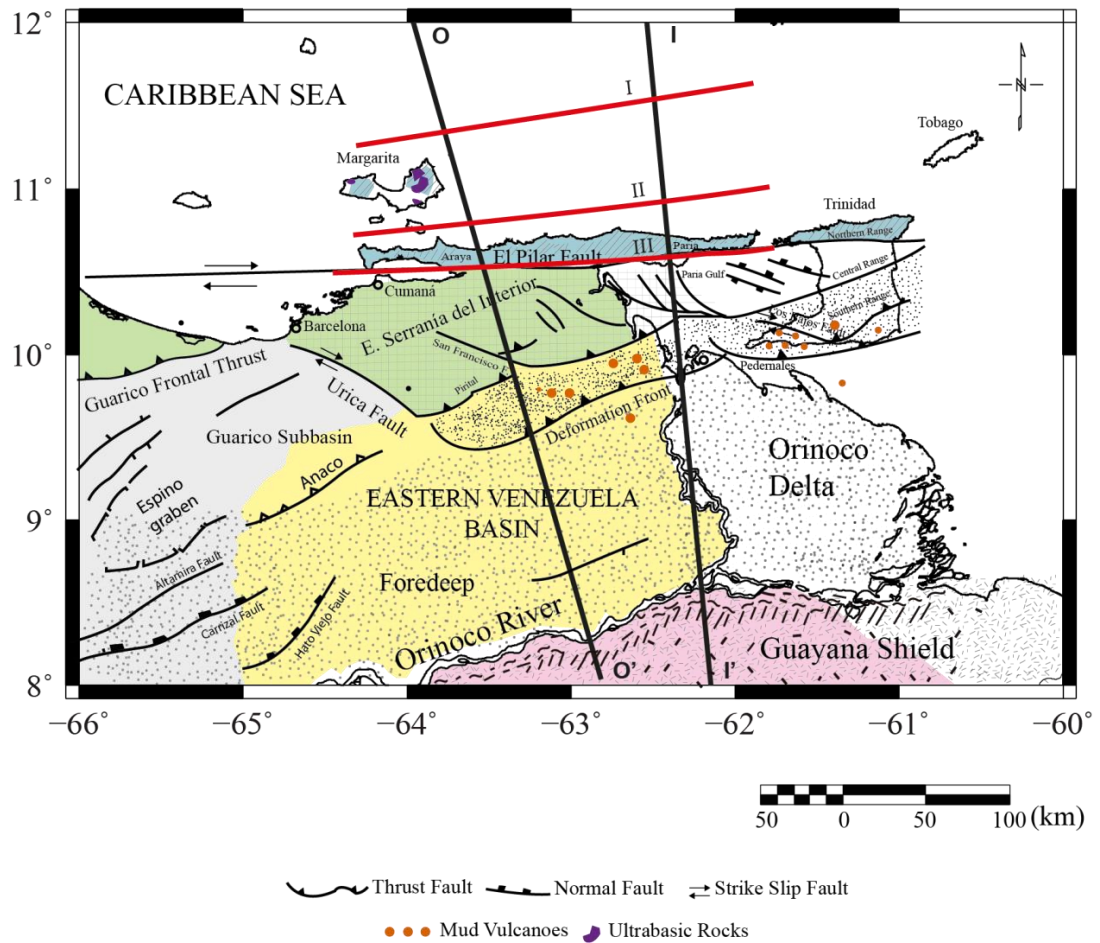


Figure 5.3. Location of profiles OO' and II' illustrating end-positions of the broken South American plate (I-II-III, shown by red lines). I= Grenada Basin (SW end). II= Margarita-Tobago forearc basin. III= El Pilar fault.

The methodology used to investigate the flexure in the area of study is illustrated in Figure 5.4. To start with, it is necessary to evaluate the flexure of the continental South American lithosphere under the loads that can be effectively constrained; i.e.: surface (topography), subsurface (thrusts and terranes).

The spectrum of the surface topography was obtained directly from the topographic maps of the area, represented along profiles OO' and II' (Figure 4.1). For this particular case, the Eastern Venezuela foreland deformed belt, the Araya-Tobago terrane and related forearc, and the magmatic belts farther north, represent an important contributory load to the deflection of the plate.

The spectrum of the thrust and terranes loads was obtained from the structural models interpreted in section 4.5.

Once the topography, thrust and terrane spectra were defined, these loads were applied over the broken elastic plate of continental South America. As the plate flexes downward, the foreland trough formed thereby is filled with sediments; the sediment load is automatically taken care of in the flexural equation (as $\Delta\rho_2$). The values of flexural rigidity, equivalent elastic thickness, densities and elastic parameters E and ν used in the calculations are listed in Table 5.1.

The flexure of the elastic plate, reflected by the wavyline of the deflected basement topography should be compared at this stage, with observed data wherever possible. At this point it is necessary to demonstrate that the amplitude and the wavelength of the flexure are correctly predicted by the model. In doing so, attention should be paid to the flexural bulge amplitude as well as the first node of the flexure or deflection.

This forebulge or outer rise is an important characteristic of the flexure profile and it is usually easy to locate geologically. The flexural bulge is a natural consequence of the existence of $\Delta\rho_2(\rho_m-\rho_s)$ and exists because material displaced from beneath the deflection moves out to the edges of the load. The first node, which represents the condition where $w(x)=0$, separates the negative deflection from the positive uplift of the flexural bulge and it is also a very useful observational parameter (Karner, 1985).

The topography can also be used as a constraint. Once the load accommodates itself into the deflection, the masses remaining above sea level should fit the current surface topography, if there is agreement between the calculated and observed deflections. Regarding the Eastern Venezuela foreland basin, borehole data providing information of the basement depth were used to constraint the calculated deflection.

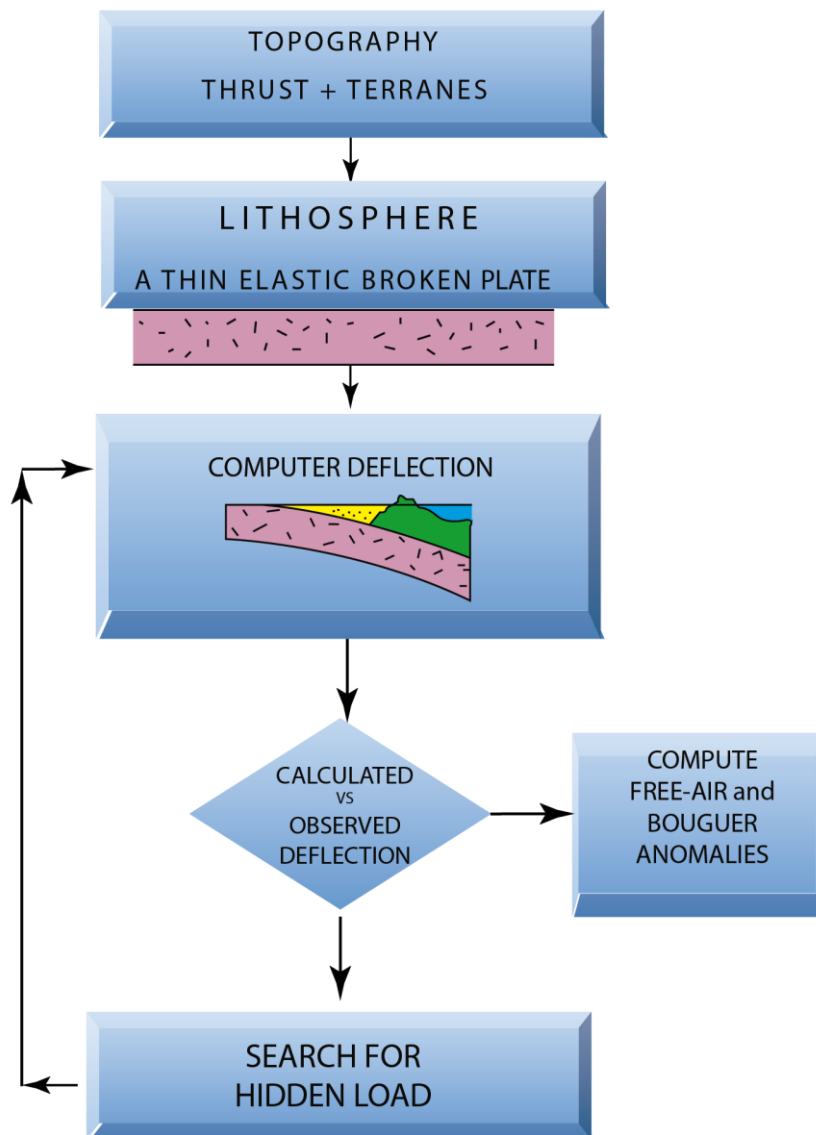


Figure 5.4. Diagram to illustrate the flexural modelling. Surface (topography) and subsurface (thrust and terranes) load spectra are applied over the lithosphere (a thin, elastic, broken plate) and the flexural response calculated and compared with the observed data.

The amplitude of the forebulge represented by the Guayana highlands is about 150-350 m and the first node is clearly defined. These were used to fit the calculated flexural response to the observational parameters.

This is a crucial point in the flexural modelling, and the following step depends on whether the loading scheme used is capable of producing the observed deflection of the basement in the study area. If it does not, it is necessary to search for some extra loads (within or below the crust) such as the *hidden load* of Karner and Watts (1983) that combined with the original scheme might be able to produce a flexural response consistent with the observed deflection. This stage usually involves a great deal of calculation, as it is necessary to look iteratively for the best load distribution to produce the deflection that fits the observed data (Fig. 5.4).

The next step is the calculation of free-air and Bouguer gravity anomalies, to determine whether the flexural model and the resulting crustal structure can satisfy the observed gravity anomalies. The shape of the gravity anomaly gives an indication of the presence of the hidden load. A positive anomaly at the hinterland may be associated with buried loads and a negative anomaly may be related to the deformation of the basement, and can also be used to test the model after the deflection is produced (Karner and Watts, 1983; Jordan and Watts, 2005). The use of gravity anomalies in this process is two-fold. The gravity anomaly depends on both, the loading history and the basement rheology, so it may be a useful constraint on the model (Watts et al., 1982). This represents a dynamic gravity modelling and regarding to the long recognized ambiguity in the gravity interpretation (Skeels, 1947; Watts and Talwani, 1974) this approach also contributes to limit the ambiguity because the loads have to produce the observed deflection and also satisfy the gravity anomaly. Mean average free-air anomalies along the transects were calculated to test for isostatic compensation of the models.

TABLE 5.1. SUMMARY OF PARAMETERS ASSUMED IN FLEXURAL MODELLING

Flexural rigidity D (dyne cm)	1.1×10^{30}	1.7×10^{31}	4.6×10^{31}	1.3×10^{32}
Elastic thickness T_e (km)	10	25	35	50
Densities (g/cm ³) ρ				
Topography	2.65		Sediments	2.50
Crust	2.80		Thrust-terranes	2.80
Mantle	3.30			
Young's modulus E	10^{12}	dyne/ cm ²		
Poisson's ratio ν	0.25			
Gravity acceleration g	981 cm/s ²			

The following references were taken into consideration to guide the choice of the parameters for flexural modelling:

(1) Anderson and Minster (1979): The unrelaxed Young's modulus determined from seismic frequencies ranges from 10^{12} dyne/cm² to 1.9×10^{12} dyne/cm², and the relaxed modulus is approximately 0.5×10^{12} to 0.9×10^{12} dyne/cm².

(2) Karner (1982, 1985): The Poisson's ratio for crustal rocks typically range from 0.15 to 0.35, value that decreases slightly on increasing confining pressure, then a value of 0.25 would seem a reasonable compromise for the lithosphere.

(3) Watts (2001): Continental rigidities are significantly greater than estimates from the oceanic lithosphere. In particular Archean-Proterozoic terranes are characterized by rigidities with values of $10^{31} - 10^{32}$ dyne.cm

(4) Density values as described in Chapter 4.

5.3. FLEXURAL MODELLING IN THE EASTERN VENEZUELA FORELAND BASIN.

5.3.1. EFFECT OF TOPOGRAPHY-THRUSTS-SEDIMENTS

To start the flexural modelling the topography and thrusts loads were defined along transects 00' and II'. At this point, profile 00' will be taken as an example to illustrate the whole procedure. The topography along this profile is very gentle and scarcely exceeds 1000 m over the narrow Eastern Serranía del Interior as seen in Figure 4.9. For the study area, the above sea level topographic load is certainly an almost negligible contributory load to the total deflection of the basement beneath the Eastern Venezuela foreland basin.

The combined effect of the topography, thrust and infilling sediments (according to the loading scheme of Figure 5.2) for the extreme-positions I and III, and for elastic thicknesses of 10, 25, 35 and 50 km is depicted in Figures 5.5 and 5.6. Two interesting facts are observed through these deflection curves: The first is the migration of the first node of the flexure towards the continent with increasing values of the elastic thickness, and the second is the way in which the load (topography + thrusts) accommodates itself into the deflection. For the same load, the greatest deflection is obviously attained for the smallest values of the elastic thickness and the model predicts that the difference between the present elevation of the topography and the predicted one increases elastic thickness increases.

Figures 5.7A-B summarize the flexural response of the South American plate to the combined loads according to the loading scheme of Figure 5.2, for a choice of elastic thicknesses of 10, 25, 35 and 50 km, and positions I, II and III of the broken end of the plate along profiles 00' and II'; the observed deflection of the basement is indicated by *---*---* (in red). It may be noticed that none of these situations can predict the observed deflection of the basement of the Eastern Venezuela foreland basin.

To elaborate further, it can be seen that the best fit for the first node of flexure is achieved with values of elastic thickness between 25 and 35 km, at the broken-position I, and that a broken edge closer to the foreland requires increasing elastic thicknesses up to 40-50 km. Small values of elastic thickness (10 km) tend to parallel the curvature of the basement deflection, but produce a narrower basin than the Eastern Venezuela foreland basin. It is also important pointing out that Moho is unlike to coincide with the base of the elastic layer, as the lower crust is much weaker than the uppermost mantle.

The maximum depth predicted by the model is about 10 km, either near the slab-end or below the topographic load. However, thicknesses of sediments around 12-13 km are expected in the foreland basin area in Eastern Venezuela as shown in Figure 3.6. Whatever the values of the elastic thicknesses assumed for the calculations, the largest depths predicted in the foredeep are around 4-6 km. These maximal values of depth in the foreland basin area correspond to an elastic thickness of 50 km. However, the deflection curve for this elastic thickness exhibits a more gentle curvature, with the first node position occurring 50 km farther towards the craton than it should.

Because of the magnitude of the predicted deflection, none of the models can accommodate the thrusts and the topographic load into the deflection, so that a significant residual topography still remains.

The conclusion from these results, as in other foreland basins (Royden and Karner, 1984; Lyon-Caen and Molnar, 1985) is straightforward. The loads represented by the foreland deformed belt, the observed thrusts and basin sediments, defined across the profiles 00' and II' are insufficient to produce the observed deflection of the basement of the Eastern Venezuela foreland basin, and hence cannot be the only factor responsible for the formation of the basin. There must be some additional load acting on the lithosphere in order to maintain the deflection of the South American lithosphere under the Eastern Venezuela foreland basin.

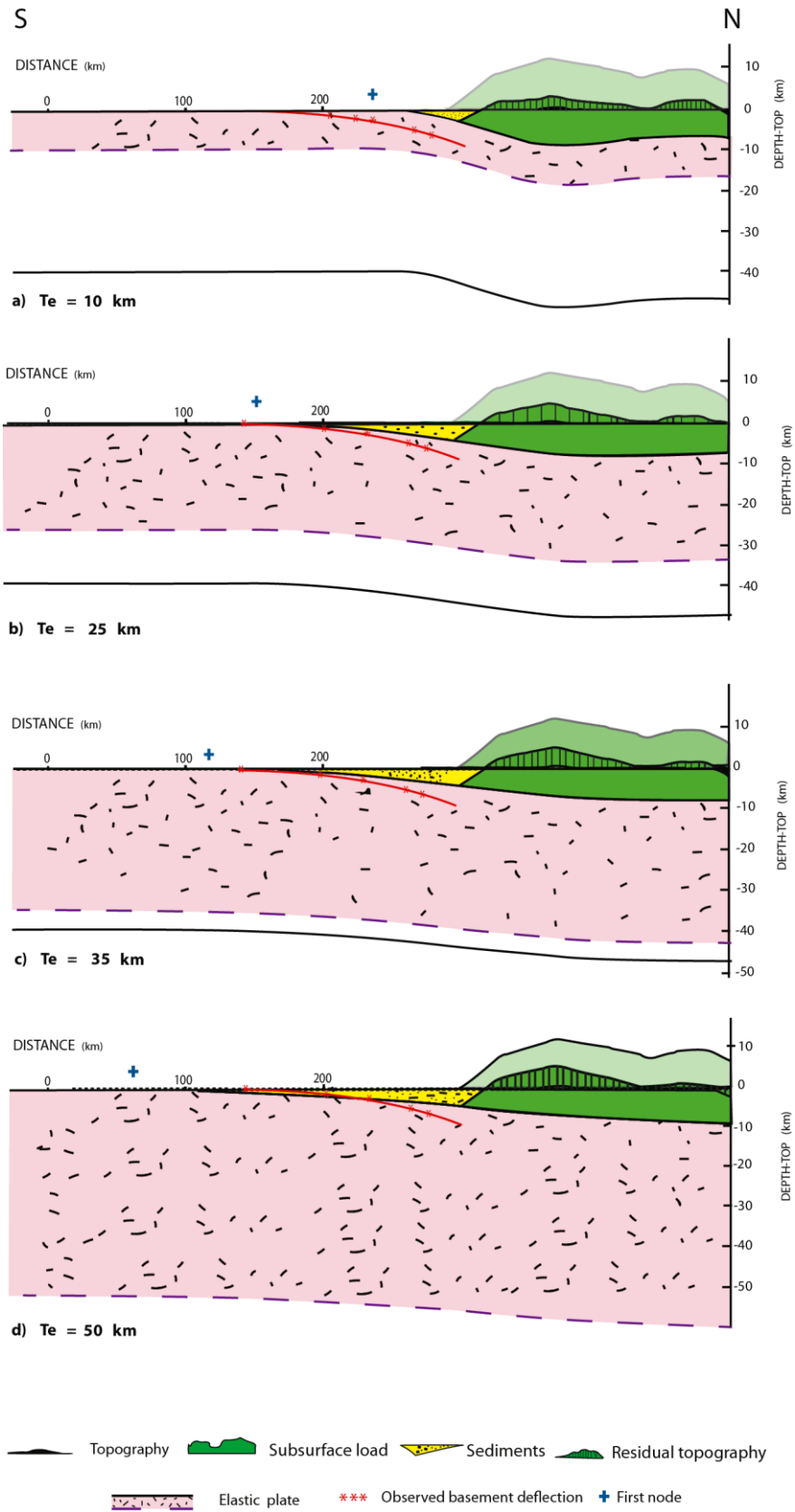


Figure 5.5. Combined effect of surface, subsurface loads and sediments in the deflection of an elastic plate with elastic thickness 10, 25, 35 and 50km, for position of the broken-end of the plate at I.

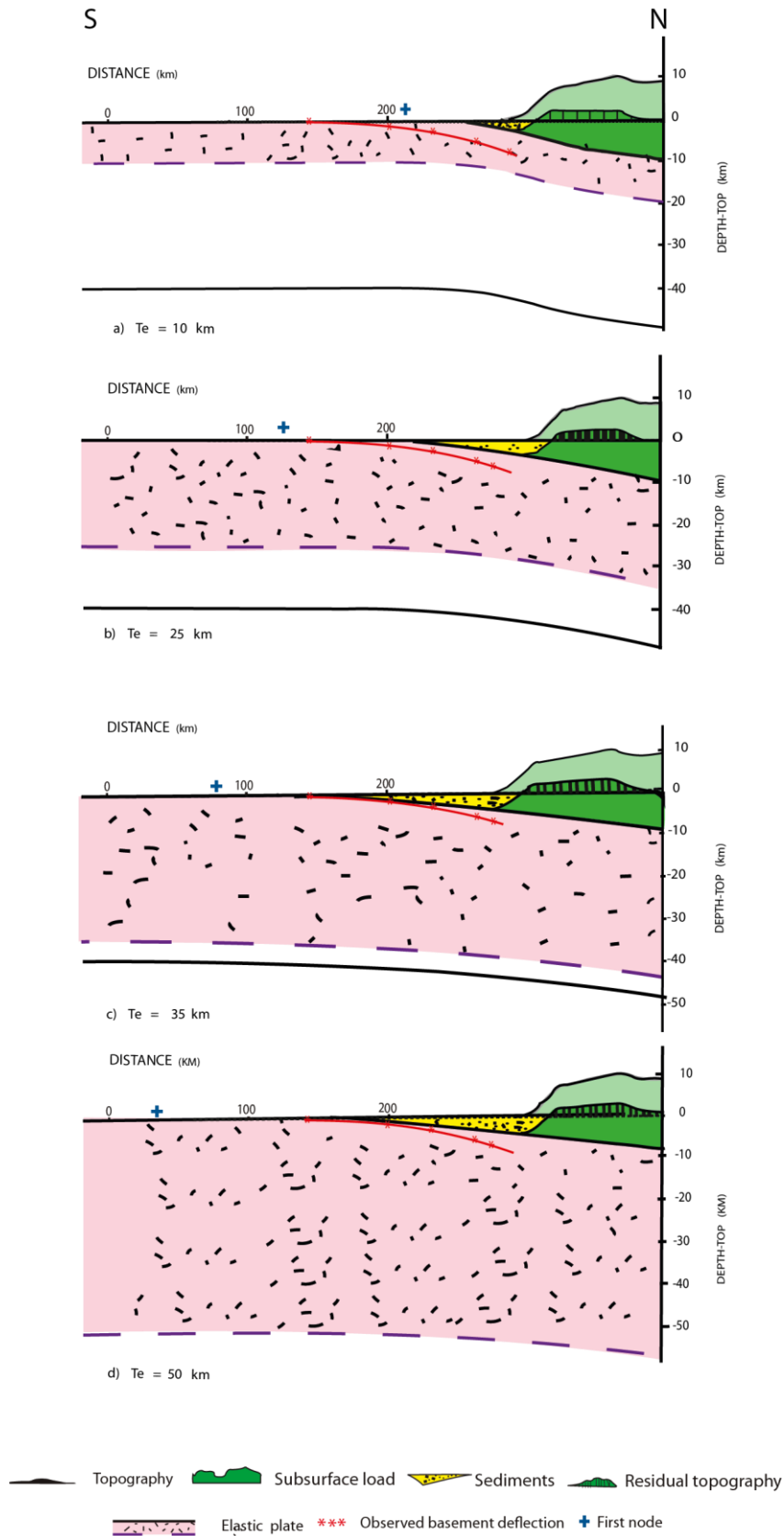
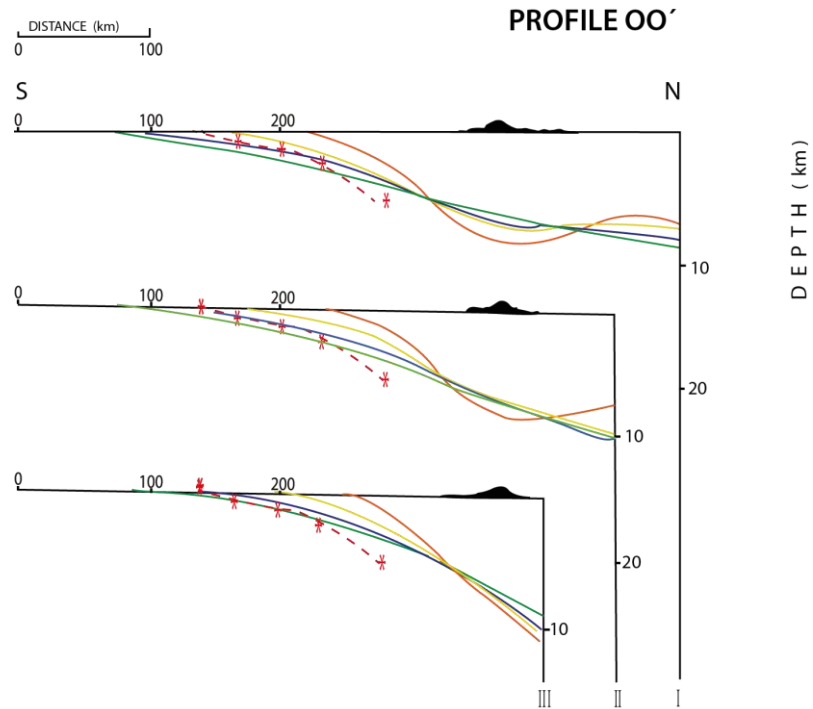


Figure 5.6. Combined effect of surface, subsurface loads and sediments in the deflection of an elastic plate with elastic thickness 10, 25, 35 and 50km, for position of the broken-end of the plate at III.

(A)



(B)

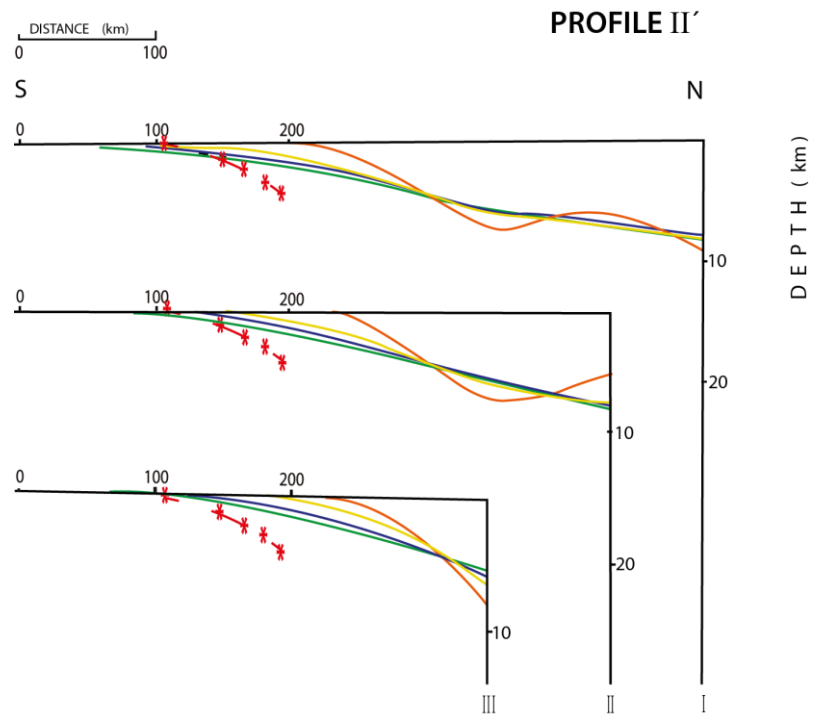


Figure 5.7. Flexural response of the South American plate to the combined surface and subsurface load, for a choice of elastic thickness of 10, 25, 35 and 50 km and positions of the broken-end of the plate at I, II and III, along: (A)- Profile OO' and (B)- Profile II'. The observed deflection of the basement is indicated by *--* (colored in red) and the calculated deflection curves are: orange line=10km, yellow line=25km, blue line=35km and green line=50km.

5.3.2. ESTIMATION OF HIDDEN LOADS

In order to search for a hidden load, the gravity anomalies were used as a constraint. The positive gravity anomaly over the complex terrane-arc north of Venezuela provides information about the buried mass causing the anomaly. As the estimated mass anomaly can be represented by different geometries, it was necessary to compute the Bouguer anomalies for the contrasting densities between crust and higher density materials, and iteratively adjust the hidden load to produce the observed deflection and the observed gravity anomaly.

At this stage special emphasis was given to fitting the amplitude and wavelength of the *positive-negative gravity anomaly couple*, rather than short wavelengths that are related to local density changes within the loads.

By using Gauss's theorem a first estimate of the effective mass of the subsurface load can be produced, from:

$$\Delta M = \frac{1}{2\pi G} \int_S \Delta g \, ds \quad (5.9)$$

where Δg is the gravity anomaly and S is the surface area covered by the anomaly. Bouguer anomaly applies to just subsurface load, free-air anomaly to both surface and subsurface loads. From the two-dimensional Bouguer anomalies (Figures 4.16 and 4.17) estimates of the subsurface mass range from 1.2×10^{13} g/cm for OO' profile, to 1.9×10^{13} g/cm for II' profile. These values were used to start the flexural modelling due to the combined effect of the previously included loads (surface (topography), subsurface (thrusts) with the additional hidden load effect.

A rough estimate of the anomalous isostatic load acting on the region (surface and subsurface) was also estimated for the specified areas illustrated in Figure 5.8, by determining the average free-air anomaly over the region and multiplying by the area. In doing this, I choose two adjoining equal-area rectangular blocks (orientated in the direction of transects OO')

and II') separated by a line along strike (~ N85°E) with the negative region to the south and the positive region to the north approximately. The southern rectangle approximately covers the main negative anomaly, and the northern rectangle covers the same width northwards. The load is much more irregular to the north of course.

The mean free-air anomaly value over each rectangular area gives the average load per unit area σ from the mean anomaly A using the relation $A=2\pi G\sigma$. This exercise gives an indication of the relative magnitude of the loads to north and south of the El Pilar fault which separates the two terrains and this value demonstrates a source for the *gravity couple*.

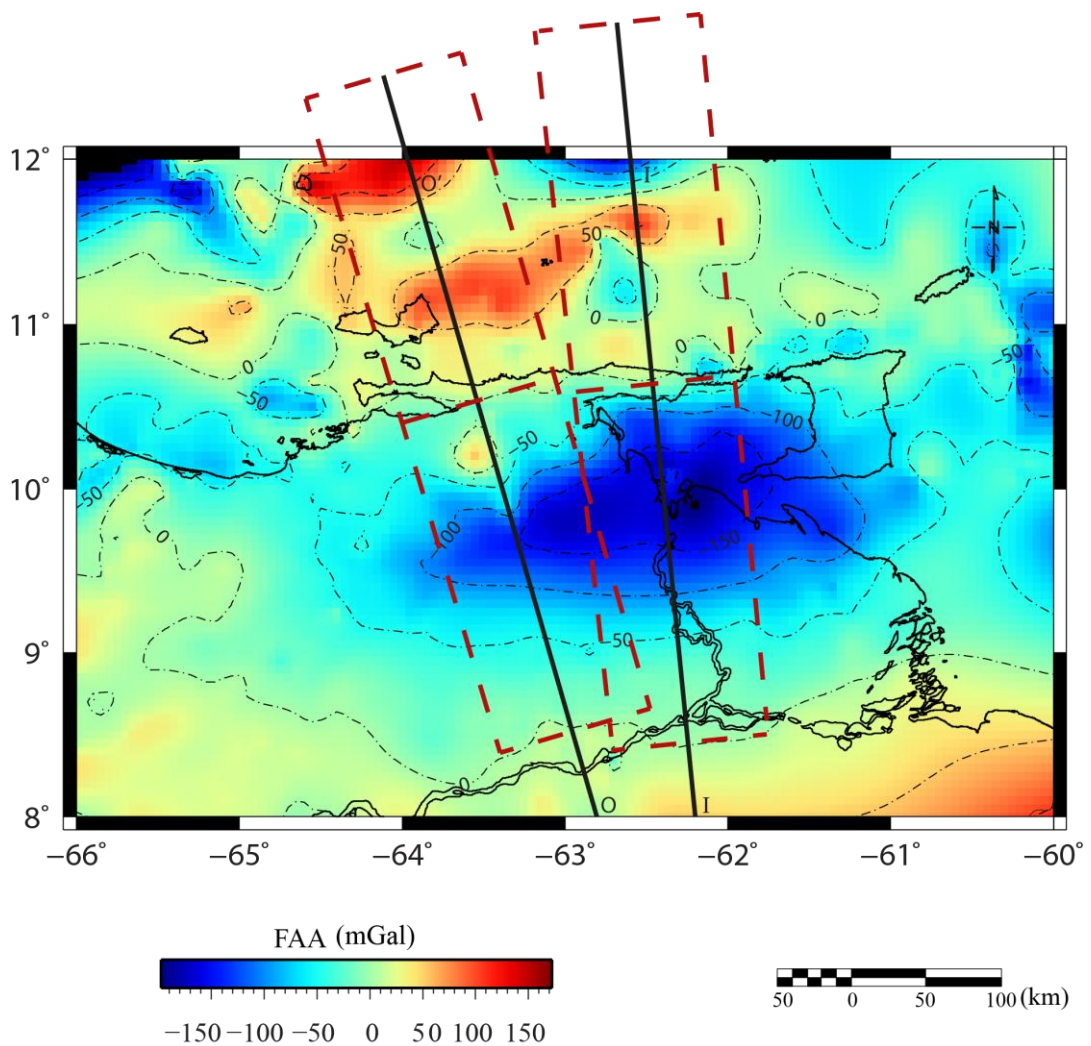


Figure 5.8. Free-air anomaly map with corridors 100 km wide, used to evaluate the mean free-air anomaly and estimate the average load per unit area.

The calculated values of average load per unit area are as follows:

PROFILE OO'

MEAN FREE-AIR (SOUTH) -67.95 mGal

AVERAGE LOAD PER UNIT AREA: $1.6213723 \times 10^5 \text{ g/cm}^2$

MEAN FREE-AIR (NORTH) +25.63 mGal

AVERAGE LOAD PER UNIT AREA: $0.61156397 \times 10^5 \text{ g/cm}^2$

PROFILE II'

MEAN FREE-AIR (SOUTH) -92.52 mGal

AVERAGE LOAD PER UNIT AREA: $2.2076433 \times 10^5 \text{ g/cm}^2$

MEAN FREE-AIR (NORTH) -28.10mGal

AVERAGE LOAD PER UNIT AREA: $0.67050127 \times 10^5 \text{ g/cm}^2$

5.3.3. HIDDEN LOAD EFFECT

The deflection curves due to the combined effect of the surface (topography), subsurface (thrust-nappes) loads, sediments and an additional 'hidden load', applied at the end-position of an elastic broken plate have been calculated for elastic thicknesses of 20, 25 and 30 km. The best fit for both the basement deflection and the first node position is attained for the elastic thickness $T_e=25 \text{ km}$.

It is also concluded that a load of the estimated magnitudes may be the additional load required to produce the observed deflection of the basement at the Eastern Venezuela foreland basin. This cannot be a surface or supracrustal load, because the loads shown in this example predict a reasonable basement deflection to accommodate the thrust and nappes, although there is still some remaining topography to be adjusted. This additional load should therefore be an intracrustal load. Accordingly, the original loading scheme was modified to include an intracrustal contributory load to predict the deflection of the basement in the study area (Figure 5.9A-5.9B).

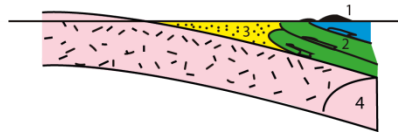


Figure 5.9A. Loading scheme for flexural modelling at the Eastern Venezuela foreland basin. 1 = Surface Load. 2 = Subsurface Load. 3 = Sediments. 4 = Hidden Load.

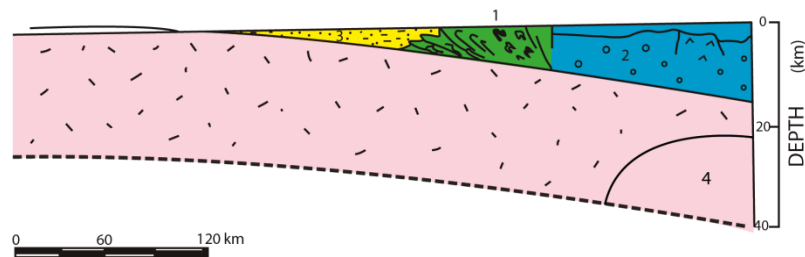


Figure 5.9B. Geological crust-section illustrating the loading scheme in the area of study. 1 = Above sea level topography. 2 = Subsurface load including the thrusts of the Eastern Serranía del Interior, Araya-Paria terrane and the magmatic arc-platform Margarita-Los Testigos. 3 = Infilling sediments of the Eastern Venezuela foreland basin. 4 = Hidden Load.

This stage involves a significant amount of computing work in search of the most appropriate mass, both in terms of magnitude and geometry, to account for the observed deflection and satisfy the gravity anomaly. The effect of the modified loading scheme applied to the foreland plate of elastic thickness $T_e=25$ km is illustrated in Figure 5.10, where the deflection of the plate as a result of the previously defined loads together with an intracrustal load of 1.2×10^{13} g/cm has been calculated. Figure 5.10 shows the Bouguer gravity anomaly calculated only for points located between the minimum gravity anomaly and the craton (controlling the basement deflection) obtained during the process of searching for the hidden load. Figure 5-11 illustrates the flexural model for the considered example, with the intracrustal load shown as a patterned area. Free-air and Bouguer anomalies are also shown and exhibit a reasonable fit to the long wavelength of the observed anomalies.

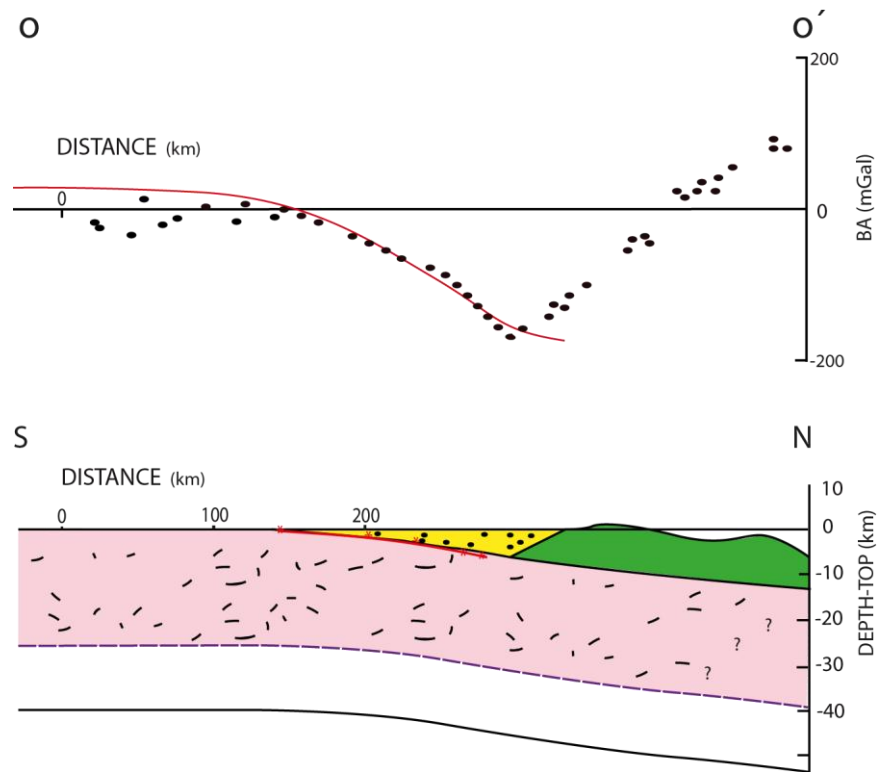


Figure 5.10. Effect of the modified loading scheme onto the foreland plate, $T_e=25\text{km}$. Bouguer anomaly controlling the basement deflection; hidden load not included into calculations of gravity anomalies. Continuous line in free-air and Bouguer anomaly profiles represent calculated anomalies for the crustal section and dots are observed gravity values.

5.4. RESULTS FROM FLEXURAL MODELLING

In the following sections the results of the flexural modelling along profiles 00' and II' will be discussed. The values of the loading masses are listed in Table 5.2 and data used for deflection calculations are in Table 5.1.

The models have been produced accordingly to the modified loading scheme (Figure 5.9) in which the intracrustal load has been modelled as denser material underlying South American plate. The best fits for both, observed deflection of the basement and gravity anomalies, are shown for the different positions of the broken edge of the plate, along transects 00' and II'.

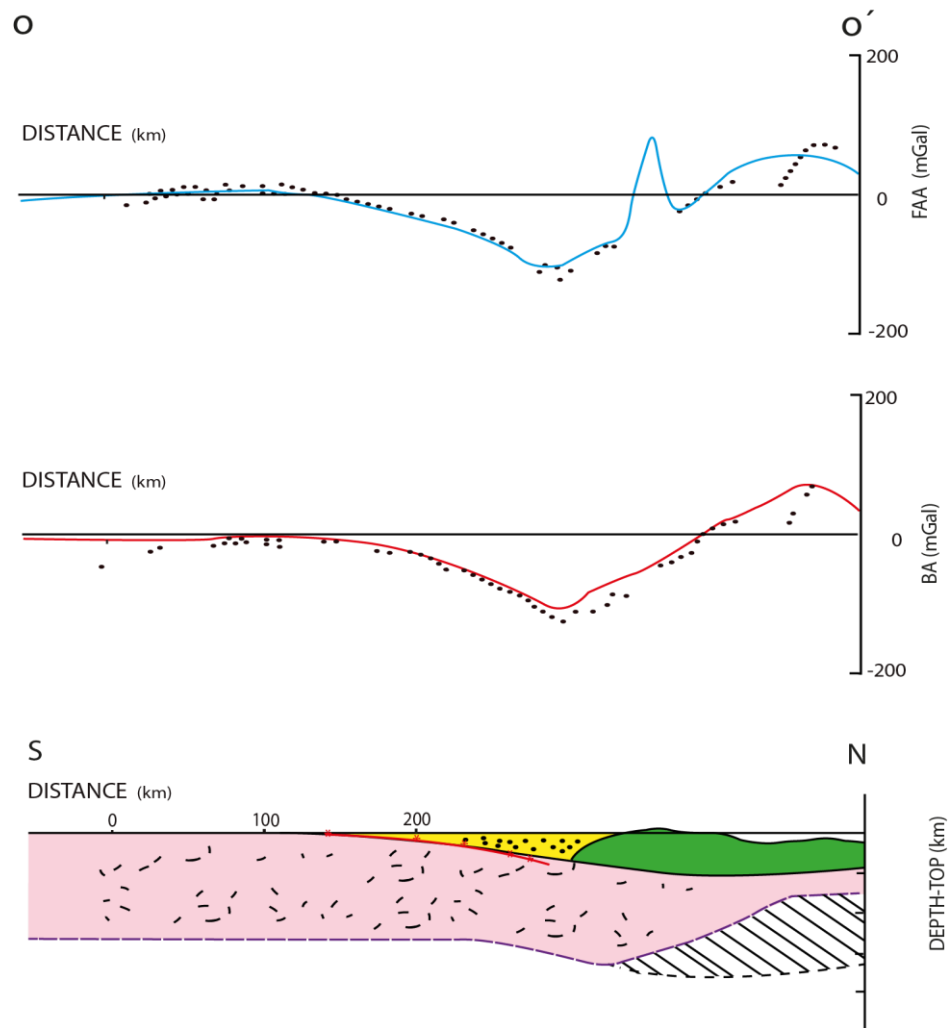


Figure 5.11. Effect of the modified loading scheme onto the foreland plate, $T_e=25\text{km}$. Flexural model as in Figure 5.11 but hidden load included in gravity calculations. Continuous line in free-air and Bouguer anomaly profiles represent calculated anomalies for the crustal section and dots are observed gravity values.

TABLE 5.2. LOADING MASSES FOR FLEXURAL MODELLING (g/cm)

	END POSITIONS		
	I	II	III
PROFILE 00'			
Topography	0.35×10^{13}	0.35×10^{13}	0.30×10^{13}
Thrust-terrane	3.50×10^{13}	2.90×10^{13}	2.20×10^{13}
Intracrustal	1.40×10^{13}	0.90×10^{13}	0.60×10^{13}
PROFILE II'			
Topography	0.06×10^{13}	0.06×10^{13}	0.02×10^{13}
Thrust-terrane	4.00×10^{13}	2.70×10^{13}	0.89×10^{13}
Intracrustal	1.60×10^{13}	1.30×10^{13}	0.77×10^{13}

5.4.1. RESULTS PROFILE 00'.

The best fit for the flexural model along profile 00' with end-position I (SW end Grenada Basin) is depicted in Figure 5.12. A distributed load of 1.40×10^{13} g/cm has been required to produce the deflection of the basement, with maximum depths occurring beneath the foreland deformed belt. A good fit for long wavelength free-air and Bouguer anomalies has been obtained, and even for some short wavelength free-air anomalies such as the one associated to the Eastern Serranía del Interior.

A model is depicted in Figure 5.13 to illustrate the flexural response of the elastic plate, along profile 00', end-position II (Margarita-Tobago forearc basin). In order to fit the observed deflection of the basement it was necessary to model the elastic plate with thicknesses of 23-20 km, and to apply a distributed load of 0.9×10^{13} g/cm representing the intracrustal load. To improve the fit between calculated and observed gravity anomalies, it seems to be necessary to decrease the magnitude of the mass of the intracrustal load, but it would imply, on the whole, producing a minor deflection of the basement shown in Figure 5.13, for elastic thickness 23 km. A good fit can be obtained for the observed deflection along this profile, applying a load of 0.6×10^{13} g/cm.

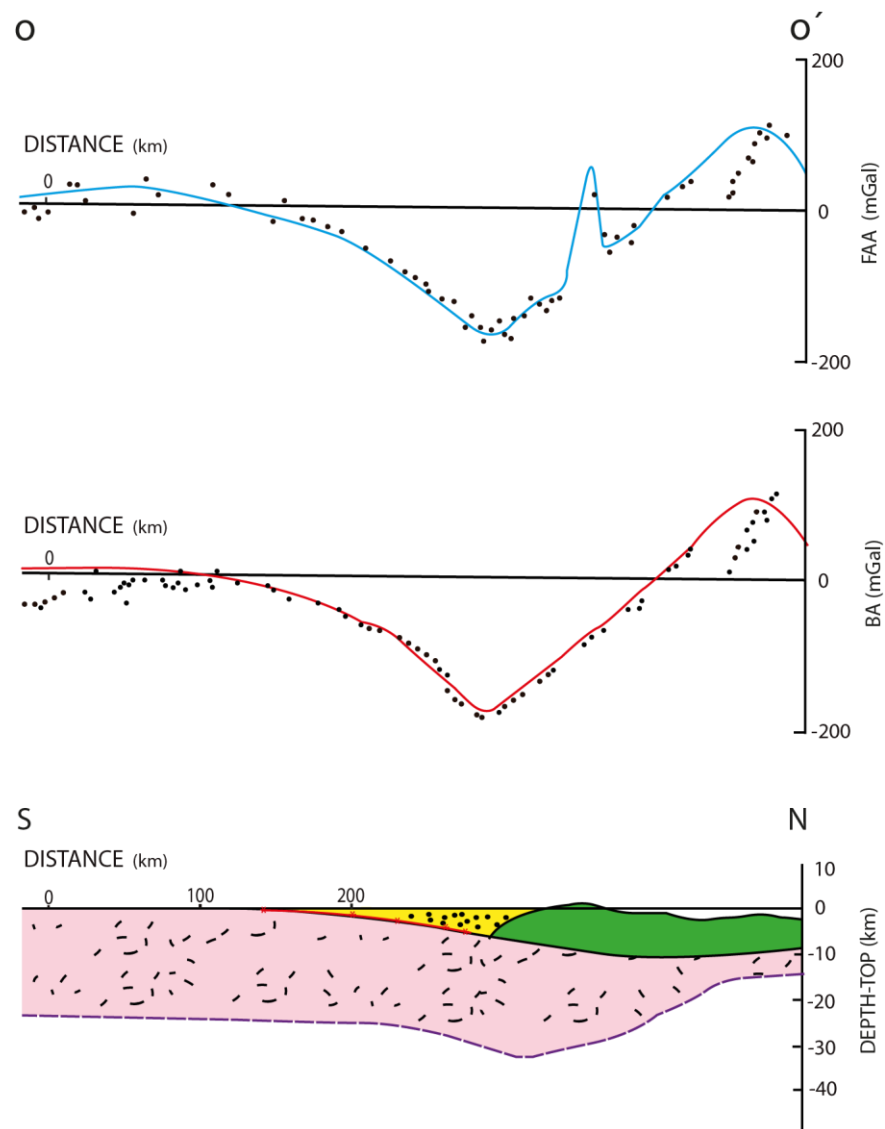


Figure 5.12. Flexural model along profile OO', with broken-end position I (SW Grenada basin) produced according to the modified loading scheme. Continuous line in free-air and Bouguer anomaly profiles represent calculated anomalies for the crustal section and dots are observed gravity values. A good fit for long wavelength FAA and BA is attained with the model $T_e=25\text{km}$.

The result of flexural modelling for profile OO', end-position III (El Pilar fault) is shown in Figure 5.14; reducing the elastic thickness down to 20 km improves the fit to the basement deflection and also decreases the residual topography, as observed in the resulting free-air anomaly over the Eastern

Serranía del Interior. However, the calculated Bouguer gravity anomalies suggest that there should be less mantle material beneath the deformed foreland belt to get a better fit between observed and calculated Bouguer anomalies.

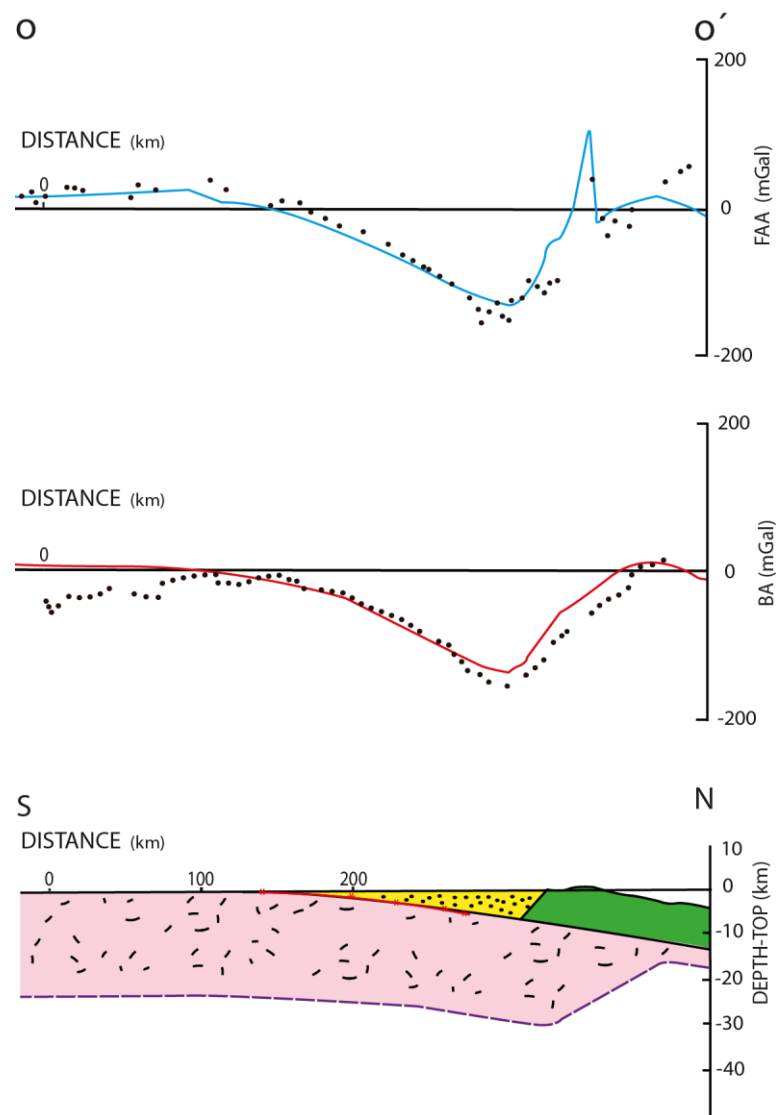


Figure 5.13. Flexural model along profile OO', with end-position II.(Margarita-Tobago forearc basin). $T_e=23\text{km}$. Continuous line in free-air and Bouguer anomaly profiles represent calculated anomalies for the crustal section and dots are observed gravity values.

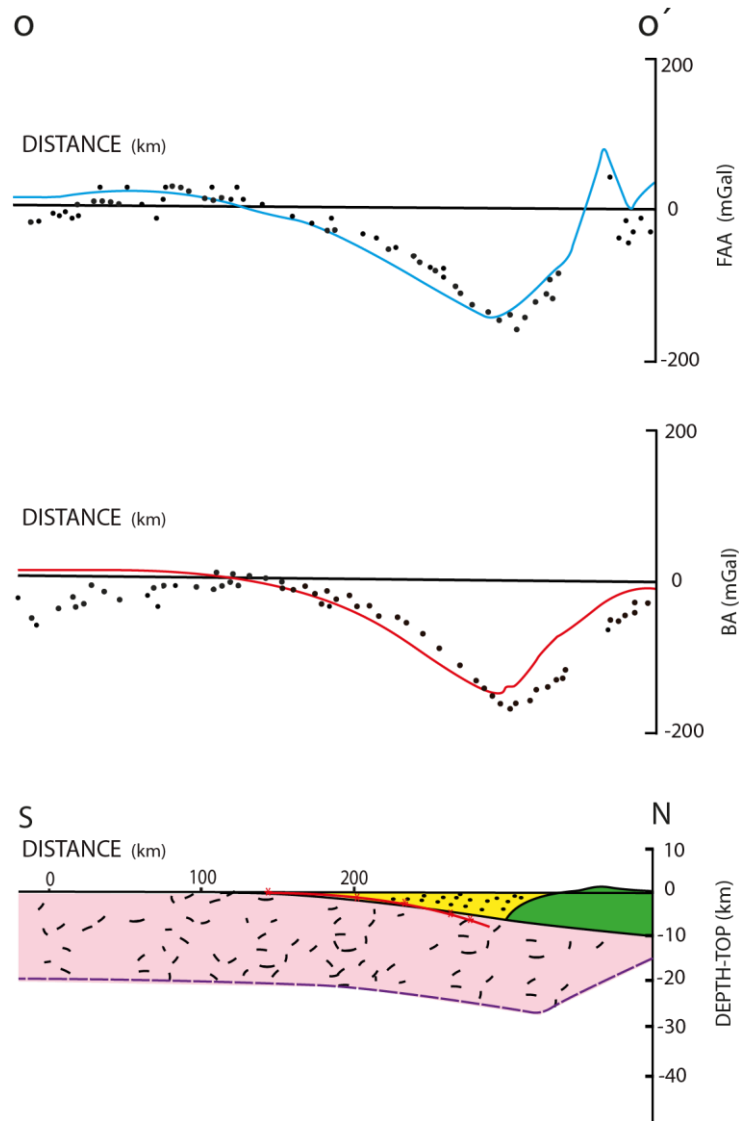


Figure 5.14. Flexural model along profile OO', with end-position III (El Pilar Fault). $T_e=20\text{km}$. Continuous line in free-air and Bouguer anomaly profiles represent calculated anomalies for the crustal section and dots are observed gravity values.

5.4.2. RESULTS PROFILE II'

The best fit for the flexural model along profile II' with end-position I (SW Grenada Basin) is shown in Figure 5.15. A distributed load of $1.6 \times 10^{13} \text{ g/cm}$ has been applied to produce the observed deflection of the basement in a plate with elastic thickness 20 km. A good fit for the long wavelength gravity anomalies has been attained, especially over the gravity minimum; some additional high-density rock masses should probably be required to improve the fit of the positive anomaly at the northern end of the profile.

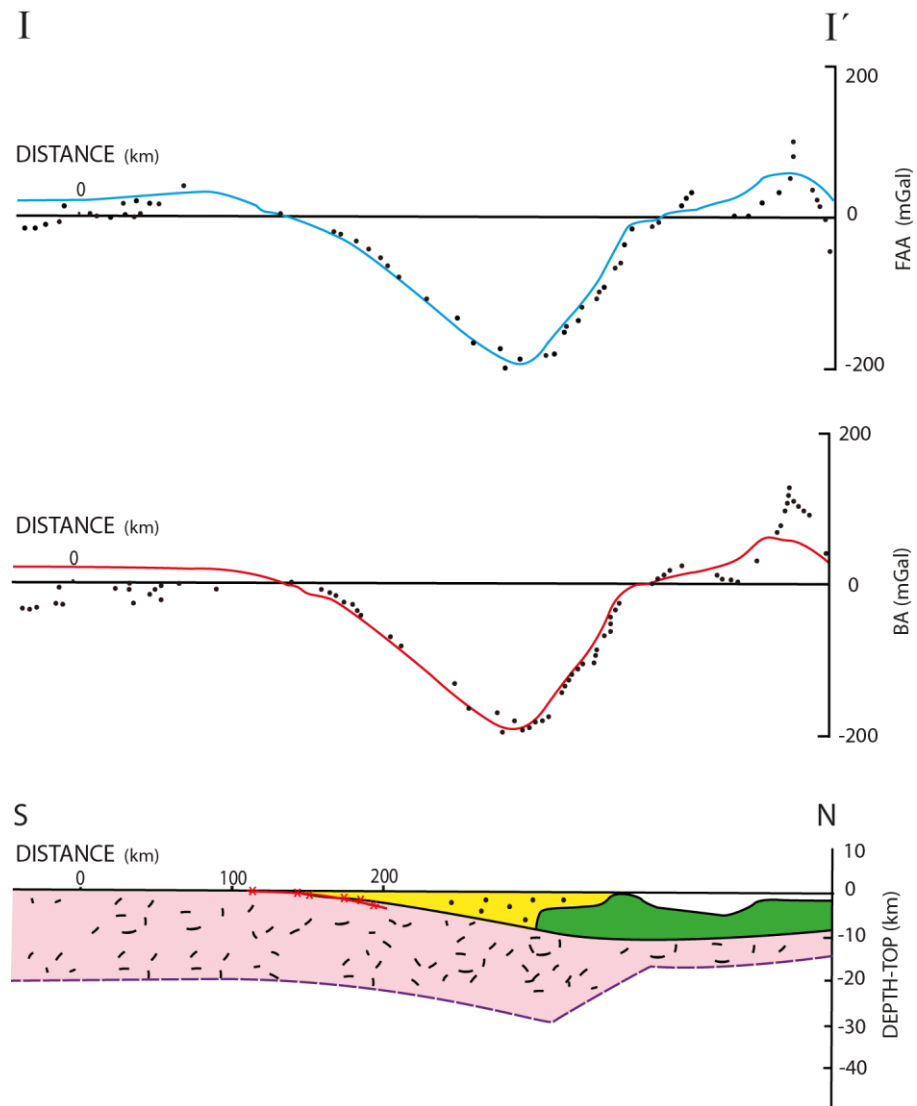


Figure 5.15. Flexural model along profile II', with end-position I (SW Grenada basin) produced according to the modified loading scheme. Best fit for $T_e=20\text{km}$. Continuous line in free-air and Bouguer anomaly profiles represent calculated values for the modeled crustal section and dots are observed values.

A section is illustrated in Figure 5.16, along profile II, end-position II (Margarita-Tobago forearc basin) to show the flexural response of the elastic plate to an intracrustal load of $1.3 \times 10^{13} \text{ g/cm}$. Reducing the elastic thickness from 20 to 15 km contributes to improve the fit between observed and calculated gravity anomalies, particularly over the positive anomaly area (north of the profile).

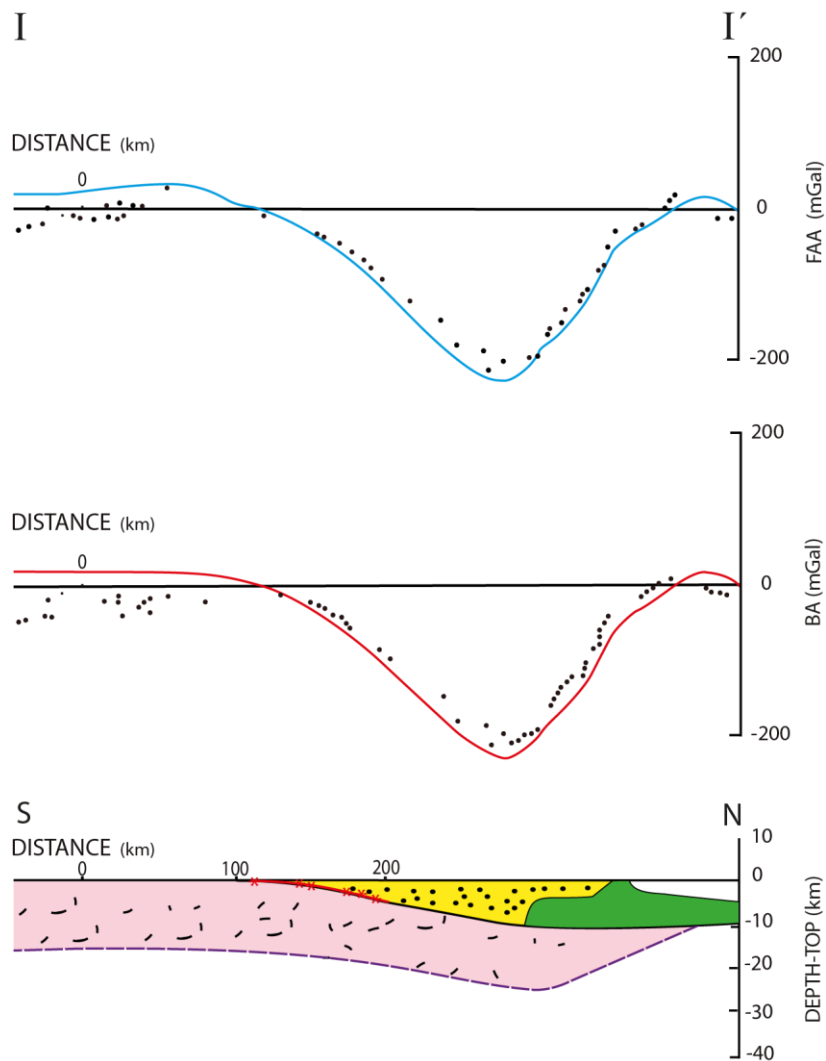


Figure 5.16. Flexural model along profile II', with end-position II (Margarita-Tobago forearc basin). $T_e=15\text{km}$. Continuous line in free-air and Bouguer anomaly profiles represent calculated values for the modeled crustal section and dots are observed values.

The result of flexural modelling along profile II', end position III (El Pilar fault) is depicted in Figure 5.17; an elastic thickness of the plate $T_e=15\text{ km}$ produces the best fit for this model in response to an applied load of $0.77 \times 10^{13}\text{ g/cm}$. A good fit between observed and calculated gravity anomalies has also been attained.

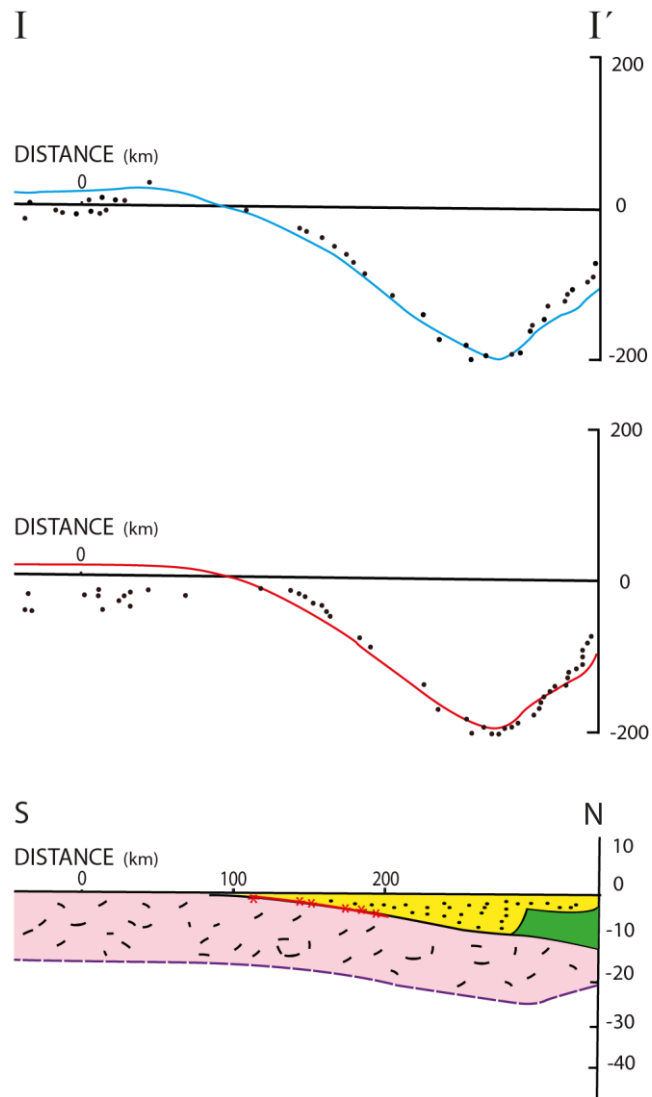


Figure 5.17. Flexural model along profile II', with end-position III (El Pilar Fault). $T_e=15\text{km}$. Continuous line in free-air and Bouguer anomaly profiles represent calculated values for the modeled crustal section and dots are observed values.

Modelling of the loading process has also been carried out using the finite element computer package FEMFLEX (Arnaiz-Rodríguez, 2012) and the results fit quite well with the previous one. These results are illustrated in Appendix C where details of the calculations are shown.

5.5. THE ORIGIN OF THE “HIDDEN LOAD”.

In discussing the “hidden load” approach to explain the formation of the Eastern Venezuelan basin, two main questions need to be considered. First, is the “hidden load” a gravitational load? If so, then it might give rise to a gravity anomaly able to explain the deflection and vertical subsidence of the basin. However, there is a major misfit between the gravity anomaly computed for the structural model which takes into account all the geological and geophysical constraints (Figs 4.16 and 4.17) when the contribution of the “hidden load” is included in the calculations. As we see in Figs 5.18 and 5.19, this misfit implies that it cannot be a gravitational load.

The models presented in Figs 5.18 and 5.19 are the same as those in Figs 4.16 and 4.17 except that they were modified by including the gravity effects caused by the postulated hidden loads as estimated in Chapter 4. The best estimates of the loads for OO' and II' are 1.4×10^{13} g/cm and 1.6×10^{13} g/cm respectively. These loads have been added to the original models by incorporating a region of density 3.1 g/cm^3 where previously there was mainly less dense crust. This means that this region has an excess density of $+0.4 \text{ g/cm}^3$ (excess positive load) where it overlaps the upper crustal layer of density 2.7 g/cm^3 , but -0.2 g/cm^3 relative to the density of the upper mantle of 3.3 g/cm^3 where it overlaps.

The second question is: What is the origin of that load? Not being a gravitational load, the only possible cause is release of compressional strain energy by crustal shortening involving faulting. I, therefore, explored a fault-based hypothesis which does not depend on hidden gravitational loads, but takes into account the clear relationship between the subsidence and the complementary uplift.

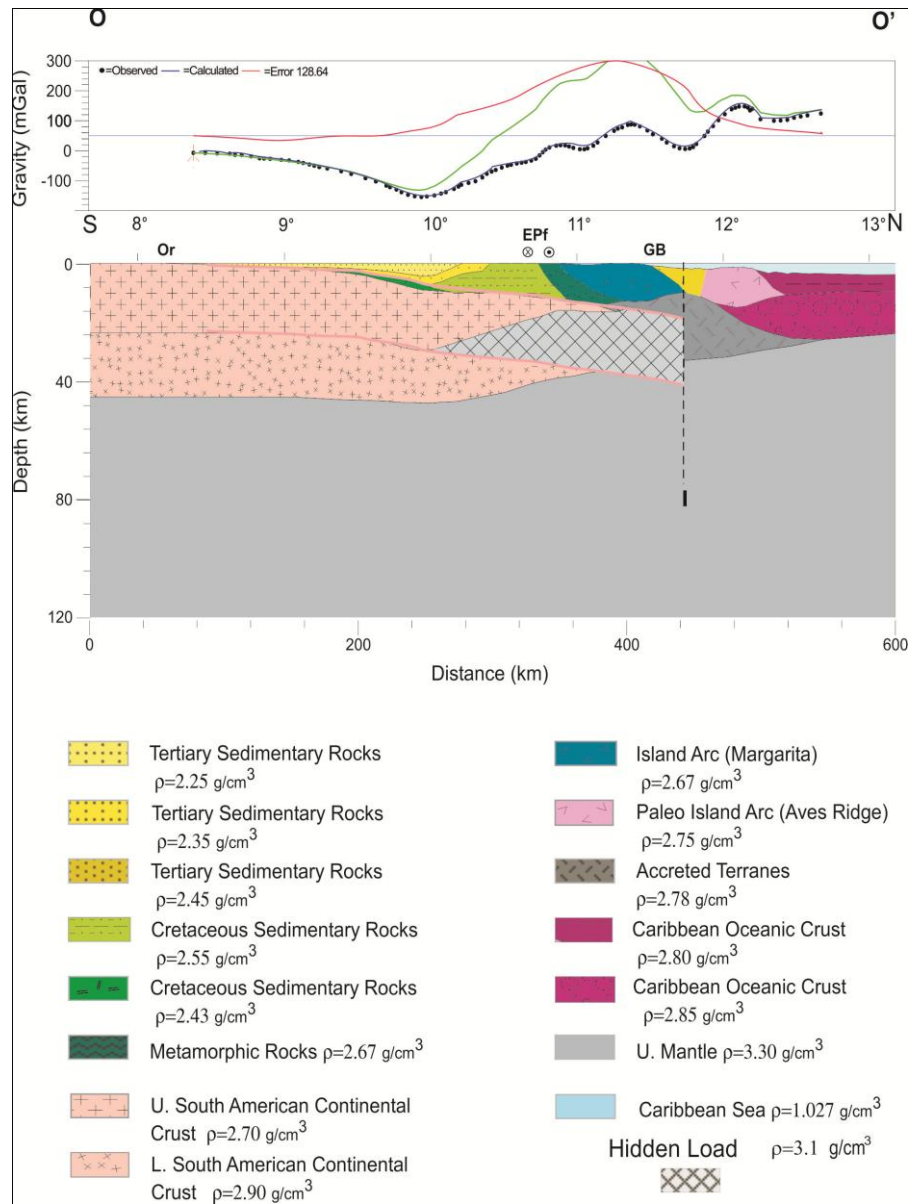


Figure 5.18. Bouguer gravity model along profile OO' illustrating the effect of the "hidden load" when it is included in the calculations. End position I of the slab as in Fig.5.3. The Bouguer anomaly of the original model (Fig. 4.16) is shown in blue. The Bouguer anomaly of the modified model, including the hidden load effect, is shown in green.

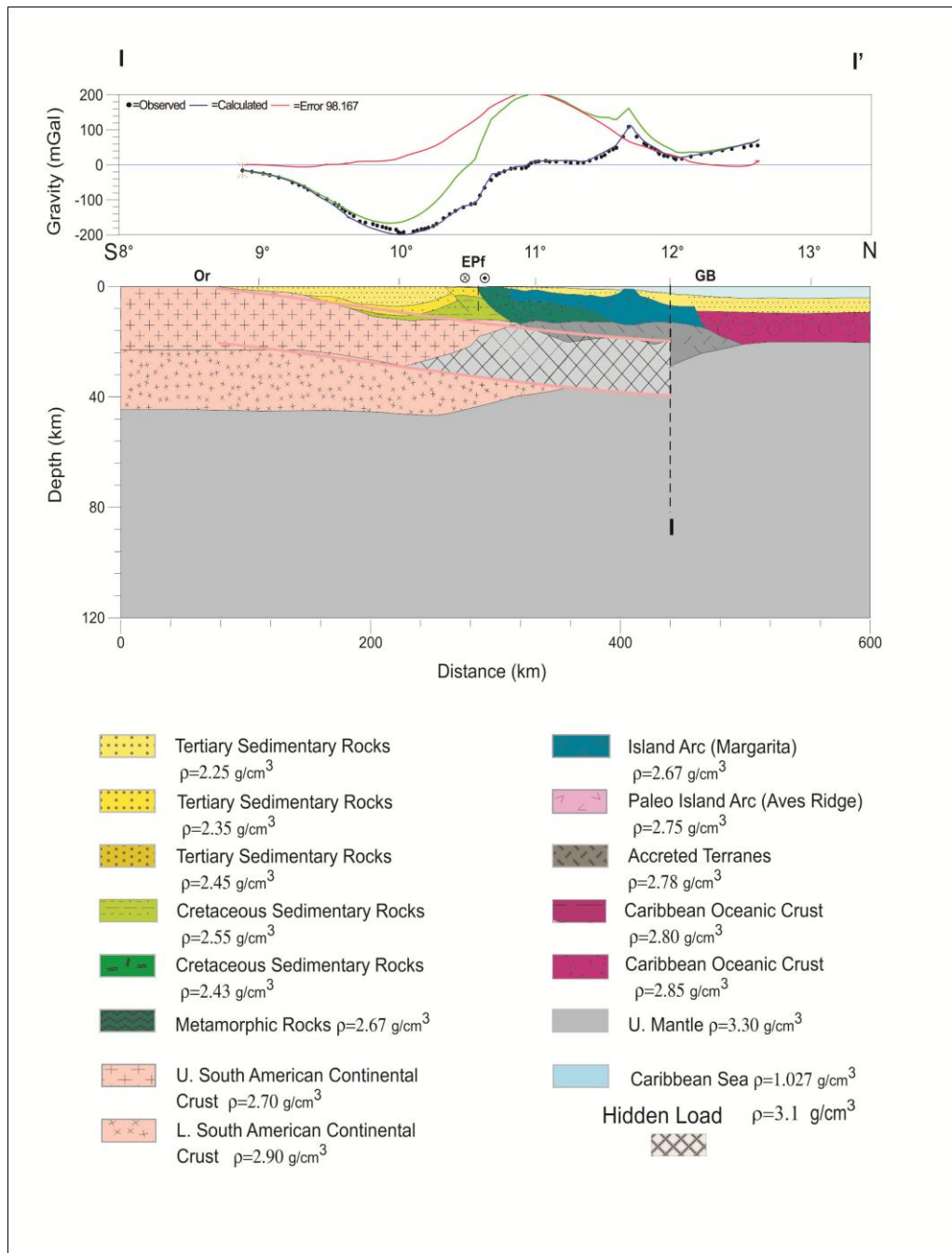


Figure 5.19. Bouguer gravity model along profile II' illustrating the effect of the "hidden load" when it is included in the calculations. End position I of the slab as in Fig.5.3. The Bouguer anomaly of the original model (Fig. 4.17) is shown in blue. The Bouguer anomaly of the modified model, including the hidden load effect, is shown in green.

5.6. THE STRESS RELEASE MECHANISM.

Stress release on thrust faults planes is a mechanism to explain the linked uplift and subsidence caused by dip slip faulting. Faulting is caused by release of strain energy in the strong lithosphere. Horizontal deviatoric tension, if sufficient in magnitude, causes normal faulting and horizontal deviatoric compression causes reverse faulting. The strain energy is released partly as heat and partly as increased gravitational energy associated with uplift on the upthrow and subsidence on the downthrown sides. The fault motion is driven by equal but opposite vertical tractions, which act on each side of the fault plane and can be approximated by equal but opposite vertical forces acting at the centre of each side. Each side responds by flexure as the fault moves and the deformation of each side can be represented (approximately) by the equations of thin plate flexure in response to a vertical edge force or computed by finite element analysis.

Bott (1996) provided the background for understanding normal faulting. In his study of flexure associated with planar faulting, the fault gives rise to equal vertical end loads acting in opposite directions on the faulted edges of the plates. In his study of normal faulting in simple models driven by relief of horizontal stress and consequent reduction of strain energy, Bott (2009) pointed out that release of strain energy gives rise to increase of gravitational potential energy as both plates are thrown out of isostatic equilibrium in opposite senses across the fault plane. However, the thin plate flexure equations need to be modified if the plate loading densities differ because the two opposing fault planes are constrained to be in contact (Bott, 1996).

Exactly the same principle applies to reverse (thrust) faulting as models of Zhang and Bott (2000) show. It is also important mentioning that although flexure theory also applies to the foreland basin hypothesis, the boundary conditions at the edge of the plate differ so that different flexural profiles will apply.

This mechanism primarily depends on the forces acting on the opposite sides of a weak thrust fault or zone, but only when it is in motion. Equal and opposite vertical components of these forces cause opposite flexure of the adjoining plates; at the same time the horizontal components release an increment of the applied compressive stress. Thus the prime cause of the evolution of the system depends not on hidden loads but on the forces on fault planes as they move.

A main release of strain energy in shortening the lithosphere occurs on faults which produce isostatic disequilibrium equally on both of the plates when the fault is active. There are two main states for such a fault, *active* when fault motion is occurring and there are two plates separated by the fault plane, and *locked* when friction inhibits motion and the two plates are locked together to form a single composite plate.

The diagram shown in Figure 5.20 demonstrates how the tractions on a thrust fault develop when a frictionless fault occurs in response to horizontal compression of an elastic layer. In (A) the crustal section illustrates the state of stress in equilibrium, before faulting occurs or when the fault is locked. As horizontal compressive stress is applied at the edges of the plate, horizontal deviatoric compression and vertical tension will develop. In (B) we show the effect when the fault, cutting across the layer, becomes frictionless and the stresses are re-orientated. This implies zero shear stress in the fault plane with the corresponding effect of rotating the principal stresses parallel and perpendicular to the fault plane. In (C), a more detailed view, we show the total force R and the vertical and horizontal components acting on the fault plane. The resultant compressive stress is represented by a single vector R acting perpendicularly at the center of the fault plane, causing release of horizontal compression and vertical displacement of the plates. These resultant forces and their components represent the resultant force applied to each fault plane by the opposite fault plane.

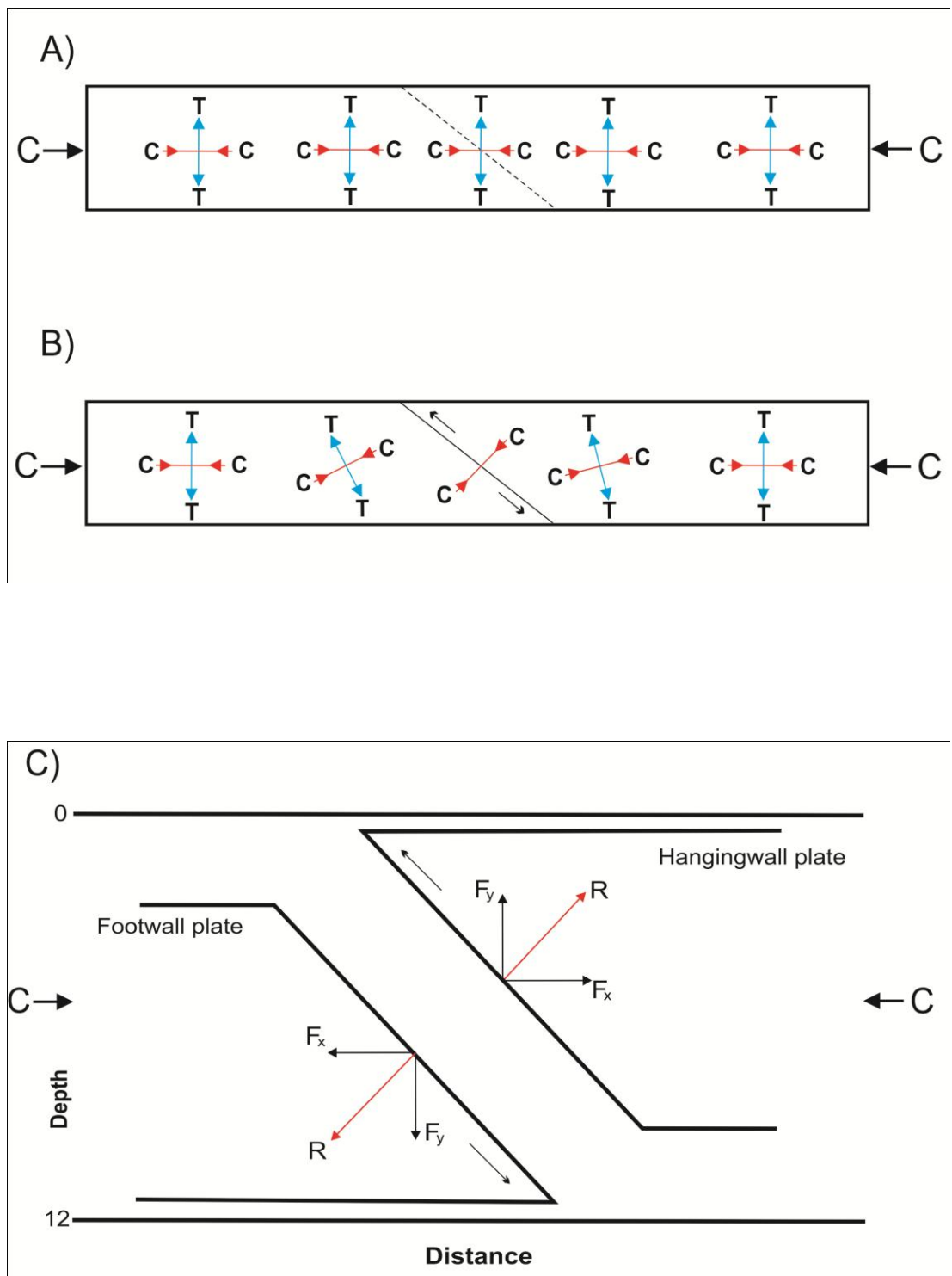


Figure 5.20. Schematic diagram to demonstrate how the tractions on a thrust fault develop when a frictionless fault occurs in response to horizontal compression of an elastic layer. C = horizontal compressive stress, R = Total force, F_x and F_y are the horizontal and vertical components.

Stresses in *active* and *locked* situations of the major fault are as follows:

(1) *Active fault*: At times when the compressive stress is sufficient to move the dipping fault plane, the release of stress produces equal but opposite tractions on the upper and lower faulted surface. As the plates move along the fault plane in opposite directions, the vertical component of the tractions forces the upper plate upwards and the lower plate downwards against gravity (Bott, 1996). This is the origin of the edge forces which act vertically on the fault plane and which are not gravitational in origin, rather they increase the gravitational potential on both sides of the fault to produce the characteristic isostatic dipole which Bott (1997) thinks is probably characteristic of all dip-slip faulting, normal and reverse. Zhang and Bott (2000) modelled this stage showing the overall displacement of a reverse fault bounding an asymmetric basin caused by release of strain energy.

(2) *Locked fault*: when the fault is locked, elastic strain energy cannot be released by displacement of the fault and the two plates effectively become a single plate. The equal but opposite edge forces which drive deformation of the separate plates cannot be present and the fault no longer affects the stress distribution with the stresses building up over a long time until the fault fails again. Deviations from isostatic equilibrium can only act on the combined plate to cause flexure of the whole plate, not just part of it.

The single combined plate is thus a lot more resistant to bending in response to the isostatic couple than the separated plates are to the stress-release couple when the fault is active.

Presumably the evolution of the system occurs by repetition of a two-stage cycle:

(1) A short stage of faulting driven by stress release when the two plates deform in opposite directions in response to release of strain energy.

(2) A prolonged period when the two plates are locked to form a single near-infinite plate and erosion/deposition takes place to make the opposite isostatic loads unequal in magnitude.

The strong plate deforms slightly isostatically in elastic (plus slow non-elastic response?) to the opposite but now unequal gravity loads (couple plus force). The compressive stress then builds up until the fault is triggered again. Successive applications of this cycle since the Oligocene - early Miocene (?) thus produce the present structure without need to invoke a hidden load.

Both normal and reverse faulting produce isostatic dipoles using the strain energy released and, taking erosion into account, it gives by far the simplest explanation of horst/half graben for extensional stress release and linked foreland basins and compressional uplift (Bott, 1997) as in Eastern Venezuela. These principles may apply (not without local complications) to the area of the Eastern Venezuela basin, as an upper uplifted northern plate is overthrust southwards over the complementary subsiding foreland basin. For this particular case, the Eastern Venezuela foreland basin is dynamically linked to the associated orogenic belts, the Eastern Serranía del Interior and the Araya-Paria metamorphic belt, whose evolution is important for basin development in a number of ways.

The distribution of earthquake foci in eastern Venezuela demonstrates that these faults are approximately planar down to the base of the brittle layer at 6-15 km depth where the earthquakes nucleate and that their dip is between 30° and 60° (Jackson, 1987; Yeats et al., 1997). They may terminate at a subhorizontal detachment surface on the transitional region between the upper brittle and lower ductile crust; the vertical displacement can be in excess of 5 km. As Bott (2009) recognizes further more sophisticated modelling is needed to follow the changing stress environment associated with the earthquake cycle involving locking and unlocking of the fault. It is also interesting to point out that deep earthquakes (Figs. 2.12 to 2.14 and Figs. 4.20-4.21) may be associated to deep cool subducting mantle, proto Caribbean or Atlantic subduction that may help pulling down the South American plate. It is not well known enough to calculate its contribution to the gravity anomaly and it surely should be too small because of its depth, but certainly must be contributing to the compressive stress.

5.7. THE NATURE OF THE HIDDEN SUBSURFACE LOAD REQUIRED TO EXPLAINING THE EASTERN VENEZUELA BASIN SUBSIDENCE AND ITS RELATION TO SUBDUCTION.

As I have illustrated (Figs 5.18 and 5.19) and described in section 5.5, a hidden gravitation load of substantial magnitude cannot explain the origin of the Eastern Venezuelan foreland basin because of the major discrepancy between observed and calculated gravity anomalies. However, I have shown that the complementary forces acting on the El Pilar fault system are adequate to explain the subsidence of the foreland basin and complementary uplift of the Eastern Serranía tectonic belt to the north of the basin. Then, there is no 'hidden gravitational load' in the strict sense of the word, but there are forces which demonstrably occur on the fault plane when the shearing stress exceeds the strength. As I have demonstrated in the model I used to illustrate the process (Fig. 5.20), the vertical forces on the downthrown side of the fault, which develop when the fault-plane is unable to withstand the shearing stress, pull it vertically downwards. Those on the upthrown side are equal in magnitude but opposite in direction and pull it upwards. The vertical forces which drive the complementary uplift and subsidence occur as a result of reduction of the shearing stress acting along the fault plane in opposite vertical and horizontal directions when slip takes place. As a result the gravitational energy on both sides is increased equally as elastic strain energy is lost. Thus the effect of faulting (normal or reverse) is to produce an isostatic plus/minus situation, positive topography on one side, and negative on the other.

This is the mechanism by which the twin positive/negative isostatic anomalies occur with erosion and deposition reducing the positive and increasing the negative anomalies as observed. Of course, existing gravitational loads may affect the response in a secondary, passive way. Gravitational loads, either positive or negative, on the surface or beneath the lithosphere, cause vertical motion, but not major *differential* vertical motion. Either the lithosphere is depressed by a positive load, or raised by a negative

load. Thus, there are no hidden gravitational loads but release of elastic strain energy that gives rise to forces on fault planes which drive complementary subsidence and uplift.

The complex tectonic setting present nowadays in the zone of interaction of northeastern Venezuela, southeastern Caribbean and the Atlantic oceanic plate dipping westward along the Lesser Antilles can be explained in terms of shortening involving compression, faulting and erosion affecting the strong upper crust and presumably thickening of the underlying continental crust producing some subsidence at the level of the Moho discontinuity. Shortening of the upper mantle involves sinking of the dense cool Caribbean upper mantle beneath the tectonic zone by near-vertical subduction, which may be a source for compressive stress but has very small contribution to the gravity anomaly because of its depth.

The lack of deep seismicity beneath the Eastern Venezuela foreland basin, south of the tectonic zone, indicates that the dense subducting material cannot underlie the main part of the foreland basin and therefore cannot be the main explanation for the subsidence of the basin. I have shown that an additional crustal gravitational load is not consistent with the gravity field, and therefore cannot be the main explanation for the basin subsidence. However, I have shown that the complementary forces acting on the El Pilar fault system are adequate to explain the subsidence of the foreland basin and complementary uplift of the Eastern Serranía tectonic belt to the north of the basin.

There are still considerable uncertainties in the interpretation of the crustal and upper mantle structure beneath the tectonic zone and a full understanding must wait for further evidence, particularly from seismology.

5.8. MANTLE DYNAMIC TOPOGRAPHY AND TECTONIC OVERVIEW.

Dynamic topography is topography caused by flow within the mantle below the lithosphere produced by loading of the lithosphere, an idea that was first proposed by Pekeris (1935). It is “dynamic” because the mass anomalies driving the density are moving towards isostatic equilibrium, and this contrasts with isostatic topography, in which the mass anomalies are in a state of quasi-equilibrium (Flament et al., 2012).

Two well-known examples of dynamic topography include: (1) The widespread use of it in studies of icecap loading/unloading and corresponding changes of volume of the oceans, where the vertical response and recovery is due to lateral flow within the mantle (upper mainly) depending on the viscosity (and used to estimate this), also applicable to loading by seamount (Gurnis, 1990; Flament et al., 2012). (2) Ocean trenches which are held down out of equilibrium by the ongoing downpull of the sinking dense oceanic lithosphere (Husson et al., 2012).

Whenever there is dip slip faulting (normal or reverse), each episode of fault movement throws both sides further out of isostatic equilibrium by equal but opposite amounts, immediately producing positive (mainly topographical) loading on the upthrown side and negative loading on the downthrown side. The two laterally displaced opposite loads effectively compensate each other, but put local strain on the elastic lithosphere. The isostatic situation is then further modified over time in two main ways: (1) Lateral migration of sediments caused by erosion and deposition. Erosion reduces the topographical uplift adjacent to the fault, transferring material deposited onto the downthrown plate and also to more distant parts of the uplifted plate, thus progressively modifying the loading pattern. (2) There must also be lateral flow beneath the fault to accommodate the displacement, which often takes place by power-law creep in a hot and weak lower crustal layer in continental normal faulting, but may also take place in large scale structures by slow sublithospheric flow from downthrown to upthrown place, as is relevant to Venezuelan tectonics.

The initial activity in eastern Venezuela was the Late Mesozoic development of the passive continental margin which now separates the Caribbean and South American plates, with northward shallowing of the Moho covered by northward thickening Cretaceous sediments. This probably warmed the underlying crust, weakening it relative to the Guayana Shield crust to the south and the cooling oceanic lithosphere to the north, and thus making it the place where later N-S crustal shortening by faulting was initiated.

The eastern Venezuela tectonic evolution during the Tertiary may be described as follows:

(1) The primary and dominant cause is the thrust faulting in the brittle upper crust in response to N-S compression where it is weakest roughly above the underlying passive margin. This causes downthrowing of the plate to the south to initiate the Eastern Venezuela foreland basin and upthrowing of the plate to the north where the maximum uplift gives rise to the elevated topography above the tectonic fault belt and also raises the surface further north in the Caribbean Sea. This area was subsequently affected by the development of the transpressional plate boundary between the South America and Caribbean plates as they were forced together in a N-S direction. The faulting may have included some obduction of oceanic crust. In between episodes of faulting when the faults are locked, whole plate flexural isostatic adjustment would be expected to occur mainly by minor elastic strain, so that the northern and southern loads compensate each other approximately along the combined plate.

(2) Accompanying the upper crustal shortening due to (1), the underlying ductile lower crust must be thickened and shortened by ductile flow, contributing to the uplift and local deepening of the Moho, but not greatly affecting distant parts of the plates.

(3) A critical contribution to the tectonics in this area is the transfer of sediments by erosion of the uplifted Eastern Serranía tectonic belt and surface transport mainly by rivers to south and north. The removal of load

from the tectonic belt encourages further uplift in this belt and also increases the sediment load on the more distant low-lying parts of both plates. The sediment load considerably increases the fault-related subsidence of the subsiding southern South American plate (foreland basin) but to a lesser extent, it reduces the fault-related uplift of the bordering Caribbean Sea to the north, so that the dynamic topography to the south subsides more than the corresponding uplift to the north.

(4) Mantle slab contribution: Beneath the Moho, the mantle part of the lithosphere has to adapt to the north-south lithospheric shortening, and it does this by subduction of the cooler, stronger, denser Caribbean uppermost mantle, as indicated by deep earthquakes (Figs. 4.20-4.21). This will give rise to a gravitational load which will pull down the Moho affecting both plates, but with a greater subsidence above the South American continental side because of its location (as in normal subduction) mainly to the south.

A fuller assessment of the dynamic Moho (or top of the mantle) topography and lateral asthenospheric flow which is related to this, may be described as follows:

(1) Beneath the Eastern Venezuela foreland basin, the subsidence which has taken place must be approximately equal to the thickness of the sediment infill. In absence of creep in the lower crust, the Moho should have subsided by this amount. According to the gravity profiles (Figs 4.16 & 4.17), this is about 8 to 9 km in the centre of the basin and approximately following the shape and size of the basin. This subsidence is basically caused by the combined effect of faulting and added sediment load.

(2) Beneath the northern plate (north of the strongly uplifted Eastern Serranía and Araya-Paria tectonic belt), where the sediment load acts in the opposite sense to the uplift due to the faulting, the resulting uplift of the Moho beneath must be smaller than the subsidence to the south, although probably covering a larger area as indicated by the positive isostatic anomalies. Data

is insufficient, but the isostatic positive/negative twin pattern seems to indicate that the southern and northern plates have approximately equal but opposite uncompensated total loads. Separately they are out of equilibrium but together they are in equilibrium as generally occurs in simple faulting. This explains the isostatic twin positive/negative which dominates the tectonic region.

(3) As the tectonic activity has developed since the Oligocene, to compensate for the subsidence of the southern plate and the uplift of the northern plate, there must have been an ongoing flow in the underlying asthenosphere from beneath the Eastern Venezuela foreland basin northwards towards the Caribbean Sea, as indicated by the pattern of isostatic anomalies.

(4) The above is further complicated by the sinking cool mantle slab, but data is insufficient for a quantitative assessment.

CHAPTER 6
SUMMARY AND CONCLUSIONS

SUMMARY AND CONCLUSIONS

The central purpose of this work has been to investigate the structure and linked uplift of the E-W coastal ranges and subsidence of the southern major foreland basin of Eastern Venezuela, using gravity interpretation with previous geological and seismic evidence along two approximately N-S lines and geodynamic modelling.

Chapter 1 provides a description of the plate tectonic setting of the eastern part of the Caribbean plate with some emphasis on the eastern subduction boundary.

Chapter 2 describes the geological and tectonic framework of eastern Venezuela (Fig. 2.4). Of particular interest is the geological evidence for the evolution of the Eastern Venezuela basin since the Jurassic rifting, going through a passive margin phase (Cretaceous to early Oligocene) followed by uplift of the northern terranes that gave rise to the Eastern Venezuela foreland thrust and fold belt, and consequently to the linked Tertiary Eastern Venezuela foreland basin. The seismicity in eastern Venezuela is shown in Figures 2.12 to 2.14, where the shallower seismicity is mostly concentrated along the eastern segment of the El Pilar fault; this fault might represent the east-west trending fault system that marks the boundary of the Araya-Paria terrane over the continental South American plate, not being a vertical fault at the lithospheric scale. Deep seismicity down to 150 km depth occurs north of the Paria peninsula, at the southernmost end of the Lesser Antilles Arc.

Chapter 3 deals with the geohistorical analysis of wells in eastern Venezuela (Figures 3.7 to 3.9), illustrating an initial passive margin stage of the Eastern Venezuela basin, from Cretaceous to early Oligocene, starting with a high subsidence rate (except at well CA1) which decreased roughly exponentially with time. Within the limitations of sampling these results are consistent with thermal subsidence, but more detailed well data would be necessary for a full assessment.

The northern South American passive margin formed as a result of N-S separation of the North and South American plates with formation of Atlantic Ocean floor between from Jurassic to early Cretaceous. The rifting stage was followed by prolonged Cretaceous subsidence all along the northern South American passive margin.

North-South compressional tectonic activity commenced in early Oligocene and was renewed during the mid Miocene, the period of fastest rate of sedimentation. At this time the Eastern Serranía del Interior provided a new source of sediments in addition to the Guayana Shield to the south. The highest sedimentation rates (of the order of 20m/my in the Oligocene and >100m/my in the Miocene) are observed in the North (e.g.: well QUI) in contrast to the southern wells where less noticeable subsidence trends are present.

A progressively younger pattern of tectonic loading along the northern margin of the South America plate from west to east has been previously recognized. Our total and tectonic subsidence integrated curves for wells QUI, ALT, CA1 and PER (Fig. 3.9) also indicate that the tectonic loading pattern in eastern Venezuela is younger from north to south. The intensification of tectonic loading during early Miocene is well marked in the North (well QUI, Fig. 3.8B) whereas wells located in the southern part of the Eastern Venezuela basin exhibit major subsidence during Mid Miocene. Incipient uplift is inferred to have occurred during early Miocene in wells ALT, CA1 and PER which may represent the isostatic rebound caused by loads applied in the north, i.e.: emplacement of nappes and thrusts, and Caribbean obduction.

The tectonic subsidence curves, from Oligocene to Present time, illustrate that pulses of tectonic subsidence are first registered in the north (well QUI) and later on in wells located further south (CA1, PER, ALT) as shown by orange dashed lines in Fig. 3.9B representing advanced fronts of tectonic subsidence from north to south into the foreland. Some kind of periodicity in episodic pulses of major subsidence between quiescence times (13, 10, 9 my) can also be inferred and these are probably related to the spasmodic

stress release mechanism. The collision zone extends probably from the southern limit of the structural domain characterized by thrusting, up to the present southwestern extension of the Grenada basin, north of Margarita Island.

The N-S compression responsible of the Tertiary tectonic of eastern Venezuela has a transpressional origin. The collision process started when the Caribbean plate was isolated by initiation of subduction in its margins which then caused the newly isolated Caribbean plate to migrate eastwards relative to the South American plate.

Chapter 4 is devoted to the study of the gravity anomalies in the eastern part of Venezuela, based on ~1400 gravity observations in Eastern Venezuela and surface ship measurements at sea to the north. I have also determined and applied terrain corrections where relevant. The Bouguer anomaly map used to model the underlying shallow and crustal structure is shown in Fig. 4.2. The free-air (Fig. 4.3) and isostatic anomaly maps (based on local isostatic compensation, Airy (Fig. 4.5) and Pratt (Fig. 4.6)) are used to illustrate the exceptional deviations of equilibrium in eastern Venezuela.

The area of study is characterized by the existence of a prominent minimum gravity anomaly (~ -200 mGal) which may represent the largest negative free-air anomaly on Earth, with the topographic height near to sea level. This anomaly belt (seen in Bouguer, free-air and isostatic anomaly maps) with a fairly constant N70°E trend widens eastward and corresponds to the Eastern Venezuela foreland basin. The complementary northern nearly E-W positive belt (~ +100 mGal) corresponds to the coastal ranges and adjacent marine area. It is worthwhile to mention the gentle secondary gravity high (~ +50 mGal) over the Guayana Shield to the south, corresponding to the flexural bulge product of the basement deflection under the loads applied to the north during the collision between the Caribbean and the South American plate.

The gravity anomalies along profiles OO' and II', chosen for 2D interpretation of the area, are shown in Figures 4.9 and 4.10. They exhibit the characteristic positive-negative anomaly couple identified in areas such as

the Alps and the Appalachians and their associated foreland basins. In eastern Venezuela we can see the clear correlation between the gravity high coinciding with the Guayana highlands on the south, the gravity low associated to the basin at the southernmost front of the nappes of the foreland deformed province, and the northern gravity high coinciding with the Araya-Paria terrane and the Margarita-Los Testigos magmatic arc platform, with many local maximum and minimum closures reflecting the intricate structure of the area; suggesting a regional-type of compensation according to flexural mechanisms.

In constructing the interpretation of crustal structure along profiles OO' and II' the following data were used to constraint the proposed models, namely: (a) Drilling and seismic reflection data for the sedimentary structure and depth to basement; (b) Density measurements as listed in Table 4.1; (c) Seismic refraction data from the Guayana Shield and a velocity model along profile 65W for the crustal structure and depth down to Moho discontinuity.

The final models along OO and II (Figures 4.16 and 4.17) illustrate the impressive gravity anomaly minimum of -200 mGal in eastern Venezuela which is primarily caused by the low density of the 10-13 km of the sediments and the consequent downwarping of the dense lower crustal layer and the Moho reaching maximum depths of 48 km beneath the basin and foreland thrusts. The secondary gravity high over the Guayana craton is related to the amplitude of the flexural bulge represented by the Guayana highlands. The main contributions to the positive anomalies to the north are: (1) surface loading (free-air and isostatic anomalies), (2) southward thrusting of dense Caribbean lithosphere, thick passive margin sediments, metamorphic and magmatic island arc rocks to the south, (3) original thin to very thin crystalline crust beneath the Mesozoic passive margin, (4) deep cool subducting mantle indicated by deep earthquakes, (5) with an opposite negative contribution which results from horizontal compression of ductile lower crust at depth, causing some crustal thickening, obviously outweighed by (1) to (4). Contributions (2) and (5) are reflected in the Bouguer anomalies.

Hypocentral locations for earthquakes of magnitude >5 projected on OO' and II' profiles (Fig. 4.20 and 4.21 respectively) show that shallower seismicity may be associated to north dipping thrust faults within the area of the Eastern Serranía del Interior thrust belt. Intermediate seismicity (~40 km depth) may be related to the contrasting crust-mantle density zone ($\Delta\rho \sim 0.4\text{--}0.5 \text{ g/cm}^3$) that probably reflect a weakening zone product of the South-North American plates break-up. Finally, deep seismicity (~80-120 km) may be associated to the subduction of the mantle northwards, in the NE corner of the South American plate.

A quantitative analysis based on flexural and gravity modelling in eastern Venezuela was carried out in Chapter 5. Two approaches have been used to investigate the mechanism of formation of the Eastern Venezuela foreland basin and linked northern compressional ranges. These are, first the hidden load hypothesis of Karner and Watts (1983) and second a fault-based hypothesis as described by Bott (1996) in relation to the mechanism of normal faulting.

Both of the mechanisms involve flexural analysis described in section 5.2. where a "thin plate" represents the continental lithosphere whose deflection in response to applied loads is computed. Assuming different elastic thicknesses for the South American plate, and positions of the slab-end at Grenada basin, Margarita-Los Testigos platform and El Pilar fault, I computed the response of this continental plate, in cantilever at the Guayana Craton, to loads applied down its northern vertical free edge.

Following the diagram for flexural modelling (Figure 5.4) the deflection of the South American plate under the loads of the surface topography, thrusts and terranes in northern Venezuela, and sediments infilling the depression, was computed and compared with the observed deflection of the basement controlled by borehole wells and with the forebulge represented by the Guayana highlands (Figures 5.7). It was necessary to include the effect of an additional intracrustal load (the *hidden* or *buried* load of Karner and Watts, 1983) to produce the observed deflection of the basement and fit the gravity anomaly. This part of the process involved a great deal of iterative calculation

to obtain the best end-load distribution of gravitational origin required to explain the observed deformation. It is also important to mention that for the fault-based hypothesis the boundary conditions at the edge of the plate differ so that significantly different flexural profiles would apply.

The best estimate of the thickness of the elastic lithosphere is 20-25 km. The best estimate of the location of the northern end of the South America plate is at the southern end of the Grenada basin, some 110 km north of the El Pilar fault (Figure 5.3). The location of the secondary high on the Guayana Shield and the first node of flexure are accurately simulated.

There are two reasons why the hidden load approach fails; first, as shown in Fig. 5.18-5.19, there is a major misfit between the gravity anomaly computed for the structural model which takes into account all the geological and geophysical constraints when the gravitational contribution of the “hidden load” is included in the calculations. This misfit implies that it cannot be a gravitational load. Second, the hidden load approach ignores the relationship of the foreland basin to the demonstrably uplifted tectonic belt, which was being uplifted by faulting at the time of origin.

I explored a fault-based hypothesis which primarily depends on the forces acting on the opposite sides of a weak thrust fault or zone when in motion and takes into account the clear relationship between the subsidence and the complementary uplift. Thus the prime cause of the evolution of the system depends on the forces on fault planes as they move as shown in Fig. 5.20 where the tractions on a thrust fault develop when a frictionless fault occurs in response to horizontal compression of an elastic layer. The starting point of this model (section A in Fig 5.20) illustrates the state of stress in equilibrium, before faulting occurs or when the two plates of the fault are locked forming a single near-infinite plate. As compression acts at the edges of the plate, the stresses are re-orientated (section B in Fig. 5.20) producing the movement of the two plates along the dipping fault plane (like El Pilar), and leading to the formation of the Eastern Venezuela foreland basin and linked uplift of the Eastern Serranía del Interior by release of compressive strain energy.

The lapses of quiescence interpreted from backstripping studies (Fig. 3.9B) could then be associated with periods of locked faults as well as the episodic pulses of major subsidence to movement along the faults.

Relative to its development, the Eastern Venezuela foreland basin evolved on the continental South American lithosphere, which had been stretched in pre-Cretaceous times during the break-up of North and South American plates, and then accumulated sediments as a passive margin, produced by post-rift thermal subsidence, from Cretaceous to early Tertiary times.

Since the Cretaceous, and especially during metamorphism, significant convergence must have occurred between the Caribbean cool oceanic lithosphere and the warmer and thinner continental lithosphere to the south. It is energywise unlikely that most of the excess converged upper mantle lithosphere has been thrust into the crust, but rather that its largest proportion has sunk vertically or possibly slightly towards the south beneath the thinner and weaker continental mantle lithosphere. If so, it may act as a hidden mass if it has sunk deep enough to significantly attenuate its gravity signature as at typical subduction zones, pulling down the northern tectonic zone and possibly also the northern part of the marginal basin. A contribution to the vertical force acting downwards may also originate from the southwestern end of the currently subducting Atlantic Ocean floor at the south end of the Caribbean arc.

The onset of the foreland basin subsidence was during the Oligocene, being its primary cause the eastern migration of the Caribbean plate along the dextral transpressive Caribbean-South America boundary. The initiation of folding and thrusting in the uplifted Serranía del Interior was certainly a product of N-S compressive stress applied to the northern edge of the South American plate, associated with the translation of the allochthonous (Araya-Paria terrane) along reactivated faults onto the then passive continental margin of South America, which caused flexural subsidence of the Eastern Venezuela foreland basin to the south as a primary result of the vertical forces acting on the fault planes as described before.

Future work will focus on two central outstanding problems: (1) Geodynamic modelling by finite element of the fault based hypothesis in relation to the lithospheric and crustal structure, using appropriate rheology. (2) Further exploration of the deeper structure and geodynamics of the tectonic belt and plate boundary separating the foreland basin from the Caribbean plate to the north.

BIBLIOGRAPHY AND REFERENCES

BIBLIOGRAPHY AND REFERENCES.

- Ainscough, D.P. (1983) A study of the crustal structure between the southern part of the Lesser Antilles Island Arc and the northeastern corner of the South America continent. M.Sc.Dissertation. Durham University, England. 59p.
- Airy, G.B. (1855) On the computation of the effect of the attraction of mountain masses as disturbing the apparent astronomical latitude of stations of geodetic surveys. *Phil. Trans. Roy. Soc.* 145:101-104.
- Aitken, T. (2005) Cenozoic stratigraphic and tectonic history of the Grenada and Tobago basins as determined from marine seismic data, wells and onland geology. M.Sc. Thesis, University of Texas. 89p.
- Aitken, T., P. Mann, A. Escalona and G. Christeson (2011) Evolution of the Grenada and Tobago basins and implications for arc migration. *Marine and Pet. Geol.* 28:235-258.
- Allen, P.A. and J.R. Allen (2000). *Basin Analysis: Principles and Applications*. Blackwell Sci. Pub. 451p.
- Allen, P.A., P. Homewood and G.D. Williams (1986) Foreland basins: An Introduction. *Spec. Pub. Int. Ass. Sediment* 8:3-12.
- Alvarado, A. (2005) Integración geológica de la península de Araya, estado Sucre. Contribution to GEODINOS Project G-2002000478, FUNVISIS-FONACIT. *GEOS* 38:11-13.
- Anderson, D.L. and J.P. Minster (1979) The frequency dependence of Q in the Earth and implications for mantle rheology and Chandler Wobble. *Geophys. Jour. R. Astr. Soc.* 58:431-440.
- Aquino, R. (2006) Formación Macal (propuesta). In: *Léxico Estratigráfico de Venezuela online*. <http://www.pdvsa.com/lexico/>
- Aquino, R. and C. Arreaza (2005) Sedimentología y geoquímica de la unidad con capas rojas que subyace al Cretácico Temprano (Formación Barranquín), Edo. Monagas. *Geos, UCV*, 37:66.
- Arnaiz-Rodríguez, M. (2012) Femflex (versión β). Software de cómputo, UCV
- Arnaiz-Rodríguez, M. and Y. Garzón (2012) Nuevos mapas de anomalías gravimétricas del Caribe. *Interciencia* 37:3.
- Arraiz, D. y E. Dinis (2008). Interpretación integrada del Macizo ígneo-metamórfico de la región de El Baúl, Edo. Cojedes. Trabajo

Especial de Grado. Dep. Geofísica. Universidad Central de Venezuela. Caracas. 190p.

- Arraiz, D., E. Dinis, I. Rodríguez y F. Urbani (2008). Interpretación integrada del Macizo Ígneo-Metamórfico de El Baúl, Edo. Cojedes. Mem. XIV Congreso Venezolano de Geofísica.
- Arstein, R., C. Bertoret, E. Molina, L. Mompert, J. Ortega, H. Sánchez and F. Russomanno (1982). Geología petrolera de la Cuenca de Venezuela Oriental. Internal Report Corpoven S.A.
- Audemard, F.A. (2006) Surface rupture of the Cariaco July 09, 1997 earthquake on the El Pilar fault, northeastern Venezuela. *Tectonophysics* 424:19-39.
- Audemard, F.A. (2007) Revised seismic history of the El Pilar fault, northeastern Venezuela. From the Cariaco 1997 earthquake and recent preliminary paleo-seismic results. *Jour. of Seismicity* 13(3): 311-326.
- Audemard, F.A. (2009) Key issues on the post-Mesozoic southern Caribbean plate boundary. *Geol. Soc. of London, Spec. Pub.* 328:569-586.
- Audemard, F.A. and C. Giraldo (1997). Desplazamientos dextrales a lo largo de la frontera meridional de la placa Caribe, Venezuela Septentrional. Mem. VIII Congreso Geológico Venezolano. Soc. Venezolana de Geólogos. Tomo I:101-108. November 1997.
- Ave Lallemant, H.G. (1997) Transpression, displacement, partitioning and exhumation in the eastern Caribbean-South American plate boundary zone. *Tectonics* 16(2):272-289
- Aymard, R., L. Pimentel, J.G. Pereira, P. Eitz, P. Lopez, A. Chaouch, J. Navarro and J. Mijares (1990). Geological integration and evolution of northern Monagas, Eastern Venezuela basin. *Geol. Soc. of Amer. Spec. Pub.* 50:37-53.
- Bally A.W. (1980) Basins and subsidence – A summary. In: A.W. Bally, P.L. Bender, T.R. McGetchin and R.I. Walcott (Eds.) *Dynamics of Plate Interior*; Amer. Geo. Unim. and Geol. Soc. of Amer., *Geodynamics Series*. 1:5-20.
- Bally A.W. and S. Snelson (1980) Realms of Subsidence. In: A.D. Miall (Ed.) *Facts and principles of world petroleum occurrence*. Canadian Soc. of Pet. Geol. Mem. 6:1-94.
- Banks, R.J., R.L. Parker, and S.P. Huestis (1977) Isostatic compensation on a continental scale: Local versus regional mechanisms. *Geophys. Jour. R. Astr. Soc.* 51:431-452.

- Bartholomew, J. (1975) (Ed.) The Times Atlas of the World. Vol 4: The Americas. Midcentury edition. Sheets 115-116. Scale 1:5,000,000.
- Bartok, P., O. Renz and C. Westermann (1985) The Siquisique ophiolite, Northern Lara State. Venezuela: A discussion on their Middle Jurassic ammonites and tectonic implications. Geol. Soc. of Amer. Bull. 96:1050-1055.
- Bassinger, B.G., R.N. Harbison and L.A. Weeks. (1971) Marine geophysical study northeast of Trinidad-Tobago. Am. Assoc. Pet. Geol. Bull. 55(10):1730-1740.
- Beaumont, C. (1978) The evolution of sedimentary basins on a viscoelastic lithosphere: Theory and examples. Geophys. Jour. R. Astr. Soc. 55: 471-497.
- Beaumont, C. (1979) On the rheological zonation of the lithosphere during flexure. Tectonophysics 59:347-366.
- Beaumont, C. (1981) Foreland basins. Geophys. Jour. R. Astr. Soc. 65:291-329.
- Becerra, E. and I. Rodríguez (1985) Sistema para el procesamiento e interpretación de datos gravimétricos -SPIDGRA. Mem. Conv. Nacional ASOVAC, Venezuela.
- Bechtel, T.D., D.W. Forsyth, and C.J. Swain (1987) Mechanisms of isostatic compensation in the vicinity of the East African Rift, Kenya, Geophys. Jour. R. Astron. Soc. 90:445-65.
- Bechtel, D., D.W. Forsyth, V.L. Sharpton and R.A.F. Grieve (1990) Variations in effective elastic thickness of the North American lithosphere, Nature, 3J3, 636-638.
- Bell, J.S. (1971) Tectonic evolution of the central part of the Venezuelan Coast Ranges, Caribbean Geophysical, Tectonic and Petrologic Studies. Geol. Soc. Amer. Mem. 130:107-108.
- Bell, J.S. (1972) Geotectonic evolution of the southern Caribbean area. In: Shagam, R., R. Hargraves and others. (Eds.) Studies in Earth and Space Sciences. Geol. Soc. of Amer. Mem. 132:369-386.
- Bellizzia, A. (1972) Is the entire Caribbean Mountain Belt of northern Venezuela allochthonous? In: Studies in Earth and Space Sciences (Hess volume). Geol. Soc. of Amer. Mem.132:363-368.
- Bellizzia, A., N. Pimentel and R. Bajo (compilers) (1976) Mapa geológico-estructural de Venezuela. Ministerio de Energía y Minas. Venezuela, Scale: 1,500,000.

- Bellizzia, A., N. Pimentel and M.I. Muñoz (1981) Geology and tectonics of northern South America. *Geodynamics Bull. Spec. Pub.* 9, Venezuela. 140p.
- Bezada, M., M. Magnani, C. Zelt, M. Schmitz and A. Levander (2010) The Caribbean-South American plate boundary at 65°W: Results from wide-angle seismic data. *Jour.of Geophys. Res.* 115: doi:10.1029/2009JH007070.
- Biju - Duval, B., A. Mascle, L. Montadert and J. Wanneson. (1978) Seismic investigations in the Colombia, Venezuela and Grenada basins, and on the Barbados ridge for future IPOD DRILLING. *Geologic in Mijnbouw* 57 (2): 105 -116.
- Biju-Duval, B., A. Mascle, H. Rosales and G. Young (1982) Episutural Oligo-Miocene basins along the Venezuelan margin. In: Watkin, J.S. and L. Drake (Eds.) *Studies in Continental Margins Geology.* Am. Assoc. Pet. Geol. Mem. 347-358.
- Bodine J.H. and A.B. Watts. (1979) On lithospheric flexure seaward of the Bonin and Mariana Trenches. *Earth Planet. Sci. Letts.* 43:132-148.
- Bonini, W. (1978) Anomalous crust in the Eastern Venezuela basin and the Bouguer gravity anomaly field of northern Venezuela and the Caribbean borderland. *Geologie en Mijnbouw* 57(2):117-122.
- Bonini, W., C. Pimstein De Gaete and V. Graterol (compilers) (1978) Mapa de anomalías de Bouguer de la parte norte de Venezuela y áreas vecinas. Venezuela, Ministerio de Energía y Minas. Scale 1:10,000,000.
- Bott, M.H.P. (1971a) *The interior of the Earth.* Arnold Ed., London, UK, 316p.
- Bott, M.H.P. (1971b) Evolution of young continental margins and formation of shelf basins. *Tectonophysics* 11:319-327.
- Bott, M.H.P. (1976) Mechanisms of basin subsidence. An introductory review. *Tectonophysics* 36:1-4.
- Bott, M.H.P. (1980) Mechanisms of subsidence at passive continental margins. In: *Dynamics of Plate Interior.* Geodynamics Ser. Vol. 1.
- Bott, M.H.P. (1990) Stress distribution and plate boundary force associated with collision mountain ranges. *Tectonophysics* 182:193-209.
- Bott, M.H.P. (1996) Flexure associated with planar faulting. *Geophys. Jour. International* 126:F21-F24.
- Bott, M.H.P. (1997) Modelling the formation of a half graben using realistic upper crustal rheology. *Jour. of Geophys. Res.* 102:24605-24612

- Bott, M.H.P. (2009) Stresses in planar normal faulting: shallow compression caused by fault-plane mismatch. *Jour. of Structural Geology* 31: 354-365.
- Bouysse, P. (1988) Opening of the Grenada back-arc basin and evolution of the Caribbean Plate during the Mesozoic and early Paleogene. *Tectonophysics* 149:121-143.
- Bouysse, P., D. Westercamp and P. Andreieff (1990) The Lesser Antilles island arc. In: J. Moore and A. Mascle (Eds.) *Proceedings of the Ocean Drilling Program, Scientific Results*, 110:29-44.
- Bowin, C. (1976) Caribbean gravity field and plate tectonic. *Geol. Soc. of Amer. Spec. Pap.* 169. 79p.
- Boynton, C., G.K. Westbrook, M.H.P. Bott and R. Long (1979) A seismic refraction investigation of crustal structure beneath the Lesser Antilles island arc. *Geophys. Jour. R. Astr. Soc.* 58:371-393.
- Bradley, A. (1979) A gravity study of the continental margin north of the Araya-Paria Península, Venezuela. M.Sc.Dissertation. Durham University, England. 102p.
- Brown, K.M. and G.K. Westbrook (1987) The tectonic fabric of the Barbados ridge accretionary complex. *Marine and Pet. Geol.* 4:71-81.
- Brown, K.M. and G.K. Westbrook (1988) Mud diapirism and subcretion in the Barbados ridge accretionary complex: The role of fluids in accretionary processes. *Tectonics* 7(3):613-640.
- Burke, K. (1988) Tectonic evolution of the Caribbean. *Ann. Rev. Earth Planet. Sci.* 16: 201-230.
- Burke, K., J. Grippi and A. Sengor (1980) Neogene structures in Jamaica and the tectonic style of the northern Caribbean plate boundary zone. *Jour. of Geology* 88:375-386.
- Burke, K., C. Cooper, J. Dewey, P. Mann and J. Pindell (1984). Caribbean tectonic and relative plate motions. In: Bonini, W., R. Hargraves and R. Shagam (Eds.) *The Caribbean-South American plate boundary and regional tectonics*. *Geol. Soc. of Amer. Mem.* 162:31-63.
- Burov, E.B. and M. Diament (1995) The effective elastic thickness (T_e) of continental lithosphere: What does it really mean? *Jour. of Geophys. Res.* 100:3905-3927.
- Case, J.E. and T.L. Holcombe. (1980) *Geologic-Tectonic Map of the Caribbean region*. Miscellaneous Investigations. U.S. Geological Survey. Map I-1100, Scale 1: 2,500,000.

- Case, J.E., T.L. Holcombe and R.G. Martin (1984) Map of geologic provinces in the Caribbean region. In: W.E. Bonini, R.B. Hargraves and R. Shagam (Eds.) The Caribbean-South American plate boundary and regional tectonics. Geol. Soc. of Amer. Mem. 162:1-30.
- Case, J.E., W.D. MacDonald and P.J. Fox (1990) Caribbean crustal provinces. Seismic and gravity evidences. In: G. Dengo and J. Case (Eds.) The Geology of North America: The Caribbean region Geol. Soc. of Amer. Vol H:15-35.
- Chalboud, D. (2001) Determinación del espesor cortical del Escudo de Guayana a partir del análisis de información de sísmica de refracción. Trabajo Especial de Grado, Univ. Simón Bolívar, Caracas, Venezuela. 134p.
- Chandrupatla, T. and A. Belegundu (2000) Finite Elements in Engineering. 2nd Ed., Prentice Hall of India, New Delhi.
- Chase, R. and T. Bunce (1969) Underthrusting of the eastern margin of the Antilles by floor of the western North Atlantic Ocean and origin of the Barbados Ridge. Jour. of Geophys. Res. 74 (6):1413-1420.
- Chevalier, Y. (1993) A cross section from the oil rich Maturin sub-basin to Margarita Island. The geodynamic relations between South America and Caribbean plates. Tectonics and stratigraphy. Am. Assoc. Pet. Geol. and Soc. Venezolana de Geol. Field trip report. 165p.
- Chevalier, Y., G. González, S. Mata, N. Santiago and F. Spano (1995). Estratigrafía secuencial y tectónica del transecto El Pilar- Cerro Negro, Cuenca Oriental de Venezuela. Mem. VI Cong. Colombiano del Petróleo. pp:115-125.
- Choy, J., M.T. Morandi and C. Palme de Osechas (1998). Determinación de patrones de esfuerzos tectónicos en Oriente de Venezuela – Sureste del Caribe, a partir de mecanismos focales. Mem. IX Congr. Venez. de Geofísica. 9p.
- Christeson, G.L., P. Mann, A. Escalona and T.J. Aitken (2008) Crustal structure of the Caribbean-northeastern South America arc-continent collision zone. Jour. of Geophys. Res 113:B08104.
- Christofferson, E. (1973) Linear magnetic anomalies in the Colombian Basin, central Caribbean Sea. Geol. Soc. of Amer. Bull. 84:3217-3230.
- Clark, T.F., B.J. Korgen and D.M. Best (1978) Heat flow in the eastern Caribbean. Jour. of Geophys. Res. 83:5883-5891.
- Clark, S.A., M. Sobiesiak, C.A. Zelt, M.V. Magnani, M.S. Miller, M.J. Bezada and A. Levander (2008) Identification and tectonic implications of a tear in the South American Plate at the southern end of the Lesser

Antilles. *Geochem. Geophys. Geosyst* 9, Q11004, doi: 10.1029/2008GC002084.

- Cobos (2002) Interpretación estructural en el cinturón plegado de Monagas, por medio de la integración de datos sísmicos, datos de pozos y geología de superficie. Tesis Dep. Geofísica, Univ. Simón Bolívar. Caracas, Venezuela.
- Cruz, L., C. Teyssier, A. Fayon and J. Weber (2004) Thermochronological topographic and precipitation data of the transpressional orogen of the Venezuelan Paria Peninsula, SE Caribbean-South American Plate Boundary. *EOS Transactions Am. Geophys. Union* 85 (47):F1715.
- Daal, A., A. González, G. Hernández and R. Prieto (1989). Exploración para hidrocarburos en el norte de Monagas. Internal report EPHINOM, Comité Interfilial CVP-LGV-IM.
- Dewey, J. and J.M. Bird (1970). Mountain belts and the New Global Tectonics. *Jour. of Geophys. Res.* 75(14):2625-2647.
- Dickinson, W. (1974) Plate tectonics and sedimentation. In: W.R. Dickinson, (Ed.) *Tectonics and Sedimentation*. Soc. Econ. Pal. Min. Spec. Pub. 22:1-27.
- Di Croce, J. (1995). Eastern Venezuela Basin: sequence stratigraphy and structural evolution. Ph.D. Dissert. Rice Univ. Houston, Texas. 225p.
- Di Croce, J., A. Bally and P. Vail (1999). Sequence stratigraphy of the Eastern Venezuela basin. In: P. Mann (Ed.) *Caribbean Basin. Sedimentary Basins of the World*. Elsevier Amsterdam. pp:419-476.
- Di Croce, J., B. De Toni, R. Ysaccis, E. Álvarez, S. Ghosh, L. Duerto, L. Porras and R. Violino (2000). Key petroleum system elements of the Venezuela Basin in an improved chronostratigraphic framework. Annual Convention AAPG 9. Poster Session A38
- Diebold, J.B. and N. Driscoll (1995). Geophysical investigations of the Caribbean. Preliminary Report on the R/V Ewing Cruise 9501. Mesozoic crustal development of the Caribbean region: A geophysical investigation. Lamont-Doherty Earth Observatory, Columbia University, New York. 41p.
- Diebold, J.B, P.L. Stoffa, P. Buhl and M. Truchan (1981). Venezuelan basin crustal structure. *Jour. of Geophys. Res.* 86(B9):7901-7923.
- Donovan, S.K. (1994) Caribbean Geology: An Introduction. Northern South America (Chapter 13) 9:229-247. Univ. of West Indies. Publisher Assoc. Kingston, Jamaica.

- Dorman, L. M. and B.T.R. Lewis (1970). Experimental isostasy, 2. A Theory of the determination of the Earth's isostatic response to a concentrated load. *Jour. of Geophys. Res* 75:3357-3365.
- Drapper, G., S.K. Donovan and T.A. Jackson (1994) Geologic provinces of the Caribbean region. In: S.K. Donovan and T.A. Jackson (Eds.) *Caribbean Geology: The Univ. of West Indies, Pub. Assoc., Kingston, Jamaica*, pp:3-12.
- Driscoll, N. and J.B. Diebold (1999) Tectonic and stratigraphic development of the eastern Caribbean: New constraints from multichannel seismic data. In: P. Mann (Ed.) *Caribbean Basin. Sedimentary Basins of the World*. Elsevier Amsterdam. pp:591-626.
- Duerto. L. (2007) Shale Tectonics, Eastern Venezuela basin. Ph.D. Thesis. Univ. of London Royal Holloway. 424p.
- Duerto, L. and K. McClay (2002) 3D Geometry and evolution of shale diapirs in the Eastern Venezuela basin. *Amer. Assoc. Pet. Geol. Annual Convention. Houston. Abstracts*.
- Ebinger, C.J., T.D. Bechtel, D.W. Forsyth, and C.O. Bowin (1989) Effective elastic plate thickness beneath the East African and Afar plateaus and dynamic compensation of the uplifts, *Jour. of Geophys. Res.* 9: 2883-2901.
- Edgard, N. (1968) Seismic refraction and reflection in the Caribbean Sea. Ph.D. Dissertation Columbia University, 159p.
- Edgard, N., J. Ewing and J. Henion (1971) Seismic refraction and reflection in the Caribbean Sea. *Amer. Assoc. Pet. Geol. Bull* 55(6):833-870.
- Epp, D., P.J. Grim and M.G. Langseth (1970) Heat flow in The Caribbean and Gulf of Mexico. *Jour. of Geophys. Res.* 75(29):5655-5669.
- Erikson, J.P. (1994). A Lower Cretaceous shelf and delta in the Eastern Venezuela Basin. *Mem. V Simposio Bolivariano: Exploración Petrolera en las Cuencas Subandinas*. Pto. La Cruz, Venezuela. pp:174-189.
- Erikson, A.J., C.E. Helsley and G. Simmons (1972) Heat flow and continuous seismic profiles in the Cayman trough and Yucatan basin. *Geol. Soc. of Amer. Bull.* 83(5):1241-1260.
- Erlich, R.N. and S.F. Barrett (1990). Cenozoic plate tectonic history of the northern Venezuela and Trinidad area. *Tectonics* 9(1):161-184.
- Erlich, R.N. and S.F. Barrett (1992). Petroleum geology of the Eastern Venezuela basin. In: R. McQueen and D. Leckie (Eds.) *Foreland basin and Fold Belts*. *Am. Assoc. Pet. Geol. Mem.* 55:341-362.

- Escalona, A. and P. Mann (2006) Sequence-stratigraphic analysis of Eocene clastic foreland basin deposits in central Lake Maracaibo using high-resolution well correlation and 3-D seismic data. *Am. Assoc. Pet. Geol. Bull.* 90:581-623.
- Escalona, A. and P. Mann (2011) Tectonic, basin subsidence mechanisms, and paleogeography of the Caribbean-South American plate boundary zone. *Marine and Pet. Geol.* 28:8-39.
- Ewing, J., C.B. Officer, H.R. Johnson and R.S. Edwards (1957) Geophysical investigations in the eastern Caribbean: Trinidad Shelf, Tobago Trough, Barbados Ridge, Atlantic Ocean. *Geol. Soc. of Amer. Bull.* 68(7):897-912.
- Falvey, D.A. (1974) The development of continental margins in plate tectonic theory. *Aus. Petr. Expl. Assoc. Jour.* 14:95-106.
- Feo Codecido, G., F. Smith, N. Aboud and E. Di Giacomo (1984) Basement and Paleozoic rocks of the Venezuelan Llanos basins. *Geol. Soc. of Amer. Memoir* 162:175-187.
- Flament, N., M. Gurnis and R.D. Muller (2012) A review of observations and models of dynamic topography. *Geol. Soc. of Amer. Lithosphere* 5(2):189-210.
- Folinsbee, R.A. (1972) The gravity field and plate boundaries in Venezuela. Ph.D. Dissertation. Massachusetts Inst. Technology – Woods Hole Oceanographic Inst. 160 p.
- Forsyth, D.W., (1985) Subsurface loading and estimates of the flexural rigidity of continental lithosphere, *Jour. of Geophys. Res.* 90: 12,623-12,632.
- Fox, P.J. and C. Heezen (1975) Geology of the Caribbean crust. In: A. Nairn and F.G. Stehli (Eds.) *The Ocean Basins and Margins. Vol. 3. The Gulf of Mexico and the Caribbean.* *Geol. Soc. of Amer. Mem.* 132:369-386.
- Galloway, W.E. (1989) Genetic stratigraphic sequence in basin analysis I: Architecture and genesis of flooding-surface bounded depositional units. *Am. Assoc. Pet. Geol. Bull.* 73(2):125-142.
- Garrity, C., P. Hackley, A. Karlsen, F. Urbani and FUNVISIS (2005) *Geologic Shaded Relief Map of Venezuela.* Caracas.
- Garciacono, E., P. Mann and A. Escalona (2011) Regional structure and tectonic history of the obliquely colliding Columbus foreland basin, offshore Trinidad and Venezuela. *Marine and Pet. Geol.* 28:126-148.

- Geosoft (2010) Oasis montaj v.7.2.1 Gravity and Magnetic Mapping, Modelling and Interpretation. (HJ), Standard Ed. Geosoft Inc. Toronto, Canada.
- Ghosh, N., S.A. Hall and J.F. Casey. (1984) Sea Floor spreading magnetic anomalies in the Venezuelan Basin. *Geol. Soc. of Amer. Mem.* 162:65-80.
- Giraldo, C., E. Alvarez, M. Odehnal, G. González, V. De Lisa, G. Hernández (2000). New Insight into the Mud Diapirs Exploration in the Eastern Venezuela basin. Annual Meeting Expanded Abstracts. *Am. Assoc. Pet. Geol.* 55.
- Giunta, G., L. Beccaluva, M. Colorti, F. Siena and C. Vaccaro (2002). The southern margin of the Caribbean Plate in Venezuela: Tectonomagmatic setting of the ophiolitic units and kinematic evolution. *Lithos*, 63(1-2):19-40.
- Goddard, D. (1988) Seismic stratigraphy and sedimentation of the Cariaco basin and surrounding continental shelf, northeastern Venezuela. In: L. Barker (Ed.) *Trans. XI Caribbean. Geol. Conf.*, Barbados. pp:1-34.
- González de Juana, C. (1977) Tertiary tectonics of the Caribbean and the Eastern Venezuela basin. *Abstr. VIII Caribbean Geol. Conf.* p:61.
- González de Juana, C., J. Iturralde and X. Picard. (1980) *Geología de Venezuela y sus cuencas petrolíferas*. Caracas. Ed. Foninves. 2 vol. 1031p.
- Graterol, V. (1978) Mapa de Anomalías de Bouguer de Venezuela. Región 6°-9° de latitud Norte, y 59°-73° de longitud Oeste. Ministerio de Energía y Minas. Caracas, Venezuela.
- Guillaume, H.A., H.M. Bolli and J.P. Beckmann (1972) Estratigrafía del Cretáceo Inferior en la Serranía del Interior, Oriente de Venezuela. *Mem. IV Congr. Geol. Venez. Pub. Esp. N° 5. Vol III:1619-1655.*
- Gurnis, M. (1990) Bounds on global dynamic topography from Phanerozoic flooding of continental platforms. *Nature* 344(6268):754-756, doi:10.1038/344754a0
- Hackley, P.C., F. Urbani, A.W. Karlsen y C.P. Garrity (2006). Mapa Geológico de Venezuela, escala 1,750,000. U.S. Geological Survey. Open-File Report 2006-1109.
- Hammer S. (1939) Terrain corrections for gravimeter stations. *Geophysics* 4(3):184-194.

- Hartley, R., A.B. Watts and J.D. Fairhead (1996) Isostasy of Africa. *Earth Planet. Sci. Lett.* 137:1–18.
- Haxby, W.F, D.L. Turcotte and J.M. Bird. (1976) Thermal and mechanical evolution of the Michigan Basin. *Tectonophysics* 36:57-75.
- Hayford, J. and W. Bowie (1912) The effect of topography and isostatic compensation upon the intensity of gravity. U.S. Coast and Geod. Surv., Spec. Pub. N° 10. 132p.
- Hedberg, H.D. (1936) Gravitational compaction of clays and shales. *Amer. Jour. Sci.* 31:241-287.
- Hedberg, H.D. (1950) Geology of the Eastern Venezuela Basin (Anzoátegui-Monagas- Sucre-Eastern Guárico portion). *Geol. Soc. of Amer. Bull.* 61:1173-1296.
- Heiskanen, W.A. (1953) Isostatic reductions of gravity anomalies by the aid of high-speed computing machines. *Publ. Isost. Inst., I.A.G. (Helsinki)*, 28
- Heiskanen, W.A. and F. Vening-Meinez, (1958) *The Earth and its gravity field.* Mc Graw Hill, New York, 470 pp.
- Hetenyi, M. (1979) *Beams on Elastic Foundations.* University of Michigan Studies, Scientific Series, Vol. XVI. The University of Michigan Press, Ann Arbor, 255 p.
- Higgs, R. (2007) Venezuela – Trinidad, Caribbean oblique collision model. Revised 4th Geol. Conf. of the Geol. Soc. of Trinidad-Tobago. Port of Spain. Abstracts.
- Holcombe, T.L (1977) Caribbean bathymetry and sediments. In: J.D. Weaver (Ed.) *Geology, geophysics and resources of the Caribbean.* A report of the IDOE Workshop on the Geology and Marine Geophysics of the Caribbean region and its Resources. Unesco Intergovernmental Oceanographic Commission, pp:27-62.
- Holcombe, T.L., J.W. Ladd, G.K. Westbrook, N.T. Edgar and C.L. Bowland (1990). Caribbean marine geology: Ridges and basins of the plate interior. In: G. Dengo and J. Case (Eds.) *The Geology of North America: The Caribbean Region.* Geol. Soc. of Amer. Vol H:231-260.
- Holt, P.J., M. Allen, J.van Hunen and H. Morten Bjornseth (2010) Lithospheric cooling and thickening as a basin forming mechanism. *Tectonophysics* 495:184-194.
- Hung, E. (2005) Thrust belt interpretation of the Serranía del Interior and Maturín subbasin. Eastern Venezuela. In: H. Ave Lallemand and V.

- Sisson. (Eds.) Caribbean-South American Plate Interactions, Venezuela. Geol. Soc. of Amer. Spec. Pap. 394:53-89.
- Husson, L., B. Guillaume, F. Funiciello, C. Faccenna and L.H. Royden (2012) Unravelling topography around subduction zones from laboratory models. *Tectonophysics* 526-529:5-15. doi:10.1016 /j.tecto. 2011.09.001.
- Jackson, J.A. (1987) Active normal faulting and crustal extension In: M.P. Coward, J.F. Dewey and P.L. Hancock (Ed.) *Continental Extensional Tectonics*. Geol. Soc. London. Spec. Pub. 28:3-17.
- Jácome, M., N. Kuszniir, F. Audemard and S. Flint (2003) Tectonostratigraphic evolution of the Maturín foreland basin: eastern Venezuela. In: C. Bartolini, R.T. Buffler and J. Blickwed (Eds.) *The Circum-Gulf of Mexico and the Caribbean: Hydrocarbon habitats, basin formation and plate tectonic*: Am.Assoc.Pet.Geol.Mem. 79:735-749.
- Jaeger, J.C. and N.G. Cook (1976) *Fundamentals of Rock Mechanics*. 2nd Edition. Chapman and Hall, London. 585p.
- James, K. (2003) A simple synthesis of Caribbean Geology. Am. Assoc. Pet. Geol. International Conference, Barcelona, Spain.
- James, K. (2009) In situ origin of the Caribbean: Discussion of data. In: K.H. James, M.A. Lorente and J. Pindell (Eds.) *The origin and evolution of the Caribbean plate*. Geol. Soc. London. Spec. Pub. 328:77-125.
- Jarrard, R. (1986) Relations among subduction parameters. *Reviews of Geophysics* 24:217-284.
- Jarvis, G.T. and D.P. McKenzie. (1980) Sedimentary basin formation with finite extension rates. *Earth Planet. Sci. Letts.* 48:42-52.
- Jordan, T.E. (1981) Thrust loads and foreland basin evolution, Cretaceous, Western United States. *Am. Assoc. Pet. Geol. Bull.* 65(12):2506-2520.
- Jordan, T.E. and A.B. Watts (2005) Gravity anomalies flexure and the elastic thickness structure of the Indian – Eurasia collisional system. *Earth Planet Sci. Letts.* 236:732-750.
- Jordan, T.H. (1975) The present day motion of the Caribbean Plate. *Jour. of Geophys. Res.* 80:4433-4439.
- Jouanne, F., F. A. Audemard, C. Beck, A. Van Welden, R. Ollarves and C. Reinosa (2011) Present-day deformation along the El Pilar Fault in eastern Venezuela: Evidences of creep along a major transform boundary. *Jour. of Geodynamics* 51:398-410.

- Karner, G.D. (1982) Spectral representation of isostatic models. *BMR Jour. Australian Geol. and Geophys.* 7:55-62.
- Karner, G.D. (1985) *Continental Tectonics. A quantitative view of the thermal and mechanical properties of the continental lithosphere in compressional and extensional stress regimes.* University of Durham, England. 52p
- Karner, G.D. and A.B. Watts. (1983) Gravity anomalies and flexure of the lithosphere at mountain ranges. *Jour. of Geophys. Res.* 88:10449-10477.
- Karner, G.D., M.S. Steckler and J.A. Thome (1983) Long-term thermo-mechanical properties of the continental lithosphere. *Nature* 304: 250-253.
- Kearey, P. (1974) Gravity and seismic reflection investigations into the crustal structure of the Aves Ridge, eastern Caribbean. *Geophys. Jour. R. Astr. Soc.* 38:435-448.
- Kearey, P. (1976) Gravity and seismic reflection investigations into the crustal structure of the Aves Ridge, eastern Caribbean. In: *Trans. VII Caribbean Geol. Conf., Guadalupe, 1974.* pp:311-320.
- Kearey, P., G. Peter and G.K. Westbrook (1975) Geophysical maps of the eastern Caribbean. *Jour. Geol. Soc. London* 131:311-321.
- Keen, C.E. and D.L. Barret (1981) Thinned and subsided continental crust on the rifted margin of Eastern Canada: crustal structure, thermal evolution and subsidence history. *Geophys. Jour. R. Astr. Soc.* 65:443-465.
- Kellogg, J.N. and W.E. Bonini (1982). Subduction of the Caribbean plate and basement uplifts in the overriding South American plate. *Tectonics* 1:251-276.
- Ladd, J.W. (1976) Relative motions of the South America and the Caribbean Tectonics. *Geol. Soc. of Amer. Bull.* 87:969-976.
- Ladd, J., W. Truchan, M. Talwani, M. Stoffa, P.L. Buhl, R. Houtz, R. Maufret and G. Westbrook (1984) Seismic Reflection Profiles across the southern margin of the Caribbean. In: W.E. Bonini, R.B. Hargraves and R. Shagam (Eds.) *The Caribbean South American plate boundary and regional tectonics.* Geol. Soc. of Amer. Mem. 162. Boulder, Colorado pp:153-159.
- Ladd, J., T.L. Holcombe, G. Westbrook and N.T. Edgar (1990) Caribbean marine geology: active margins of the plate boundary. In: G. Dengo and J.E. Case (Eds.) *The Caribbean Region, The Geology of North America.* Geol. Soc. of Amer. Vol H:261-290. Boulder, CO.

- Lee, W.H.K. and S.P. Clark (1966) Heat flow and volcanic temperatures. In: S.P. Clark (Ed.) Handbook of physical constants. Geol. Soc. of Amer. Mem. 97:483-511.
- Levander, A., M. Schmitz, H. Ave Lallemand, C. Zelt, D. Sawyer, M. Magnani, P. Mann, G. Christeson, J.E. Wright, G. Pavilis and J. Pindell (2006). Evolution of the Southern Caribbean plate boundary. EOS Trans. AGU. 87:97-100
- Léxico Estratigráfico de Venezuela, online LEV (2008) <http://www.pdvsa.com/lexico/lexicoh.htm>.
- Lewis, B.T.R. and L.M. Dorman (1970). Experimental isostasy, 2. An isostatic model for the U.S.A derived from gravity and topography data. Jour. of Geophys. Res 75:3367-3386.
- Lilliu, A. (1990) Geophysical interpretation of Maturín foreland, north-eastern Venezuela. M.Sc. Thesis. Univ. of Houston, Houston. 110p.
- Ludwig, W., J. Nafe and C. Drake (1970) Seismic refraction. In: A.E. Maxwell (Ed.) The Sea 4(1):53-84. Wiley, Interscience, NY.
- Lugo, J. and P. Mann. (1995) Jurassic-Eocene tectonic evolution of Maracaibo basin, Venezuela. In: A. Tankard, S. Suarez and H. Welsink (Eds.) Petroleum basins of South America. Am. Assoc. Pet. Geol. Mem 62:699-725.
- Lyon-Caen, H. and P. Molnar (1985) Gravity anomalies, flexure of the Indian plate and the structure, support and evolution of the Himalaya and Ganga Basin. Tectonics 4(6):513-538.
- Macdonald, R.C., J. Hawkesworth and E. Heath (2000) The Lesser Antilles volcanic chain: A study in arc magmatism. Earth Sci. Rev. 40:1-76.
- MacDonald W.D. (1972) Continental crust, crustal evolution and the Caribbean. In: R. Shagam, R. Hargraves and others (Eds.) Studies in Earth and Space Sciences. Geol. Soc. Amer. Mem. 132:351-362.
- MacDonald W.D. (1990) Survey of Caribbean Paleomagnetism. In: G. Dengo and J. Case (Eds.) The Geology of North America: The Caribbean Region. Geol. Soc. of Amer. Vol H:393-404.
- Malfait, B. T. and M. G. Dinkelman. (1972) Circum Caribbean tectonics and igneous activity and the evolution of the Caribbean Plate. Geol. Soc. of Amer. Bull. 83:251-271.
- Mann, P. (1999) Caribbean sedimentary basins: Classification and tectonic setting from Jurassic to Present. In: P. Mann (Ed.) Caribbean Basins. Sedimentary Basins of the World. Vol. 4:3-31. Elsevier. Amsterdam, Holanda.

- Mann, P. and K. Burke (1984) Neotectonics of the Caribbean. *Reviews of Geophys. and Space Physics.* 22:309-362.
- Mann, P. and A. Escalona (2011) Introduction to the special issue of *Marine and Petroleum Geology: Tectonics, basinal framework, and petroleum systems of eastern Venezuela, the Leeward Antilles, Trinidad and Tobago, and offshore areas.* *Marine and Pet. Geol.* 28: 4-7.
- Mann, P., C. Schubert and K. Burke (1990) Review of Caribbean Neotectonics. In: G. Dengo and J. Case (Eds.) *The Geology of North America: The Caribbean Region.* *Geol. Soc. of Amer. Vol H:*307-338.
- Mann, P., A. Escalona and M. Castillo (2006) Regional geologic and tectonic setting of the Maracaibo supergiant basin, western Venezuela. *Amer. Assoc. Pet. Geol. Bull.* 90:445-478.
- Maresh, W.V. (1974) Plate tectonic origin of the Caribbean Mountain System of Northern South America: discussion and proposal. *Geol. Soc. of Amer. Bull.* 85:669-682.
- Maresh, W.V., B. Stockhert, A. Baumann, C. Kaiser, R. Kluge, G. Kuckhans-Luder, M. Brix and S. Thomson (2000a) Crustal history and plate tectonic development in the Southern Caribbean. In: *Geoscientific Cooperation with Latin America. 31st International Geological Congress, Rio de Janeiro 2000: Zeitschrift fur Angewandte Geologie* 1:283-290.
- Maresh, W.V., R. Kluge, A. Bauman, J. Pindell, G. Kruckhans-Lueden and K. Stanck (2000b) The occurrence and timing of high-pressure metamorphism of Margarita Island, Venezuela: A constraint on Caribbean – South American interaction: 705-742.
- Martín, C. (1974a) Paleotectónica del Escudo de Guayana. In: *Mem. IX Conf. Geol. Inter-Guayanas. Ciudad Guayana 1973. Venezuela, Ministerio Minas-Hidrocarburos. Bol. Geol. Spec. Pub.* 6:251-305.
- Martín, C. (1974b) Interpretación tectónica de la parte norte de América del Sur. *IV Cong. Geol. Venez. Vol. IV:*2477-2482.
- Martín, C. (1978) Mapa Tectónico, Norte de América del Sur, Venezuela. Ministerio de Energía y Minas, Venezuela. Scale 1:2,500,000.
- Martin-Kaye, P. (1969) A summary of the geology of the Lesser Antilles. Reprinted from *Overseas Geology Mineral Resources, Great Britain* 10(2):172-206.
- Maus, S., U. Barckhausen, H. Berkenbosch, N. Bournas, J. Brozena, V. Childe, F. Dostaler, J. Fairhead, C. Finn, R. Von Frese, C. Gaina, S.

- Golynsky, R. Kucks, H. Lühr, P. Milligan, S. Mogren, R. Muller, O. Olesen, M. Pilkington, R. Saltus, B. Schreckenberger, E. Thebault, F. Caratori (2009) EMAG2: A 2-arc min resolution Earth Magnetic Anomaly Grid compiled from satellite, airborne, and marine magnetic measurements (USA). *Geochem. Geophys. Geosyst. Amer. Geophys. Union.* 10, Q08005. doi:10.1029/2009GC00-2471.
- McAdoo, D. C., J. G. Caldwell and D. L. Turcotte (1978) On the elastic perfectly plastic bending of the lithosphere under generalized loading with applications to the Kuril Trench. *Geophys. Jour. R. Astr. Soc.* 54:11-26.
- McCann, W. R. and W. D. Pennington (1990) Seismicity, large earthquakes and the margin of the Caribbean plate. In: G. Dengo and J. Case (Eds.) *The Geology of North America: The Caribbean Region.* Geol. Soc. of Amer. Vol H:291-306.
- McCann, W.R., J. Dewey, A.J. Murphy and J. Harding (1982) A large normal – fault earthquake in the overriding wedge of the Lesser Antilles subduction zone. The earthquake of October 8, 1974. *Bull. Seismol. Soc. of Amer.* 72:2267-2284.
- McKenzie, D. (1978) Some remarks on the development of sedimentary basin. *Earth Planet. Sci. Letts* 40:25-32.
- McKenzie, D., E. Nisbet and J. Sclater (1980) Sedimentary basin development in the Archaean. *Earth Planet. Sci. Letts* 48:35-41.
- Menard, H. W. (1967) Transitional types of crust under small ocean basins. *Jour. of Geophys. Res.* 72(12):3061-3073
- Mendoza, V. (2005) Evolución geotectónica y recursos minerales del Escudo de Guayana en Venezuela. *GEOS* 38:61-64.
- Menevén (1982) Estudio Geológico Integrado de la Cuenca Oriental de Venezuela. Ed. N. G. Muñoz. International Report, Caracas, Venezuela. 271p.
- Menéndez, A. (1994) Cinturones de rocas verdes del Escudo de Guayana en Venezuela. Revisión estratigráfica. III Simposio Internacional del Oro en Venezuela. Mem. Asoc. del Oro. pp: 123-139.
- Meshede, M. and W. Frisch (1998) A plate tectonic model for the Mesozoic and Cenozoic history of the Caribbean Plate. *Tectonophysics* 296:269-291.
- Miall, A. D. (1990) *Principles of Sedimentary Basin Analysis.* New York. Springer-Verlag. 668p.

- Mittermayer, E. (1969) Numerical formulas for the Geodetic Reference System 1967. *Boll. Geofisica Teorica ed Applicata* 11:96-107.
- Molnar, P. and L. Sykes (1969) Tectonics of the Caribbean and Middle America regions from focal mechanisms and seismicity. *Geol. Soc. of Amer. Bull.* 80(9):1639-1684.
- Munro, S. and F. Smith (1984) The Urica fault zone, northeastern Venezuela. In: W. Bonini, R. Hargraves and R. Shagam. (Eds.) *The Caribbean South American plate boundary and regional tectonics*. *Geol. Soc. of Amer. Mem.* 162:213-215.
- Muñoz, N. G. (1985) Estudio geológico integrado de la Cuenca Oriental de Venezuela. Resumen. Menevén, S.A. Gerencia de Exploración. Caracas, Venezuela. 271p.
- Navarro, E. (1977) Eclogitas de Margarita: evidencias de polimetamorfismo. *Mem. V Cong. Geol. Venezolano*. Caracas. Vol II:651-661.
- Orihuela, N. and A. García (2011) Anomalías magnéticas bandeadas del Caribe Oriental. IV Convención Cubana de Ciencias de la Tierra, La Habana, Cuba. *Mem:*141-147.
- Ostos, M., F. Yoris and H. Ave Lallemand (2005) Overview of the southeast Caribbean-South American plate boundary zone. In: H. Ave Lallemand and V. Sisson (Eds.) *Caribbean-South American Plate Interactions, Venezuela*. *Geol. Soc. of Amer. Spec. Pap.* 394:53-89.
- Parker, R. L. (1973) The rapid calculation of potential anomalies. *Geophys. Jour. R. Astr. Soc.* 31:447-455.
- Parsons, B. and J. G. Sclater (1977) An analysis of the variation of ocean floor bathymetry and heat flow with age. *Jour. of Geophys. Res.* 82: 803-827.
- Pascal Audet. and J-C Mareschal (2007) Wavelet analysis of the coherence between Bouguer gravity and topography: application to the elastic thickness anisotropy in the Canadian Shield, *Geophys. J. Int.* 168:287–298 doi: 10.1111/j.1365-246X.2006.03231.x
- Pekeris, C.L. (1935) Thermal convection in the interior of the Earth. *Geophys. Jour. International* 3:343-367. doi:10.1111/j.1365- 246X. 1935. tb01742.x
- Perez-Gussinye, M. and A.B. Watts (2005) The long-term strength of Europe and its implications for plate forming processes, *Nature*, 436, 381–384, doi:10.1038/nature03854.
- Pérez O. and G. Aggarwal (1981) Present day tectonics of the northeastern Venezuela. *Jour. of Geophys. Res.* 86:10791-10804.

- Pérez, O., R. Bilham, R. Bendick, J. Velandia, N. Hernández, C. Moncayo, M. Hoyer and M. Kozuch (2001). Velocity field across the southern Caribbean plate boundary and estimates of Caribbean/South American plate motion using GPS geodesy 1994-2000. *Geophys. Res. Letts.* 28:2987-2990.
- Perry, R.K. (1984) Compiler Bathymetry of the Gulf of Mexico and the Caribbean Sea. *Am. Assoc. Pet. Geol.*
- Pindell, J. (1985) Plate Tectonic evolution of the Gulf of Mexico and Caribbean region. Ph.D.Thesis, Univ.of Durham, Durham, UK 227p.
- Pindell, J. (1994). Evolution of the Gulf of Mexico and the Caribbean. En S.K. Donovan and T.A. Jackson. (Eds.). *Caribbean Geology: An Introduction.* Univ. of the West Indies Publisher's Association, Kingston, Jamaica pp:13-39.
- Pindell, J. L. and S. F. Barrett (1990). Geological evolution of the Caribbean region: A plate-tectonic perspective. In: G. Dengo and J.E. Case (Eds.). *The Geology of North America: The Caribbean Region.* Geol. Soc. of Amer. Vol H:405-432.
- Pindell, J. and J. Dewey (1982) Permo-Triassic reconstruction of western Pangea and the evolution of the Gulf of Mexico – Caribbean region. *Tectonics* 1(2):179-212.
- Pindell, J. and L. Kennan (2001a). Kinematic evolution of the Gulf of Mexico and the Caribbean. Gulf Coast Association of Geological Societies Conference. Recover February 12th-2009: <http://tectonicanalysis.com/site/download/papercarib01.pdf>.
- Pindell, J. and L. Kennan (2001b). Processes and events in the terrane assembly of Trinidad and Eastern Venezuela. In: R. Fillon, N. Rosen and P. Weimar (Eds.): *Petroleum System of Deep Water Basins: Global and Gulf of Mexico Experience.* 211:159-192.
- Pindell, J. and L. Kennan (2007a). Bow-wave model for deformation and foredeep development since 10 Ma, Eastern Venezuela and Trinidad. 4th Geol. Conf. of the Geol. Soc. of Trinidad and Tobago. Port of Spain. pp:1-30
- Pindell, J. and L. Kennan (2007b). Cenozoic kinematics and dynamics of oblique collision between two convergent plate margins: The Caribbean-South America collision in Eastern Venezuela, Trinidad and Barbados. In *Proceedings of GCSSEPM 2007.*
- Pindell, J. and L. Kennan (2009). Tectonic evolution of the Gulf of Mexico, Caribbean and northern South America in the mantle reference frame: An update. In: K.H. James, M.A. Lorente and J. Pindell

(Eds.) The origin and evolution of the Caribbean plate. Geol. Soc. London. Spec. Pub. 328:1-55

- Pindell, J., J.F. Dewey, S. Cande, W. Pitman III, D. Rowley, L. LaBrecque and J. Haxby (1988) Plate kinematic framework for models of Caribbean evolution. *Tectonophysics* 155:121-138.
- Pindell, J., L. Kennan, W.V. Maresch, K.P. Stanek, G. Drapper and R. Higgs (2005). Plate-kinematics and crustal dynamics of circum-Caribbean arc-continent interactions: Tectonic controls on basin development in Proto-Caribbean margins. In: H. Ave Lallemand and V. Sissons (Eds.) *Caribbean-South American Plate Interactions, Venezuela*. Geol. Soc. of Amer. Spec. Pap. 394:7-52.
- Pratt, J. H. (1854) On the attraction of the Himalaya Mountains and of the elevated regions beyond upon the plum-line in India. *Phil. Trans. R. Soc. London*. 145:53-100.
- Price, R.A. (1973) Large-scale gravitational flow of supracrustal rocks, southern Canadian Rockies. In: K.A. de Jong and R. Sholten. (Eds.) *Gravity and Tectonics*. Wiley Sons. N.Y. pp:491-502.
- Rekowski, F. and L. Rivas. (2005) Integración geológica de la isla de Margarita, Nueva Esparta. *Contribución Proyecto GEODINOS G-2002000478. (FUNVISIS-FONACIT)*. *GEOS* 38:37-39.
- Renz, H. H., H. Alberding, F. K. Dallmus, J. M. Patterson, R. H. Robie, N. E. Weisborb, J. Masvall (1958) The Eastern Venezuelan Basin. In: L.G. Weeks (Ed.) *Habitat of Oil*. Am. Assoc. Pet. Geol. pp:551-600.
- Ríos, K. (2002) Estimación de espesores sedimentarios del Mesozoico en el Graben de Espino a lo largo de dos transectos regionales en el área de Anaco, Edo. Anzoátegui. Trabajo Especial de Grado. Dep. Geofísica, Universidad Central de Venezuela. Caracas. 116p.
- Ritter, J.B. (2007) Geomorphology and Quaternary geology of the Northern Range, Trinidad and Paria Peninsula, Venezuela: Recording Quaternary subsidence and uplift associated with a pull-apart basin. Abstracts. 4th Geological Conf. of the Geol. Soc. of Trinidad and Tobago: Caribbean exploration, planning the future.
- Robertson, P. and K. Burke (1989) Evolution of southern Caribbean plate boundary, vicinity of Trinidad and Tobago. *Am. Assoc. Pet. Geol. Bull* 73:490-509.
- Rodríguez, I., S. Grande, N. Adrian, R. Azuaje, A. Díaz, N. Escorihuela, L. Lozano, L. Morgado, M. Pérez y E: Vargas. (2009). Modelo cortical del Escudo de Guayana, Estado Bolívar, Venezuela. *Jornadas de Investigación Facultad de Ingeniería, UCV*.

- Rodríguez, J. and J. C. Sousa. (2003). Estudio geológico – estructural y geofísico de la sección cabo San Román-Barquisimeto, estados Falcón y Lara. Trabajo Especial de Grado. Dep. Geología y Geofísica. Univ. Central de Venezuela. Caracas, Venezuela. 296p.
- Romero, G., F. Audemard, M. Schmitz and Resica Working Group FUNVISIS (1998) Seismological aspects and fault characteristics of the July 9th 1997 Cariaco earthquake, eastern Venezuela. Mem. IX Cong. Venezolano de Geofísica, 30p.
- Rosales, H. (1972) La Falla de San Francisco en el oriente de Venezuela. Bol. Geol. Venezuela. Spec. Pub. 5:2322-2339.
- Ross, M. and C. Scotese (1988) A hierarchical tectonic model of the Gulf of Mexico and the Caribbean region. Tectonophysics 155:139-168.
- Royden, L. and G. D. Karner (1984) Flexure of the lithosphere beneath the Apennine and Carpathian foredeep basins: Evidence for an insufficient topographic load. Am. Assoc. Pet. Geol. Bull, 68:704-712.
- Royden, L. and C. E. Keen (1981) Rifting processes and thermal evolution of the continental margin of eastern Canada determined from subsidence curves. Earth. Planet. Sci. Letts. 51:343-361.
- Russo, R. M. and R. C. Speed (1992) Oblique collision and tectonic wedging of the South American continent and Caribbean terranes. Geology 20(5):447-450.
- Russo, R. M., R. C. Speed, E. A. Okal, J. B. Shepherd and K. C. Rowley (1993) Seismicity and Tectonics of the southeastern Caribbean, Jour. of Geophys. Res. 98(B8):14299-14319.
- Salvador, P. and R. M. Stainforth (1968) Clues in Venezuela to the geology of Trinidad and vice-versa. Mem. IV Caribbean Geol. Conf., Trinidad 1965, pp:31-40.
- Sánchez, H. and F. Russomanno (1982) Geología Petrolera de la Cuenca de Venezuela Oriental, Internal report, Corpovén. SA, Venezuela.
- Sandwell, D. and W. H. Smith (2009) Global marine gravity from retracked Geosat and ERS-1 altimetry: Ridge segmentation versus spreading rate. Jour. of Geophys. Res. 114: B01411. doi: 10.1029/2008JB006008.
- Santamaría, F. and C. Schubert (1974) Geochemistry and geochronology of the southern Caribbean-northern Venezuela plate boundary. Geol. Soc. of Amer. Bull 85:1085-1098.
- Schmitz, M., G. Romero, F. Audemard, J. Avendaño and F. De Santis (1998) Correlation of aftershocks distribution with surface rupture along El

Pilar fault related to the July 9th 1997, Cariaco earthquake, eastern Venezuela. Abstr. XV Carib. Geol. Conf. Kingston, Jamaica.

- Schmitz, M., J. Castillo, C. Izarra, S. Lüth, A. Da Silva and D. Chalboud (1999) Mediciones sísmicas de refracción, gravimétricas y magnéticas en el Escudo de Guayana. VI Congr. Venez. de Sismología e Ingeniería Sísmica, Mérida, 12-14 mayo 1999. 10p.
- Schmitz, M., A. Martins, C. Izarra, M. Jácome, J. Sánchez and V. Rocabado (2005). The major features of the crustal structure in northeastern Venezuela from deep wide-angle seismic observations and gravity modelling. *Tectonophysics* 399:109-124.
- Schmitz, M., J. Avila, M. Bezada, E. Vieira, M. Yáñez, A. Levander, C. A. Zelt, M. Jácome, M. Magnani and the Bolivar active seismic working group (2008). Crustal thickness variations in Venezuela from deep seismic observations. *Tectonophysics* 459:14-26.
- Schneider, E. D. (1972) Sedimentary evolution of rifted continental margins. *Geol. Soc. of Amer. Mem.* 132:109-118.
- Schoonmaker, J. E. and J. N. Ladd (1984) Heat flow in Lesser Antilles Arc and adjacent terranes. In: R.C. Speed, G. K. Westbrook and others. (Eds.) *Ocean Margin Drilling Program, Regional Atlas Series, Atlas 10*, Marine Science International, Woods Hole, MA, 27 sheets.
- Schubert, C. (1972) Geología de la península de Araya-Paria, estado Sucre.. *Mem. IV Congr. Geol. Venez. Pub. Esp. N° 5, Vol III:1823-1886.*
- Schubert, C. (1979) El Pilar fault zone, northeastern Venezuela. Brief review *Tectonophysics* 52:447-455.
- Schubert, C. (1984) Basin formation along the Boconó-Morón-El Pilar fault system, Venezuela. *Jour. of Geophys. Res. Bull.* 89(B7):5711-5718.
- Schwans, P. (1988) Depositional response of Pigeon. Creek Formation, Utah, to initial fold-thrust belt deformation in a differentially subsiding foreland basin. *Geol. Soc. of Amer. Mem* 171:531-556.
- Sclater, J. G. and P. A. Christie (1980) Continental stretching: An explanation of the post-Mid Cretaceous subsidence of the Central North Sea Basin. *Jour. of Geophys. Res.* 85(B7):3711-3739.
- Sclater, J. G., R. N. Anderson and M. L. Bell (1971) Elevation of ridges and evolution of the Central Pacific. *Jour. of Geophys. Res.* 76:7888-7915.
- Sheridan, R E. (1969) Subsidence of continental margins. *Tectonophysics* 7(3):219-229.

- Silver, E., J. Case and H. MacGillavri (1975) Geophysical study of the Venezuelan borderland. *Geol. Soc. of Amer. Bull.* 86(2):213-226.
- Simmons, G. and K. Horai (1968) Heat flow data 2. *Jour. of Geophys. Res.* 73(20):6608-6629.
- Sisson, V., H. Ave Lallemand, M. Ostos, A. Blythe, L. Snee, P. Copeland, J. Right, R. Donelick and L. Guth (2005) Overview of radiometric ages in three allochthonous belts of northern Venezuela: Old ones, new ones and their impact on regional geology. *Caribbean- South American plate interactions, Venezuela. Am. Assoc. Pet. Geol. Spec. Pap.* 394:91-117.
- Skeels, D. (1947) Ambiguity in gravity interpretation. *Geophysics* 12:43-56.
- Sleep, N.H. (1974) Plate Tectonics and Sedimentation. In: W.R. Dickinson. (Ed.) *Spec. Publ. Soc. Econ. Pal. Min.* 22:1-27, Tulsa.
- Sleep, N. H. and N. S. Snell (1976) Thermal contraction and flexure of mid-continent and Atlantic marginal basins. *Geophys. Jour. R. Astr. Soc.* 45:125-154.
- Sousa, J. C., J. Rodríguez , C. Giraldo, I. Rodríguez, F. Audemard and R. Alezones (2005). An integrated geological-geophysical profile across northwestern Venezuela. Presented at the 6th International Symposium on Andean Geodynamics. Barcelona, Spain.
- Speed, R. C. (1985) Cenozoic collision of the Lesser Antilles Arc and continental South America and the origin of the El Pilar fault. *Tectonics* 4:41-69.
- Speed, R.C., R. Russo, J. Weber and K.C. Rowley (1991). Evolution of southern Caribbean plate boundary, vicinity of Trinidad and Tobago: Discussion. *Am. Assoc. Pet. Geol. Bull.* 75(11):1789-1794.
- Speed, R. C., R. Torrini and P.L. Smith (1989) Tectonic evolution of the Tobago trough forearc basin. *Jour. of Geophys. Res.* 94(B3):2913-2936.
- Speed, R. C., G. K. Westbrook, B. Biju-Duval, J. W. Ladd, A. Mascle, J. C. Moore, J. B. Saunders, J. E. Schoonmaker and S. Stein (1984). Lesser Antilles arc and adjacent terranes. *Ocean Margin Drilling Program, Regional Atlas Series, Atlas 10*, Marine Science International, Woods Hole, MA, 27 sheets.
- Speed, R. C., P.L. Smith-Horowitz, K. Perch-Nielsen, J.B. Saunders and A.B. Sanfilippo (1993) Southern Lesser Antilles Arc Platform: Pre-Late Miocene stratigraphy, structure and tectonic evolution. *Geol. Soc. of Amer. Spec. Pap.* 277

- Stainforth, R. M. (1965) Internal publications on the Geology of Venezuela, 1958 to mid 1965. Am. Assoc. Pet. Geol. Bull. 49:2289-2294.
- Steckler, M. S. and A. B. Watts (1978) Subsidence of the Atlantic type continental margin off New York. Earth Planet. Sci. Letts. 41:1-13.
- Stein, S., C. DeMetz, R. Gordon, J. Brodholt, D. Argus, J. Engeln, P. Lundgren, C. Stein, D. Wiens and D. Woods. (1988). A test of alternative Caribbean Plate relative motion models. Jour. of Geophys. Res. 93(B4):3041-3050.
- Stephan, J. F., C. Beck, V. Vivas, H. Arnaud, J. Chorowicz, O. MacSotay, M. Lujan, A. Perez and A. Sequera (1985). Geometría e historia tectonosedimentaria del frente de montañas Caribe de Venezuela, desde Lara hasta el norte de Monagas. Mem. V Simposium Bolivariano: Exploracion Petrolera en las Cuencas Subandinas. Puerto La Cruz, Venezuela. pp:265-266.
- Stephan, J.F., B. Mercier de Lepinay, E. Calais, M. Tardy, C. Beck, J.C. Carfantan, J. Olivet, J. Vila, P. Bouysse, A. Mauffret, J. Bourgois, J. Thery, J. Tournon, R. Blanchet and J. Dercout (1990) Paleogeodynamic maps of the Caribbean: 14 steps from Lias to Present. Bull. Soc. Geologique de France. Series 8(VI):915-919.
- Subieta, T. (1988) Evolución tectonoestratigráfica de la Serranía del Interior y de la Subcuenca de Maturín. Internal Report. Dep. Geología. Estudios Regionales, Lagoven, Venezuela. 30p.
- Summa, L.L., E.D. Goodman, M. Richardson, I.O. Norton and A.R. Green (2003) Hydrocarbon systems of Northeastern Venezuela: plate through molecular scale-analysis of the genesis and evolution of the Eastern Venezuela basin. Marine and Pet. Geol. 20:323-349.
- Sykes, L. and M. Ewing (1965) The seismicity of the Caribbean region. Jour. of Geophys. Res. 70(10):5065-5074.
- Sykes, L., W. R. McCann and A. L. Kafka (1982) Motion of Caribbean Plate during last 7 million years and implications for early Cenozoic movements. Jour. of Geophys. Res. 87(B13):10656-10676.
- Taboada, A., L.A. Rivera, A. Fuenzalida, A. Cisternas, H. Phillip, H. Bijwaard, J. Olaya and C. Rivera (2000) Geodynamic of the Northern Andes: subduction and intra-continental deformation (Colombia). Tectonics 19:787-813.
- Talukdar, S. (1983) Petrological study of volcanic and sedimentary rocks from offshore wells of the north of Paria. Internal Report Int-83. Caracas, Venezuela.

- Talukdar, S. and D. Loureiro (1982) Geología de una zona ubicada en el segmento norcentral de la Cordillera de La Costa, Venezuela: Metamorfismo y deformación, Evolución del margen septentrional de Sudamérica en el marco de la Tectónica de Placas. Ed. UCV Geos 27:15-76
- Talwani, M., J.L. Worzel and M. Landisman (1959) Rapid gravity computations for two-dimensional bodies with applications to the Mendocino submarine fracture zone. Jour. of Geophys. Res. 64(1):49-59.
- Tassara, A., C. Swain, R. Hackney and J. Kirby (2007). Elastic thickness of South America estimated using wavelets and satellite-derived gravity data. Earth Planet. Sci. Letts. 253:17-36.
- Thomas, M. (1983) Tectonic significance of paired gravity anomalies in the southern and central Appalachians. Geol. Soc of Amer. Mem. 158:113-124.
- Tomblin, J.F. (1975) The Lesser Antilles the Aves Ridge, The Ocean Basins and margins, 3:1-64.
- Torrini, R. and R. Speed (1989) Tectonic wedging in the forearc basin-accretionary prism transition, Lesser Antilles Forearc. Jour. of Geophys. Res. 94(B8):10549-10584
- Trenkamp, R., J.N. Kellogg, J.T. Freymuller, H.P. Mora (2002) Wide plate margin deformation, southern Central America and northwestern South America. Jour. of South American Earth Science 15:157-171.
- Turcotte, D. L. (1979) Flexure: Advances in Geophysics 21:51-86.
- Turcotte, D.L. (1980) Models for the evolution of sedimentary basins. In: A.W. Bally, P.L. Bender, T.R. McGetchin and R. I. Walcott. (Eds.) Dynamics of plate interiors. Geodynamic Series 1:21-26. Amer. Geophys. Union, Washington DC.
- Turcotte, D.L. and J.L. Ahern. (1977) On the thermal and subsidence history of sedimentary basins. Jour. of Geophys. Res. 82 (26):3762-3766.
- Turcotte, D. and G. Schubert. (1982) Geodynamics applications of continuum Physics to Geological Problems. J. Wiley & Sons, New York, 450p.
- Turcotte, D. and G. Schubert (2002) Geodynamics, 2nd Ed., Cambridge University Press, 528p.
- Turcotte, D.L., J.L. Ahern and J.M. Bird (1977) The state of stress at the continental margins. Tectonophysics 42:1-28.
- Turcotte, D.L., D.C. McAdoo and J.G. Caldwell (1978) An elastic perfectly

plastic analysis of the bending of the lithosphere at a trench. *Tectonophysics*. 47:193-205

- Ughi, A. (2009) Modelado geofísico integrado en la zona de subducción activa del arco de islas de las Antillas Menores. Trabajo de Grado M.Sc. Fac. de Ciencias. Univ. Central de Venezuela. Caracas.101p.
- Urbani, F. (1989) Recursos geotermales en Venezuela. Mem. Jornadas 50 Aniv. Esc. Geol., Minas y Geof., Univ. Central de Venezuela.
- Urbani, F. (1991) Fuentes de Aguas Termales de Venezuela. Geotermia en Venezuela. In: LEV: www.pdvsa.com/lexico.menes/
- Vail, P.R., R.M. Mitchum and S. Thompson. (1977) Seismic stratigraphy and global changes of sea level, part four: global cycles of relative changes of sea level. *Am. Assoc. Pet. Geol. Mem* 26:83-98.
- Vajk, R. (1956) Bouguer corrections with varying surface density. *Geophysics* 21(4):1004-1020.
- Van der Hilst, R. and P. Mann (1994) Tectonic implications of tomographic images of subducted lithosphere beneath NW South America. *Geology* 22:451-454.
- Veevers, J.J. (1981) Morphotectonics of rifted continental margins in embryo (East Africa), youth (Africa-Arabia) and maturity (Australia). *Jour. Geol. Chicago* 89:57-82
- Vening Meinesz, F.A. (1931) Une nouvelle method pour la reduction isostatique regionale de l'intensite de la pesanteur. *Bull. Geod.* 29:33-51.
- Vierbuchen, R.C. (1979) The Tectonics of northeastern Caribbean Sea. Ph. D. Thesis, Princeton Univ., Princeton N.Y. 193p.
- Vierbuchen, R. C. (1984) The geology of the El Pilar fault zone and adjacent areas in northeastern Venezuela. *Geol. Soc. of Amer. Mem.* 162:189-212.
- Vignali, M. (1977) Geology between Casanay and El Pilar (El Pilar fault zone), Estado Sucre, Venezuela. *Abstr. VIII Caribbean Geol. Conf.* p:215.
- Vignali, M. (1979) Estratigrafía y estructura de las cordilleras metamórficas de Venezuela oriental (Península de Araya-Paria e Isla de Margarita). *Geos* 25:19-66.
- Viscarret, P. and F. Urbani (2005) Algunos aspectos de la geología de la región del El Baúl, Edo. Cojedes, Venezuela. *Geos* 38:49-51.

- Wadge, G. (1984) Comparison of volcanic production rates and subduction rates at Lesser Antilles and Central America. *Geology* 12:555-558
- Wadge, G. (1994) The Lesser Antilles. In: S.K. Donovan and T.A. Jackson (Eds.) *Caribbean Geology: An Introduction*. The Univ. of West Indies, Pub. Assoc., Kingston, Jamaica, pp:167-177.
- Wadge, G. and J. Shepherd (1984) Segmentation of the Lesser Antilles zone. *Earth Planet. Sci. Letts.* 71:297-304.
- Walcott, R.I. (1970a) Flexural rigidity, thickness and viscosity of the lithosphere. *Jour. of Geophys. Res.* 75(20):3941-3954.
- Walcott, R.I. (1970b) Flexure of the lithosphere at Hawaii. *Tectonophysics* 9:435-446.
- Walcott, R.I. (1972) Gravity, flexure and the growth of sedimentary basins at continental edge. *Geol. Soc. of Amer. Bull.* 83:1845-1848.
- Walcott, R.I. (1976) Gravity, flexure and the growth of sedimentary basins at a continental edge. *Geol. Soc. of Amer. Bull.* 83:1845-1848
- Waltham, D. (2001) *Decompact, Software for Backstripping*. Royal Holloway, Univ. of London. UK.
- Watts, A. B. (1978) An analysis of isostasy in the world's oceans: 1. Hawaiian-Emperor seamount chain. *Jour. of Geophys. Res.* 83:5989-6004
- Watts, A. B. (1992) The elastic thickness of the lithosphere and the evolution of sedimentary basins. *Basin Research* 4:169-178
- Watts, A. B. (2001) *Isostasy and Flexure of the Lithosphere*. Cambridge Univ. U.K. Press, 1st Edition, 480 p.
- Watts, A.B. and W.B. Ryan (1976) Flexure of the lithosphere and continental margin basins. *Tectonophysics* 36:25-44.
- Watts, A.B. and M. Talwani (1974) Gravity anomalies seaward of deep-sea trenches and their tectonic implications. *Geophys. Jour. R. Astr. Soc.* 36:57-90.
- Watts, A.B., G.D. Karner and M.S. Steckler (1982) Lithospheric flexure and the evolution of sedimentary basins. In: *The evolution of sedimentary basins*. *Phil. Trans. R. Soc. Series A* 305:249-281.
- Weber, J.C., T.H. Dixon, C. De Mets, W.B. Ambeh, P. Jansma, G. Mattioli, J. Saleh, G. Sella, R. Bilhzm and O. Perez (2001) GPS estimate of relative motion between the Caribbean and South American plates,

and geologic implications for Trinidad and Venezuela. *Geology* 29: 75-78.

- Weber, J.C., J. Saleh, S. Balkaransingh, T. Dixon, W. Arnbeth, T. Leong, A. Rodriguez and K. Miller (2010). Triangulation-to-GPS and GPS-to-GPS geodesy in Trinidad, West Indies: Neotectonics, seismic risk and geologic implications. 23(1):110-121.
- Wessel, P. and W.H. Smith (1995) New version of the GMT (Generic Mapping Tool, Free software helps map and display data) released. *EOS Trans. AGU* 76:329.
- Westbrook, G.K. (1975) The structure of the crust and upper mantle in the region of Barbados and the Lesser Antilles. *Geophys. Jour. R. Astr. Soc.* 43:201-242.
- Westbrook, G.K. and W.R. McCann (1986) Subduction of Atlantic lithosphere beneath the Caribbean. In: P.R. Vogt and B.E. Tucholke. (Eds.) *The Geology of North America: The western North Atlantic Region.* Geol. Soc. of Amer. Vol M:341-350.
- Westbrook, G.K. and J.M. Smith (1983) Long decollements and mud volcanoes: Evidence from the Barbados Ridge Complex for the role of high pore-fluid pressure in the development of an accretionary complex. *Geology* 11:279-283.
- Westbrook, G.K., J.W. Ladd, P. Buhl, N. Bangs, G.J. Tiley (1988) Cross section of an accretionary wedge: Barbados Ridge Complex. *Geology* 16:631-635.
- Yeats, R.S., K. Sich and G.R. Allen (1987) *The Geology of Earthquakes.* Oxford University Press.
- Ysaccis, R. (1997) Tertiary evolution of the northeastern Venezuela offshore. Ph.D. Thesis, Rice University. Houston, USA. 285p.
- Yoris, F. and M. Ostos (1997) *Geología de Venezuela: Geología General y avances petrolíferos.* In: J. Singer (Ed.). WEC 1997, Evaluación de pozos. Texas. Joyel Printing Schlumberger Surencos CA. pp:24-44
- Young, G., A. Bellizzia, H. H. Renz, F. W. Johnson, R. H. Robie and J. Masvall (1956) *Geología de las cuencas sedimentarias de Venezuela y de sus campos petrolíferos.* Mem. XX Internat. Geol. Cong. Mexico. Symposium sobre yacimientos de petróleo y gas. Vol. IV:161-322.
- Zhang, G. and M. H. P. Bott (2000) Modelling the evolution of asymmetrical basins bounded by high-angle reverse faults application to foreland basins. *Tectonophysics* 322:203-218.

APPENDIX A.1

SEDIMENTATION vs. SUBSIDENCE

A.1. STRATIGRAPHIC ZONAL DISTRIBUTION EASTERN VENEZUELA

Based on the data cited in section 3.5. Chapter 3, a brief description of subzones 1 to 10 is given hereinafter, to provide a better idea of the relation between sedimentation and subsidence all over the area of this study. A location map of boreholes is shown in Figure 3.3.

As a rule of thumb the following general remarks should be kept in mind throughout the ensuing discussion:

- Regional unconformities limit the stratigraphic units and are identified as follows: Precambrian crystalline basement (PC), Paleozoic (PZ), Cretaceous (KK), Paleocene-Eocene (PE), Oligocene (OL), Lower Miocene (LM), Mid Miocene (MM) and Upper Miocene-Pliocene (UMP).
- All thickness, subsidence and sedimentary rate referred are average values

Subzone 1 (Figure A.1)

The stratigraphic pattern of subzone 1 is governed by the formula PZ/KK-OL-LM, which means that the subsurface stratigraphic sequence in this region comprises lower Miocene and Oligocene deposits plus an undifferentiated age Cretaceous section overlying rocks of Paleozoic age. Twenty eight wells were evaluated to describe this subzone; three wells (75, 76 and 77) reached Paleozoic basement at depths of about 2,500 m. Cretaceous sedimentary rocks have been drilled in all these locations, so the Oligocene deposits overlie directly the Cretaceous, except at one well where a thin section of Paleocene-Eocene has been reported (Arstein et al., 1982).

The sedimentation rate was maximum during the lower Miocene (200 m/my) in contrast with the 15-20 m/my recorded during the Oligocene, which marks the onset of subsidence in this subzone. The Mid-Miocene and Upper Miocene-Pliocene are periods of non-deposition/erosion all over this area.

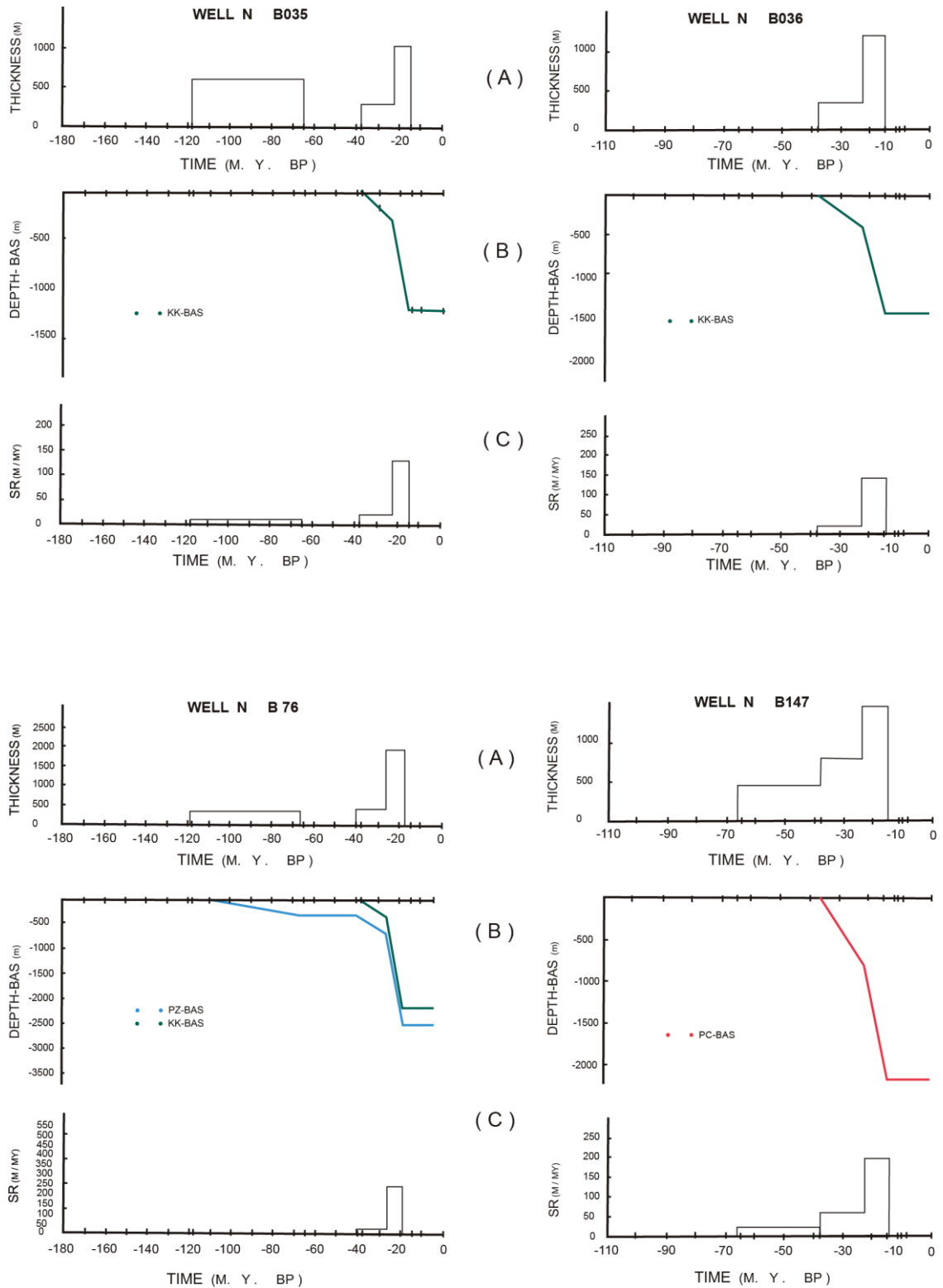


Figure A.1. Diagrams illustrating (A) Thickness of sediments, (B) Depth to basement and (C) Rate of sedimentation characteristic of subzone 1 in Eastern Venezuela.

Histograms (A) and (C) have been drawn using information of sedimentary thickness and time interval for sedimentary sequences limited by well-identified unconformities. Curves (B) represent accumulated thicknesses of sediments up to de top of Paleocene-Eocene (PE), Cretaceous (KK), Paleozoic (PZ) and/or Precambrian (PC) crystalline basement, whichever of these horizons had been reached at the well.

Subzone 2 (Figure A.2a)

The formula PC/PZ-KK-OL-MM characterizes this subzone where six wells were analyzed. The crystalline Precambrian basement was reached at well N° 1, while the oldest rocks drilled at the other locations are of Paleozoic age; there, thicknesses up to 1,700 m have been preserved and might overlay Precambrian rocks. Cretaceous sedimentary strata, some 300 m thick, are present all over the area. In this area, the subsidence history starts with Oligocene deposits (15 m/my) and recurs at a higher rate (170 m/my) during the Mid Miocene after a period of non-deposition/erosion in the Lower Miocene.

Subzone 3 (Figure A.3)

Fourteen wells were evaluated and a sequence PC/PZ-KK-MM-UMP was found to typify subzone 3; the complete section has been drilled only at location N° 108. All the boreholes in this region exhibit Cretaceous section with thicknesses around 500-800 m and six of them overlay Paleozoic rocks. The onset and also the period of major subsidence in this subzone is Mid Miocene, with sedimentation rates increasing northwards from 125 to 350 m/my. Deposition through the Upper Miocene to Pliocene times occurs at a rate of 35 m/my.

Subzone 4 (Figure A.2b)

The stratigraphic sequence that characterizes this subzone is PC/MM-UMP. Data from eighteen boreholes was used to describe this subzone where the crystalline basement of Precambrian age has been reached at all well-locations underlying deposits of the Mid Miocene. A slow subsidence, if compared with subzones 2 and 3, is recorded in this area where the rate of sedimentation is found to decrease in a westerly direction from values of 100 m/my down to 17 m/my. The Upper Miocene-Pliocene sedimentary rates are about 54 m/my, with minimum values of 7.5 m/my at the southernmost locations close to the Guayana outcrops.

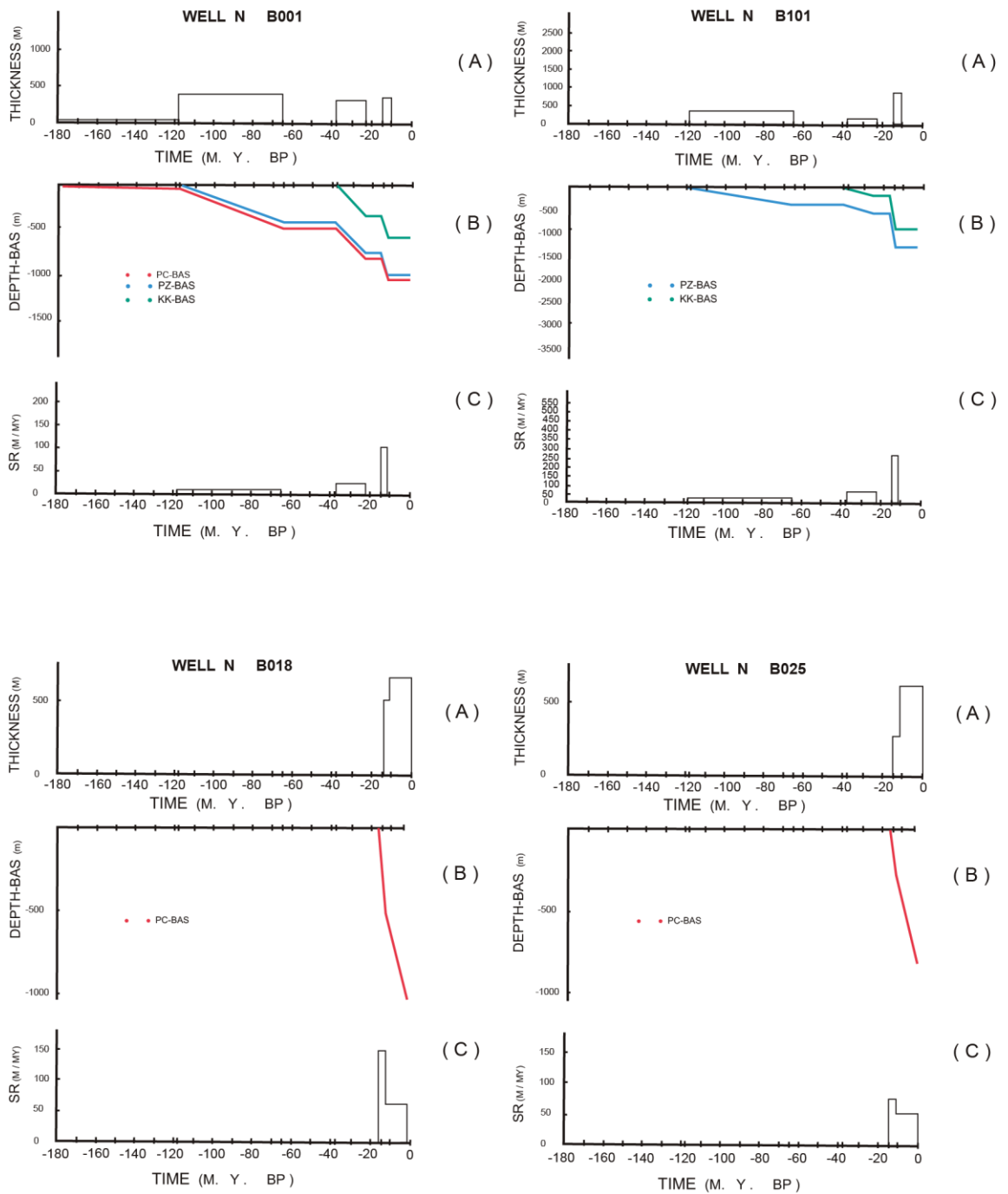


Figure A.2. Diagrams illustrating (A) Thickness of sediments, (B) Depth to basement and (C) Rate of sedimentation characteristic of subzones 2 and 4 in Eastern Venezuela.

Subzone 2 (A.2a, wells 1 and 101)

Subzone 4 (A.2b, wells 18 and 25)

Histograms (A) and (C) have been drawn using information of sedimentary thickness and time interval for sedimentary sequences limited by well-identified unconformities. Curves (B) represent accumulated thicknesses of sediments up to the top of Paleocene-Eocene (PE), Cretaceous (KK), Paleozoic (PZ) and/or Precambrian (PC) crystalline basement, whichever of these horizons had been reached at the well.

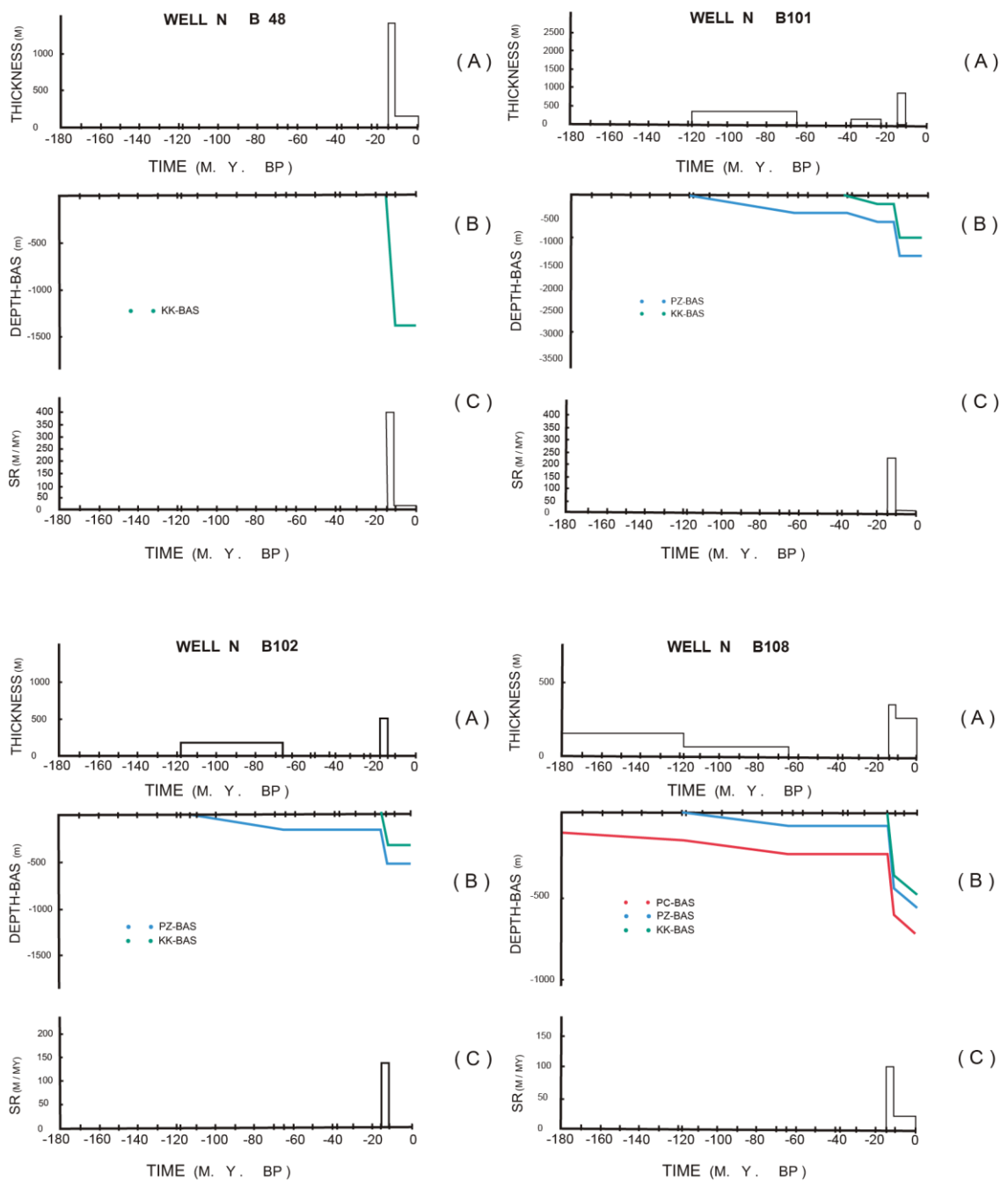


Figure A.3. Diagrams illustrating (A) Thickness of sediments, (B) Depth to basement and (C) Rate of sedimentation characteristic of subzone 3 in Eastern Venezuela.

Histograms (A) and (C) have been drawn using information of sedimentary thickness and time interval for sedimentary sequences limited by well-identified unconformities. Curves (B) represent accumulated thicknesses of sediments up to the top of Paleocene-Eocene (PE), Cretaceous (KK), Paleozoic (PZ) and/or Precambrian (PC) crystalline basement, whichever of these horizons had been reached at the well.

Subzone 5 (Figure A.4)

A formula PC/UMP was found to typify subzone 5, where Upper Miocene-Pliocene strata overlay directly the crystalline basement. Apparently, either there has not been deposition of other units, or they have all been eroded. A very slow subsidence, increasing northwards is evident in this subzone. The four wells drilled in the area show sedimentary thickness increasing towards the north, as in a wedge, from 230 m to 600 m over a south-north distance of about 30 km, which reflects a gradient of the top of the basement of the order of 12m/km. Sedimentary rate varies from 3 to 5 m/my.

Subzone 6 (Figure A.5a)

The stratigraphic pattern that typifies this subzone is controlled by the formula PC/KK-MM-UMP. There, Cretaceous sections 100 - 600 m thick have been preserved and rest directly over the Precambrian crystalline basement; only 3 out of 45 wells drilled in this area did not reach the basement. Maximum subsidence has occurred at the western part of this subzone with sedimentary rates of Mid Miocene deposits of 200 m/my decreasing eastwards down to 110 m/my. Trends of rates of sedimentation at the Upper Miocene-Pliocene sections evidence major subsidence at the north, with values of 185 m/my in contrast with the 72 m/my recorded in the southern part of this subzone.

Subzone 7 (Figure A.6)

This region exhibits by far the most complete stratigraphic sequence throughout the Eastern Venezuela foreland basin. Data from 30 boreholes was processed and a formula KK-PE-OL-LM-MM-UMP was obtained to characterize this zone. Tertiary sedimentary sections, a few thousand meters thick, have been drilled with the top of Cretaceous strata being reached at seven wells; the Paleozoic, beneath some 600 m of Cretaceous sedimentary rocks was reached at one location (Nº 79) on the western part of this subzone. Locally, a few hundred meters of Paleocene-Eocene deposits have also been preserved (as in wells 140, 142 and 145) over sedimentary rocks of Cretaceous age.

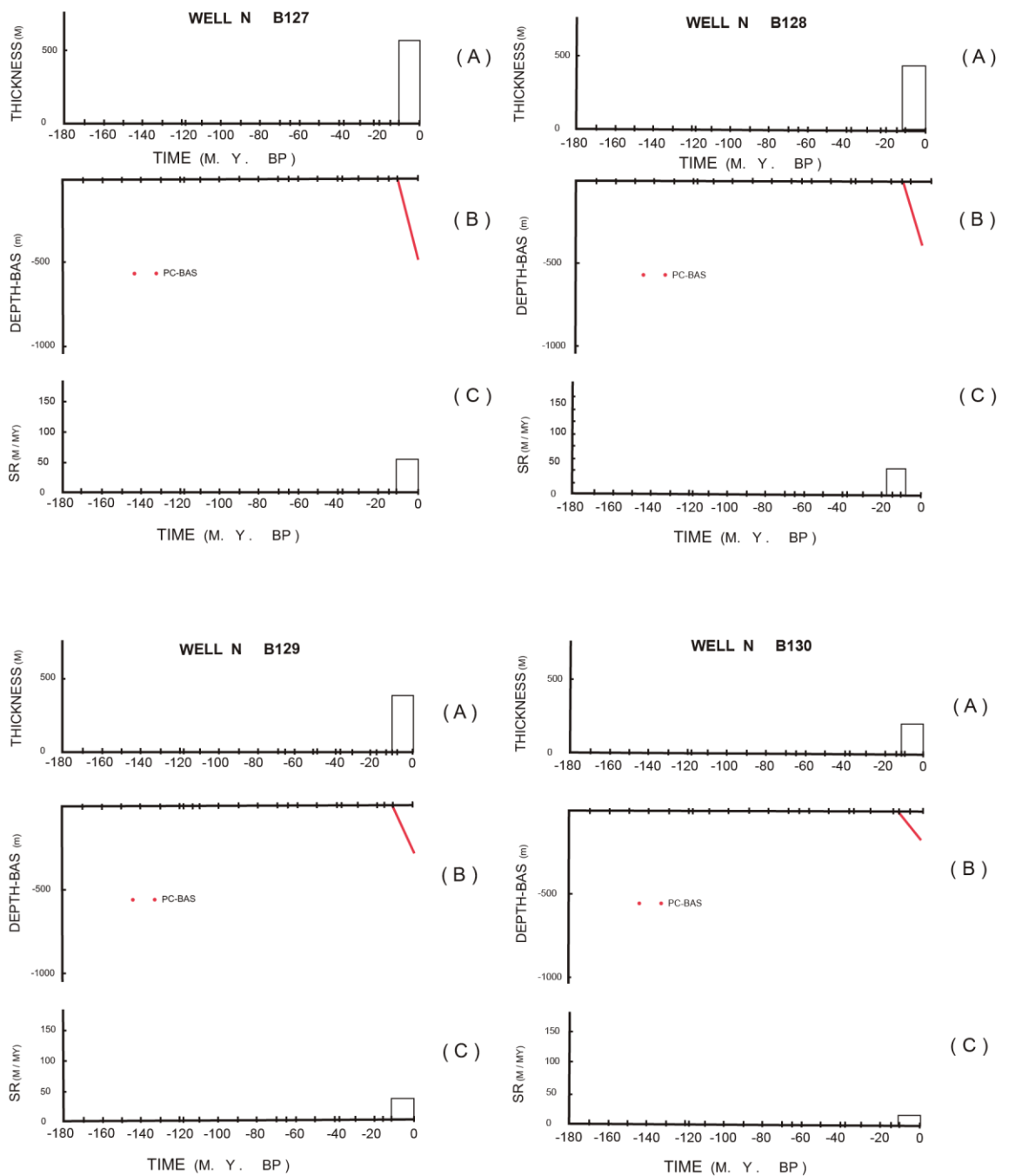


Figure A.4. Diagrams illustrating (A) Thickness of sediments, (B) Depth to basement and (C) Rate of sedimentation characteristic of subzone 5 in Eastern Venezuela. Observe the subsidence increasing towards the North through wells 130, 129, 128 and 127.

Histograms (A) and (C) have been drawn using information of sedimentary thickness and time interval for sedimentary sequences limited by well-identified unconformities. Curves (B) represent accumulated thicknesses of sediments up to the top of Paleocene-Eocene (PE), Cretaceous (KK), Paleozoic (PZ) and/or Precambrian (PC) crystalline basement, whichever of these horizons had been reached at the well.

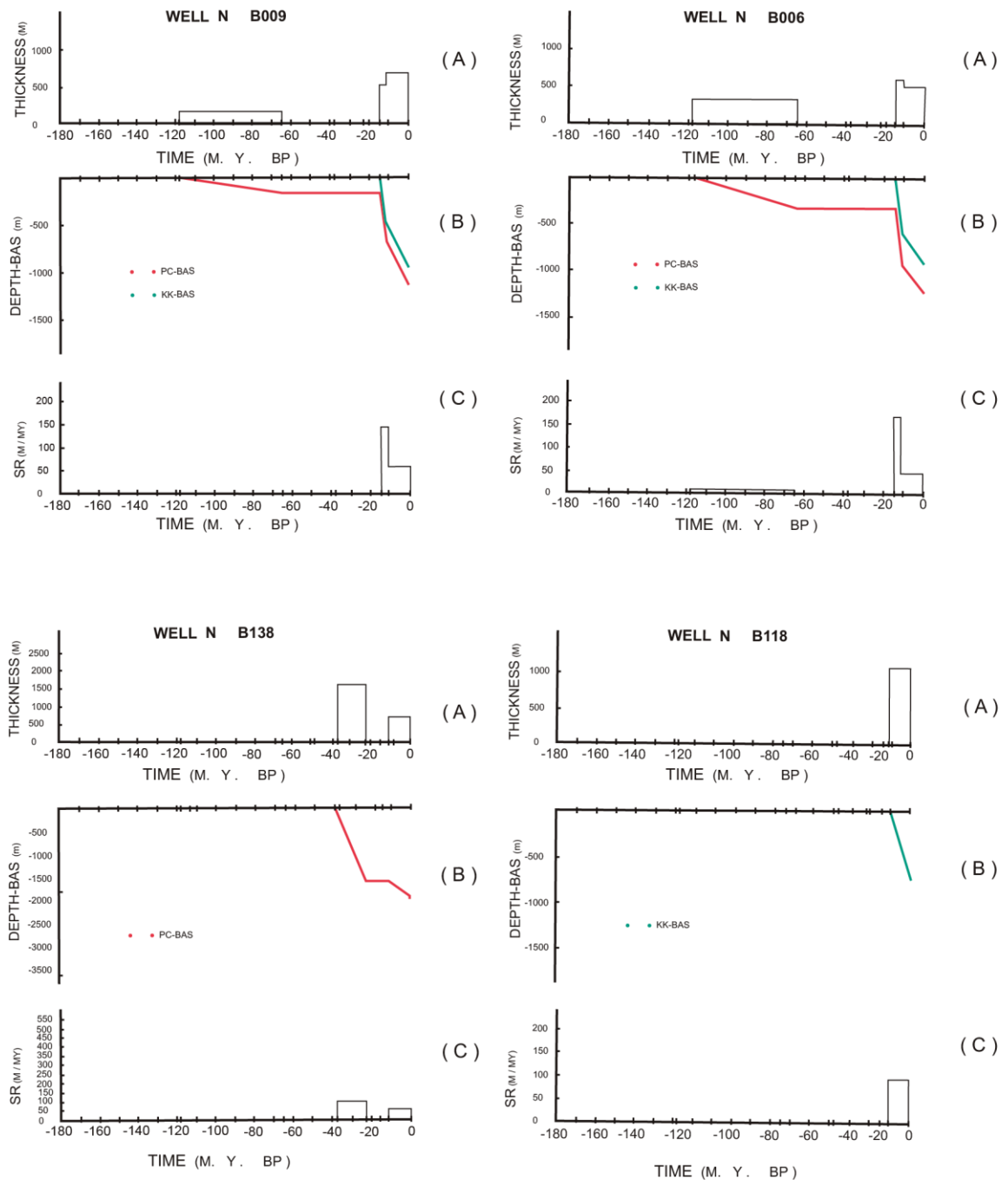


Figure A.5. Diagrams illustrating (A) Thickness of sediments, (B) Depth to basement and (C) Rate of sedimentation characteristic of subzones 6 and 8 in Eastern Venezuela.
 Subzone 6 (A.5a, wells 9 and 6)
 Subzone 8 (A.5b, wells 138 and 118)

Histograms (A) and (C) have been drawn using information of sedimentary thickness and time interval for sedimentary sequences limited by well-identified unconformities. Curves (B) represent accumulated thicknesses of sediments up to de top of Paleocene-Eocene (PE), Cretaceous (KK), Paleozoic (PZ) and/or Precambrian (PC) crystalline basement, whichever of these horizons had been reached at the well.

The subsidence history began in the Oligocene, with a fairly constant sedimentary rate of 20 m/my all over this zone. A few Low Miocene deposits, although scarce, have been identified (wells N° 142-145) overlying the Oligocene or directly Eocene strata. Then, a Mid Miocene sequence with sedimentary rates of about 340 m/my is widespread all over this subzone, where they may overlay Low Miocene, Oligocene and even Cretaceous sediments directly.

The thick Upper Miocene-Pliocene sequence is in some cases the only stratigraphic unit penetrated by drill in subzone 7. Maximum subsidence is recorded at around 63.5°W – 64.0° W of longitude, with the sedimentary rate grading southwards from 255 m/my down to 140 m/my. In the Paria Gulf, the eastern extension of the Eastern Venezuela Basin, well N° 92 has drilled a sedimentary sequence including Lower Miocene (150 m/my), Mid Miocene (100 m/my) and Upper Miocene-Pliocene (200 m/my). The bottom of the Lower Miocene was not reached at this borehole.

Subzone 8 (Figure A.5b)

The formula KK-PE-OL-UMP describes the stratigraphic sequence drilled in this region corresponding to the southwestern piedmont of the Eastern Serrania del Interior and the Serrania itself. Four wells were available for studying the area where some 800 m of Paleocene-Eocene strata overlay the Cretaceous.

Subsidence is recorded from the Oligocene with low sedimentary rates of the order of 7.5 m/my (where it has been reached by drill). Lower and Middle Miocene deposits are absent, or very sparse, probably as a result of non-deposition or erosion

An 800-1000 m thick section of Upper Miocene-Pliocene sediments overlies the Cretaceous rocks of the Eastern Serrania del Interior, which are also exposed over extensive parts of northeastern Venezuela. The rate of sedimentation of the Upper Miocene-Pliocene cover varies from 100 m/my at the western piedmont to 1000 m/my at the Serrania.

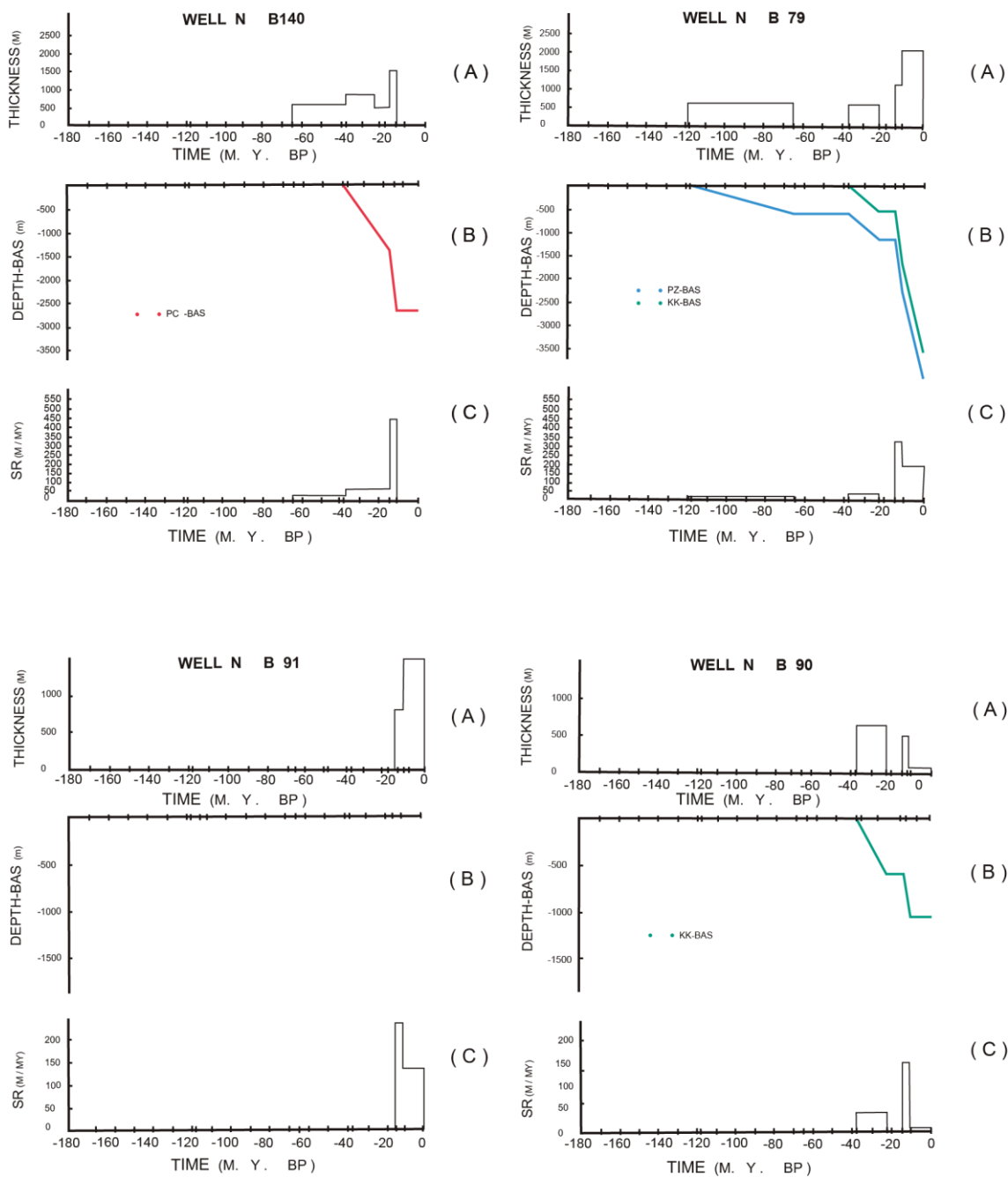


Figure A.6. Diagrams illustrating (A) Thickness of sediments, (B) Depth to basement and (C) Rate of sedimentation characteristic of subzone 7 in Eastern Venezuela. Exhibit the most complete stratigraphic sequence throughout the Eastern Venezuela foreland basin.

Histograms (A) and (C) have been drawn using information of sedimentary thickness and time interval for sedimentary sequences limited by well-identified unconformities. Curves (B) represent accumulated thicknesses of sediments up to the top of Paleocene-Eocene (PE), Cretaceous (KK), Paleozoic (PZ) and/or Precambrian (PC) crystalline basement, whichever of these horizons had been reached at the well.

Subzone 9 (Figure A.7)

This region is located offshore Venezuela, north of the Paria peninsula. Data from eight wells were evaluated and the sequence drilled in the area includes KK(metamorphic) - KK(sedimentary)-OL-LM-MM-UMP. The metamorphic basement (KKm) was reached at 3,115 m depth at B01 where it includes volcanic rocks (mid-oceanic ridge basalts MORB) very low to low grade regional metamorphism of high P/T type developed during the Upper Cretaceous (?) as suggested by Talukdar (1983) who also stated that the MORB of B01 might represent earlier Atlantic Ocean floor if not older than Jurassic. Maximum subsidence related to sedimentary rates exceeding 400 m/my is recorded during the Mid Miocene to the north of Paria.

A similar stratigraphic sequence comprising KKm-EO-OL-LMMM-UMP is found northwest of Margarita Island and north of the Cariaco trough; eight wells have reached the metamorphic basement in the area around the Cariaco Basin, at depths variable between 1,347 and 3,673 m. The earliest sedimentary sequence known in the basin fill consists of deep marine shales of Eocene age, overlying upper Cretaceous igneous -metamorphic rocks (KKm) that have been correlated to similar rocks exposed in Margarita Island and Araya-Paria Peninsula (Talukdar and Loureiro, 1982).

Subzone 10

Subzone 10 comprises the area south of Cariaco trough over the platform of Venezuela. There Upper Miocene sediments consisting of silts and clays deposited in an estuarine environment, overlie directly basement rocks of Upper Cretaceous age. Unconformably over the Miocene lies the Pliocene sequence of coastal-deltaic environment.

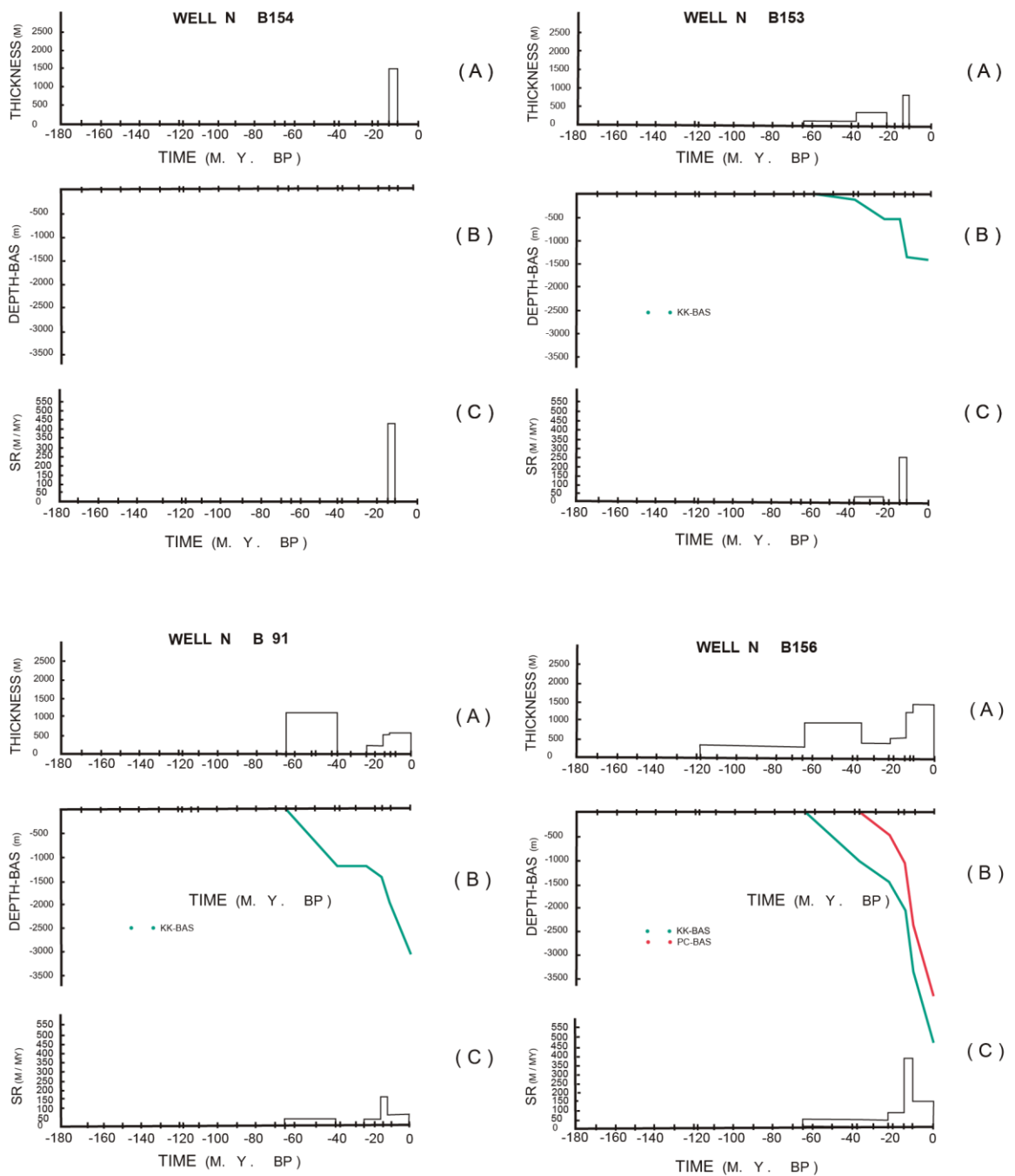


Figure A.7. Diagrams illustrating (A) Thickness of sediments, (B) Depth to basement and (C) Rate of sedimentation characteristic of subzone 9 in Eastern Venezuela. Basement is Cretaceous metamorphic rocks as those exposed in Araya-Paria peninsula.

Histograms (A) and (C) have been drawn using information of sedimentary thickness and time interval for sedimentary sequences limited by well-identified unconformities. Curves (B) represent accumulated thicknesses of sediments up to the top of Paleocene-Eocene (PE), Cretaceous (KK), Paleozoic (PZ) and/or Precambrian (PC) crystalline basement, whichever of these horizons had been reached at the well.

APPENDIX A.2

SEDIMENT LOADING EFFECT BACKSTRIPPING

A.2. SEDIMENT LOADING EFFECT - BACKSTRIPPING

Wells CAI, ALT, PER and QUI were backstripped using the computer package for Backstripping and Subsidence from Waltham (2001, Royal Holloway). The program corrects a file of stratigraphic horizons for the effects of compaction assuming Airy sediment loading.

Compaction is defined by digitizing data from the porosity-depth relationship observed within the well being backstripped. It is assumed that the porosity-depth equation is valid throughout the geological sequence and also through geological time. Sediments are decompacted by moving them vertically up the exponential porosity curve. This is calculated by removing the appropriate amount of sediments off the bottom of the porosity curve until the mass of sediments removed from the top of the well equals the mass of sediments removed from the bottom of the well.

Porosity estimates for the wells being backstripped were obtained from porosity logs of wells CAI and QUI. Surface porosity is of the order of 36% to 38 % and average porosity values of 20% (Quiriquire Formation), 18-20% (Oficina Formation) and 15-20% (Merecure Formation) have been referred in Gonzalez de Juana et al. (1980).

The program uses Vail et al. (1977) values for eustatic sea level correction and the relative sea level values (relative depositional water-depth values similar to Vail's values but more rounded in a gentle curve) for paleobathymetric corrections. Estimates of paleobathymetry in the area of study were approximately given by lithology, geologic history and paleontology (Gonzalez de Juana et al. (op.cit.)).

Input data consist of:

- 1) Age in Ma. before Present time, for the base of each unit.
- 2) The corresponding depth at the base of each unit (m).

- 3) The porosity of each unit at the time of deposition, i.e.: before compaction.
- 4) The corresponding “c” factor .

As a reference, values of porosity and “c” can be obtained from Sclater and Christie (1980), who give:

LITHOLOGY	INITIAL POROSITY	“c” (m ⁻¹)
Shale	0.63	0.00051
Sand	0.49	0.00027
Chalk	0.70	0.00071
Shaley sand	0.56	0.00039

Output is the depth, porosity, age and depth to basement with and without the backstripped sediments. The output of the program for wells PER, QUI, CA1 and ALT is shown in Table A.1. and graphic outputs exhibiting the calculated subsidence curves are illustrated in Figures 3.7A-B and 3.8A-B in Chapter 3. There the subsidence curves correspond respectively to: Total subsidence (cumulative depth to basement, shown in yellow line) and the tectonic subsidence after backstripping (without sea level and palaeobathymetric corrections, shown in green line).

TABLE A.1.

INPUT AND OUTPUT DATA FOR BACKSTRIPPING WELLS QUI, ALT, PER AND CA1.

Well : QUI

Level	Input Data				Output Data	
	Thickness	Age (Ma)	Porosity	C	Total Subsidence	Tectonic Subsidence
1	0	0	0,00	0,00000	3575,00	1131,33
2	0	2	0,45	0,0003	3575,00	1131,33
3	534	5	0,35	0,0003	3147,81	996,14
4	775	8	0,34	0,0003	2944,24	931,72
5	1145	10	0,32	0,0003	2622,25	829,83
6	1425	18	0,30	0,0004	2362,26	747,55
7	1995	25	0,32	0,0004	1815,11	574,40
8	2025	37	0,32	0,0004	1784,97	564,86
9	2205	44	0,31	0,0004	1602,17	507,02
10	2425	68	0,31	0,00052	1366,81	432,53
11	2625	74	0,28	0,00052	1145,28	362,43
12	2965	78	0,30	0,00052	765,79	242,34
13	3575	100	0,30	0,00052	0,00	0,00

Well : ALT

Level	Input Data				Output Data	
	Thickness	Age (Ma)	Porosity	C	Total Subsidence	Tectonic Subsidence
1	0	0	0,00	0,00000	832,00	263,29
2	0	12	0,35	0,0003	832,00	263,29
3	223	12,5	0,33	0,0003	610,22	193,11
4	247	25	0,33	0,0003	586,11	185,48
5	347	33	0,30	0,0003	486,04	153,81
6	488	36	0,28	0,0003	345,18	109,23
7	610	86	0,20	0,0002	222,88	70,53
8	832	100	0,15	0,0002	0,00	0,00

Well : PER

Level	Input Data				Output Data	
	Thickness	Age (Ma)	Porosity	C	Total Subsidence	Tectonic Subsidence
1	0	0	0,00	0,00000	1204,00	381,01
2	0	5	0,35	0,0003	1204,00	381,01
3	152	11	0,30	0,0003	1061,39	335,88
4	335	16	0,28	0,0003	884,45	279,89
5	411	17	0,30	0,0003	808,92	255,99
6	507	23	0,30	0,0003	711,82	225,26
7	564	25	0,30	0,0003	653,25	206,73
8	628	35	0,27	0,0003	587,25	185,84
9	853	86	0,20	0,0002	359,03	113,62
10	1204	100	0,15	0,0002	0,00	0,00

Well : CA1

Level	Input Data				Output Data	
	Thickness	Age (Ma)	Porosity	C	Total Subsidence	Tectonic Subsidence
1	0	0	0	0,00000	960,00	303,80
2	0	1	0,4	0,0003	960,00	303,80
3	183	3	0,37	0,0003	778,22	246,27
4	229	9	0,33	0,0003	732,11	231,68
5	305	11	0,3	0,0003	656,07	207,62
6	430	12	0,29	0,0003	530,89	168,00
7	543	13	0,24	0,0003	418,22	132,35
8	768	16	0,33	0,0003	193,18	61,13
9	960	90	0,2	0,0002	0,00	0,00

APPENDIX B

FINITE ELEMENT METHOD FOR FLEXURE

B. FINITE ELEMENTS METHOD (FEM) FOR FLEXURE

Finite Element Method (FEM) is a methodology applied to solve differential equations starting from the simplification of the initial problem to a mesh of small elements whose behaviour is well known. The extreme points of each element, where the nodal loads are applied, are called nodes. The nodal loads are usually a generalization of the real forces applied to the body, and boundary conditions are also generalized to the nodes. Finally, the stress, strain and displacement are computed from matrix relations between the mechanical properties of the entire body, the loads and the boundary conditions (Chandrupatla and Belegundu, 2000). The final solution and the complexity of the calculation will depend on the geometry of the element used to represent the body. For the lithospheric flexure we used triangular elements since they are simple and reliable for 2D applications.

In this case, we have discretized the “plate” into 12,500 triangles. The rigidity of each one of these elements relates to its thickness (t_e), its area (A_e), its flexural rigidity (D) and B , a matrix associated to the geometrical and mechanical properties of a constant unitary strain triangle:

$$K_e = [t_e A_e B^T D B]$$

$$D = \frac{E}{1-\nu^2} \begin{bmatrix} 1 & \nu & 0 \\ \nu & 0 & 1 \\ 0 & 0 & \frac{(1-\nu)}{2} \end{bmatrix}$$

$$B = \frac{1}{\det J} \begin{bmatrix} y_{23} & 0 & y_{31} & 0 & y_{12} & 0 \\ 0 & x_{32} & 0 & x_{13} & 0 & x_{21} \\ x_{32} & y_{23} & x_{13} & y_{31} & x_{21} & y_{12} \end{bmatrix}$$

$$\det J = 2A$$

Once the rigidity matrix of each element is computed, the general rigidity matrix of the entire plate is assembled (K). This matrix will uniquely depend on the way we have created the FEM mesh and the way the triangles are connected to

each other (Chandrupatla and Belegundu, 2000). The boundary conditions for a semi-infinite broken plate are set as a loose end and a fix one; all the nodes on the fix side get an extremely high rigidity. The displacement vector of all the nodes (Q) relates to K and to the nodal loads as:

$$KQ = F$$

Using the superposition theorem we will apply now the conditions of the sedimentary load (q), and the mantle restoration force as a Winkler foundation (p) from the displacement vector Q (Watts, 2001).

$$p = g\rho_{mantle}y$$
$$q = g\rho_{sed}y$$

The final flexure of the plate is computed as a superposition of the deformation due to these loads and the previous ones, using the algorithm developed by Arnaiz-Rodriguez (2011).

The methodology used to investigate the flexure in the study area through the finite element computer package FEMFLEX (Arnaiz-Rodriguez, 2011) is illustrated in Figure B.1.

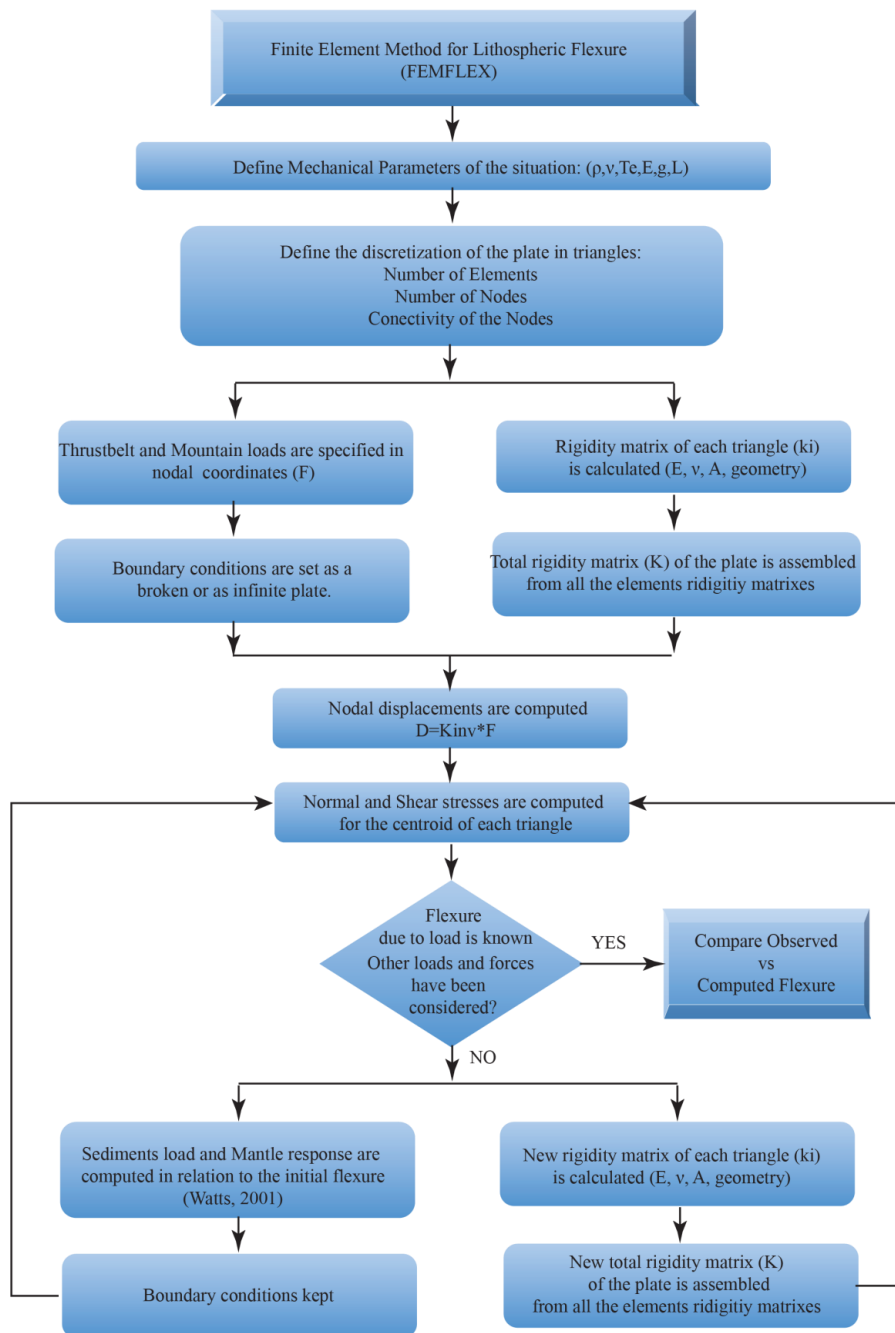


Figure B.1. Diagram to illustrate the flexural modelling applying Finite Elements Method – FEMFLEX (From Arnaiz-Rodriguez, 2011).

A simple elastic finite element model of a 25 km thick uniform upper crust above an inviscid substratum has been used to study the flexure of the South American continental plate, having a free edge at its northern boundary in the zone of interaction with the Caribbean plate. These are the same basic calculations used before, in section 5.3, except that the load is not gravitational. The deformation profiles for the upper plate, for different combinations of loads and stresses, are shown as follows:

(1) Combined effect of surface (topography) and subsurface (thrust belt) loads (L). The maximum deflection of the elastic plate ($T_e=25$ km) is about 8 km. Similar results obtained from flexural analysis are shown in Figure 5.6.

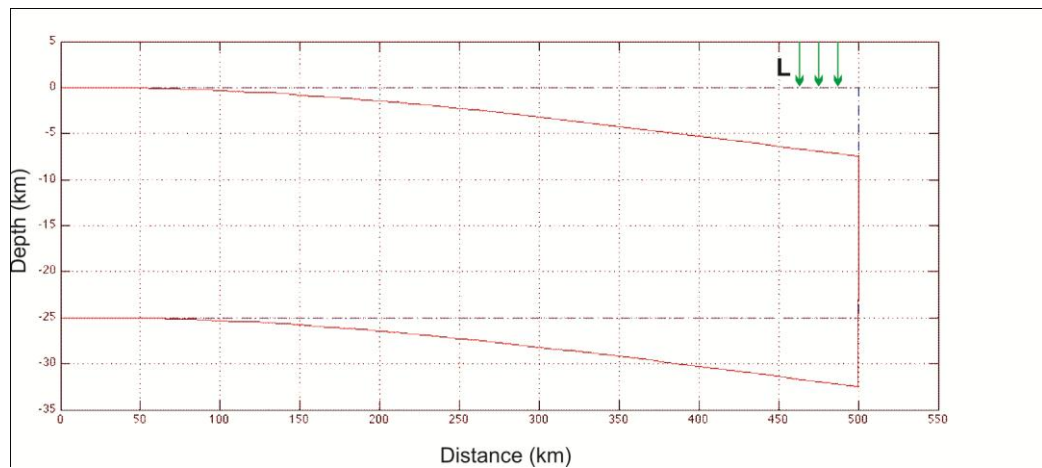


Figure B.1.1. Flexure of the South American plate in response to the surface (topography) plus subsurface (foreland thrust belt) loads.

(2) Flexural response of the South American plate to a vertical force (F_P), acting downwards. To produce the deflection of the plate up to about 12 km in depth, the magnitude of the force needed is 0.505 (0.4-0.5 times) the load (always topography + thrust) distributed along the surface, the last 50 km of the plate. This force is enough to flex the plate and fits also the first node.

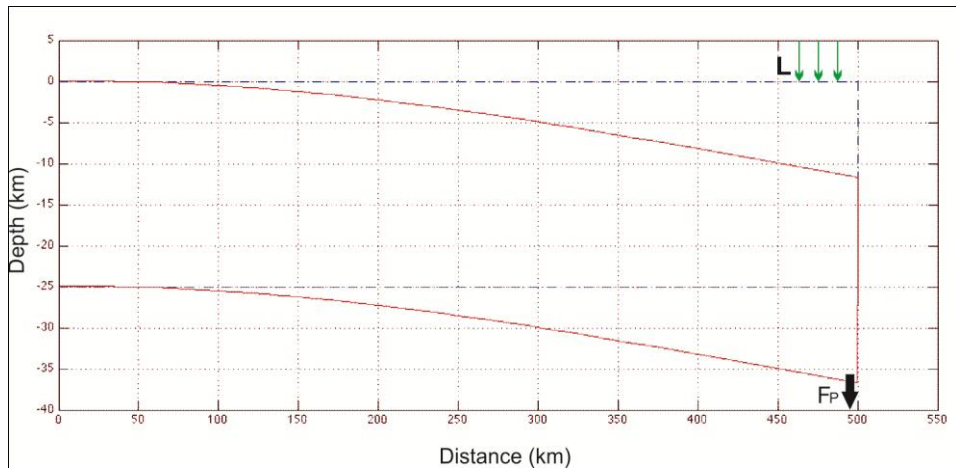


Figure B.1.2. Flexural response of the South American plate to the combined effect of surface and subsurface loads, plus a vertical force F_P acting downwards.

(3) Flexural response of the South American plate to the gravitational loads (topography plus thrust belt) plus a horizontal force ($F_H=0.1$ times the same load) applied at the top of the plate. The effect on the deflection of the South American plate is minimum (in fact, it reduces 100m the deflection).

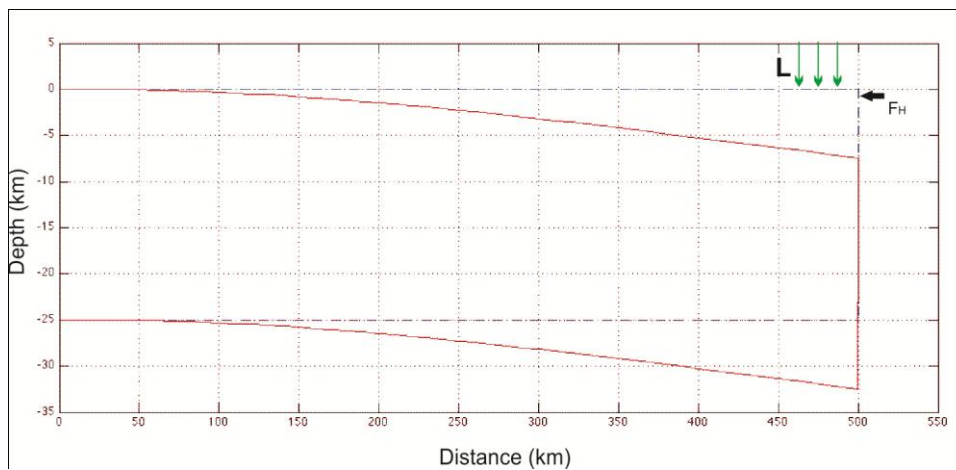


Figure B.1.3. Flexural response of the South American plate to the combined effect of surface and subsurface loads, plus a horizontal force F_H acting at the top of the plate.

(4) Flexural response of the South American plate to the surface and subsurface loads plus two horizontal forces (magnitude equal to 0.5 the load of the topography + thrust, plus an additional vertical force (0.1 the same load) applied on the top of the plate. The two horizontal forces at this stage are equal

in magnitude but opposite sense, acting as a couple. The deflection is slightly bigger but not too much because the assumed vertical force F_V is very small.

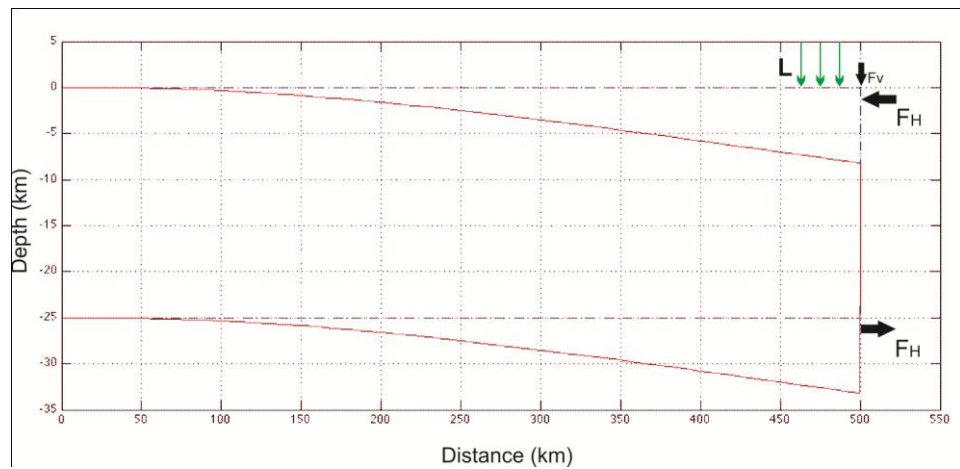


Figure B.1.4. Flexural response of the South American plate to the combined effect of surface and subsurface loads, a small vertical force F_V plus two horizontal forces F_H acting as a couple at the top and bottom of the plate.

(5) Flexural response of the South American plate to the gravitational loads (topography plus thrust belt) plus a couple of horizontal forces (pushing the South American plate leftwards at the top and pulling the plate rightwards at the bottom) simulating a reverse fault. The magnitude of both forces is 0.5 the load (topography + thrust). Additionally we include a vertical force F_V of 0.5 times the load (which would be difficult to justify according to the geology of the area). The combined effect of all these loads and forces let the deflection reach about 12 km.

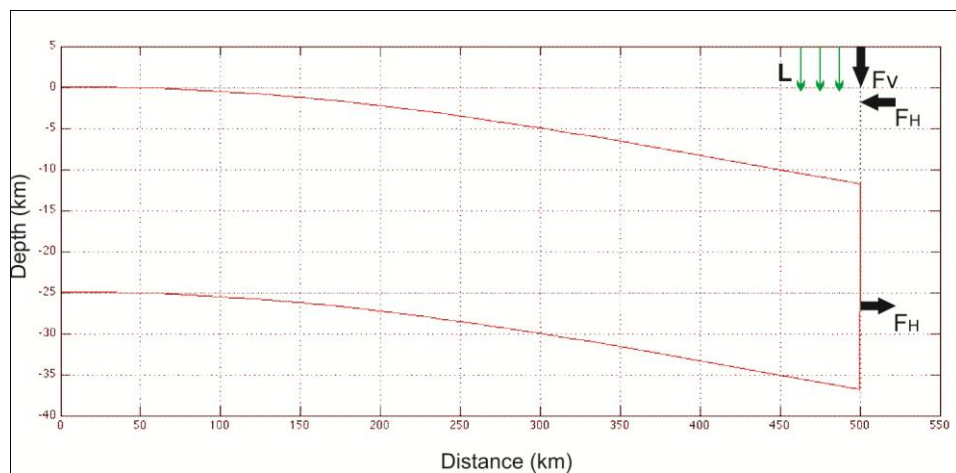


Figure B.1.5. Flexural response of the South American plate to the combined effect of surface and subsurface loads, a vertical force $F_V = 0.5L$ plus a couple of horizontal forces F_H acting at the top and bottom of the plate.

(6) Flexural response of the South American plate to the gravitational loads (topography plus thrust belt) combined with the couple of forces F_H characteristic of the reverse fault, a vertical force F_V of 0.1 the topography (probably related to the thrusting of the nappes during their emplacement) plus a downwards force F_P of the order of 0.4-0.45 times the load of the topography + thrust. This combination of loads and forces produces the deflection of the South American plate up to 12 km deep and it's a good fit to the first node of flexure.

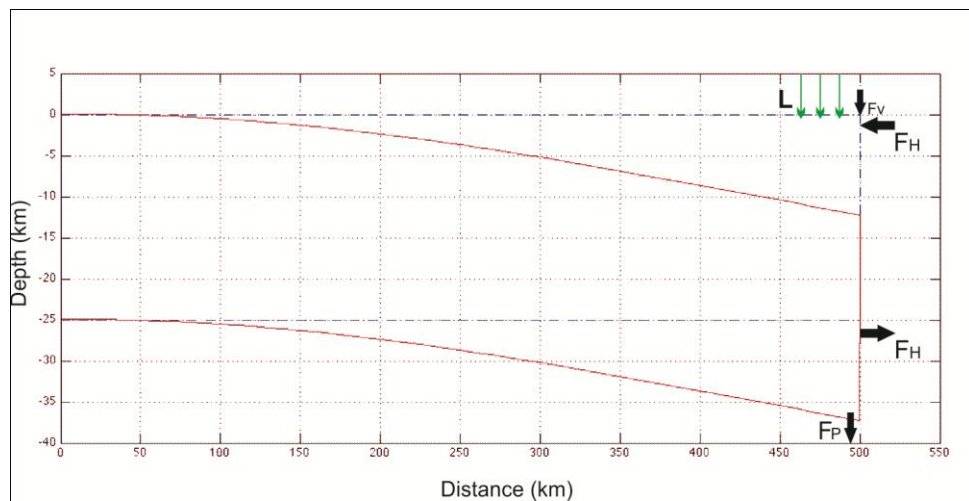


Figure B.1.6. Flexural response of the South American plate to the combined effect of surface and subsurface loads, plus a couple of horizontal forces F_H acting at the top and bottom of the plate, a vertical force F_V acting at the top and a vertical force F_P acting downwards.

On comparing the results which have been found through the Finite Element Method in eastern Venezuela, it is important to point out that:

(1) The load of the topography plus thrust belt (Eastern Serrania del Interior) is important but not enough to flex the South American plate up to 12 km. Similar results were obtained from the flexural analysis illustrated in Fig. 5.5 and 5.6. where the deflection of the plate reaches about 8 km at the broken end.

(2) The major impact in flexing the plate is achieved by applying a vertical force ($F_P \sim 0.5L$) acting downwards at the broken end of the plate. The combination of the load L plus the vertical force pulling the plate downwards is able to produce a deflection of the order of 12 km, which represents the

thickness of sediments infilling the basin (see Figure 3.6). To produce a similar deflection of the South America continental plate, following the Karner and Watts (1983) approach, an intracrustal load whose magnitude is of the order of a third of the surface plus subsurface loads was computed through an iterative process.

(3) A couple of horizontal forces (pushing the South American plate southwards at the top and pulling the plate northwards at the bottom) is used to simulate compressional faulting at the broken edge of the plate.

The strain release mechanism provides a simpler method to explain the flexure of the Eastern Venezuela basin, which could be attributed to the combined effect of supracrustal loading (surface and subsurface loads (L)) acting upon the South American continental crust, plus a vertical force ($F_P = 0.5L$) acting downwards and a couple of horizontal forces ($F_H = 0.5L$) simulating a reverse fault.

APPENDIX C

GRAVITY DATA CATALOGUE
EASTERN VENEZUELAN BASIN

GRAVITY DATA CATALOGUE - EASTERN VENEZUELA BASIN

STN-N°	STN-REF	LONG (deg)	LAT (deg)	HEIGHT (m)	FAA (mGal)	BA (mGal)	AIRY 35 (mGal)	PRATT 100 (mGal)
1	1	-60,92	8,92	2,00	8,81	8,64	8,66	8,66
2	10	-61,43	8,48	3,00	16,00	15,80	15,90	15,50
3	11	-61,25	8,50	1,00	16,81	16,80	16,87	16,60
4	12	-61,50	8,50	3,00	16,00	15,82	15,92	15,54
5	13	-61,13	8,60	1,00	15,75	15,67	15,70	15,61
6	14	-61,25	8,60	2,00	13,81	13,64	13,68	13,57
7	15	-61,65	8,62	4,00	5,00	4,66	4,71	4,53
8	16	-61,71	8,62	6,00	-8,06	-8,58	-8,53	-8,73
9	17	-61,45	8,63	2,00	13,88	13,70	13,73	13,63
10	18	-61,53	8,75	4,00	-7,94	-8,27	-8,24	-8,31
11	19	-61,63	8,75	4,00	-13,94	-14,26	-14,23	-14,31
12	20	-61,18	8,77	1,00	5,69	5,61	5,63	5,61
13	21	-61,37	8,82	5,00	-7,88	-8,32	-8,30	-8,33
14	22	-61,23	8,87	2,00	-2,13	-2,29	1,17	2,60
15	23	-61,93	8,88	9,80	-19,56	-20,42	-20,37	-20,48
16	24	-61,15	8,90	2,00	-6,19	-6,36	-6,34	-6,35
17	25	-61,35	8,92	4,00	-19,00	-19,34	-19,31	-19,35
18	26	-61,51	8,92	6,60	-28,00	-28,56	-28,53	-28,59
19	27	-62,00	8,93	10,30	-23,75	-24,66	-24,62	-24,72
20	28	61,42	8,97	3,90	-29,88	-30,21	-30,18	-30,23
21	29	-61,10	8,98	2,00	-16,19	-16,35	-16,33	-16,34
22	30	-61,86	9,00	8,40	-39,19	-39,92	-39,88	-39,97
23	115	-62,93	8,02	115,20	4,75	-8,11	-7,65	-8,73
24	116	-62,78	8,07	92,70	4,88	-3,83	-3,32	-4,67
25	117	-62,82	8,12	117,00	7,38	-5,32	-4,98	-6,13
26	118	-62,46	8,13	386,40	32,63	-9,76	-9,10	-11,13
27	119	-62,65	8,16	100,40	12,88	1,75	2,21	0,94
28	120	-62,73	8,25	153,60	18,19	1,87	2,11	0,78
29	121	-62,90	8,29	93,30	11,31	1,24	1,41	0,48
30	122	-62,76	8,34	111,40	14,00	2,10	2,25	1,27
31	123	-62,55	8,34	104,30	3,00	-8,42	-8,19	-9,30
32	124	-62,71	8,35	0,00	-27,63	-27,18	-27,00	-27,90
33	125	-62,92	8,36	35,70	2,75	-0,33	-0,17	-0,90
34	126	-62,64	8,37	121,10	13,56	0,66	0,84	-0,24
35	127	-62,99	8,41	40,60	-1,38	-4,89	-4,74	-5,51
36	128	-62,31	8,43	32,50	-0,81	-3,64	-3,51	-4,17
37	129	-62,68	8,44	43,70	5,69	2,02	2,17	1,42
38	130	-62,85	8,51	88,90	12,00	3,65	3,80	3,01
39	131	-62,73	8,53	77,40	1,25	-6,01	-5,86	-6,67
40	132	-62,60	8,56	78,20	2,00	-5,11	-4,96	-5,73
41	133	-62,91	8,57	89,00	-3,13	-11,69	-11,51	-12,30
42	134	-62,79	8,65	72,80	-12,00	-18,94	-18,77	-19,59
43	135	-62,64	8,66	71,40	-9,88	-16,72	-16,57	-17,20
44	136	-62,98	8,68	89,50	-18,94	-27,51	-27,31	-28,34
45	137	-62,88	8,69	84,20	-13,94	-22,04	-21,85	-22,80
46	138	-62,19	8,70	12,40	-7,63	-8,65	-8,58	-8,83
47	139	-62,44	8,72	21,30	-14,81	-16,87	-16,78	-17,18
48	140	-62,11	8,72	11,90	-12,06	-13,07	-13,02	-13,20
49	141	-62,59	8,75	51,00	-16,19	-21,06	-20,92	-21,50
50	142	-62,91	8,78	80,30	-17,56	-25,30	-25,09	-26,02
51	143	-62,85	8,81	62,30	-21,81	-27,73	-27,53	-28,38
52	144	-62,94	8,81	87,20	-22,31	-30,64	-30,42	-31,37

STN-N°	STN-REF	LONG	LAT	HEIGHT	FAA	BA	AIRY 35	PRATT 100
		(deg)	(deg)	(m)	(mGal)	(mGal)	(mGal)	(mGal)
53	145	-62,07	8,85	11,00	-16,63	-17,58	-17,53	-17,65
54	146	-62,62	8,85	48,60	-18,75	-23,36	-23,20	-23,80
55	147	-62,52	8,86	37,10	-17,25	-20,74	-20,05	-20,67
56	148	-62,92	8,91	61,60	-31,94	-37,73	-37,53	-38,42
57	149	-62,69	8,92	40,30	-32,44	-36,27	-36,12	-36,73
58	150	-62,52	8,94	23,50	-29,19	-31,32	-31,21	-31,64
59	151	-62,78	8,94	45,50	-37,69	-42,02	-41,85	-42,56
60	152	-62,85	8,98	60,60	-52,25	-57,97	-57,79	-58,57
61	153	-62,06	8,98	9,60	-27,44	-28,25	-28,21	-28,34
62	188	-63,24	8,03	140,80	13,25	-2,01	-1,54	-2,76
63	189	-63,14	8,11	272,70	32,56	3,77	4,09	2,55
64	190	-63,21	8,13	43,80	15,44	11,28	11,61	10,32
65	191	-63,00	8,15	149,60	8,94	-6,80	-6,50	-7,83
66	192	-63,52	8,15	0,00	1,81	2,55	2,84	1,64
67	193	-63,98	8,17	167,20	15,69	0,55	0,76	-0,48
68	194	-63,05	8,28	138,80	9,25	-2,48	-2,29	-3,31
69	195	-63,39	8,32	84,20	3,13	-4,02	-3,82	-4,92
70	196	-63,69	8,40	132,90	-14,38	-27,04	-26,80	-28,03
71	197	-63,07	8,41	160,10	12,06	-0,90	-0,72	-1,98
72	198	-63,82	8,43	77,40	-24,88	-32,09	-31,85	-33,24
73	199	-63,24	8,54	90,80	-13,56	-22,19	-21,98	-23,02
74	200	-63,10	8,57	202,60	7,13	-11,14	-10,94	-12,35
75	201	-63,46	8,57	120,70	-13,13	-24,75	-24,48	-25,83
76	202	-63,57	8,62	155,00	-10,31	-25,14	-24,82	-26,43
77	203	-63,36	8,62	116,50	-5,31	-16,52	-16,25	-17,51
78	204	-63,03	8,66	94,20	-18,69	-27,72	-27,51	-28,57
79	205	-63,12	8,71	82,70	-15,25	-23,19	-22,96	-24,03
80	206	-63,05	8,73	81,30	-18,75	-26,55	-26,32	-27,43
81	207	-63,68	8,78	181,20	-29,25	-46,65	-46,25	-48,38
82	208	-63,91	8,83	203,80	-28,63	-47,73	-47,22	-50,06
83	209	-63,10	8,84	88,60	-24,56	-33,08	-32,81	-34,02
84	210	-63,66	8,84	173,00	-29,81	-46,41	-45,98	-47,98
85	211	-63,54	8,85	165,00	-28,75	-44,48	-44,08	-45,85
86	212	-63,02	8,89	87,90	-31,25	-39,69	-39,45	-40,41
87	213	-63,73	8,94	198,80	-37,19	-56,14	-55,63	-58,11
88	214	-63,14	8,96	103,50	-45,00	-54,83	-54,58	-55,68
89	215	-63,37	8,96	94,40	-43,69	-52,67	-52,37	-53,80
90	216	-63,95	8,97	211,00	-35,75	-55,65	-55,05	-58,14
91	217	-63,66	8,99	152,90	-45,69	-60,07	-59,60	-61,77
92	407	-64,99	8,00	112,90	14,94	5,38	5,57	4,84
93	408	-64,87	8,01	125,20	14,06	3,55	3,74	2,98
94	409	-64,55	8,04	115,10	0,06	-10,52	-10,30	-11,04
95	410	-64,73	8,05	132,90	2,75	-8,36	-8,15	-8,96
96	411	-64,66	8,05	133,70	-3,69	-14,84	-14,62	-15,44
97	413	-64,06	8,12	146,30	20,94	7,70	7,91	6,85
98	412	-64,47	8,07	114,30	0,75	-8,84	-8,64	-9,74
99	414	-64,75	8,13	157,50	9,69	-3,53	-3,29	-4,51
100	415	-64,82	8,15	146,10	12,56	-0,02	0,25	-0,99
101	416	-64,98	8,17	167,20	15,69	1,25	1,51	0,19
102	417	-64,67	8,18	152,60	5,94	-8,18	-7,94	-9,23
103	418	64,75	8,21	165,80	12,31	-2,95	-2,67	-4,21
104	419	64,96	8,26	172,50	17,06	1,91	2,22	0,77
105	420	-64,86	8,27	139,60	12,81	0,65	0,97	-0,66
106	421	-64,69	8,29	149,20	11,69	-2,14	-1,87	-3,60
107	422	-64,86	8,34	139,50	11,88	-1,45	-1,10	-2,84

STN-N°	STN-REF	LONG	LAT	HEIGHT	FAA	BA	AIRY 35	PRATT 100
		(deg)	(deg)	(m)	(mGal)	(mGal)	(mGal)	(mGal)
108	423	-64,97	8,37	162,00	17,88	2,69	3,04	1,17
109	424	-64,64	8,39	199,50	17,06	-1,39	-1,07	-2,95
110	425	-64,74	8,45	138,40	9,25	-3,95	-3,55	-5,54
111	426	-64,86	8,46	222,00	18,13	-2,91	-2,50	-4,58
112	427	-64,94	8,46	175,60	16,00	-0,65	-0,26	-2,20
113	428	-64,62	8,46	163,20	9,44	-5,88	-5,52	-7,39
114	429	-64,08	8,52	185,70	-7,69	-25,36	-25,02	-26,95
115	430	-64,65	8,53	161,90	5,38	-9,28	-8,87	-11,34
116	431	-64,27	8,53	226,60	2,91	-18,40	-18,02	-20,14
117	432	-64,77	8,55	172,10	8,13	-8,26	-7,80	-10,22
118	433	-64,85	8,56	206,30	10,13	-9,27	-8,81	-11,18
119	434	-64,55	8,56	158,30	1,31	-13,86	-13,47	-15,48
120	435	-64,93	8,57	203,50	10,63	-8,47	-8,02	-10,33
121	436	-64,30	8,60	174,00	-0,56	-16,51	-16,09	-18,48
122	437	-64,92	8,61	218,10	8,38	-12,29	-11,83	-14,12
123	438	-64,78	8,61	173,50	3,25	-13,33	-12,84	-15,38
124	439	-64,64	8,63	183,10	-0,19	-17,75	-17,27	-19,67
125	440	-64,54	8,64	199,50	-4,06	-22,85	-22,38	-24,85
126	441	-64,14	8,69	202,50	-10,69	-29,96	-29,47	-31,98
127	442	-64,19	8,70	167,40	-10,50	-26,60	-26,07	-28,75
128	443	-64,74	8,72	241,70	-3,06	-26,21	-25,67	-28,33
129	444	-64,97	8,73	150,00	-0,13	-14,46	-13,99	-16,29
130	445	-64,02	8,74	233,10	-15,38	-37,65	-37,15	-39,59
131	446	-64,85	8,75	195,10	-4,00	-22,20	-21,68	-24,09
132	447	-64,17	8,76	222,90	-12,94	-33,94	-33,38	-36,35
133	448	-64,54	8,76	214,90	-10,31	-30,58	-30,03	-32,90
134	449	-64,45	8,76	280,60	-4,31	-31,06	-30,51	-33,27
135	450	-64,36	8,78	274,20	-5,00	-31,27	-30,69	-33,76
136	451	-64,36	8,81	295,30	-5,06	-33,30	-32,69	-35,64
137	452	-64,21	8,82	254,10	-11,31	-35,76	-35,16	-38,08
138	453	-64,02	8,83	230,10	-22,00	-43,90	-43,35	-46,21
139	454	-64,33	8,83	205,90	-6,69	-25,98	-25,44	-28,26
140	455	-64,55	8,84	246,60	-18,31	-42,04	-41,42	-44,46
141	456	-64,18	8,84	256,40	-15,63	-40,27	-39,63	-42,64
142	457	-64,27	8,84	267,20	-13,56	-39,24	-38,59	-41,66
143	458	-64,45	8,84	311,50	-13,00	-42,62	-41,98	-45,15
144	459	-64,91	8,85	166,80	-3,06	-19,10	-18,63	-20,82
145	460	-64,68	8,85	238,80	-14,94	-37,78	-37,16	-40,08
146	461	-64,74	8,87	205,50	-14,44	-33,70	-32,86	-35,67
147	462	-64,67	8,91	253,90	-15,88	-40,34	-39,73	-42,54
148	463	-64,27	8,93	283,00	-19,06	-46,25	-45,55	-48,93
149	464	-64,86	8,93	144,10	-10,19	-23,73	-23,23	-25,67
150	465	-64,99	8,94	140,30	-9,13	-22,54	-22,12	-24,06
151	466	-64,56	8,94	308,00	-21,56	-50,72	-50,05	-53,32
152	467	-64,37	8,94	321,50	-22,69	-53,33	-52,64	-56,08
153	468	-64,76	8,96	45,20	-35,13	-37,70	-37,13	-39,54
154	470	-64,14	8,97	270,00	-28,81	-54,78	-54,12	-57,32
155	469	-64,46	8,96	298,40	-27,19	-55,93	-55,24	-58,47
156	612	-65,62	8,02	52,00	32,31	27,93	28,07	27,51
157	613	-65,15	8,03	110,60	18,25	7,77	7,95	7,24
158	614	-65,52	8,03	81,60	27,63	20,96	21,10	20,56
159	615	-65,31	8,08	134,40	17,88	6,82	7,03	5,93
160	616	-65,65	8,10	63,00	23,31	17,94	18,11	17,44
161	617	-65,87	8,12	74,90	17,69	11,21	11,39	10,63
162	618	-65,06	8,12	146,30	20,94	7,36	7,60	6,43

STN-N°	STN-REF	LONG	LAT	HEIGHT	FAA	BA	AIRY 35	PRATT 100
		(deg)	(deg)	(m)	(mGal)	(mGal)	(mGal)	(mGal)
163	619	-65,42	8,15	42,80	19,06	15,08	15,24	14,45
164	620	-65,52	8,15	95,00	19,19	11,11	11,28	10,44
165	621	-65,22	8,20	113,00	17,69	7,28	7,48	6,38
166	622	-65,72	8,21	69,10	21,56	15,71	15,91	14,85
167	623	-65,62	8,23	110,00	16,50	6,93	7,14	6,05
168	624	-65,22	8,24	116,30	16,69	5,89	6,11	4,92
169	625	-65,13	8,25	78,80	17,94	10,47	10,72	9,41
170	626	-65,50	8,26	121,60	19,19	8,84	9,07	7,90
171	627	-65,05	8,26	108,10	16,06	5,77	6,05	4,69
172	628	-65,52	8,27	110,00	14,50	5,04	5,24	4,15
173	629	-65,13	8,32	105,30	15,88	5,89	6,15	4,70
174	630	-65,48	8,32	105,70	17,56	7,43	7,65	6,48
175	631	-65,94	8,33	101,50	37,31	28,92	29,22	27,85
176	632	-65,07	8,34	163,30	18,25	3,22	3,53	1,79
177	633	-65,62	8,37	130,00	24,19	13,20	13,46	11,93
178	634	-65,53	8,37	170,00	24,88	9,27	9,52	7,91
179	635	-65,48	8,41	97,40	19,00	9,64	9,89	8,51
180	636	-65,36	8,42	161,60	14,75	0,63	1,00	-0,56
181	637	-65,14	8,42	98,40	11,44	1,97	2,27	0,78
182	638	-65,04	8,44	150,50	17,06	2,68	3,02	1,34
183	639	-65,99	8,47	133,40	2,94	-8,39	-8,01	-9,56
184	640	-65,55	8,48	175,00	31,25	14,92	15,22	13,38
185	641	-65,63	8,48	180,00	35,63	19,16	19,50	17,35
186	642	-65,13	8,53	101,40	11,44	1,81	2,14	0,43
187	643	-65,05	8,54	135,90	13,56	0,52	0,89	-0,90
188	644	-65,96	8,57	197,90	1,56	-17,31	-16,88	-18,49
189	645	-65,47	8,57	181,90	34,31	17,36	17,68	15,69
190	646	-65,75	8,53	84,20	9,38	3,09	3,53	0,76
191	647	-65,56	8,58	123,00	31,13	19,80	20,18	18,15
192	648	-66,00	8,62	163,40	5,31	-8,88	-8,44	-10,06
193	649	-65,37	8,63	160,00	21,88	6,51	6,85	5,23
194	650	-65,57	8,63	185,00	15,06	-2,60	-2,18	-4,24
195	651	-65,02	8,63	135,30	6,63	-6,41	-6,00	-8,06
196	652	-65,08	8,76	119,80	8,00	-3,38	-2,97	-4,94
197	653	-65,20	8,80	143,50	2,00	-11,73	-11,34	-12,87
198	654	-65,15	8,80	144,30	1,88	-11,82	-11,45	-13,07
199	655	-65,32	8,82	125,60	6,31	-5,57	-5,21	-6,98
200	656	-65,02	8,84	151,30	3,19	-11,27	-10,82	-12,76
201	657	-65,98	8,86	169,20	6,50	-9,80	-9,32	-10,99
202	658	-65,13	8,95	108,80	-10,00	-20,14	-19,79	-21,52
203	659	-65,09	8,96	129,80	-9,56	-22,01	-21,62	-23,20
204	660	-65,96	8,99	182,30	31,88	14,38	14,81	13,33
205	2	-60,88	9,08	1,00	-24,25	-24,34	-24,32	-24,31
206	3	-60,98	9,08	1,00	-34,25	-34,34	-34,31	-34,29
207	4	-60,95	9,30	1,30	-36,31	-36,42	-36,40	-36,39
208	5	-60,97	9,31	0,70	-38,81	-38,87	-38,84	-38,84
209	6	-60,96	9,47	0,50	-38,19	-38,23	-38,21	-38,18
210	31	-61,36	9,03	1,30	-29,94	-30,02	-30,00	-30,03
211	32	-61,46	9,04	1,10	-35,94	-35,99	-35,96	-36,01
212	33	-61,55	9,04	1,00	-35,44	-35,49	-35,46	-35,52
213	34	-61,25	9,05	2,00	-13,19	-13,35	-13,33	-13,34
214	35	-61,25	9,13	1,10	-23,63	-23,72	-23,61	-23,59
215	36	-61,17	9,13	1,00	-24,88	-24,95	-24,93	-24,94
216	37	-61,83	9,13	6,00	-42,81	-43,33	-43,29	-43,38
217	38	-61,37	9,15	1,10	-41,31	-41,40	-41,38	-41,40

STN-Nº	STN-REF	LONG	LAT	HEIGHT	FAA	BA	AIRY 35	PRATT 100
		(deg)	(deg)	(m)	(mGal)	(mGal)	(mGal)	(mGal)
218	39	-61,41	9,15	1,50	-44,19	-44,31	-44,12	-44,45
219	40	-61,59	9,17	0,10	-58,44	-58,42	-58,39	-58,44
220	41	-61,08	9,18	2,10	-33,81	-33,99	-33,97	-33,97
221	42	-61,59	9,21	0,30	-51,75	-51,77	-51,75	-51,78
222	43	-61,35	9,22	1,50	-44,44	-44,56	-44,54	-44,55
223	44	-61,80	9,24	6,40	-67,94	-68,50	-68,47	-68,52
224	45	-61,85	9,25	8,00	-58,63	-59,31	-59,28	-59,34
225	46	-61,61	9,26	0,10	-67,88	-67,86	-67,84	-67,87
226	47	-61,25	9,27	0,20	-56,25	-56,25	-56,23	-56,24
227	48	-61,46	9,27	1,50	-54,25	-54,37	-54,35	-54,37
228	49	-61,18	9,30	1,00	-47,38	-47,45	-47,43	-47,43
229	50	-61,17	9,34	1,00	-50,25	-50,34	-50,32	-50,32
230	51	-61,39	9,34	1,50	-129,11	-61,37	-61,35	-61,36
231	52	-61,09	9,35	0,50	-46,81	-46,85	-46,83	-46,83
232	53	-61,62	9,35	0,10	-82,06	-82,05	-82,02	-82,05
233	54	-61,44	9,36	1,50	-64,00	-64,12	-64,09	-64,11
234	55	-61,29	9,38	1,00	-59,00	-59,08	-59,04	-59,03
235	56	-61,88	9,38	9,00	-90,56	-91,34	-91,31	-91,36
236	57	-61,21	9,41	0,50	-56,06	-56,09	-56,07	-56,07
237	58	-61,37	9,42	4,40	-99,75	-100,09	-100,06	-100,11
238	59	-61,63	9,43	4,10	-86,19	-86,53	-86,51	-86,53
239	60	-61,09	9,44	0,20	-48,31	-48,32	-48,30	-48,30
240	61	-61,34	9,45	0,30	-79,31	-79,32	-79,30	-79,31
241	62	-61,17	9,49	0,70	-68,13	-68,10	-68,17	-68,16
242	63	-61,04	9,52	0,50	-46,06	-46,11	-46,09	-46,05
243	64	-61,59	9,56	3,10	-95,69	-95,94	-95,91	-95,92
244	65	-61,16	9,58	0,20	-74,69	-74,70	-74,68	-74,65
245	66	-61,33	9,75	0,50	-136,19	-136,23	-136,20	-136,19
246	67	-61,66	9,88	0,50	-138,75	-138,77	-138,75	-138,69
247	154	-62,57	9,02	24,60	-41,75	-44,06	-43,96	-44,33
248	155	-62,87	9,04	53,00	-46,19	-51,17	-51,01	-51,71
249	156	-62,69	9,05	31,20	-43,69	-46,65	-46,53	-46,96
250	157	-62,05	9,06	9,00	-41,06	-41,85	-41,80	-41,91
251	158	-62,74	9,07	36,90	-50,63	-54,15	-54,01	-54,46
252	159	-62,10	9,10	8,60	-44,88	-45,62	-45,57	-45,68
253	160	-62,88	9,12	37,00	-58,31	-61,79	-61,64	-62,27
254	161	-62,75	9,17	12,80	-68,69	-69,78	-69,67	-70,06
255	162	-62,67	9,17	12,00	-67,31	-68,38	-68,29	-68,60
256	163	-62,92	9,23	35,30	-73,44	-76,81	-76,67	-77,24
257	164	-62,10	9,24	7,20	-69,00	-69,61	-69,57	-69,66
258	165	-62,34	9,28	6,50	-84,00	-84,56	-84,52	-84,60
259	166	-62,81	9,32	13,30	-92,31	-93,54	-93,45	-93,76
260	167	-63,00	9,38	27,40	-101,06	-103,67	-103,47	-103,93
261	168	-62,41	9,43	5,40	-116,00	-116,47	-116,43	-116,49
262	169	-63,00	9,47	33,60	-118,44	-121,53	-121,42	-121,89
263	173	-62,44	9,58	4,40	-136,31	-136,67	-136,63	-136,70
264	171	-62,31	9,73	3,00	-167,81	-168,07	-167,99	-168,00
265	172	-62,07	9,88	0,90	-174,63	-174,69	-174,66	-174,65
266	173	-62,97	9,93	10,00	-161,50	-162,27	-162,18	-162,61
267	174	-62,25	9,97	1,30	-183,44	-183,55	-183,53	-183,48
268	218	-63,33	9,03	120,80	-47,13	-58,54	-58,24	-59,72
269	219	-63,13	9,03	85,70	-44,75	-52,87	-52,62	-53,78
270	220	-63,21	9,03	104,40	-43,56	-53,58	-53,32	-54,49
271	221	-63,33	9,08	183,70	-51,81	-69,32	-68,77	-71,86
272	222	-63,58	9,08	141,60	-52,94	-66,50	-66,10	-68,21

STN-N°	STN-REF	LONG	LAT	HEIGHT	FAA	BA	AIRY 35	PRATT 100
		(deg)	(deg)	(m)	(mGal)	(mGal)	(mGal)	(mGal)
273	223	-63,82	9,09	195,40	-50,31	-68,54	-67,99	-70,98
274	224	-63,14	9,14	83,30	-55,69	-63,70	-63,47	-64,42
275	225	-63,36	9,15	94,70	-59,13	-67,91	-67,61	-69,04
276	226	-63,64	9,15	139,50	-62,38	-75,59	-75,11	-77,49
277	227	-63,84	9,15	245,80	-51,44	-75,08	-74,49	-77,22
278	228	-63,75	9,17	185,10	-61,06	-78,39	-77,84	-80,58
279	229	-63,05	9,20	62,40	-63,56	-69,52	-69,32	-70,09
280	230	-63,13	9,22	63,90	-67,19	-73,17	-72,96	-73,94
281	231	-63,41	9,22	118,20	-67,50	-78,85	-78,53	-79,99
282	232	-63,23	9,23	79,90	-67,81	-75,45	-75,19	-76,36
283	233	-63,04	9,23	57,70	-70,13	-75,66	-75,48	-76,19
284	234	-63,95	9,24	183,70	-70,38	-87,23	-86,58	-89,90
285	235	-63,76	9,26	229,60	-67,75	-89,65	-89,09	-91,71
286	236	-63,83	9,27	247,10	-69,00	-92,79	-92,17	-95,02
287	237	-63,55	9,31	160,60	-80,44	-95,91	-95,48	-97,34
288	238	-63,17	9,32	62,00	-86,75	-92,58	-92,37	-93,32
289	239	-63,96	9,33	232,00	-74,94	-96,88	-96,20	-99,80
290	240	-63,75	9,33	226,70	-78,56	-100,15	-99,52	-102,35
291	241	-63,07	9,35	38,50	-92,69	-96,11	-95,95	-96,71
292	242	-63,83	9,35	175,40	-88,50	-105,20	-104,57	-107,73
293	243	-63,46	9,38	125,00	-93,88	-105,75	-105,37	-107,12
294	244	-63,62	9,38	177,70	-92,75	-109,68	-109,22	-111,62
295	245	-63,27	9,39	85,30	-96,56	-104,72	-104,43	-105,45
296	246	-63,61	9,42	178,30	-100,25	-117,42	-116,95	-119,20
297	247	-63,05	9,42	35,50	-108,25	-111,52	-111,38	-111,99
298	248	-63,28	9,44	90,80	-106,38	-115,06	-114,83	-115,92
299	249	-63,13	9,45	50,90	-111,56	-116,42	-116,24	-116,97
300	250	-63,93	9,47	299,80	-86,25	-115,03	-114,31	-117,88
301	251	-63,46	9,47	131,20	-111,31	-123,95	-123,60	-125,19
302	252	-63,53	9,47	148,10	-111,06	-125,30	-124,87	-126,99
303	253	-63,77	9,47	230,10	-100,06	-121,96	-121,34	-124,55
304	254	-63,34	9,49	99,30	-116,00	-125,56	-125,29	-126,49
305	255	-63,09	9,52	43,60	-126,06	-130,25	-130,11	-130,69
306	256	-63,83	9,54	216,50	-106,44	-126,71	-126,02	-129,44
307	257	-63,22	9,54	65,60	-127,06	-133,34	-133,09	-134,02
308	258	-63,64	9,55	185,50	-125,38	-143,25	-142,72	-145,12
309	259	-63,52	9,55	144,60	-129,31	-143,19	-142,69	-144,60
310	260	-63,35	9,56	104,50	-130,19	-140,15	-139,87	-141,11
311	261	-63,44	9,56	132,80	-130,25	-143,02	-142,66	-144,28
312	262	-63,19	9,57	56,80	-134,31	-139,77	-139,58	-140,41
313	263	-63,74	9,57	242,30	-113,38	-136,64	-135,95	-138,99
314	264	-63,92	9,58	274,20	-97,75	-123,89	-123,20	-126,86
315	265	-63,63	9,62	179,10	-128,69	-145,16	-144,65	-147,47
316	266	-63,36	9,63	90,30	-142,69	-151,23	-150,94	-152,35
317	267	-63,73	9,64	258,60	-106,44	-131,26	-130,62	-133,63
318	268	-63,47	9,65	113,20	-139,75	-150,47	-150,09	-151,95
319	269	-63,21	9,66	63,30	-152,19	-158,16	-157,94	-158,79
320	270	-63,55	9,66	188,10	-131,50	-149,32	-148,86	-151,08
321	271	-63,85	9,68	282,70	-85,44	-112,64	-111,95	-115,52
322	272	-63,18	9,68	55,00	-157,44	-162,63	-162,45	-163,28
323	273	-63,94	9,70	283,90	-74,81	-102,13	-101,38	-105,13
324	274	-63,95	9,71	221,20	-77,75	-98,52	-97,73	-101,31
325	275	-63,53	9,72	197,30	-129,38	-148,19	-147,72	-150,19
326	276	-63,26	9,73	97,60	-152,38	-161,75	-161,52	-162,53
327	277	-63,16	9,74	67,10	-162,69	-169,13	-168,96	-169,63

STN-N°	STN-REF	LONG	LAT	HEIGHT	FAA	BA	AIRY 35	PRATT 100
		(deg)	(deg)	(m)	(mGal)	(mGal)	(mGal)	(mGal)
328	278	-63,46	9,75	143,00	-136,25	-149,82	-149,41	-151,32
329	279	-63,16	9,75	65,90	-162,44	-168,74	-168,57	-169,27
330	280	-63,66	9,75	263,50	-108,75	-134,06	-133,48	-136,09
331	281	-63,06	9,77	25,80	-174,88	-177,05	-176,93	-177,43
332	282	-63,85	9,77	250,80	-78,75	-102,92	-102,20	-105,49
333	283	-63,75	9,77	249,50	-93,06	-116,88	-116,24	-119,53
334	284	-63,19	9,78	26,70	-168,31	-170,28	-170,10	-171,08
335	285	-63,73	9,80	301,10	-89,81	-118,82	-118,90	-121,49
336	286	-63,21	9,81	62,30	-158,06	-163,46	-163,24	-164,26
337	287	-63,87	9,84	269,30	-69,81	-95,41	-94,62	-98,10
338	288	-63,46	9,85	202,40	-115,19	-134,66	-134,20	-136,36
339	289	-63,16	9,86	32,70	-163,13	-165,86	-165,69	-166,52
340	290	-63,55	9,86	258,20	-103,06	-127,91	-127,37	-130,01
341	291	-63,64	9,88	170,00	-99,69	-115,29	-114,66	-117,69
342	292	-63,15	9,90	26,50	-157,56	-159,74	-159,56	-160,43
343	293	-63,73	9,91	168,10	-96,44	-112,24	-111,46	-114,24
344	294	-63,35	9,91	412,60	-58,75	-97,40	-96,34	-100,36
345	295	-63,50	9,92	342,70	-86,13	-118,18	-117,59	-120,48
346	296	-63,49	9,94	215,60	-88,50	-108,77	-108,14	-110,61
347	297	-63,16	9,94	62,20	-143,88	-149,10	-148,89	-150,06
348	298	-63,65	9,96	229,60	-85,38	-107,20	-106,45	-109,72
349	299	-63,27	9,96	135,60	-108,94	-121,59	-121,19	-123,10
350	300	-63,17	9,97	87,80	-134,25	-142,39	-142,13	-143,71
351	301	-63,16	9,98	46,80	-134,63	-139,00	-138,74	-140,14
352	471	-64,26	9,02	308,50	-32,69	-62,32	-61,59	-65,15
353	472	-64,67	9,03	196,40	-20,81	-39,08	38,45	-41,67
354	473	-64,54	9,03	322,40	-23,81	-54,64	-53,96	-57,17
355	474	-64,88	9,04	123,30	-14,94	-26,63	-26,16	-28,39
356	475	-64,78	9,05	171,10	-17,13	-32,77	-32,24	-35,03
357	476	-64,41	9,05	295,30	-34,06	-62,48	-61,74	-65,11
358	477	-64,60	9,10	206,10	-28,31	-47,63	-46,95	-49,82
359	478	-64,73	9,13	174,50	-22,81	-39,58	-38,91	-41,42
360	479	-64,53	9,13	260,50	-30,31	-55,26	-54,55	-57,85
361	480	-64,94	9,14	91,70	-13,19	-21,77	-21,41	-23,04
362	481	-64,34	9,16	288,20	-43,00	-70,65	-69,92	-73,31
363	482	-64,44	9,16	309,30	-35,06	-62,17	-61,46	-64,68
364	483	-64,87	9,17	124,60	-17,19	-29,14	-28,73	-30,53
365	484	-64,08	9,21	234,60	-57,13	-79,57	-78,91	-82,29
366	485	-64,65	9,23	166,30	-29,50	-45,32	-44,79	-47,33
367	486	-64,38	9,24	130,00	-16,69	-29,11	-28,74	-30,41
368	487	-64,57	9,25	176,80	-35,44	-52,11	-51,52	-54,36
369	488	-64,02	9,25	221,90	-67,63	-88,69	-88,02	-91,40
370	489	-64,00	9,26	206,00	-63,69	-83,05	-82,39	-85,71
371	490	-64,26	9,27	262,50	-57,69	-82,96	-82,24	-85,58
372	491	-64,35	9,27	252,80	-51,19	-75,37	-74,67	-78,02
373	492	-64,91	9,29	105,60	-11,88	-21,94	-21,63	-23,11
374	493	-64,78	9,29	87,30	-16,44	-24,59	-24,21	-26,01
375	494	-64,44	9,29	200,80	-45,75	-64,34	-63,68	-66,92
376	495	-64,80	9,32	137,30	-22,56	-35,44	-35,06	-36,88
377	496	-64,23	9,32	285,30	-60,00	-87,44	-86,74	-90,43
378	497	-64,05	9,33	289,90	-66,50	-94,22	-93,52	-97,08
379	498	-64,66	9,33	145,30	-35,13	-49,08	-48,61	-50,84
380	499	-64,34	9,35	228,10	-56,75	-78,27	-77,59	-81,03
381	500	-64,56	9,35	151,90	-39,00	-53,61	-53,06	-55,53
382	501	-64,96	9,36	95,40	-3,44	-12,47	-12,15	-13,44

STN-N°	STN-REF	LONG	LAT	HEIGHT	FAA	BA	AIRY 35	PRATT 100
		(deg)	(deg)	(m)	(mGal)	(mGal)	(mGal)	(mGal)
383	502	-64,16	9,38	355,90	-59,31	-92,78	-92,06	-96,07
384	503	-64,44	9,39	193,50	-49,19	-67,76	-67,13	-70,13
385	504	-64,85	9,39	90,40	-13,06	-21,56	-21,30	-22,87
386	505	-64,93	9,42	71,60	-6,31	-13,45	-13,16	-14,56
387	506	-64,23	9,42	324,30	-60,06	-91,25	-90,55	-94,21
388	507	-64,73	9,43	103,80	-30,19	-39,84	-39,45	-41,41
389	508	-64,47	9,43	218,30	-43,44	-64,05	-63,45	-66,40
390	509	-64,52	9,43	193,20	-42,56	-60,93	-60,40	-63,05
391	510	-64,07	9,46	328,40	-73,69	-105,32	-104,59	-107,97
392	511	-64,47	9,46	200,00	-45,38	-64,49	-63,90	-66,81
393	512	-64,82	9,46	110,90	-17,88	-28,55	-28,22	-29,74
394	513	-64,14	9,47	356,20	-66,25	-100,41	-99,67	-103,32
395	514	-64,70	9,48	163,10	-29,00	-44,68	-44,29	-46,15
396	515	-64,37	9,48	250,70	-53,06	-77,01	-76,35	-79,52
397	516	-64,19	9,53	371,00	-66,13	-101,43	-100,64	-104,30
398	517	-64,45	9,55	197,40	-53,13	-72,07	-71,49	-73,88
399	518	-64,64	9,55	173,90	-36,25	-52,91	-52,50	-54,34
400	519	-64,29	9,55	314,40	-62,69	-92,94	-92,19	-95,54
401	520	-64,54	9,56	161,20	-48,56	-64,00	-63,51	-65,65
402	521	-64,73	9,56	166,50	-26,38	-42,35	-42,00	-43,59
403	522	-64,37	9,57	233,80	-58,63	-80,42	-79,65	-82,93
404	523	-64,08	9,57	313,40	-81,75	-111,89	-111,11	-115,09
405	524	-64,86	9,58	81,30	-15,44	-23,06	-22,76	-24,13
406	525	-64,47	9,64	171,40	-54,88	-71,08	-70,51	-73,14
407	526	-64,55	9,64	157,20	-48,81	-63,94	-63,48	-65,59
408	527	-64,27	9,64	477,10	-41,38	-85,48	-84,75	-87,78
409	528	-64,65	9,65	132,40	-40,94	-53,34	-52,96	-54,66
410	529	-64,76	9,65	131,00	-29,00	-41,56	-41,22	-42,68
411	530	-64,86	9,65	74,20	-19,25	-26,09	-25,80	-27,16
412	531	-64,35	9,66	223,50	-56,06	-77,19	-76,54	-79,63
413	532	-64,13	9,68	355,00	-62,31	-95,92	-95,14	-99,28
414	533	64,04	9,69	267,20	-77,44	-102,82	-102,05	-105,83
415	534	-64,43	9,73	144,50	-56,06	-69,92	-69,38	-72,08
416	535	-64,08	9,73	363,00	-58,38	-93,22	-92,38	-96,65
417	536	-64,12	9,73	437,40	-49,38	-90,56	-89,74	-93,91
418	537	-64,37	9,73	177,40	-58,25	-74,54	-73,91	-77,19
419	533	-64,74	9,74	90,40	-36,94	-45,32	-45,00	-46,56
420	539	-64,25	9,74	234,40	-54,25	-76,12	-75,39	-78,89
421	540	-64,82	9,74	72,50	-29,06	-35,63	-35,33	-36,86
422	541	-64,55	9,75	155,70	-45,50	-60,43	-60,01	-61,85
423	542	-64,66	9,77	149,10	-39,00	-52,94	-52,59	-54,32
424	543	-64,54	9,85	76,70	-49,81	-56,95	-56,54	-58,53
425	544	-64,85	9,87	81,80	-35,38	-43,02	-42,73	-44,25
426	545	-64,99	9,90	74,10	-30,75	-37,54	-37,30	-38,45
427	546	-64,99	9,91	69,10	-32,69	-38,95	-38,72	-39,88
428	547	-64,89	9,94	90,90	-34,75	-43,37	-43,09	-44,48
429	548	-64,85	9,95	89,60	-37,13	-45,64	-45,35	-46,87
430	549	-64,56	9,98	40,00	-50,94	-54,15	-53,72	-55,53
431	550	-64,81	9,99	111,40	-36,13	-46,71	-46,42	-48,26
432	661	-65,74	9,00	119,40	7,88	-3,09	-2,67	-4,85
433	662	-65,93	9,03	150,00	26,94	12,70	13,14	11,54
434	663	-65,21	9,04	99,70	-17,44	-26,71	-26,37	-27,95
435	664	-65,03	9,04	94,20	-12,38	-20,95	-20,60	-22,45
436	665	-65,32	9,09	68,70	-6,19	-12,44	-12,12	-13,72
437	666	-65,78	9,10	97,00	14,25	5,37	5,81	3,83

STN-N°	STN-REF	LONG	LAT	HEIGHT	FAA	BA	AIRY 35	PRATT 100
		(deg)	(deg)	(m)	(mGal)	(mGal)	(mGal)	(mGal)
438	667	-65,97	9,12	185,50	39,31	21,66	22,08	20,70
439	668	-65,02	9,15	98,80	-10,75	-20,20	-19,84	-21,37
440	669	-65,16	9,15	61,20	-3,69	-9,15	-8,84	-10,36
441	670	-65,62	9,18	80,00	3,75	-3,51	-3,18	-4,90
442	671	-65,16	9,21	91,90	1,81	-7,01	-6,73	-8,00
443	672	-65,22	9,26	55,30	2,75	-2,13	-1,84	-3,28
444	673	-65,56	9,27	83,90	10,13	2,50	2,83	1,16
445	674	-65,77	9,28	140,40	27,06	13,59	13,96	12,18
446	675	-65,05	9,28	82,70	-0,50	-8,20	-7,91	-9,30
447	676	-65,07	9,31	91,30	3,94	-4,74	-4,46	-5,75
448	677	-65,30	9,32	53,00	2,31	-2,33	-2,06	-3,40
449	678	-65,62	9,32	95,00	10,06	1,30	1,62	-0,04
450	679	-65,93	9,32	140,00	17,06	3,63	4,03	2,63
451	680	-65,35	9,37	52,00	4,19	-0,39	-0,13	-1,46
453	682	-65,15	9,39	46,70	10,00	6,15	6,41	5,09
454	683	-65,15	9,40	60,00	5,00	-0,28	-0,02	-1,20
455	684	-65,77	9,40	110,00	8,44	-1,78	-1,41	-3,34
456	685	-65,95	9,42	138,90	4,50	-8,77	-8,34	-9,81
457	686	-65,27	9,43	45,00	3,63	-0,48	-0,24	-1,40
458	687	-65,43	9,43	55,00	1,50	-3,30	-3,01	-4,45
459	688	-65,09	9,44	70,10	3,69	-2,62	-2,37	-3,59
460	689	-65,90	9,45	129,00	0,81	-11,44	-11,01	-12,50
461	690	-65,68	9,47	125,00	9,75	-2,13	-1,76	-3,70
462	691	-65,85	9,47	119,00	-1,50	-12,62	-12,21	-14,28
463	692	-65,85	9,48	136,30	-1,13	-14,11	-13,70	-15,73
464	693	-65,53	9,48	85,00	5,19	-2,56	-2,24	-3,88
465	694	-65,81	9,49	166,80	15,25	-0,64	-0,24	-2,24
466	695	-65,22	9,50	45,00	2,63	-1,60	-1,37	-2,38
467	696	-65,09	9,50	65,20	10,19	4,07	4,30	3,28
468	697	-65,75	9,51	139,20	10,25	-3,04	-2,62	-4,64
469	698	-65,68	9,53	159,00	17,25	2,02	2,42	0,43
470	699	-65,73	9,53	200,00	7,31	-11,41	-10,97	-13,19
471	700	-65,40	9,55	85,00	1,13	-6,96	-6,67	-7,73
472	701	-65,60	9,55	150,00	11,88	-2,35	-1,94	-3,55
473	702	-65,15	9,57	60,00	3,00	-2,78	-2,57	-3,48
474	703	-65,63	9,58	179,90	20,44	3,33	3,73	1,79
475	704	-65,63	9,58	198,80	23,00	3,86	4,24	2,38
476	705	-65,19	9,60	30,30	2,13	-0,54	-0,34	-1,29
477	706	-65,32	9,62	50,00	-7,00	-11,71	-11,51	-12,42
478	707	-65,67	9,63	195,90	18,63	0,34	0,77	-1,58
479	708	-65,22	9,63	45,00	-6,38	-10,65	-10,45	-11,26
480	709	-65,90	9,63	260,00	-0,38	-24,77	-24,23	-26,48
481	710	-65,73	9,65	205,00	2,81	-16,34	-15,86	-18,29
482	711	-65,53	9,65	125,60	13,06	1,30	1,63	0,00
483	712	-65,53	9,66	121,60	12,94	1,52	1,85	0,27
484	713	-65,72	9,67	166,80	6,94	-8,10	-7,62	-10,43
485	714	-66,00	9,69	165,60	-5,44	-20,88	-20,29	-22,33
486	715	-65,78	9,69	186,90	1,31	-15,89	-15,38	-18,10
487	716	-65,40	9,70	75,90	-1,00	-8,20	-7,95	-8,94
488	717	-65,91	9,72	224,20	-4,75	-25,85	-25,25	-27,69
489	718	-65,73	9,72	200,00	-1,69	-20,96	-20,45	-22,93
490	719	-65,97	9,72	174,80	-5,75	-21,76	-21,13	-23,52
491	720	-65,53	9,73	100,00	-2,56	-12,09	-11,73	-13,44
492	721	-65,84	9,74	215,40	1,50	-18,87	-18,28	-20,94
493	722	-65,34	9,74	51,60	-11,50	-16,45	-16,26	-17,11

STN-N°	STN-REF	LONG	LAT	HEIGHT	FAA	BA	AIRY 35	PRATT 100
		(deg)	(deg)	(m)	(mGal)	(mGal)	(mGal)	(mGal)
494	723	-65,28	9,77	44,80	-16,19	-20,45	-20,28	-21,09
495	724	-65,84	9,78	220,10	1,69	-19,08	-18,46	-21,18
496	725	-65,05	9,78	54,20	-16,56	-21,51	-21,31	-22,31
497	726	-65,21	9,81	29,90	-22,56	-25,33	-25,18	-25,97
498	727	-65,83	9,82	280,80	6,56	-20,38	-19,66	-23,15
499	728	-65,14	9,84	16,00	-28,19	-29,52	-29,35	-30,28
500	729	-65,81	9,86	225,40	0,69	-20,21	-19,48	-22,35
501	730	-65,81	9,86	225,80	-0,06	-21,00	-20,27	-23,03
502	731	-65,07	9,87	33,40	-31,38	-34,51	-34,30	-35,32
503	732	-65,77	9,88	260,00	5,31	-19,63	-18,92	-22,04
504	733	-65,56	9,90	243,50	5,13	-17,34	-16,85	-19,37
505	734	-65,61	9,90	230,00	5,88	-15,73	-15,16	-17,71
506	735	-65,15	9,90	22,30	-34,63	-36,74	-36,56	-37,42
507	736	-65,74	9,91	341,70	14,19	-18,27	-17,54	-21,07
508	737	-65,68	9,91	273,00	10,50	-15,51	-14,87	-17,97
509	738	-65,51	9,92	132,30	-9,44	-21,11	-20,67	-22,82
510	739	-65,51	9,92	133,30	-10,13	-21,90	-21,46	-23,65
511	740	-65,44	9,93	89,30	-19,13	-27,65	-27,27	-28,72
512	741	-65,44	9,93	82,80	-20,88	-28,71	-28,33	-29,74
513	742	-65,71	9,94	350,30	13,63	-19,57	-18,82	-22,74
514	743	-65,16	9,94	32,80	-36,88	-40,01	-39,82	-40,86
515	744	-65,26	9,95	22,30	-37,50	-39,23	-39,03	-40,19
516	745	-65,16	9,96	10,50	-39,31	-40,04	-39,85	-40,98
517	746	-65,46	9,96	363,80	2,88	-29,98	-29,58	-32,35
518	747	-65,31	9,98	56,20	-37,00	-42,04	-41,78	-43,05
519	748	-65,48	9,99	417,30	12,56	-24,97	-24,53	-27,76
520	749	-65,18	9,99	7,10	-42,81	-43,18	-42,99	-43,92
521	750	-65,39	9,99	60,40	-36,75	-42,12	-41,92	-43,20
522	7	-61,00	10,40	35,90	-71,81	-75,27	-75,20	-75,14
523	8	-60,97	10,75	15,40	-6,13	-7,84	-7,78	-7,32
524	9	-60,94	10,83	29,30	-12,63	-15,20	-15,10	-14,31
525	68	-61,13	10,05	70,40	-77,06	-83,79	-83,72	-83,64
526	69	-61,51	10,07	2,70	-125,63	-125,89	-125,84	-125,94
527	70	-61,91	10,07	1,80	-159,63	-159,80	-159,77	-159,62
528	71	-61,67	10,08	10,60	-142,88	-143,90	-143,87	-143,90
529	72	-61,15	10,11	39,30	-79,81	-83,60	-83,53	-83,51
530	73	-61,74	10,12	31,40	-151,13	-154,15	-154,11	-153,99
531	74	-61,04	10,14	3,00	-69,38	-69,66	-69,58	-69,22
532	75	-61,36	10,14	33,80	-98,06	-101,32	-101,26	-101,63
533	76	-61,46	10,16	10,60	-114,25	-115,27	-115,22	-115,55
534	77	-61,54	10,17	22,00	-124,56	-126,68	-126,63	-126,78
535	78	-61,64	10,19	9,70	-133,25	-134,18	-134,14	-134,09
536	79	-61,01	10,21	15,10	-71,88	-73,33	-73,26	-73,00
537	80	-61,15	10,25	16,60	-78,00	-79,60	-79,53	-80,27
538	81	-61,35	10,26	79,40	-89,13	-96,78	-96,70	-97,75
539	82	-61,43	10,26	67,00	-97,19	-103,65	-103,59	-104,21
540	83	-61,24	10,29	55,90	-83,44	-88,83	-88,75	-90,03
541	84	-61,18	10,30	34,70	-79,38	-82,72	-82,64	-83,62
542	85	-61,24	10,33	59,20	-78,19	-83,89	-83,57	-85,24
543	86	-61,34	10,36	116,90	-66,63	-77,88	-77,79	-78,87
544	87	-61,01	10,37	1,50	-73,19	-73,33	-75,69	-67,40
545	88	-61,47	10,37	4,50	-91,94	-92,33	-92,24	-92,71
546	89	-61,15	10,42	26,30	-60,13	-62,66	-62,57	-63,44
547	90	-61,24	10,43	135,30	-44,56	-57,59	-57,49	-58,33
548	91	-61,04	10,45	1,80	-57,75	-57,92	-57,85	-57,99

STN-N°	STN-REF	LONG	LAT	HEIGHT	FAA	BA	AIRY 35	PRATT 100
		(deg)	(deg)	(m)	(mGal)	(mGal)	(mGal)	(mGal)
549	92	-61,42	10,46	16,30	-70,38	-71,95	-71,87	-72,42
550	93	-61,34	10,47	33,50	-62,19	-65,42	-65,33	-66,32
551	94	-61,40	10,51	16,00	-62,44	-63,85	-63,77	-64,34
552	95	-61,13	10,52	32,60	-43,13	-46,27	-46,19	-46,86
553	96	-61,20	10,55	100,00	-38,75	-48,39	-48,29	-49,22
554	97	-61,37	10,55	10,30	-58,00	-58,91	-58,82	-59,53
555	98	-61,04	10,56	11,80	-33,81	-34,95	-34,88	-35,00
556	99	-61,35	10,60	17,00	-54,50	-56,00	-55,91	-56,74
557	100	-61,34	10,63	24,20	-35,63	-38,06	-37,96	-38,71
558	101	-61,27	10,64	60,40	-28,25	-33,57	-33,45	-34,33
559	102	-61,20	10,64	55,90	-29,06	-33,98	-33,91	-34,69
560	103	-61,45	10,65	14,80	-34,19	-35,68	-35,61	-35,81
561	104	-61,61	10,67	0,00	-29,75	-29,75	-29,69	-29,07
562	105	-61,60	10,68	2,00	-31,75	-31,97	-31,91	-31,25
563	106	-61,55	10,68	10,00	-32,31	-33,42	-33,37	-32,95
564	107	-61,60	10,68	2,40	-32,25	-32,52	-32,46	-31,79
565	108	-61,03	10,69	15,10	-8,44	-10,11	-10,05	-10,10
566	109	-61,60	10,69	2,50	-31,19	-31,47	-31,42	-30,68
567	110	-61,55	10,71	27,50	-26,25	-29,30	-29,24	-28,66
568	111	-61,32	10,75	240,10	-7,63	-31,72	-31,64	-31,70
569	112	-61,44	10,75	8,80	-30,44	-31,41	-31,34	-30,94
570	113	-61,36	10,80	23,30	-27,88	-30,22	-30,13	-29,83
571	114	-61,01	10,84	12,10	-19,75	-20,97	-21,07	-20,09
572	175	-62,85	10,02	3,00	-162,19	-162,37	-162,31	-162,60
573	176	-62,97	10,03	4,00	-149,06	-149,06	-148,96	-149,90
574	177	-62,37	10,12	2,00	-129,31	-129,49	-129,42	-129,91
575	178	-62,97	10,13	10,00	-104,56	-105,44	-105,30	-106,48
576	179	-62,75	10,17	1,00	-124,38	-124,46	-124,42	-124,62
577	180	-62,85	10,22	2,00	-88,31	-88,49	-88,40	-88,94
573	181	-62,97	10,25	40,00	-73,94	-77,77	-77,60	-78,87
580	183	-62,85	10,35	1,00	-64,38	-64,46	-64,36	-64,82
581	184	-62,98	10,45	1,00	-45,38	-45,45	-45,26	-46,42
582	185	-62,98	10,55	3,00	-43,19	-43,44	-43,21	-44,56
583	186	-62,54	10,60	47,20	-22,50	-27,72	-27,48	-28,00
584	187	-62,43	10,61	53,90	-21,56	-27,53	-27,35	-27,63
585	302	-63,14	10,01	37,40	-129,69	-132,92	-132,66	-134,17
586	303	-63,10	10,04	20,20	-127,31	-128,80	-128,51	-130,12
587	304	-63,12	10,05	50,00	-110,00	-114,75	-114,42	-116,08
588	305	-63,07	10,07	20,00	-113,69	-115,44	-115,26	-116,64
589	306	-63,09	10,09	9,40	-111,38	-112,18	-111,95	-113,34
590	307	-63,09	10,13	9,60	-95,00	-95,81	-95,50	-97,17
591	308	-63,07	10,17	5,00	-89,00	-89,41	-89,15	-90,76
592	309	-63,12	10,18	60,00	-77,13	-83,13	-82,69	-84,94
593	310	-63,16	10,20	24,60	-76,94	-79,25	-78,68	-81,06
594	311	-63,54	10,22	1136,20	55,63	-58,43	-56,82	-64,69
595	312	-63,23	10,25	100,00	-63,63	-73,26	-72,38	-75,54
596	313	-63,90	10,25	233,40	-36,13	-59,26	-57,13	-61,16
597	314	-63,21	10,25	27,90	-60,63	-63,10	-62,34	-64,99
598	315	-63,03	10,27	100,00	-43,63	-53,64	-53,32	-55,37
599	316	-63,22	10,28	14,00	-55,69	-56,83	-56,02	-58,62
600	317	-63,24	10,31	30,40	-47,13	-49,98	-49,09	-51,85
601	318	-63,64	10,32	332,10	-8,81	-42,04	-40,36	-46,25
602	319	-63,31	10,33	29,70	-40,06	-42,79	-41,62	-44,42
603	320	-63,25	10,35	7,00	-45,81	-46,42	-45,50	-47,88
604	321	-63,36	10,36	17,20	-37,56	-39,04	-37,82	-40,40

STN-N°	STN-REF	LONG	LAT	HEIGHT	FAA	BA	AIRY 35	PRATT 100
		(deg)	(deg)	(m)	(mGal)	(mGal)	(mGal)	(mGal)
605	322	-63,41	10,38	20,60	-35,31	-37,18	-35,89	-38,39
606	323	-63,39	10,42	31,30	-26,25	-29,30	-28,22	-30,56
607	324	-63,57	10,44	47,90	-5,56	-10,20	-8,98	-11,37
608	325	-63,77	10,44	3,30	-22,25	-22,43	-21,24	-22,87
609	326	-63,79	10,44	0,90	-22,06	-21,91	-20,65	-22,29
610	327	-63,87	10,44	8,60	-20,75	-21,46	-20,29	-21,72
611	328	-63,89	10,45	7,50	-23,63	-24,24	-23,01	-24,37
612	329	-63,93	10,45	5,50	-21,69	-22,14	-21,01	-22,28
613	330	-63,44	10,45	228,40	-4,50	-27,42	-26,30	-30,97
614	331	-63,68	10,46	0,80	-25,31	-25,31	-24,15	-26,03
615	332	-63,70	10,47	14,30	-18,75	-20,06	-19,06	-20,82
616	333	-63,55	10,48	11,80	-27,50	-28,62	-27,49	-29,63
617	334	-63,44	10,49	40,70	-20,31	-24,32	-23,33	-25,85
618	335	-63,44	10,50	31,30	-19,94	-23,02	-22,09	-24,36
619	336	-63,55	10,50	11,50	-26,94	-28,04	-27,05	-29,05
620	337	-63,53	10,54	34,80	12,25	8,77	9,58	7,46
621	338	-63,15	10,55	74,90	-11,00	-19,31	-18,88	-20,75
622	339	-63,11	10,58	44,60	4,69	-0,26	0,07	-1,64
623	340	-63,20	10,60	116,60	0,19	-12,73	-12,31	-14,62
624	341	-63,24	10,60	120,40	-4,44	-17,77	-17,32	-19,52
625	342	-63,65	10,61	64,10	23,69	16,59	17,01	15,80
626	343	-63,53	10,63	1,10	18,44	18,33	18,74	17,99
627	344	-63,49	10,64	1,00	21,38	21,28	21,69	21,12
628	345	-63,48	10,65	1,90	21,69	21,49	21,91	21,21
629	346	-63,26	10,66	19,90	7,44	5,28	5,70	4,83
630	347	-63,34	10,66	17,30	16,63	14,76	15,18	14,35
631	343	-63,75	10,66	13,40	23,69	22,22	22,52	22,02
632	349	-63,25	10,67	16,00	7,94	6,21	6,62	5,83
633	350	-63,33	10,67	1,30	18,25	18,15	18,57	17,97
634	351	-63,40	10,68	0,40	28,06	28,04	28,43	27,87
635	352	-63,82	10,68	1,70	25,88	25,70	25,93	25,71
636	353	-63,11	10,70	0,30	22,50	22,51	22,83	22,41
637	354	-63,10	10,71	4,40	22,88	22,42	22,75	22,33
638	355	-63,17	10,71	0,30	22,94	22,95	23,29	22,89
639	356	-63,89	10,90	1,50	20,56	20,43	20,52	20,62
640	357	-63,93	10,90	1,50	18,31	18,18	18,26	18,33
641	358	-63,96	10,90	1,20	16,75	16,64	16,71	16,78
642	359	-63,89	10,93	1,50	27,00	26,87	26,99	27,08
643	360	-63,98	10,94	8,50	22,44	21,69	21,93	22,02
644	361	-63,91	10,95	12,10	36,13	34,78	34,94	34,98
645	362	-63,88	10,95	14,90	43,13	41,81	41,95	42,05
646	363	-63,95	10,95	17,60	34,56	32,61	32,74	32,78
647	364	-63,34	10,96	2,10	47,75	47,57	47,71	47,85
648	365	-63,84	10,96	13,70	51,00	49,79	49,91	50,06
649	366	-63,83	10,97	12,20	51,44	50,36	50,49	50,64
650	367	-63,83	10,97	14,60	52,38	51,09	51,21	51,36
651	368	-63,86	10,98	18,80	49,81	47,72	47,84	47,93
652	369	-63,38	10,99	46,00	54,56	49,46	49,57	49,59
653	370	-63,98	10,99	29,50	49,50	46,23	46,33	46,34
654	371	-63,82	11,00	7,00	57,50	56,88	57,01	57,17
655	372	-63,79	11,00	3,00	56,69	56,42	56,55	56,68
656	551	-64,37	10,02	245,90	-37,69	-62,25	-61,31	-64,33
657	552	-64,78	10,04	58,90	-42,81	-46,23	-45,92	-48,25
658	553	-64,74	10,05	8,10	-48,13	-48,44	-48,14	-49,66
659	554	-64,74	10,05	7,20	-49,31	-49,67	-49,37	-50,79

STN-N°	STN-REF	LONG	LAT	HEIGHT	FAA	BA	AIRY 35	PRATT 100
		(deg)	(deg)	(m)	(mGal)	(mGal)	(mGal)	(mGal)
660	555	-64,81	10,06	28,40	-46,56	-49,02	-48,75	-49,92
661	556	-64,89	10,08	9,40	-54,94	-55,74	-55,49	-56,26
662	557	-64,94	10,08	17,40	-55,31	-56,80	-56,56	-57,42
663	558	-64,63	10,08	12,00	-46,13	-47,26	-46,87	-48,11
664	559	-64,70	10,11	6,30	-53,13	-53,67	-53,32	-54,62
665	560	-64,68	10,11	8,50	-52,00	-52,74	-52,42	-53,54
666	561	-64,68	10,11	4,60	-53,94	-54,33	-54,01	-55,02
667	562	-64,68	10,14	3,80	-44,00	-44,32	-43,94	-44,99
668	563	-64,68	10,15	4,20	-54,38	-54,73	-54,37	-55,34
669	564	-64,68	10,18	3,30	-29,63	-29,91	-29,58	-30,36
670	565	-64,62	10,19	93,30	-21,88	-31,22	-30,83	-32,37
671	566	-64,64	10,22	2,30	-24,38	-24,58	-24,21	-24,62
672	567	-64,46	10,23	39,90	-21,94	-25,76	-24,95	-26,28
673	568	-64,53	10,23	156,70	-10,63	-26,33	-25,76	-27,62
675	570	-64,58	10,24	25,10	-24,00	-26,41	-25,87	-26,81
676	571	-64,45	10,26	2,10	-26,50	-26,59	-25,78	-26,68
677	572	-64,42	10,28	3,20	-24,06	-24,20	-23,37	-24,40
678	573	-64,39	10,29	4,00	-24,56	-24,81	-23,83	-25,06
679	574	-64,34	10,31	52,00	-16,75	-21,75	-20,64	-22,39
680	575	-64,31	10,34	383,40	22,94	-15,54	-14,26	-17,78
681	576	-64,33	10,35	134,80	-6,81	-20,26	-19,23	-21,24
682	577	-64,25	10,37	76,60	-7,50	-15,12	-13,88	-15,93
683	578	-64,25	10,38	31,30	-10,19	-13,26	-12,04	-13,83
684	579	-64,23	10,40	13,40	-9,00	-10,28	-9,27	-10,62
685	580	-64,02	10,43	49,50	-11,50	-16,38	-15,20	-16,87
686	581	-64,01	10,44	5,40	-17,44	-17,87	-16,94	-17,44
687	582	-64,07	10,45	0,20	-13,69	-13,65	-12,64	-13,63
688	583	-64,15	10,45	1,90	-8,94	-9,07	-8,16	-9,04
689	584	-64,18	10,45	1,40	-9,13	-9,21	-8,31	-9,15
690	585	-64,13	10,47	5,50	-9,38	-9,83	-8,95	-9,82
691	586	-64,25	10,57	0,10	30,69	30,74	31,30	31,25
692	587	-64,09	10,90	3,00	7,81	7,55	7,62	7,90
693	588	-64,06	10,93	34,70	20,19	17,13	17,24	17,36
694	589	-64,25	10,95	8,80	26,19	25,22	25,55	25,83
695	590	-64,21	10,95	5,40	28,44	27,84	28,05	28,40
696	591	-64,29	10,95	9,10	29,38	28,39	28,69	28,98
697	592	-64,02	10,95	16,40	25,69	23,87	23,98	24,06
698	593	-64,10	10,96	20,10	29,06	27,29	27,42	27,54
699	594	-64,34	10,96	10,00	31,69	30,61	30,93	31,03
700	595	-64,16	10,96	0,40	28,88	28,84	28,97	29,23
701	596	-64,15	10,97	7,00	32,13	31,51	31,63	31,82
702	597	-64,18	10,97	1,50	28,75	28,62	28,75	28,99
703	598	-64,40	10,98	3,00	12,13	11,84	12,20	12,25
704	599	-64,36	10,98	6,70	41,63	40,92	41,25	41,30
705	600	-64,03	10,99	3,00	40,13	39,79	39,90	39,93
706	601	-64,19	11,00	14,00	32,50	31,27	31,39	31,83
707	751	-65,32	10,02	135,30	-31,25	-44,00	-43,80	-45,10
708	752	-65,52	10,02	248,60	-4,31	-26,07	-25,55	-29,40
709	753	-65,20	10,02	3,90	-47,75	-47,64	-47,44	-48,28
710	754	-65,32	10,04	263,40	-19,50	-43,01	-42,75	-44,59
711	755	-65,02	10,06	63,30	-45,44	-50,97	-50,75	-51,59
712	756	-65,35	10,06	16,90	-45,44	-47,01	-46,72	-47,68
714	758	-65,04	10,07	6,60	-58,13	-58,72	-58,51	-59,18
715	759	-65,37	10,09	4,00	-43,50	-43,82	-43,52	-44,23
716	760	-65,98	10,09	44,60	-22,19	-26,26	-25,35	-27,12

STN-N°	STN-REF	LONG	LAT	HEIGHT	FAA	BA	AIRY 35	PRATT 100
		(deg)	(deg)	(m)	(mGal)	(mGal)	(mGal)	(mGal)
717	761	-65,43	10,13	8,20	-39,88	-40,58	-40,19	-40,93
718	762	-65,50	10,15	9,50	-45,75	-46,57	-46,10	-46,80
719	763	-65,90	10,16	11,70	-33,50	-34,55	-33,77	-35,20
720	764	-65,97	10,16	31,80	-25,63	-28,60	-27,80	-29,37
721	765	-65,65	10,17	15,70	-28,50	-29,97	-29,36	-30,43
722	766	-65,70	10,17	17,50	-26,44	-28,08	-27,47	-28,49
723	767	-65,57	10,17	14,50	-37,06	-38,43	-37,93	-38,73
724	768	-65,77	10,17	11,90	-23,19	-24,28	-23,61	-24,92
725	769	-65,83	10,18	20,40	-17,13	-19,02	-18,30	-19,75
726	770	-65,95	10,21	23,10	-37,94	-40,12	-39,43	-40,61
727	771	-65,95	10,24	13,60	-38,06	-39,23	-38,67	-39,71
728	772	-65,96	10,27	3,40	-44,06	-44,33	-43,79	-44,77
729	773	-65,99	10,30	5,20	-49,94	-50,31	-49,86	-50,70
730	774	-65,88	10,31	0,70	-53,56	-53,61	-53,30	-53,73
731	775	-65,93	10,35	0,20	-48,81	-48,82	-48,53	-48,77
732	824	-62,26	9,89	-4,00	-197,88	-197,63	-197,60	-197,60
733	778	-60,96	10,95	-94,00	-40,69	-35,68	-35,59	-34,77
734	779	-60,92	10,96	-89,00	-38,06	-33,33	-33,21	-32,36
735	780	-60,87	10,97	-88,00	-35,06	-30,38	-30,27	-29,40
736	781	-60,82	10,99	-77,00	-23,13	-19,03	-18,91	-18,01
737	782	-61,82	10,05	-8,00	-160,69	-160,26	-160,22	-160,14
738	783	-61,73	10,07	-2,00	-149,81	-149,71	-149,66	-149,68
739	784	-61,87	10,13	-7,00	-156,81	-156,44	-156,41	-156,18
740	785	-61,93	10,13	-10,00	-161,44	-160,91	-160,87	-160,61
741	786	-61,66	10,25	-19,00	-123,25	-122,24	-122,20	-122,03
742	787	-61,57	10,27	-5,00	-119,44	-119,17	-119,12	-119,16
743	788	-61,73	10,27	-22,00	-131,81	-130,64	-130,60	-130,28
744	789	-61,87	10,27	-24,00	-153,25	-151,97	-151,93	-151,44
745	790	-61,93	10,27	-26,00	-154,63	-153,24	-153,20	-152,67
746	791	-61,53	10,33	-11,00	-110,63	-110,04	-109,96	-110,08
747	792	-61,67	10,33	-21,00	-124,69	-123,57	-123,52	-123,10
748	793	-61,73	10,33	-22,00	-131,88	-130,70	-130,06	-131,13
749	794	-61,97	10,33	-24,00	-149,25	-147,97	-147,92	-147,32
750	795	-61,53	10,47	-11,00	-73,63	-73,04	-72,98	-72,84
751	796	-61,67	10,47	-18,00	-92,06	-91,10	-91,05	-90,43
752	797	-61,73	10,47	-23,00	-94,06	-92,84	-92,79	-92,11
753	798	-61,87	10,47	-28,00	-96,06	-94,57	-94,52	-93,73
754	799	-61,96	10,47	-33,00	-110,88	-109,12	-109,06	-108,34
755	800	-61,53	10,53	-11,00	-66,63	-66,04	-65,98	-65,85
756	801	-61,67	10,53	-18,00	-74,00	-73,04	-72,98	-72,31
757	802	-61,73	10,53	-24,00	-84,25	-82,97	-82,89	-82,12
758	803	-61,94	10,64	-9,00	-33,69	-33,20	-33,04	-32,29
759	804	-61,84	10,66	-26,00	-73,19	-71,79	-71,67	-70,59
760	805	-61,81	10,74	-297,00	-46,31	-30,44	-30,14	-30,04
761	806	-61,70	10,77	-50,00	-52,13	-49,46	-49,36	-47,70
762	807	-61,65	10,78	-40,00	-43,00	-40,87	-40,78	-39,23
763	808	-61,60	10,79	-42,00	-44,50	-42,26	-42,17	-40,72
764	809	-61,56	10,80	-50,00	-41,56	-38,90	-38,81	-37,49
765	810	-61,51	10,82	-56,00	-43,06	-40,08	-39,98	-38,73
766	811	-61,46	10,83	-58,00	-39,94	-36,85	-36,74	-35,74
767	812	-61,41	10,84	-55,00	-47,50	-44,57	-44,45	-43,44
768	813	-61,36	10,85	-55,00	-61,19	-58,26	-58,09	-57,25
769	814	-61,80	10,85	-118,00	-40,75	-34,47	-34,29	-31,88
770	815	-61,31	10,86	-46,00	-76,44	-73,99	-73,27	-72,78
771	816	-61,26	10,88	-30,00	-80,63	-79,03	-78,73	-78,21

STN-N°	STN-REF	LONG	LAT	HEIGHT	FAA	BA	AIRY 35	PRATT 100
		(deg)	(deg)	(m)	(mGal)	(mGal)	(mGal)	(mGal)
772	817	-61,21	10,89	-26,00	-71,38	-69,99	-69,85	-69,29
773	818	-61,16	10,90	-30,00	-56,56	-54,97	-54,85	-54,26
774	819	-61,11	10,91	-38,00	-35,13	-33,10	-33,00	-32,35
775	820	-61,78	10,92	-118,00	-30,88	-24,59	-24,39	-22,13
776	821	-61,06	10,92	-51,00	-28,19	-25,47	-25,37	-24,72
777	822	-61,01	10,93	-77,00	-36,94	-32,84	-32,72	-31,93
778	823	-61,81	10,98	-129,00	-9,75	-2,88	-2,69	-0,76
779	825	-62,21	10,01	-4,00	-194,88	-194,59	-194,56	-194,48
780	826	-62,15	10,06	-7,00	-191,75	-191,38	-191,35	-191,16
781	827	-62,14	10,11	-18,00	-186,50	-185,54	-185,51	-185,24
782	828	-62,05	10,15	-22,00	-175,56	-174,39	-174,35	-174,03
783	829	-62,36	10,16	-7,00	-181,75	-181,38	-181,35	-181,16
784	830	-62,44	10,16	-6,00	-179,44	-179,12	-179,09	-178,97
785	831	-62,64	10,22	-6,00	-136,25	-135,93	-135,90	-135,94
786	832	-62,56	10,24	-6,00	-143,38	-143,06	-143,03	-142,95
787	833	-62,16	10,25	-30,00	-153,19	-151,59	-151,55	-151,04
788	834	-62,43	10,25	-7,00	-150,88	-150,50	-150,46	-150,23
789	835	-62,36	10,26	-12,00	-141,94	-141,30	-141,27	-140,92
790	836	-62,05	10,27	-18,00	-158,50	-157,54	-157,50	-156,90
791	837	-62,25	10,29	-16,00	-128,31	-127,46	-127,42	-126,91
792	838	-62,32	10,33	-16,00	-115,13	-114,27	-114,22	-113,77
793	839	-62,03	10,33	-18,00	-158,50	-157,54	-157,40	-156,83
794	840	-62,18	10,34	-24,00	-138,00	-136,72	-136,65	-136,04
795	841	-62,47	10,34	-10,00	-137,56	-137,03	-136,93	-136,74
796	842	-62,64	10,35	-3,00	-120,06	-119,90	-119,87	-119,81
797	843	-62,54	10,38	-9,00	-135,94	-135,46	-135,43	-135,24
798	844	-62,25	10,38	-20,00	-117,00	-115,94	-115,89	-115,36
799	845	-62,47	10,42	-10,00	-134,81	-134,28	-134,24	-133,99
800	846	-62,62	10,43	-6,00	-128,56	-128,24	-128,20	-128,14
801	847	-62,18	10,43	-24,00	-107,56	-106,29	-106,23	-105,64
802	848	-62,32	10,43	-19,00	-117,31	-116,30	-116,25	-115,83
803	849	-62,05	10,44	-30,00	-114,13	-112,53	-112,47	-111,76
804	850	-62,25	10,47	-18,00	-95,19	-94,23	-94,18	-93,78
805	851	-62,54	10,47	-6,00	-117,06	-116,74	-116,71	-116,65
806	852	-62,07	10,51	-28,00	-98,94	-97,45	-97,36	-96,75
807	853	-62,32	10,53	-4,00	-70,06	-69,85	-69,72	-69,70
808	854	-62,47	10,54	-3,00	-65,63	-65,46	-65,30	-65,40
809	855	-62,54	10,54	-3,00	-65,63	-65,46	-65,30	-65,59
810	856	-62,62	10,55	-4,00	-59,13	-58,90	-58,70	-59,12
811	857	-62,18	10,57	-15,00	-66,38	-65,58	-65,45	-65,20
812	858	-62,25	10,60	-9,00	-37,31	-36,82	-36,66	-36,55
813	859	-62,11	10,61	-9,00	-34,75	-34,26	-34,13	-33,79
814	860	-63,09	10,77	-56,00	23,75	26,74	27,00	27,38
815	861	-63,27	10,80	-80,00	18,00	22,27	22,55	23,07
816	862	-63,07	10,84	-56,00	19,25	22,23	22,58	23,44
817	863	-63,31	10,86	-69,00	-1,00	2,67	2,90	3,73
818	864	-63,35	10,91	-42,00	21,31	23,55	23,71	24,67
819	865	-63,02	10,96	-69,00	8,44	12,11	12,28	13,26
820	866	-64,33	10,16	-28,00	-53,50	-52,01	-51,80	-51,85
821	867	-64,95	10,18	-21,00	-47,38	-46,26	-46,07	-45,98
822	868	-64,98	10,24	-44,00	-59,75	-57,41	-57,26	-56,54
823	869	-64,64	10,25	-15,00	-26,75	-25,92	-25,57	-25,69
824	870	-64,73	10,25	-34,00	-29,75	-27,93	-27,71	-27,39
825	871	-64,88	10,26	-60,00	-52,50	-49,31	-49,15	-48,35
826	872	-64,70	10,30	-44,00	-17,50	-15,14	-14,77	-14,11

STN-N°	STN-REF	LONG	LAT	HEIGHT	FAA	BA	AIRY 35	PRATT 100
		(deg)	(deg)	(m)	(mGal)	(mGal)	(mGal)	(mGal)
827	873	-64,81	10,32	-67,00	-22,75	-19,16	-18,93	-17,88
828	874	-64,56	10,40	-119,00	-2,31	4,13	4,82	5,50
829	875	-64,55	10,42	-225,00	-24,00	-11,87	-11,10	-10,80
830	876	-64,55	10,47	-1309,00	-81,81	-11,27	-10,43	1,30
831	877	-64,85	10,47	-1063,00	-58,69	-1,65	-1,05	4,84
832	878	-64,95	10,47	-11,00	-31,38	-30,44	-29,95	-28,80
833	879	-64,85	10,50	-1275,00	-77,88	-9,64	-8,83	-1,02
834	880	-64,54	10,51	-1339,00	-94,81	-23,22	-22,25	-10,40
835	881	-64,54	10,52	-1341,00	-93,06	-21,45	-20,43	-11,68
836	882	-64,99	10,54	-30,00	-16,63	-14,06	-13,32	-12,36
837	883	-64,85	10,55	-1322,00	-91,75	-21,24	-20,24	-14,47
838	884	-64,54	10,56	-1287,00	-72,19	-3,54	-2,50	7,10
839	885	-64,85	10,59	-1242,00	-82,81	-16,61	-15,46	-7,96
840	886	-64,54	10,61	-878,00	-15,00	31,91	33,09	36,15
841	887	-64,85	10,64	-984,00	-57,19	-4,75	-3,47	2,36
842	888	-64,54	10,66	-342,00	27,88	46,30	47,46	51,70
843	889	-64,57	10,66	-360,00	17,38	36,76	37,94	42,29
844	890	-64,57	10,67	-404,00	9,25	30,89	32,09	36,62
845	891	-64,85	10,68	-759,00	-34,00	6,45	7,74	11,63
846	892	-64,57	10,71	-519,00	-18,81	8,88	10,04	13,41
847	893	-64,86	10,73	-594,00	-17,63	14,05	15,33	16,86
848	894	-64,57	10,75	-556,00	-28,00	1,65	2,73	4,40
849	895	-64,86	10,77	-424,00	-7,25	15,38	16,60	18,51
850	896	-64,86	10,82	-265,00	4,06	18,22	19,25	21,53
851	897	-64,56	10,83	-245,00	-11,13	1,95	2,77	7,18
852	898	-64,86	10,86	-232,00	7,56	19,94	20,89	23,52
853	899	-64,56	10,87	-315,00	-28,63	-11,85	-10,97	-4,20
854	900	-64,56	10,91	-338,00	-34,31	-16,32	-15,76	-8,51
855	901	-64,97	10,94	-118,00	26,81	33,10	33,80	35,52
856	902	-64,56	10,95	-358,00	-35,19	-16,13	-15,60	-10,14
857	903	-64,56	10,99	-318,00	-23,19	-6,26	-5,79	-0,64
858	904	-65,99	10,08	-4,00	-68,25	-67,51	-66,57	-68,44
859	905	-65,12	10,08	-7,00	-78,81	-78,43	-78,25	-78,69
860	906	-65,88	10,08	-7,00	-78,81	-78,21	-77,36	-78,97
361	907	-65,06	10,12	-16,00	-76,69	-75,83	-75,66	-75,94
862	908	-65,94	10,12	-16,00	-76,69	-75,62	-74,78	-76,33
863	909	-65,23	10,13	-7,00	-81,44	-81,05	-80,82	-81,21
864	910	-65,77	10,13	-7,00	-81,44	-80,93	-80,19	-81,61
865	911	-65,17	10,14	-12,00	-83,44	-82,80	-82,63	-82,84
866	912	-65,34	10,14	-6,00	-74,94	-74,61	-74,35	-74,79
867	913	-65,83	10,14	-12,00	-83,44	-82,60	-81,82	-83,24
868	914	-65,44	10,17	-7,00	-68,56	-68,17	-67,80	-68,24
869	915	-65,44	10,20	-8,00	-68,75	-68,31	-67,97	-68,04
870	916	-65,17	10,24	-37,00	-71,69	-69,72	-69,59	-68,91
871	917	-65,66	10,24	-47,00	-75,13	-72,60	-72,16	-72,26
872	918	-65,32	10,24	-7,00	-63,38	-63,00	-62,80	-62,27
873	919	-65,44	10,27	-60,00	-66,75	-63,55	-63,29	-62,53
874	920	-65,77	10,28	-50,00	-66,19	-63,52	-63,13	-63,36
875	921	-65,26	10,29	-30,00	-67,13	-65,53	-65,38	-64,17
876	922	-65,81	10,29	-8,00	-62,94	-62,50	-62,11	-62,60
377	923	-65,02	10,30	-65,00	-52,38	-48,92	-48,79	-47,62
878	924	-65,97	10,30	-65,00	-52,38	-48,87	-48,46	-48,99
879	925	-65,61	10,31	-68,00	-54,94	-51,31	-51,02	-50,23
880	926	-65,83	10,32	-67,00	-57,69	-54,11	-53,79	-53,88
881	927	-65,42	10,32	-65,00	-57,88	-54,41	-54,21	-52,91

STN-N°	STN-REF	LONG	LAT	HEIGHT	FAA	BA	AIRY 35	PRATT 100
		(deg)	(deg)	(m)	(mGal)	(mGal)	(mGal)	(mGal)
882	928	-65,32	10,34	-68,00	-58,50	-54,88	-54,69	-53,06
883	929	-65,06	10,36	-7,00	-52,06	-51,67	-51,52	-49,95
884	930	-65,43	10,44	-445,00	-36,25	-12,42	-12,05	-10,81
385	931	-65,06	10,45	-40,00	-49,81	-47,60	-47,26	-45,81
886	932	-65,48	10,46	-499,00	-43,25	-16,54	-16,09	-14,42
887	933	-65,13	10,47	-65,00	-52,38	-48,87	-48,53	-47,03
888	934	-65,48	10,48	-644,00	-44,69	-10,29	-9,82	-7,59
889	935	-65,48	10,49	-715,00	-52,63	-14,46	-13,98	-10,25
890	970	-60,30	9,99	-88,00	-67,00	-62,22	-62,09	-60,84
391	971	-60,29	9,98	-88,00	-32,00	-27,22	-27,09	-25,90
892	140	-60,54	10,00	-74,00	-46,00	-41,96	-41,85	-40,82
893	141	-60,51	9,99	-77,00	-43,00	-38,75	-38,63	-37,53
894	142	-60,45	9,99	-83,00	-42,00	-37,45	-37,33	-36,19
895	143	-60,40	9,98	-83,00	-39,00	-34,45	-34,33	-33,23
896	144	-60,37	9,99	-84,00	-37,00	-32,39	-32,27	-31,09
897	145	-60,33	9,97	-81,00	-38,00	-33,57	-33,44	-32,32
898	146	-60,30	9,99	-86,00	-38,00	-33,33	-33,20	-31,98
899	972	-62,33	10,99	-95,00	10,00	15,06	15,26	16,73
900	973	-62,30	10,87	-104,00	-3,00	2,54	2,77	4,77
901	974	-62,29	10,83	-102,00	-6,00	-0,56	-0,29	1,48
902	975	-62,27	10,73	-102,00	-14,00	-8,56	-8,32	-6,87
903	976	-62,25	10,76	-96,00	-10,00	-4,87	-4,63	-3,48
904	977	-62,17	10,75	-100,00	-77,00	-71,65	-71,41	-70,23
905	978	-62,05	10,75	-109,00	-64,00	-58,07	-57,88	-56,60
906	55	-62,33	10,98	-95,00	10,00	15,06	15,26	16,75
907	56	-62,33	10,96	-95,00	10,00	15,06	15,33	16,94
908	57	-62,32	10,92	-104,00	9,00	14,54	14,80	16,80
909	58	-62,30	10,88	-104,00	7,00	12,54	12,77	14,81
910	59	-62,67	10,96	-66,00	30,00	33,51	33,82	34,87
911	60	-62,72	10,90	-66,00	36,00	39,52	39,82	40,96
912	61	-62,71	10,86	-83,00	37,00	41,43	41,75	42,70
913	62	-62,52	10,90	-85,00	15,00	19,53	19,85	21,39
914	63	-62,47	10,96	-85,00	17,00	21,52	21,84	23,20
915	64	-62,47	11,00	-74,00	17,00	20,94	21,14	22,57
916	979	-61,95	10,77	-107,00	11,00	16,74	16,91	18,52
917	980	-61,89	10,79	-92,00	-2,00	2,91	3,07	5,08
918	981	-61,82	10,80	-116,00	-27,00	-20,83	-20,67	-18,50
919	982	-61,78	10,82	-95,00	-42,00	-36,94	-36,80	-34,66
920	983	-61,69	10,85	-95,00	-50,00	-44,94	-44,78	-42,50
921	984	-61,71	10,84	-90,00	-53,00	-48,21	-48,01	-45,80
922	985	-61,74	10,80	-102,00	-43,00	-37,57	-37,45	-35,48
923	986	-61,76	10,76	-154,00	-42,00	-33,78	-33,67	-31,93
924	987	-61,77	10,77	-135,00	-38,00	-30,80	-30,69	-28,74
925	988	-61,79	10,74	-223,00	-26,00	-14,09	-13,93	-13,19
926	989	-61,87	10,67	-53,00	-39,00	-36,17	-36,05	-35,02
927	990	-61,90	10,61	-32,00	-63,00	-61,30	-61,19	-60,33
928	991	-61,91	10,57	-28,00	-71,00	-69,51	-69,40	-68,69
929	992	-61,93	10,54	-28,00	-78,00	-76,51	-76,37	-75,67
930	993	-61,94	10,51	-34,00	-96,00	-94,19	-94,12	-93,40
931	994	-61,95	10,49	-34,00	-104,00	-102,19	-102,14	-101,39
932	995	-61,91	10,59	-53,00	-45,00	-42,17	-42,06	-41,29
933	996	-61,86	10,72	-123,00	-26,00	-19,43	-19,28	-17,97
934	997	-61,79	10,75	-130,00	-27,00	-20,07	-19,92	-18,22
935	998	-61,70	10,82	-96,00	-48,00	-42,89	-42,78	-40,81
936	999	-61,57	10,86	-100,00	-60,00	-54,68	-54,47	-52,58

STN-N°	STN-REF	LONG	LAT	HEIGHT	FAA	BA	AIRY 35	PRATT 100
		(deg)	(deg)	(m)	(mGal)	(mGal)	(mGal)	(mGal)
937	0	-61,50	10,86	-83,00	-50,00	-45,58	-45,25	-43,70
938	1	-61,41	10,87	-73,00	-48,00	-44,11	-43,87	-42,74
939	2	-61,31	10,88	-55,00	-70,00	-67,07	-66,91	-66,07
940	3	-61,25	10,90	-36,00	-71,00	-69,08	-68,95	-68,31
941	4	-61,19	10,92	-160,00	-22,00	-13,46	-13,35	-13,05
942	5	-61,21	11,00	-178,00	-16,00	-6,52	-6,38	-6,07
943	65	-61,80	10,96	-125,00	2,00	8,65	8,85	11,01
944	66	-61,80	10,94	-125,00	0,00	6,65	6,99	9,80
945	67	-61,80	10,91	-123,00	-6,00	0,55	0,72	3,27
946	68	-61,49	10,83	-81,00	-37,00	-32,69	-32,57	-31,29
947	69	-61,49	10,89	-107,00	-44,00	-38,30	-38,15	-36,45
948	70	-61,49	10,93	-123,00	-36,00	-29,45	-29,30	-27,56
949	71	-61,49	10,97	-125,00	-20,00	-13,35	-13,19	-11,52
950	72	-61,49	10,99	-129,00	-3,00	3,87	4,03	5,72
951	73	-61,03	10,99	-77,00	-12,00	-7,90	-7,79	-7,16
952	74	-61,00	10,98	-96,00	-36,00	-30,89	-30,79	-30,05
953	6	-60,13	10,92	-1585,00	-88,00	-2,23	-0,84	4,26
954	7	-60,11	10,89	-1542,00	-90,00	-6,51	-5,23	-0,82
955	8	-60,10	10,85	-1459,00	-94,00	-15,58	-14,19	-12,18
956	9	-60,08	10,81	-1313,00	-94,00	-23,73	-22,43	-21,05
957	10	-60,07	10,78	-1173,00	-94,00	-31,39	-30,08	-28,93
958	11	-60,07	10,77	-1147,00	-88,00	-26,80	-25,46	-24,31
959	12	-60,07	10,80	-1103,00	-94,00	-35,12	-33,79	-30,93
960	13	-60,06	10,82	-1235,00	-111,00	-45,04	-43,60	-42,35
961	14	-60,08	10,83	-1458,00	-159,00	-80,94	-79,64	-78,24
962	15	-60,11	10,83	-1533,00	-159,00	-76,75	-75,58	-74,02
963	16	-60,16	10,86	-1556,00	-160,00	-75,23	-73,96	-70,45
964	17	-60,32	11,00	-426,00	-335,00	-311,84	-310,95	-310,87
965	18	-60,31	10,98	-660,00	-333,00	-297,26	-296,45	-295,48
966	19	-60,30	10,95	-858,00	-332,00	-285,51	-284,60	-282,75
967	20	-60,29	10,94	-407,00	-332,00	-309,42	-308,47	-308,23
968	21	-60,20	10,91	-438,00	-331,00	-304,87	-303,68	-303,35
969	22	-60,27	10,88	-486,00	-330,00	-303,52	-302,56	-302,08
970	23	-60,26	10,86	-550,00	-329,00	-299,23	-298,17	-297,98
971	24	-60,26	10,83	-773,00	-328,00	-286,31	-285,53	-281,59
972	25	-60,25	10,82	-896,00	-328,00	-279,79	-278,99	-271,21
973	26	-60,24	10,80	-871,00	-200,00	-153,21	-152,42	-145,29
974	27	-60,24	10,79	-1041,30	-100,00	-44,08	-43,35	-38,28
975	28	-60,23	10,77	-1062,00	-69,00	-12,05	-11,31	-7,65
976	29	-60,22	10,75	-977,00	-81,00	-28,65	-27,91	-20,30
977	30	-60,22	10,74	-942,00	-79,00	-28,53	-27,83	-20,00
978	31	-60,23	10,74	-965,00	-79,00	-27,29	-26,62	-19,72
979	32	-60,23	10,73	-971,00	-32,00	20,09	20,78	27,31
980	33	-60,23	10,72	-890,00	-86,00	-38,32	-37,64	-29,71
981	34	-60,22	10,70	-945,00	-87,00	-36,24	-35,56	-28,23
982	35	-60,22	10,68	-909,00	-89,00	-40,20	-39,57	-32,64
983	36	-60,22	10,67	-856,00	-89,00	-43,14	-42,52	-35,51
984	37	-60,21	10,65	-760,00	-134,00	-93,38	-92,74	-88,83
985	38	-60,18	10,43	-587,00	-82,00	-50,65	-50,19	-49,24
986	39	-60,18	10,41	-594,00	-86,00	-54,24	-53,81	-52,95
987	40	-60,17	10,39	-596,00	-86,00	-54,13	-53,72	-52,96
988	41	-60,16	10,16	-88,00	-86,00	-81,31	-81,05	-79,02
989	42	-60,16	10,17	-92,00	-44,00	-39,09	-38,83	-36,78
990	43	-60,16	10,16	-92,00	-50,00	-45,09	-44,83	-42,67
991	44	-60,16	10,15	-92,00	-48,00	-43,09	-42,84	-40,87

STN-N°	STN-REF	LONG	LAT	HEIGHT	FAA	BA	AIRY 35	PRATT 100
		(deg)	(deg)	(m)	(mGal)	(mGal)	(mGal)	(mGal)
992	45	-60,16	10,15	-92,00	-57,00	-52,09	-51,84	-49,79
993	46	-60,16	10,14	-92,00	-98,00	-93,09	-92,84	-90,76
994	47	-60,15	10,14	-92,00	-34,00	-29,09	-28,83	-26,77
995	48	-60,14	10,12	-92,00	-77,00	-72,09	-71,84	-69,77
996	49	-60,14	10,12	-92,00	-46,00	-41,09	-40,83	-38,71
997	50	-60,14	10,11	-92,00	-70,00	-65,09	-64,84	-62,74
998	51	-60,14	10,12	-92,00	-102,00	-97,09	-96,83	-94,68
999	52	-60,13	10,12	-92,00	-39,00	-34,09	-33,84	-31,96
1000	53	-60,14	10,11	-92,00	-96,00	-91,09	-90,84	-88,80
1001	75	-60,22	10,11	-113,00	-53,00	-46,99	-46,79	-44,31
1002	76	-60,16	10,09	-121,00	-51,00	-44,56	-44,36	-42,17
1003	77	-60,06	10,07	-156,00	-51,00	-42,69	-42,38	-41,11
1004	78	-60,03	10,06	-239,00	-52,00	-39,26	-38,94	-37,85
1005	79	-60,00	10,05	-297,00	-53,00	-37,13	-36,72	-35,78
1006	80	-60,98	10,98	-83,00	-16,00	-11,58	-11,47	-10,86
1307	81	-60,96	10,98	-86,00	-28,00	-23,42	-23,31	-22,49
1008	82	-60,92	10,98	-111,00	-35,00	-29,09	-28,98	-28,13
1009	83	-60,87	10,97	-100,00	-41,00	-35,68	-35,57	-34,70
1010	84	-60,83	10,96	-62,00	-27,00	-23,70	-23,58	-22,62
1011	85	-60,79	10,94	-46,00	-11,00	-8,55	-8,42	-7,28
1012	86	-60,73	10,93	-46,00	-9,00	-6,55	-6,42	-5,16
1013	87	-60,67	10,91	-62,00	-8,00	-4,70	-4,57	-3,10
1014	88	-60,64	10,90	-60,00	-13,00	-9,81	-9,68	-8,32
1015	89	-60,60	10,89	-60,00	-16,00	-12,81	-12,64	-11,17
1016	90	-60,58	10,90	-71,00	-22,00	-18,22	-18,07	-16,60
1017	91	-60,55	10,92	-73,00	-31,00	-27,11	-26,95	-25,49
1018	92	-60,53	10,86	-79,00	-29,00	-24,80	-24,36	-22,76
1019	93	-60,51	10,84	-95,00	-27,00	-21,94	-21,75	-20,01
1020	94	-60,48	10,79	-79,00	-36,00	-31,80	-31,63	-29,82
1021	95	-60,46	10,76	-88,00	-42,00	-37,32	-37,13	-35,25
1022	96	-60,43	10,73	-79,00	-37,00	-32,80	-32,60	-30,62
1023	97	-60,41	10,68	-84,00	-30,00	-25,52	-25,26	-23,03
1024	98	-60,42	10,64	-39,00	-38,00	-35,91	-35,71	-33,74
1025	99	-60,42	10,61	-86,00	-48,00	-43,42	-43,22	-40,78
1026	100	-60,43	10,58	-102,00	-54,00	-48,57	-48,38	-45,77
1027	101	-60,43	10,55	-102,00	-58,00	-52,57	-52,40	-49,87
1028	102	-60,43	10,51	-102,00	-64,00	-58,57	-58,40	-55,55
1029	103	-60,46	10,45	-88,00	-66,00	-61,32	-61,16	-58,88
1030	104	-60,48	10,41	-90,00	-66,00	-61,21	-61,06	-58,69
1031	105	-60,48	10,38	-96,00	-64,00	-58,89	-58,69	-56,71
1032	106	-60,51	10,34	-88,00	-62,00	-57,32	-57,11	-55,11
1033	107	-60,51	10,31	-79,00	-55,00	-50,80	-50,65	-48,51
1034	108	-60,54	10,27	-83,00	-55,00	-50,58	-50,45	-48,53
1035	109	-60,57	10,22	-84,00	-52,00	-47,53	-47,41	-45,45
1036	110	-60,59	10,17	-81,00	-51,00	-46,69	-46,57	-44,76
1037	111	-60,60	10,12	-79,00	-47,00	-42,80	-42,69	-41,05
1038	112	-60,54	10,07	-77,00	-45,00	-40,90	-40,77	-39,39
1030	113	-60,57	10,01	-73,00	-44,00	-39,99	-39,88	-38,68
1040	114	-60,25	10,05	-88,00	-32,00	-27,22	-27,07	-25,32
1041	115	-60,24	10,09	-86,00	-35,00	-30,42	-30,15	-28,08
1042	116	-60,25	10,15	-92,00	-41,00	-36,10	-35,91	-33,22
1043	117	-60,25	10,20	-92,00	-42,00	-37,10	-36,89	-33,99
1044	118	-60,25	10,24	-123,00	-45,00	-38,45	-38,22	-34,96
1045	119	-60,25	10,26	-156,00	-50,00	-41,69	-41,46	-37,68
1046	120	-60,25	10,30	-198,00	-56,00	-45,45	-45,18	-41,23

STN-N°	STN-REF	LONG	LAT	HEIGHT	FAA	BA	AIRY 35	PRATT 100
		(deg)	(deg)	(m)	(mGal)	(mGal)	(mGal)	(mGal)
1047	121	-60,24	10,33	-216,00	-63,00	-51,49	-50,50	-47,42
1048	122	-60,23	10,37	-225,00	-65,00	-53,02	-52,65	-48,26
1049	123	-60,24	10,41	-265,00	-68,00	-53,89	-53,54	-48,78
1050	124	-60,25	10,43	-239,00	-67,00	-54,28	-53,95	-48,17
1051	125	-60,25	10,52	-191,00	-66,00	-55,82	-55,40	-51,30
1052	126	-60,25	10,55	-163,00	-66,00	-57,29	-56,87	-53,70
1053	127	-60,25	10,59	-183,00	-61,00	-51,23	-50,74	-47,24
1054	128	-60,25	10,61	-218,00	-57,00	-45,37	-44,37	-41,16
1055	129	-60,25	10,65	-197,00	-52,00	-41,45	-40,89	-38,25
1056	130	-60,24	10,67	-191,00	-46,00	-35,72	-35,11	-32,69
1057	131	-60,25	10,69	-160,00	-36,00	-27,27	-26,64	-24,73
1058	132	-60,25	10,74	-150,00	-33,00	-24,63	-23,98	-22,04
1059	133	-60,24	10,78	-129,00	-22,00	-14,70	-13,97	-12,44
1060	134	-60,23	10,79	-106,00	-12,00	-5,69	-4,95	-3,74
1061	135	-60,27	10,89	-289,00	-3,00	13,01	13,81	14,38
1062	136	-60,26	10,93	-380,00	-7,00	14,59	15,59	15,77
1063	137	-60,25	10,96	-647,00	-21,00	14,87	15,90	17,75
1064	138	-60,26	10,97	-1024,00	-36,00	19,40	20,43	22,42
1065	139	-60,25	11,00	-1307,00	-48,00	22,33	23,51	24,28
1066	3102	-63,86	11,00	49,30	58,56	57,79	57,92	53,39
1067	3103	-63,96	11,00	42,00	57,00	57,84	57,95	53,80
1068	3104	-63,88	11,01	368,10	89,75	53,39	53,52	48,99
1069	3105	-63,81	11,01	19,20	63,06	63,19	63,32	61,13
1070	3106	-63,92	11,02	103,90	67,38	62,98	63,10	55,91
1071	3107	-63,84	11,02	38,40	64,69	61,82	61,95	60,57
1072	3108	-63,87	11,02	143,80	73,63	58,37	58,50	57,61
1073	3109	-63,95	11,02	60,60	70,44	63,98	64,12	63,73
1074	3110	-63,85	11,03	31,30	67,94	65,92	66,08	63,86
1075	3112	-63,87	11,05	43,50	79,13	75,67	75,74	74,44
1076	3113	-63,78	11,05	10,60	72,13	71,17	71,29	71,17
1077	3114	-63,97	11,05	27,10	65,19	62,68	62,83	62,06
1078	3115	-63,89	11,05	122,80	93,38	80,59	80,72	80,08
1080	3117	-63,90	11,06	48,40	86,19	90,36	90,50	80,62
1081	3118	-63,92	11,07	59,40	92,00	85,70	85,82	85,16
1082	3119	-63,86	11,08	33,20	87,06	84,82	84,95	83,32
1083	3120	-63,84	11,08	66,40	64,00	57,85	57,97	56,57
1084	3121	-63,97	11,08	2,40	59,69	60,08	60,19	59,32
1085	3122	-63,97	11,08	2,10	61,06	61,49	61,60	60,71
1086	3123	-63,93	11,09	19,50	79,94	85,32	85,44	77,51
1087	3124	-63,39	11,10	71,00	98,56	92,40	92,52	90,54
1088	3125	-63,95	11,10	6,00	72,69	82,22	82,34	71,86
1089	3126	-63,86	11,10	23,10	88,94	95,82	95,95	86,39
1090	3127	-63,87	11,10	58,80	98,31	97,87	97,99	91,81
1091	3128	-63,92	11,11	3,00	84,06	88,65	88,77	84,22
1092	3129	-63,85	11,12	1,30	87,44	87,96	88,09	88,84
1093	3130	-63,84	11,12	4,80	88,63	88,70	88,83	89,63
1096	3133	-63,91	11,13	97,20	96,13	93,22	93,36	85,27
1097	3134	-63,86	11,14	10,00	96,88	96,31	96,43	97,28
1098	3135	-63,87	11,15	18,20	90,88	89,34	89,47	90,30
1099	3137	-63,89	11,16	5,40	89,75	89,74	89,86	90,66
1100	3162	-64,38	11,01	2,30	41,25	43,68	43,98	41,38
1101	3163	-64,38	11,01	1,50	41,56	44,89	45,18	41,83
1102	3164	-64,29	11,02	80,70	47,94	45,32	45,52	39,11
1103	3165	-64,22	11,03	19,50	31,75	30,06	30,24	29,87
1104	3167	-64,01	11,04	19,20	52,81	57,16	57,45	51,14

STN-N°	STN-REF	LONG	LAT	HEIGHT	FAA	BA	AIRY 35	PRATT 100
		(deg)	(deg)	(m)	(mGal)	(mGal)	(mGal)	(mGal)
1105	3168	-64,25	11,04	35,90	39,81	36,20	37,24	35,87
1106	3169	-64,36	11,04	27,70	49,88	47,23	48,17	47,10
1107	3170	-64,33	11,05	16,10	46,25	44,97	45,25	44,67
1108	3171	-64,21	11,05	1,60	25,00	35,15	35,33	25,13
1109	3173	-64,29	11,06	18,80	44,00	43,67	43,86	42,01
1110	3000	-60,24	11,00	-1110,00	-75,00	-12,47	-11,27	-11,22
1112	3002	-60,14	11,01	-1592,00	-111,50	-20,64	-19,03	-21,29
1113	3003	-60,10	11,01	-1586,00	-117,06	-31,87	-30,07	-27,24
1114	3004	-60,01	11,01	-1384,00	-120,75	-46,55	-44,67	-44,44
1115	3005	-60,73	11,03	-68,00	-5,31	-1,56	-1,42	-0,81
1116	3006	-60,69	11,05	-80,00	-6,31	-2,04	-1,89	-1,21
1117	3007	-60,64	11,07	-88,00	-8,81	-4,10	-3,95	-3,37
1118	3008	-60,60	11,09	-80,00	-10,69	-6,43	-6,20	-5,67
1119	3009	-60,56	11,11	-82,00	-14,06	-8,81	-8,14	-8,55
1120	3010	-60,52	11,13	-84,00	-4,19	0,31	0,74	1,02
1121	3011	-60,47	11,15	-158,00	-3,06	5,51	6,11	6,09
1122	3012	-60,43	11,17	-290,00	-11,44	4,67	5,40	5,66
1123	3013	-60,34	11,20	-935,00	-41,06	16,09	17,33	11,36
1124	3014	-60,30	11,21	-1625,00	-84,63	3,08	5,72	5,49
1125	3015	-60,30	11,22	-1205,00	-52,00	15,58	17,19	16,10
1126	3016	-60,25	11,23	-1325,00	-61,31	9,92	11,84	12,74
1127	3017	-60,04	11,24	-1722,00	-81,38	10,70	13,37	13,23
1128	3018	-60,17	11,25	-1676,00	-77,25	12,41	14,82	14,79
1129	3019	-60,08	11,26	-1785,00	-80,06	15,05	17,79	17,97
1130	3020	-60,12	11,26	-1740,00	-80,88	12,50	15,07	14,69
1131	3021	-60,07	11,26	-1758,00	-84,81	8,99	11,68	11,56
1132	3022	-60,32	11,27	-1750,00	-79,44	13,98	16,71	16,42
1133	3023	-60,12	11,28	-1726,00	-68,94	27,74	30,23	25,67
1134	3024	-60,16	11,31	-1428,00	-55,63	22,64	25,16	24,19
1135	3025	-60,20	11,33	-1296,00	-42,63	31,53	33,92	30,71
1136	3026	-60,24	11,35	-1259,00	-38,56	28,80	31,05	31,15
1137	3027	-60,28	11,38	-1189,00	-58,19	5,22	7,55	7,48
1138	3028	-60,32	11,40	-1488,00	-89,88	-9,17	-7,33	-4,56
1139	3029	-60,36	11,42	-1475,00	-108,31	-29,45	-27,78	-23,87
1140	3030	-60,40	11,45	-1332,00	-105,38	-26,58	-25,09	-28,77
1141	3031	-60,44	11,47	-1101,00	-90,31	-31,65	-30,42	-25,93
1142	3032	-60,84	11,43	-358,00	-0,81	18,33	18,78	19,92
1143	3033	-60,67	11,48	-480,00	-21,06	4,69	5,30	6,97
1144	3034	-60,89	11,49	-376,00	-1,38	22,79	23,23	20,42
1145	3035	-60,63	11,49	-560,00	-22,81	11,11	11,77	10,00
1146	3036	-60,48	11,49	-893,00	-72,13	-20,69	-19,50	-20,26
1147	3037	-60,93	11,49	-404,00	-14,00	12,91	13,38	9,46
1148	3038	-60,58	11,50	-660,00	-34,25	3,73	4,59	3,94
1149	3039	-60,98	11,50	-492,00	-34,56	-3,81	-3,35	-6,29
1150	3040	-61,86	11,03	-118,00	2,50	8,79	9,10	10,70
1151	3041	-61,90	11,08	-137,00	4,00	13,11	13,32	12,50
1152	3042	-61,95	11,13	-143,00	2,19	9,98	10,24	10,68
1153	3043	-61,02	11,51	-498,00	-50,38	-21,44	-20,95	-21,34
1154	3044	-61,06	11,52	-516,00	-57,19	-29,24	-28,67	-27,03
1155	3045	-61,11	11,52	-550,00	-59,44	-26,82	-26,33	-27,19
1156	3046	-61,15	11,53	-602,00	-59,81	-26,66	-26,10	-24,39
1157	3047	-61,19	11,54	-650,00	-59,56	-23,01	-22,46	-21,29
1158	3048	-61,24	11,54	-670,00	-57,31	-20,71	-20,15	-17,93
1159	3049	-61,28	11,55	-644,00	-49,94	-14,88	-14,31	-12,12
1160	3050	-61,33	11,56	-696,00	-51,31	-13,98	-13,36	-10,93

STN-N°	STN-REF	LONG	LAT	HEIGHT	FAA	BA	AIRY 35	PRATT 100
		(deg)	(deg)	(m)	(mGal)	(mGal)	(mGal)	(mGal)
1161	3051	-61,37	11,57	-610,00	-43,25	-10,53	-9,92	-8,03
1162	3052	-61,41	11,57	-552,00	-34,25	0,67	1,27	-1,93
1163	3053	-61,46	11,58	-540,00	-32,50	-2,95	-2,34	-0,89
1164	3054	-61,50	11,59	-540,00	-29,50	-0,34	0,28	2,12
1165	3055	-61,54	11,60	-550,00	-26,88	9,68	10,36	5,20
1166	3056	-61,59	11,60	-580,00	-25,13	7,10	7,75	7,87
1167	3057	-61,70	11,62	-658,00	-17,69	18,86	19,50	19,57
1168	3058	-61,74	11,62	-670,00	-11,69	24,16	24,85	26,59
1169	3059	-61,84	11,62	-681,00	7,69	44,17	44,85	46,61
1170	3060	-61,89	11,62	-698,00	16,06	58,23	58,83	55,96
1171	3061	-61,93	11,62	-710,00	25,25	63,41	64,06	65,60
1172	3062	-61,98	11,62	-740,00	30,94	70,84	71,49	73,08
1173	3063	-62,97	11,08	-31,00	18,56	20,28	20,38	20,74
1174	3064	-62,93	11,13	-31,00	15,38	17,04	17,17	17,42
1175	3065	-62,39	11,18	-31,00	14,19	15,92	16,01	16,05
1176	3066	-62,04	11,23	-143,00	-7,38	0,32	0,55	0,64
1177	3067	-62,85	11,24	-42,00	0,75	3,11	3,23	3,17
1178	3068	-62,13	11,34	-118,00	-3,25	3,07	3,31	3,34
1179	3069	-62,83	11,43	-69,00	65,19	68,93	69,07	69,05
1180	3070	-62,22	11,45	-137,00	20,19	27,49	27,77	28,06
1181	3071	-62,31	11,55	-531,00	31,69	61,99	62,44	63,25
1182	3072	-62,31	11,56	-216,00	72,81	85,06	85,33	85,50
1183	3073	-62,99	11,60	-408,00	49,06	71,11	71,46	72,98
1184	3074	-62,95	11,60	-458,00	49,44	81,57	81,91	76,10
1185	3075	-62,36	11,61	-665,00	44,94	88,37	88,91	83,12
1186	3076	-62,90	11,61	-450,00	50,19	74,19	74,56	76,32
1187	3077	-62,86	11,61	-396,00	54,50	76,61	77,00	77,35
1188	3078	-62,82	11,61	-416,00	56,81	82,51	82,88	80,84
1189	3079	-62,02	11,62	-750,00	39,19	79,67	80,29	81,62
1190	3080	-62,06	11,62	-784,00	38,88	81,36	82,05	83,40
1191	3081	-62,11	11,62	-806,00	39,44	85,18	85,82	85,27
1192	3082	-62,15	11,62	-810,00	43,38	86,62	87,30	89,47
1193	3083	-62,77	11,62	-460,00	62,75	87,33	87,73	89,44
1194	3084	-62,20	11,62	-822,00	49,19	95,90	96,54	96,02
1195	3085	-62,24	11,62	-788,00	51,81	94,02	94,71	96,88
1196	3086	-62,33	11,62	-736,00	53,88	93,82	94,43	96,07
1197	3087	-62,38	11,62	-700,00	61,88	99,71	100,36	101,93
1198	3088	-62,42	11,62	-616,00	73,75	106,93	107,46	109,27
1199	3089	-62,46	11,62	-566,00	81,44	111,69	112,27	113,98
1200	3090	-62,51	11,62	-424,00	101,63	127,49	127,97	126,13
1201	3091	-62,55	11,62	-412,00	106,94	129,11	129,61	130,81
1202	3092	-62,59	11,62	-400,00	98,25	123,53	123,95	121,34
1203	3093	-62,73	11,62	-478,00	70,81	96,44	96,84	98,58
1204	3094	-62,64	11,63	-416,00	84,75	107,01	107,47	108,83
1205	3095	-62,68	11,63	-448,00	78,25	102,38	102,77	104,21
1206	3096	-62,78	11,69	-598,00	43,94	76,58	77,10	78,94
1207	3097	-62,76	11,75	-848,00	12,63	58,61	59,50	61,38
1208	3098	-62,49	11,76	-1086,00	25,56	84,48	85,61	88,16
1209	3099	-62,74	11,52	-1458,00	-39,19	39,09	40,45	45,03
1210	3100	-62,58	11,17	-1924,00	-65,75	38,49	40,28	45,78
1211	3101	-62,70	11,87	-1874,00	-76,38	28,71	30,47	32,62
1212	3111	-63,42	11,03	-42,00	54,06	56,33	56,56	57,03
1214	3138	-63,54	11,22	-31,00	102,81	104,48	104,55	104,58
1215	3139	-63,62	11,33	-42,00	83,38	85,64	85,71	85,72
1216	3140	-63,75	11,49	-56,00	-2,44	0,98	1,09	0,80

STN-N°	STN-REF	LONG	LAT	HEIGHT	FAA	BA	AIRY 35	PRATT 100
		(deg)	(deg)	(m)	(mGal)	(mGal)	(mGal)	(mGal)
1217	3141	-63,89	11,54	-84,00	-6,94	-1,66	-1,41	-2,09
1218	3142	-63,80	11,54	-93,00	-8,81	3,42	3,74	-3,46
1219	3143	-63,80	11,54	-78,00	2,06	13,86	14,13	6,60
1220	3144	-63,75	11,55	-74,00	9,81	14,33	14,51	14,13
1221	3145	-63,71	11,55	-74,00	11,19	23,17	23,38	15,50
1222	3146	-63,66	11,55	-76,00	14,56	18,71	18,88	19,03
1223	3147	-63,61	11,56	-72,00	14,06	18,14	18,33	18,29
1224	3148	-63,57	11,56	-68,00	19,06	23,11	23,27	23,05
1225	3149	-63,52	11,56	-70,00	22,06	26,22	26,40	26,19
1226	3150	-63,48	11,57	-72,00	21,63	26,05	26,23	25,82
1227	3151	-63,43	11,57	-76,00	18,31	22,93	23,12	22,75
1228	3152	-63,38	11,57	-84,00	16,50	21,06	21,25	21,38
1229	3153	-63,44	11,58	-102,60	18,38	24,28	24,47	24,42
1230	3154	-63,29	11,58	-148,00	22,81	35,11	35,31	31,47
1231	3155	-63,24	11,53	-154,00	33,44	42,08	42,29	42,45
1232	3156	-63,17	11,59	-192,00	41,44	52,28	52,49	52,81
1233	3157	-63,13	11,59	-202,00	42,94	58,55	58,77	54,92
1234	3158	-63,08	11,59	-194,00	44,31	57,40	57,68	55,78
1235	3159	-63,04	11,60	-344,00	46,88	71,28	71,57	67,27
1236	3160	-63,90	11,65	-622,00	6,81	47,75	48,25	43,30
1237	3161	-63,95	11,70	-548,00	42,94	79,95	80,56	73,44
1238	3166	-64,56	11,04	-119,00	-3,06	3,42	3,78	4,11
1239	3172	-64,93	11,06	-105,00	34,75	40,42	40,77	42,06
1240	3174	-64,97	11,09	-86,00	67,81	72,66	72,97	73,56
1241	3175	-64,56	11,10	-40,00	16,38	25,53	25,87	19,20
1242	3176	-64,90	11,12	-129,00	39,25	48,76	49,09	47,29
1243	3177	-64,93	11,12	-103,00	62,81	69,08	69,45	69,51
1244	3178	-64,89	11,16	-283,00	33,00	49,96	50,34	49,82
1245	3179	-64,87	11,13	-441,00	15,88	40,66	41,06	41,99
1246	3180	-64,88	11,18	-383,00	14,69	36,10	36,48	37,36
1247	3181	-64,86	11,19	-543,00	9,00	40,58	41,05	41,17
1248	3182	-64,82	11,23	-728,00	-7,00	32,01	32,53	35,81
1249	3183	-64,84	11,25	-855,00	-20,50	25,92	26,58	30,00
1250	3184	-64,79	11,26	-713,00	-10,13	28,48	29,14	31,97
1251	3185	-64,78	11,27	-726,00	-10,31	29,06	29,73	32,57
1252	3186	-64,81	11,30	-1051,00	-37,00	19,26	20,20	23,59
1253	3187	-64,76	11,31	-878,00	-21,88	27,32	28,11	28,08
1254	3188	-64,77	11,34	-1046,00	-30,25	25,76	26,74	29,57
1255	3189	-64,77	11,37	-1123,00	-32,31	28,19	29,25	32,13
1256	3190	-64,79	11,39	-1362,00	-45,06	28,85	30,09	33,44
1257	3191	-64,81	11,42	-1472,00	-41,19	39,31	40,90	40,00
1258	3192	-64,74	11,42	-1123,00	-26,81	34,94	36,45	35,49
1259	3193	-64,83	11,46	-1593,00	-31,69	53,18	55,20	56,67
1260	3194	-64,92	11,47	-2034,00	-51,44	57,13	59,52	63,53
1261	3195	-64,97	11,47	-2150,00	-62,13	53,20	55,70	59,83
1262	3196	-64,88	11,43	-1814,00	-43,25	54,49	56,69	58,43
1263	3197	-64,79	11,48	-1544,00	-37,81	44,64	46,47	49,79
1264	3198	-64,83	11,48	-1640,00	-33,75	53,80	55,87	57,47
1265	3199	-64,74	11,48	-1440,00	-35,88	41,14	42,86	45,53
1266	3200	-64,65	11,48	-1042,00	-12,44	43,42	44,79	47,31
1267	3201	-64,69	11,48	-1240,00	-28,44	40,56	42,10	42,94
1268	3202	-64,60	11,48	-938,00	0,75	52,45	53,74	54,70
1269	3203	-64,45	11,49	-810,00	36,31	82,01	82,86	83,48
1270	3204	-64,40	11,50	-766,00	46,38	87,25	88,00	90,42
1271	3205	-64,84	11,50	-1562,00	-21,31	69,29	71,67	64,69

STN-N°	STN-REF	LONG	LAT	HEIGHT	FAA	BA	AIRY 35	PRATT 100
		(deg)	(deg)	(m)	(mGal)	(mGal)	(mGal)	(mGal)
1272	3206	-64,36	11,50	-655,00	58,75	101,41	102,02	95,68
1273	3207	-64,31	11,51	-567,00	49,50	80,85	81,37	80,96
1274	3208	-64,26	11,51	-482,00	40,88	67,03	67,49	68,95
1275	3209	-64,22	11,51	-412,00	31,38	57,98	58,39	55,18
1276	3210	-64,17	11,52	-334,00	25,75	44,16	44,53	44,96
1277	3211	-64,13	11,52	-282,00	19,19	35,09	35,42	35,24
1278	3212	-64,08	11,52	-244,00	8,38	22,20	22,49	22,81
1279	3213	-64,03	11,53	-215,00	1,44	13,86	14,18	14,14
1280	3214	-64,67	11,53	-1404,00	-38,06	37,23	39,07	41,30
1281	3215	-64,86	11,54	-1503,00	-4,06	76,05	78,72	79,30
1282	3216	-64,88	11,59	-1463,00	8,25	91,59	94,50	90,04
1283	3217	-64,96	11,63	-2268,00	-14,13	108,12	111,86	110,73
1284	3218	-64,91	11,63	-1472,00	8,56	89,75	93,16	94,73
1285	3219	-64,87	11,63	-1503,00	13,56	94,67	97,85	96,63
1286	3220	-64,83	11,63	-812,00	39,25	87,22	90,34	90,15
1287	3221	-64,32	11,63	-1097,00	35,38	97,07	99,98	99,33
1288	3222	-64,77	11,63	-1653,00	-17,13	71,13	73,90	74,55
1289	3223	-64,72	11,63	-1682,00	-36,88	52,77	55,42	56,46
1291	3225	-64,92	11,67	-1489,00	22,13	104,08	107,70	109,42
1292	3226	-64,94	11,71	-1441,00	31,44	110,45	114,29	115,79
1293	3227	-64,98	11,79	-1223,00	38,13	107,80	111,90	112,39
1294	3228	-64,53	11,83	-18,00	168,13	170,40	172,10	178,48
1295	3229	-65,00	11,84	-1920,00	6,19	115,10	119,29	113,84
1296	3230	-64,82	11,85	-1993,00	-21,63	85,55	88,87	88,91
1297	3231	-64,09	11,86	-259,00	133,06	148,19	149,00	149,31
1298	3232	-64,95	11,87	-1783,00	6,13	102,05	106,00	105,13
1299	3233	-65,00	11,91	-2099,00	-8,94	102,95	107,10	109,43
1300	3234	-64,96	11,91	-2037,00	-7,13	102,32	106,28	107,65
1301	3235	-64,92	11,92	-1990,00	-4,38	107,12	110,83	107,43
1302	3236	-64,88	11,92	-1887,00	-5,06	97,03	100,45	99,19
1303	3237	-64,84	11,93	-1960,00	-8,75	96,89	100,32	99,92
1304	3238	-64,80	11,93	-2251,00	-16,81	109,15	112,26	108,58
1305	3239	-64,77	11,94	-2628,00	-19,00	122,35	125,43	126,71
1306	3240	-64,73	11,95	-2076,00	-9,31	103,30	106,29	106,29
1307	3241	-64,48	11,95	-1025,00	71,88	127,73	128,90	133,06
1308	3242	-64,17	11,98	-216,00	127,63	142,33	143,30	142,08
1309	3243	-65,48	11,09	-77,00	27,63	35,17	35,75	32,29
1310	3244	-65,18	11,12	-110,00	37,94	44,20	44,55	44,44
1311	3245	-65,99	11,14	-421,00	14,63	38,36	38,81	39,06
1312	3246	-65,48	11,14	-269,00	16,38	31,16	31,47	32,40
1313	3247	-65,18	11,17	-391,00	18,44	40,38	40,75	41,73
1314	3248	-65,49	11,19	-391,00	12,13	35,12	35,61	35,40
1315	3249	-65,18	11,22	-585,00	5,38	36,91	37,36	39,70
1316	3250	-65,49	11,25	-529,00	7,00	35,30	35,89	37,99
1317	3251	-65,18	11,27	-761,00	0,19	41,43	42,12	45,18
1318	3252	-65,49	11,30	-699,00	2,19	40,50	41,21	43,08
1319	3253	-65,18	11,32	-938,00	-4,38	47,40	48,38	48,78
1320	3254	-65,49	11,35	-823,00	0,38	45,19	46,17	47,05
1321	3255	-65,18	11,37	-1233,00	-13,13	52,94	54,33	57,87
1322	3256	-65,49	11,40	-956,00	-1,38	49,65	50,89	52,89
1323	3257	-65,18	11,42	-1673,00	-28,69	62,26	64,04	65,39
1324	3258	-65,49	11,45	-1086,00	-5,69	54,04	55,55	54,85
1325	3259	-65,43	11,46	-1168,00	-10,75	51,60	53,27	54,82
1326	3260	-65,48	11,46	-1142,00	-9,94	51,15	52,76	54,03
1327	3261	-65,38	11,46	-1248,00	-15,00	51,82	53,56	55,95

STN-N°	STN-REF	LONG	LAT	HEIGHT	FAA	BA	AIRY 35	PRATT 100
		(deg)	(deg)	(m)	(mGal)	(mGal)	(mGal)	(mGal)
1328	3262	-65,29	11,47	-1688,00	-35,38	56,24	58,27	61,65
1329	3263	-65,34	11,47	-1492,00	-26,56	54,50	56,24	59,00
1330	3264	-65,18	11,47	-2048,00	-49,13	60,30	62,64	67,54
1331	3265	-65,25	11,47	-1760,00	-40,75	54,17	56,18	60,46
1332	3266	-65,15	11,47	-2165,00	-67,19	49,02	51,31	56,31
1333	3267	-65,20	11,47	-1995,00	-56,81	54,89	57,10	57,32
1334	3268	-65,11	11,47	-2210,00	-69,06	53,99	56,50	56,94
1335	3269	-65,02	11,47	-2175,00	-68,13	48,16	50,63	54,97
1336	3270	-65,06	11,47	-2200,00	-69,25	48,54	50,97	55,33
1337	3271	-65,49	11,50	-1163,30	-2,94	59,16	61,02	61,40
1338	3272	-65,18	11,52	-2458,00	-64,75	66,86	69,73	72,79
1339	3273	-65,18	11,53	-2816,00	-82,88	73,37	76,86	75,92
1340	3274	-65,50	11,60	-1545,00	-4,56	78,19	80,92	81,07
1341	3275	-65,49	11,63	-1893,00	-15,94	86,04	88,68	90,33
1342	3276	-65,44	11,63	-1933,00	-19,94	84,01	87,05	89,03
1343	3277	-65,39	11,63	-2149,00	-32,75	82,03	85,01	87,64
1344	3278	-65,34	11,63	-2152,00	-41,63	73,36	76,85	79,11
1345	3279	-65,29	11,63	-2579,00	-65,44	77,31	80,95	78,26
1346	3280	-65,25	11,63	-3091,00	-84,13	81,57	85,62	90,03
1347	3281	-65,23	11,63	-3438,00	-95,00	93,45	97,43	98,94
1348	3282	-65,15	11,63	-3008,00	-94,00	69,48	73,76	73,48
1349	3283	-65,10	11,63	-3255,00	-92,19	86,59	90,64	89,48
1350	3284	-65,06	11,63	-3301,00	-80,25	96,76	100,91	103,17
1351	3285	-65,01	11,63	-2908,00	-48,69	112,95	116,80	111,15
1352	3286	-65,47	11,84	-3888,00	-128,00	80,07	85,54	93,49
1353	3287	-65,46	11,84	-3894,00	-132,94	75,40	80,85	88,88
1354	3288	-65,44	11,84	-3901,00	-144,19	64,44	69,95	78,01
1355	3289	-65,42	11,84	-3904,00	-144,50	64,20	69,88	77,69
1356	3290	-65,38	11,85	-3904,00	-153,19	54,97	60,87	66,42
1357	3291	-65,35	11,85	-3899,00	-153,38	54,51	60,55	65,68
1358	3292	-65,30	11,86	-3899,00	-150,63	64,24	70,19	67,09
1359	3293	-65,27	11,87	-3899,00	-137,94	70,59	76,57	77,03
1360	3294	-65,23	11,87	-3873,00	-115,38	91,85	98,28	97,91
1361	3295	-65,19	11,88	-3694,00	-92,94	109,75	115,31	112,70
1362	3296	-65,02	11,88	-2158,00	-16,13	104,83	109,13	103,05
1363	3297	-65,15	11,88	-2862,00	-62,44	91,81	97,22	96,70
1364	3298	-65,11	11,89	-2249,00	-35,94	86,45	91,55	93,76
1365	3299	-65,33	11,89	-2065,00	-15,44	100,77	105,23	99,48
1366	3300	-65,07	11,89	-2196,00	-21,38	100,63	105,46	100,22
1367	3301	-65,04	11,90	-2145,00	-15,63	105,70	110,41	103,64
1368	3302	-65,14	11,92	-3317,00	-86,44	96,24	101,60	96,79
1369	3303	-65,03	11,92	-2229,00	-23,06	96,02	100,61	102,29
1370	3304	-65,46	11,93	-3894,00	-122,88	85,17	91,67	91,65
1374	966	-60,26	10,73	-274,30	-75,00	-60,18	-59,55	-57,82
1375	936	-60,09	9,78	-91,40	-82,00	-77,04	-76,87	-76,44
1376	937	-60,85	10,05	-54,90	-86,00	-83,08	-82,99	-82,20
1377	938	-60,83	10,07	-73,20	-84,00	-80,10	-80,01	-79,13
1378	939	-60,79	10,09	-64,00	-7,90	-4,49	-4,39	-3,34
1379	940	-60,18	10,37	-356,60	-93,00	-74,00	-73,59	-69,58
1380	941	-60,06	10,43	-585,20	-96,00	-64,81	-64,03	-62,12
1381	942	-61,09	10,96	-73,20	-31,00	-27,10	-26,99	-26,38
1382	943	-62,02	10,80	-100,60	-12,50	-7,13	-6,94	-5,20
1383	944	-62,05	10,80	-91,40	-14,00	-9,12	-8,92	-7,35
1384	945	-63,55	10,97	-18,30	41,00	41,97	42,08	42,81
1385	946	-64,68	10,83	-201,20	-15,00	-4,27	-3,48	-1,18

STN-N°	STN-REF	LONG	LAT	HEIGHT	FAA	BA	AIRY 35	PRATT 100
		(deg)	(deg)	(m)	(mGal)	(mGal)	(mGal)	(mGal)
1386	948	-64,87	10,40	-82,30	-16,00	-11,53	-11,21	-9,92
1387	949	-61,57	10,95	-109,70	-46,00	-40,16	-39,95	-37,88
1388	950	-61,56	10,95	-109,70	-49,00	-43,16	-42,96	-41,08
1389	951	-61,51	10,96	-100,90	-50,00	-44,63	-44,46	-42,83
1390	952	-61,25	10,96	-73,20	-65,00	-61,10	-60,97	-60,23
1391	953	-61,19	10,97	-64,00	-50,00	-46,59	-46,47	-45,82
1392	954	-61,13	10,97	-82,30	-34,00	-29,62	-29,51	-28,87
1393	955	-61,36	10,97	-89,60	-27,00	-22,23	-22,13	-21,48
1394	958	-60,91	10,94	-73,20	-44,00	-40,10	-40,67	-38,19
1395	959	-60,86	10,90	-54,90	-28,00	-25,08	-24,97	-23,81
1396	960	-60,77	10,84	-64,00	-30,00	-26,59	-26,45	-25,09
1397	961	-60,77	10,83	-69,50	-35,00	-31,30	-31,19	-29,83
1398	962	-60,77	10,77	-64,00	-37,00	-33,59	-33,50	-32,17
1399	963	-60,78	10,64	-54,90	-50,00	-47,08	-46,95	-45,71
1400	964	-60,53	10,68	-64,00	-66,00	-62,59	-62,47	-60,83
1401	965	-60,35	10,72	-100,60	-52,00	-46,63	-46,25	-44,60
1402	966	-60,26	10,73	-274,30	-75,00	-60,18	-59,55	-57,82

APPENDIX D

EARTHQUAKE DATA CATALOGUE EASTERN VENEZUELAN BASIN

YEAR	MON	DAY	HOUR	MIN	SEC	LAT (N)	LONG (W)	DEPTH (KM)	SOURCE	MAG	TYPE
------	-----	-----	------	-----	-----	------------	-------------	---------------	--------	-----	------

1910	1	23	18	49	40.0	12.000	-60.500	100.0	GUTE	7.2	
1918	2	24	23	0	20.0	12.000	-62.000	0.0	GUTE	6.3	
1923	8	8	12	1	27.0	10.500	-63.500	110.0	GUTE	6.5	
1926	2	1	1	17	33.0	10.500	-63.500	100.0	GUTE	6.5	
1928	9	27	0	44	05.0	12.000	-60.000	0.0	GUTE	6.5	
1935	4	10	22	32	31.0	10.500	-62.000	100.0	GUTE	6.5	
1946	7	31	0	28	57.0	12.500	-60.000	50.0	GUTE	6.0	
1957	10	2	12	27	54.2	10.940	-62.800	0.0	SYKE	6.1	
1957	10	4	5	26	07.2	10.920	-62.810	32.0	SYKE	6.7	
1957	10	6	0	54	05.2	10.860	-62.770	0.0	SYKE	5.1	
1957	12	25	16	26	04.0	10.460	-62.580	29.0	SYKE	5.9	
1962	1	15	8	22	18.0	13.000	-60.400	60.0	TRN	6.7	
1962	11	24	7	31	44.0	10.200	-62.900	0.0	CAR	5.5	
1962	12	21	0	46	55.0	11.100	-61.400	80.0	TRN	5.2	
1962	12	28	8	7	01.0	10.300	-61.700	0.0	TRN	6.1	
1963	3	2	15	43	03.0	11.000	-61.400	0.0	TRN	5.1	
1964	8	10	16	58	44.6	9.150	-62.020	59.0	ISC	5.4	
1965	7	15	16	55	00.0	11.230	-61.250	10.0	TRN	5.1	
1965	7	20	4	28	00.0	10.200	-64.450	10.0	TRN	5.1	
1965	11	10	9	24	00.0	11.210	-61.770	50.0	TRN	5.8	
1966	3	16	16	10	00.0	10.460	-63.310	10.0	TRN	5.2	
1966	5	14	20	27	30.7	10.370	-63.040	38.0	ISC	5.3	
1966	8	2	6	1	24.1	11.090	-62.130	14.0	ISC	5.3	
1966	8	8	0	38	27.6	12.410	-60.190	164.0	ISC	5.2	
1966	8	18	17	39	00.0	10.410	-63.800	10.0	TRN	5.3	
1966	9	24	19	56	57.4	9.950	-62.990	68.0	ISC	5.3	
1966	10	16	11	23	00.0	11.340	-64.050	160.0	TRN	5.0	
1967	1	4	20	15	59.0	10.930	-62.520	94.0	ISC	5.4	
1967	3	18	19	34	12.3	13.250	-64.370	180.0	ISC	5.0	
1967	3	30	18	23	35.4	10.610	-61.450	9.0	TRN	5.3	
1967	5	31	11	38	39.8	12.480	-60.310	70.0	ISC	5.2	
1967	6	24	9	11	18.2	11.540	-64.890	86.0	ISC	5.0	
1968	9	20	6	0	03.3	10.760	-62.700	103.0	ISC	6.2	
1969	10	22	12	52	22.8	10.920	-62.550	87.0	ISC	5.4	
1972	3	10	10	25	03.8	10.818	-62.979	129.0	ISC	5.1	
1972	8	29	3	29	25.0	10.665	-62.347	84.0	ISC	5.2	
1974	6	12	16	25	45.2	10.611	-63.469	0.0	ISC	5.7	
1974	10	29	3	10	16.9	10.584	-63.450	33.0	ISC	5.0	
1975	4	15	9	47	44.8	9.418	-61.466	52.0	ISC	5.3	
1975	8	24	1	5	15.1	10.751	-62.653	111.0	ISC	5.1	
1976	8	23	13	56	12.3	11.073	-62.357	90.4	ISC	5.0	
1977	9	21	16	5	13.7	10.421	-62.556	42.1	ISC	5.1	
1977	10	4	13	44	57.0	9.953	-62.230	45.7	FUN	5.1	
1981	3	2	7	54	07.3	12.322	-60.262	65.3	ISC	5.0	
1981	12	4	21	44	58.2	10.522	-61.420	64.6	ISC	5.0	
1981	12	25	12		48.2	10.936	-62.357	96.0	ISC	5.1	

1982	1	20	15	15	49.1	13.763	-60.472	77.9	ISC	5.1	
1982	5	10	1	25	57.3	10.698	-62.505	99.7	ISC	5.2	
1982	9	20	16	26	43.8	11.251	-60.773	1.1	ISC	5.2	
1982	10	25	17	6	54.9	11.318	-62.092	105.0	ISC	5.0	
1983	3	8	17	6	37.5	10.897	-62.038	76.1	FUN	5.9	
1983	4	11	8	18	10.1	10.351	-62.541	52.6	FUN	5.1	
1984	1	15	20	14	10.1	11.083	-60.610	62.3	ISC	5.1	
1984	2	11	13	57	45.1	12.088	-60.002	63.2	ISC	5.3	
1984	8	20	23	55	11.8	10.452	-62.450	10.0	ISC	5.1	
1985	11	28	0	14	00.0	11.763	-61.369	75.3	ISC	5.2	
1986	6	11	13	48	01.5	10.417	-62.914	10.2	FUN	5.9	
1988	3	10	6	17	15.9	10.169	-60.139	22.1	USGS	7.0	
1988	3	12	4	32	07.4	10.195	-60.209	45.0	FUN	5.3	
1988	3	16	5	47	58.7	9.722	-60.476	0.4	FUN	5.2	
1989	4	15	14	24	41.6	8.399	-61.068	0.5	FUN	5.0	
1993	9	11	18	56	54.5	10.856	-62.598	40.6	FUN	5.2	
1994	5	3	16	36	42.0	10.064	-60.367	64.0	FUN	5.7	
1994	6	1	3	13	46.5	11.922	-60.680	52.6	FUN	5.5	
1996	2	25	23	20	49.9	11.350	-60.316	58.9	FUN	5.1	
1997	4	2	6	14	40.0	11.076	-61.379	37.5	FUN	5.6	
1997	4	8	17	11	53.8	10.885	-60.569	4.4	FUN	5.1	
1997	4	22	9	31	20.0	11.134	-60.386	0.1	FUN	5.7	
1997	4	22	10	11	44.6	10.954	-60.230	20.2	FUN	5.1	
1997	5	4	1	44	49.7	10.870	-60.600	9.6	FUN	5.2	
1997	7	7	1	41	38.0	11.210	-62.195	14.7	FUN	5.1	
1997	7	9	19	24	10.8	10.545	-63.515	9.4	FUN	6.9	
2000	10	4	14	37	49.2	11.016	-62.295	98.3	FUN	5.9	Mw
2002	8	27	4	31	13.1	10.294	-60.637	55.2	FUN	5.4	Mw
2004	1	15	10	56	20.3	10.872	-62.221	71.0	FUN	5.2	Mw
2004	12	2	19	16	30.4	10.468	-61.013	11.4	FUN	5.0	Mw
2004	12	2	19	16	30.4	10.468	-61.013	11.4	FUN	5.0	Mw
2004	12	2	19	16	30.3	10.511	-60.903	24.9	FUN	5.2	Mw
2004	12	2	19	16	30.4	10.468	-61.013	11.4	FUN	5.0	Mw
2005	10	24	9	19	17.9	11.049	-62.205	116.9	FUN	5.3	Mw
2005	10	28	22	31	0.8	10.850	-61.885	76.3	FUN	5.5	Mw
2006	6	13	12	25	27.2	10.879	-62.106	67.4	FUN	5.0	Mw
2006	9	29	13	8	24.8	10.797	-61.300	54.1	FUN	6.1	Mw
2006	9	29	18	23	3.4	10.781	-61.323	25.6	FUN	5.5	Mw
2008	6	27	5	8	12.7	11.124	-62.244	128.2	FUN	5.2	Mw
2008	7	3	6	34	53.1	10.344	-60.199	41.8	FUN	5.3	Mw
2008	8	11	7	19	26.4	10.523	-64.168	13.7	FUN	5.2	Mw
2010	1	15	18	0	47.0	10.505	-63.494	5.0	FUN	5.4	Mw

SOURCES:

FUN = FUNVISIS, VENEZUELA
 USGS = U. S. GEOLOGICAL SURVEY
 ISC = INTERNATIONAL SEISMOLOGY CENTER
 TRN = TRINIDAD
 GUTE = Gutenberg & Richter Catalogue (1954)
 SYKE = Sykes et al., 1982
 CAR = CARACAS